Springer Proceedings in Complexity

Clemens Mensink
Volker Matthias *Editors*

Air Pollution Modeling and its Application XXVII

Springer

Springer Proceedings in Complexity

Springer Proceedings in Complexity publishes proceedings from scholarly meetings on all topics relating to the interdisciplinary studies of complex systems science. Springer welcomes book ideas from authors. The series is indexed in Scopus.

Proposals must include the following:

- name, place and date of the scientific meeting
- a link to the committees (local organization, international advisors etc.)
- scientific description of the meeting
- list of invited/plenary speakers
- an estimate of the planned proceedings book parameters (number of pages/articles, requested number of bulk copies, submission deadline)

Submit your proposals to: Hisako.Niko@springer.com

More information about this series at https://link.springer.com/bookseries/11637

Clemens Mensink · Volker Matthias
Editors

Air Pollution Modeling and its Application XXVII

Springer

Editors
Clemens Mensink
VITO NV
Mol, Belgium

Volker Matthias
Helmholtz-Zentrum Hereon
Geesthacht, Germany

ISSN 2213-8684 ISSN 2213-8692 (electronic)
Springer Proceedings in Complexity
ISBN 978-3-662-63759-3 ISBN 978-3-662-63760-9 (eBook)
https://doi.org/10.1007/978-3-662-63760-9

© The Editor(s) (if applicable) and The Author(s), under exclusive license to Springer-Verlag GmbH, DE, part of Springer Nature 2021
This work is subject to copyright. All rights are solely and exclusively licensed by the Publisher, whether the whole or part of the material is concerned, specifically the rights of translation, reprinting, reuse of illustrations, recitation, broadcasting, reproduction on microfilms or in any other physical way, and transmission or information storage and retrieval, electronic adaptation, computer software, or by similar or dissimilar methodology now known or hereafter developed.
The use of general descriptive names, registered names, trademarks, service marks, etc. in this publication does not imply, even in the absence of a specific statement, that such names are exempt from the relevant protective laws and regulations and therefore free for general use.
The publisher, the authors and the editors are safe to assume that the advice and information in this book are believed to be true and accurate at the date of publication. Neither the publisher nor the authors or the editors give a warranty, expressed or implied, with respect to the material contained herein or for any errors or omissions that may have been made. The publisher remains neutral with regard to jurisdictional claims in published maps and institutional affiliations.

This Springer imprint is published by the registered company Springer-Verlag GmbH, DE part of Springer Nature.
The registered company address is: Heidelberger Platz 3, 14197 Berlin, Germany

Organizing Committee

Members of the Scientific Committee for the 37th International Technical Meeting on Air Pollution Modeling and its Application

Clemens Mensink, Belgium
Ekaterina Batchvarova, Bulgaria
Wanmin Gong, Canada
Ari Karppinen, Finland
Laurent Deguillaume, France
Volker Matthias, Germany
Maria Kanakidou, Greece
Silvia Trini Castelli, Italy
Hilde Fagerli, Norway
Ana Isabel Miranda, Portugal
Oriol Jorba, Spain
Renske Timmermans, The Netherlands
Ulas Im, Turkey
Tony Dore, UK
Rohit Mathur,USA

Honorary Life Members

Chris De Wispelaere, Belgium
Douw Steyn, Canada
Sven-Erik Gryning, Denmark
Werner Klug, Germany
Carlos Borrego, Portugal
Han van Dop, The Netherlands
S. T. Rao, USA
Frank Schiermeier, USA

Preface—50th Anniversary of ITM

This 37th edition of the International Technical Meeting (ITM) on Air Pollution Modeling and its Application is a special edition because of the celebration of its 50th anniversary.

The ITM series of conferences were initiated in 1969 under the auspices of the North Atlantic Treaty Organization's Committee on Challenges of Modern Society (NATO-CCMS). The ITM series became independent of NATO since 2013. Over its long history, the ITM conference series provided a broadly independent international meeting of the highest scientific stature. ITM has become one of the most prominent forums for discussing the latest scientific developments and applications related to air pollution modeling at scales ranging from local to global.

Back in 1969, air quality researchers were actively involved in air pollution modeling, notably in Gaussian dispersion modeling, both in the USA and Europe, and the ITM was initiated as a platform where they could share knowledge and experience. The fate of pollutants such as SO_2 and black carbon were studied, as well as lead deposition, and dispersion applications related to security and defense, hence the NATO umbrella. Later, other types of air quality models were developed, applied, and discussed in the ITM, such as the 3D Eulerian and Lagrangian models to simulate long range transport of air pollutants. More recently, developments in CFD such as large eddy simulations (LES) and direct numerical simulations (DNS) to study local and micro-scale air pollution gained interest.

Since the beginning of the nineties, ITM has shown a much stronger focus on regional scale modeling, certainly after 1991, when part of the Gaussian dispersion modeling activities were taken over by the Harmonization Initiative and its conferences. For an excellent overview of the activities over the past 50 years, we refer to the keynote paper presented by Douw Steyn at the ITM in Chania in 2016 which appeared as a book chapter in the 35th ITM proceedings with the title "The Intellectual History of Air Pollution Modeling as Represented by the ITM Meeting Series."

Besides ITM's contribution to the science of air pollution modeling and its application, as published in the Springer Proceedings on Complexity series, there are at

least two more aspects of the ITM that have substantiated its success over the last 50 years.

The second key to its success is ITM's contribution to air quality policy and legislation. Over the last 50 years, strong efforts have been made to clean the air and to regulate air polluting activities, both at national and international levels. There is, for example, the Clean Air Act in the USA that has a proven record of public health and environmental protection since 1970. Various Air Quality Directives in Europe got in place since 1970 including the overarching Air Quality Framework Directive in 1996 and its various extensions and revisions since then. The activities under the UNECE Convention on Long Range Transboundary Air Pollution should be mentioned here as well. Work that started in 1979 was extended by eight protocols up till now, e.g., by the Gothenburg protocol in 1999. Finally, it is important to mention the various national air quality programs and plans in many countries. Over the past 50 years, all this work was and still is hugely supported and scientifically underpinned by the air quality modeling work presented at ITM.

A third element in the success of ITM is its strong community. ITM has always brought together scientists and policy makers to exchange knowledge, insights, and ideas, as well as to inspire and share the feeling that the work we do is relevant and contributes to a more sustainable world. This observation that ITM can build on a strong community is, for example, shown by the fact that the return ratio of participants over the last years is up to 60%. So that means that more than half of its participants was there at one of the previous meetings. This loyalty and maintained interest in ITM are an important asset and strength. But even more important is the fact that ITM keeps attracting young scientists and students and makes them enthusiastic about our work and our scientific domain. A good illustration is that for this 37th ITM conference, we have attracted 28 young scientists who subscribed for the 10th edition of Early Career Award, which is the contest for the best paper or poster award for researchers under 35.

Based on these three strong pillars of ITM, i.e., its contribution to the scientific developments, its societal relevance for air quality policy and legislation, and its community that is both loyal and open for newcomers, ITM's continuity and its future will be guaranteed.

This volume contains the papers and posters presented at the 37th International Technical Meeting on Air Pollution Modeling and its Application, held at the Katholische Akademie in Hamburg, from September 23 to 27, 2019. It was organized by Helmholtz-Zentrum Hereon in Germany (host country) and VITO in Belgium (pilot country). It was attended by 130 participants from 24 countries. Keynotes were given by Annica Ekman (Stockholm University), Silvia Trini Castelli (NRC, Institute of Atmospheric Sciences and Climate), Peter Builtjes (Free University Berlin), and Guy Brasseur (Max Planck Institute for Meteorology).

On behalf of the steering committee, we like to thank all who contributed to the success of the meeting. We like to acknowledge the keynote speakers for their outstanding contributions, the session chairpersons and rapporteurs for their efforts, and the institutions that organized and sponsored this conference: the team from Helmholtz-Zentrum Hereon for their financial and organizational support of ITM,

University of Hamburg for supporting this conference, Ramboll for sponsoring the Early Career Awards, and VITO in Belgium for financially supporting some of the graduate students to participate in this conference.

The 38th ITM conference will take place in Barcelona, Spain, October 18–22, 2021.

Mol, Belgium
Geesthacht, Germany

Clemens Mensink
Chair of the Steering Committee
Volker Matthias
Conference Organizer

Contents

Contributors

Eeva Aarrevaara Faculty of Technology, LAB University of Applied Sciences, Lahti, Finland

Christine Achberger COWI, Gothenburg, Sweden

Valentina Agresti RSE Spa, Milano, Italy

Ayodeji Akingunola Air Quality Research Division, Science and Technology Branch, Environment and Climate Change Canada, Toronto, ON, Canada

Sebnem Aksoyoglu Laboratory of Atmospheric Chemistry, Paul Scherrer Institute (PSI), Villigen, Switzerland

K. W. Appel Atmospheric and Environmental Systems Modeling Division, Center for Environmental Measurements and Modeling, US Environmental Protection Agency, Research Triangle Park, NC, USA

Patrick Armand CEA, DAM, DIF, Arpajon, France

Holger Baars Leibniz Institute for Tropospheric Research (TROPOS), Leipzig, Germany

Erik Bäck COWI, Gothenburg, Sweden

Alessandra Balzarini RSE Spa, Milano, Italy

Sabine Banzhaf Institute of Meteorology, Freie Universität Berlin, Berlin, Germany

F. Barmpas Laboratory of Heat Transfer and Environmental Engineering, Aristotle University, Thessaloniki, Greece

Jo Barnes University of the West of England, Bristol, UK

Rosa Maria Gonzalez Barras Department of Physics and Meteorology, Faculty of Physics, Complutense University of Madrid (UCM), Madrid, Spain

J. O. Bash Atmospheric and Environmental Systems Modeling Division, Center for Environmental Measurements and Modeling, US Environmental Protection Agency, Research Triangle Park, NC, USA

Ekaterina Batchvarova Climate, Atmosphere and Water Research Institute, Bulgarian Academy of Sciences (CAWRI-BAS), Sofia, Bulgaria

Stephen Beagley Air Quality Research Division, Science and Technology Branch, Environment and Climate Change Canada, Toronto, ON, Canada

Johannes Bieser Department of Chemical Transport Modeling, Institute of Coastal Research, Helmholtz-Zentrum Hereon, Geesthacht, Germany

Andrea Bisignano Department of Civil, Environmental and Mechanical Engineering, University of Trento, Trento, Italy

Anna Bjurbäck COWI, Gothenburg, Sweden

Hans Bolscher Trinomics Bv, Rotterdam, Netherlands

Carlos Borrego CESAM and Department of Environment and Planning, University of Aveiro, Aveiro, Portugal

Evert Bouman Norsk Institutt for Luftforskning, Kjeller, Norway

Yvonne Breitenbach IVU Umwelt GmbH, Freiburg, Germany

Nicolas Bruffaerts Belgian Scientific Institute of Public Health (SCIENSANO), Elsene, Belgium

Riccardo Buccolieri Dipartimento di Scienze e Tecnologie Biologiche ed Ambientali, University of Salento, Lecce, Italy

Peter Builtjes Free University Berlin, Berlin, Germany

Steven Caluwaerts Department of Physics and Astronomy, University of Ghent, Brussels, Belgium

Claudio Carnevale Department of Industrial and Mechanical Engineering, University of Brescia, Brescia, Italy

Silvia Trini Castelli Institute of Atmospheric Sciences and Climate, National Research Council, Torino, Italy

Rita Cesari National Research Council of Italy, Institute of Atmospheric Sciences and Climate (CNR-ISAC), Lecce, Italy

Hana Chaloupecká Institute of Thermomechanics, Academy of Sciences of the Czech Republic, Prague, Czechia

Edward C. Chan Institute of Meteorology, Freie Universität Berlin, Berlin, Germany

M. Chatziparaschos Environmental Chemical Processes Laboratory, Department of Chemistry, University of Crete, Heraklion, Greece

Eleftherios Chourdakis Laboratory of Heat Transfer and Environmental Engineering, Aristotle University, Thessaloniki, Greece

Giancarlo Ciarelli Department of Chemical Engineering, Carnegie Mellon University, Pittsburgh, PA, USA

Sílvia Coelho CESAM and Department of Environment and Planning, University of Aveiro, Aveiro, Portugal

N. Daskalakis Laboratory for Modeling and Observation of the Earth System (LAMOS), Institute of Environmental Physics (IUP), University of Bremen, Bremen, Germany

Elena De Angelis Department of Industrial and Mechanical Engineering, University of Brescia, Brescia, Italy

Veerle De Bock Royal Meteorological Institute of Belgium, Ukkel, Belgium

Andy Delcloo Royal Meteorological Institute of Belgium (RMI), Brussels, Belgium;
Department of Physics and Astronomy, University of Ghent, Brussels, Belgium;
Royal Meteorological Institute of Belgium (KMI), Ukkel, Belgium

Silvana Di Sabatino Department of Physics and Astronomy, ALMA MATER STUDIORUM - University of Bologna, Bologna, Italy

Iason Diafas Planbureau Voor de Leefomgeving, The Hague, Netherlands

Volker Diegmann IVU Umwelt GmbH, Freiburg, Germany

Reneta Dimitrova Sofia University "St. Kliment Ohridski", Sofia, Bulgaria;
NIGGG-BAS, Sofia, Bulgaria

François Duchêne Royal Meteorological Institute of Belgium (RMI), Brussels, Belgium

Christophe Duchenne CEA, DAM, DIF, Arpajon, France

Sébastien Dujardin Department of Geography, University of Namur, Namur, Belgium

Hendrik Elbern Institute for Energy and Climate Research - Troposphere (IEK-8), Forschungszentum Jülich, Jülich, Germany;
Rhenish Institute for Environmental Research (RIU) at the University of Cologne, Cologne, Germany

A. Eleftheriou Laboratory - Isle of Excellence of Environmental Fluid Mechanics, Department of Civil & Environmental Engineering, School of Engineering, University of Cyprus, Nicosia, Cyprus

Rohinton Emmanuel School of Computing, Engineering and Built Environment, Glasgow Caledonian University, Galsgow, UK

G. Fanourgakis Environmental Chemical Processes Laboratory, Department of Chemistry, University of Crete, Heraklion, Greece

Josefine Feldner Department of Chemical Transport Modeling, Institute of Coastal Research, Helmholtz-Zentrum Hereon, Geesthacht, Germany

Ana Patrícia Fernandes CESAM and Department of Environment and Planning, University of Aveiro, Aveiro, Portugal

Francisco Ferreira Center for Environmental and Sustainability Research, NOVA School of Science and Technology, NOVA University Lisbon, Lisbon, Portugal

Joana Ferreira CESAM and Department of Environment and Planning, University of Aveiro, Aveiro, Portugal

Giovanna Finzi Department of Industrial and Mechanical Engineering, University of Brescia, Brescia, Italy

K. M. Foley Atmospheric and Environmental Systems Modeling Division, Center for Environmental Measurements and Modeling, US Environmental Protection Agency, Research Triangle Park, NC, USA

Renate Forkel Institute for Meteorology and Climate Research (IMK-IFU), Karlsruhe Institute of Technology (KIT), Garmisch-Partenkirchen, Germany

Jens Forssén Chalmers University of Technology, Gothenburg, Sweden

E. Fragkou Laboratory of Heat Transfer and Environmental Engineering, Aristotle University, Thessaloniki, Greece

Martina Frid Department of Earth Science, University of Gothenburg, Gothenburg, Sweden;
Section of Environmental Modeling and Sustainability Analyses, COWI, Gothenburg, Sweden

Maria Gaeta RSE Spa, Milano, Italy

Gotzon Gangoiti Faculty of Engineering Bilbao, University of the Basque Country (UPV/EHU), Bilbao, Spain

Zhi Gao School of Architecture and Urban Planning, Nanjing University, Nanjing, China

Marian Ramos Garcia COWI, Gothenburg, Sweden

Juan Luis Garrido Atmospheric Pollution Unit, CIEMAT, Avda. Complutense, Madrid, Spain

Elisa Gatto Dipartimento di Scienze e Tecnologie Biologiche ed Ambientali, University of Salento, Lecce, Italy

Christa Genz Leibniz Institute for Tropospheric Research (TROPOS), Leipzig, Germany

George K. Georgiou Climate and Atmosphere Research Center, The Cyprus Institute, Nicosia, Cyprus

Roya Ghahreman Air Quality Research Division, Science and Technology Branch, Environment and Climate Change Canada, Toronto, ON, Canada

Paolo Giani RSE Spa, Milano, Italy;
Department of Civil and Environmental Engineering and Earth Science, University of Notre Dame, Notre Dame, IN, USA

Theodoros Giannaros National Observatory of Athens, Institute for Environmental Research and Sustainable Development, Athens, Greece

Victoria Gil Atmospheric Pollution Unit, CIEMAT, Avda. Complutense, Madrid, Spain

Samuel Gilbert Scientific Application Development Section, ECCC, Montreal, QC, Canada

David Gonçalves Institute of Science and Environment, University of Saint Joseph, Macau, China

Wanmin Gong Air Quality Research Division, Science and Technology Branch, Environment and Climate Change Canada, Toronto, ON, Canada

David Grawe Meteorological Institute, CEN, University of Hamburg, Hamburg, Germany

Marie Haeger-Eugensson Department of Earth Sciences, Gothenburg University, Gothenburg, Sweden;
Section of Environmental Modeling and Sustainability Analyses, COWI, Gothenburg, Sweden

Gayle Hagler National Exposure Research Laboratory, US Environmental Protection Agency, Research Triangle Park, NC, USA

Amir Hakami Carleton University, Ottawa, Canada

Rafiq Hamdi Royal Meteorological Institute of Belgium (RMI), Brussels, Belgium;
Department of Physics and Astronomy, University of Ghent, Brussels, Belgium

Enda Hayes University of the West of England, Bristol, UK

Bernd Heinold Leibniz Institute for Tropospheric Research, Department Modelling of Atmospheric Processes, Leipzig, Germany

Marijke Hendrickx Belgian Scientific Institute of Public Health (SCIENSANO), Elsene, Belgium

Hartmut Herrmann Leibniz Institute for Tropospheric Research, Atmospheric Chemistry Department (ACD), Leipzig, Germany

Christian Hogrefe Atmospheric and Environmental Systems Modeling Division, Center for Environmental Measurements and Modeling, US Environmental Protection Agency, Research Triangle Park, NC, USA;
National Exposure Research Laboratory, US Environmental Protection Agency, Research Triangle Park, NC, USA

Yongtao Hu School of Civil and Environmental Engineering, Georgia Institute of Technology, Atlanta, GA, USA

Trond Husby Planbureau Voor de Leefomgeving, The Hague, Netherlands

Ulas Im Department of Environmental Science, Aarhus University, Roskilde, Denmark

Michala Jakubcová Institute of Thermomechanics, Academy of Sciences of the Czech Republic, Prague, Czechia

Zbyněk Jaňour Institute of Thermomechanics, Academy of Sciences of the Czech Republic, Prague, Czechia

Jianhui Jiang Laboratory of Atmospheric Chemistry, Paul Scherrer Institute (PSI), Villigen, Switzerland

Pedro Jiménez-Guerrero Department of Physics, University of Murcia, Murcia, Spain;
Biomedical Research Institute of Murcia (IMIB-Arrixaca), Murcia, Spain

Roberto San José Environmental Software and Modeling Group, Computer Science School, Technical University of Madrid (UPM), Madrid, Spain

Klára Jurčáková Institute of Thermomechanics, Academy of Sciences of the Czech Republic, Prague, Czechia

M. Kanakidou Environmental Chemical Processes Laboratory, Department of Chemistry, University of Crete, Heraklion, Greece;
Laboratory for Modeling and Observation of the Earth System (LAMOS), Institute of Environmental Physics (IUP), University of Bremen, Bremen, Germany

Farah Kanani-Sühring Institute of Meteorology and Climatology, Leibniz Universität Hannover, Hannover, Germany

Daiwen Kang Center for Environmental Measurement & Modeling, U.S. Environmental Protection Agency, RTP, NC, USA

Matthias Karl Department of Chemical Transport Modeling, Institute of Coastal Research, Helmholtz-Zentrum Hereon, Geesthacht, Germany

Radka Kellnerová Institute of Thermomechanics, Academy of Sciences of the Czech Republic, Prague, Czechia

Klaus Ketelsen Independent Software Consultant, Hannover/Berlin, Germany

Angreine Kewo Danmarks Tekniske Universitet, Lyngby, Denmark

Basit Khan Institute for Meteorology and Climate Research (IMK-IFU), Karlsruhe Institute of Technology (KIT), Garmisch-Partenkirchen, Germany

Hristina Kirova National Institute of Meteorology and Hydrology, Sofia, Bulgaria

Oswald Knoth Leibniz Institute for Tropospheric Research (TROPOS), Leipzig, Germany

Svein Knudsen Norsk Institutt for Luftforskning, Kjeller, Norway

Rostislav Kouznetsov Finnish Meteorological Institute (FMI), Helsinki, Finland

Mona Kurppa Institute for Atmospheric and Earth System Research, University of Helsinki, Helsinki, Finland

Jonilda Kushta Climate and Atmosphere Research Center, The Cyprus Institute, Nicosia, Cyprus

Quentin Laffineur Royal Meteorological Institute of Belgium, Ukkel, Belgium

Fabio Lanati RSE Spa, Milano, Italy

Hugo Landry Scientific Application Development Section, ECCC, Montreal, QC, Canada

Man Tat Lei Department of Sciences and Environmental Engineering, NOVA School of Science and Technology, NOVA University Lisbon, Lisbon, Portugal; Institute of Science and Environment, University of Saint Joseph, Macau, China

Jos Lelieveld Climate and Atmosphere Research Center, The Cyprus Institute, Nicosia, Cyprus;
Max Planck Institute for Chemistry, Mainz, Germany

Diogo Lopes CESAM and Department of Environment and Planning, University of Aveiro, Aveiro, Portugal

Myriam Lopes CESAM and Department of Environment and Planning, University of Aveiro, Aveiro, Portugal

Alexandru Lupu Air Quality Research Division, Environment and Climate Change Canada (ECCC), Toronto, Canada

Marie Luise Luttkus Leibniz Institute for Tropospheric Research, Department Modelling of Atmospheric Processes, Leipzig, Germany

Paul A. Makar Air Quality Research Division, Science and Technology Branch, Environment and Climate Change Canada, Toronto, ON, Canada

Alexander Mangold Royal Meteorological Institute of Belgium, Ukkel, Belgium

Patrick M. Manseau Air Quality Policy-Issue Response Section, Canadian Meteorological Centre, ECCC, Montreal, Canada

Björn Maronga Institute of Meteorology and Climatology, Leibniz Universität Hannover, Hannover, Germany

Fernando Martín Atmospheric Pollution Unit, CIEMAT, Avda. Complutense, Madrid, Spain

Rohit Mathur Atmospheric and Environmental Systems Modeling Division, Center for Environmental Measurements and Modeling, U.S. Environmental Protection Agency, RTP, NC, USA;
National Exposure Research Laboratory, US Environmental Protection Agency, Research Triangle Park, NC, USA

Volker Matthias Helmholtz-Zentrum Hereon, Geesthacht, Germany

Matthias Mauder Institute for Meteorology and Climate Research (IMK-IFU), Karlsruhe Institute of Technology (KIT), Garmisch-Partenkirchen, Germany

Alberto Maurizi National Research Council of Italy, Institute for Microelectronics and Microsystems (CNR-IMM), Bologna, Italy

Benedetto Mele Industrial Engineering Department, University of Naples "Federico II", Naples, Italy

Sylvain Ménard Numerical Weather Prediction Section, ECCC, Montreal, QC, Canada

Luisa Mendes Department of Sciences and Environmental Engineering, NOVA School of Science and Technology, NOVA University Lisbon, Lisbon, Portugal

Joana Monjardino Center for Environmental and Sustainability Research, NOVA School of Science and Technology, NOVA University Lisbon, Lisbon, Portugal

Alexandra Monteiro CESAM and Department of Environment and Planning, University of Aveiro, Aveiro, Portugal

Michael Moran Air Quality Research Division, Environment and Climate Change Canada (ECCC), Toronto, Canada

Nicolas Moussiopoulos Laboratory of Heat Transfer and Environmental Engineering, Aristotle University, Thessaloniki, Greece

P. Mouzourides Laboratory - Isle of Excellence of Environmental Fluid Mechanics, Department of Civil & Environmental Engineering, School of Engineering, University of Cyprus, Nicosia, Cyprus

Thomas Müller Leibniz Institute for Tropospheric Research (TROPOS), Leipzig, Germany

Fabio Murena Chemical, Materials and Production Engineering Department, University of Naples "Federico II", Naples, Italy

S. Myriokefalitakis Institute for Environmental Research and Sustainable Development, National Observatory of Athens, Penteli, Athens, Greece

M. K. -A. Neophytou Laboratory - Isle of Excellence of Environmental Fluid Mechanics, Department of Civil & Environmental Engineering, School of Engineering, University of Cyprus, Nicosia, Cyprus

Theodoros Nitis Laboratory of Environmental Quality and Geospatial Applications, Department of Marine Sciences, University of the Aegean, Mytilene, Lesvos, Greece

Leonidas Ntziachristos Laboratory of Heat Transfer and Environmental Engineering, Aristotle University, Thessaloniki, Greece

Helen Nygren COWI, Gothenburg, Sweden

M. Talat Odman School of Civil and Environmental Engineering, Georgia Institute of Technology, Atlanta, GA, USA

Emmanouil Oikonomakis Laboratory of Atmospheric Chemistry, Paul Scherrer Institute (PSI), Villigen, Switzerland

Kevin Oliveira CESAM and Department of Environment and Planning, University of Aveiro, Aveiro, Portugal

Laura Palacios-Peña Department of Physics, University of Murcia, Murcia, Spain

Peter Papics Transport & Mobility Leuven, Leuven, Belgium

Radenko Pavlovic Air Quality Policy-Issue Response Section, Canadian Meteorological Centre, ECCC, Montreal, Canada

Si Jun Peng Air Quality Policy-Issue Response Section, Canadian Meteorological Centre, ECCC, Montreal, Canada

Juan L. Pérez Environmental Software and Modeling Group, Computer Science School, Technical University of Madrid (UPM), Madrid, Spain

Libia Pérez Environmental Software and Modeling Group, Computer Science School, Technical University of Madrid (UPM), Madrid, Spain

Leonardo Perronace Fagus Lab S.R.L, Roma, Italy

Guido Pirovano RSE Spa, Milano, Italy

Enzo Piscitello TECHNE Consulting, SRL, Milano, Italy

Laurent Poulain Leibniz Institute for Tropospheric Research, Atmospheric Chemistry Department (ACD), Leipzig, Germany

André S. H. Prévôt Laboratory of Atmospheric Chemistry, Paul Scherrer Institute (PSI), Villigen, Switzerland

Markus Quante Helmholtz-Zentrum Hereon, Geesthacht, Germany

Siegfried Raasch Institute of Meteorology and Climatology, Leibniz Universität Hannover, Hannover, Germany

Sandra Rafael CESAM and Department of Environment and Planning, University of Aveiro, Aveiro, Portugal

Martin Otto Paul Ramacher Department of Chemical Transport Modeling, Institute of Coastal Research, Helmholtz-Zentrum Hereon, Geesthacht, Germany

David Rayner Department of Earth Science, University of Gothenburg, Gothenburg, Sweden

Vera Rodrigues CESAM and Department of Environment and Planning, University of Aveiro, Aveiro, Portugal

S. Roselle Atmospheric and Environmental Systems Modeling Division, Center for Environmental Measurements and Modeling, US Environmental Protection Agency, Research Triangle Park, NC, USA

Armistead G. Russell School of Civil and Environmental Engineering, Georgia Institute of Technology, Atlanta, GA, USA

Estibaliz Sáez de Cámara Faculty of Engineering Bilbao, University of the Basque Country (UPV/EHU), Bilbao, Spain

Jose Luis Santiago Department of Environment, CIEMAT, Madrid, Spain

Golam Sarwar Center for Environmental Measurement & Modeling, U.S. Environmental Protection Agency, RTP, NC, USA

Verica Savic-Jovcic Air Quality Research Division, Environment and Climate Change Canada (ECCC), Toronto, Canada

Martijn Schaap Institute of Meteorology, Freie Universität Berlin, Berlin, Germany

Bert Van Schaeybroeck Royal Meteorological Institute of Belgium (RMI), Brussels, Belgium

K. Heinke Schlünzen Meteorological Institute, CEN, University of Hamburg, Hamburg, Germany

Roland Schrödner Leibniz Institute for Tropospheric Research (TROPOS), Leipzig, Germany

D. Schwede Atmospheric and Environmental Systems Modeling Division, Center for Environmental Measurements and Modeling, US Environmental Protection Agency, Research Triangle Park, NC, USA

Vânia Seixas CESAM and Department of Environment and Planning, University of Aveiro, Aveiro, Portugal

Stefan Seum Institute of Transport Research, German Aerospace Center (DLR), Berlin, Germany

T. Nash Skipper School of Civil and Environmental Engineering, Georgia Institute of Technology, Atlanta, GA, USA

Stephan Slingerland Trinomics Bv, Rotterdam, Netherlands

Mikhail Sofiev Finnish Meteorological Institute (FMI), Helsinki, Finland

Nathalie Steenhuyzen University of Antwerp, Antwerp, Belgium

Matthias Sühring Institute of Meteorology and Climatology, Leibniz Universität Hannover, Hannover, Germany

James Szykman National Exposure Research Laboratory, US Environmental Protection Agency, Research Triangle Park, NC, USA

Patricia Tarín-Carrasco Department of Physics, University of Murcia, Murcia, Spain

Florian Tautz IVU Umwelt GmbH, Freiburg, Germany

Piet Termonia Royal Meteorological Institute of Belgium (RMI), Brussels, Belgium;
Department of Physics and Astronomy, University of Ghent, Brussels, Belgium

Mark R. Theobald Atmospheric Pollution Unit, CIEMAT, Avda. Complutense, Madrid, Spain

Andreas Tilgner Leibniz Institute for Tropospheric Research, Atmospheric Chemistry Department (ACD), Leipzig, Germany

Gianni L. Tinarelli ARIANET Srl, Milano, Italy

Valeria Tolari Department of Industrial and Mechanical Engineering, University of Brescia, Brescia, Italy

Liina Tõnisson Leibniz Institute for Tropospheric Research (TROPOS), Leipzig, Germany

Eduardo Torre-Pascual Faculty of Engineering Bilbao, University of the Basque Country (UPV/EHU), Bilbao, Spain

Domenico Toscano Chemical, Materials and Production Engineering Department, University of Naples "Federico II", Naples, Italy

Silvia Trini Castelli Institute of Atmospheric Sciences and Climate (ISAC), National Research Council (CNR), Torino, Italy

Rozemien De Troch Royal Meteorological Institute of Belgium (RMI), Brussels, Belgium

Carlo Trozzi TECHNE Consulting, SRL, Milano, Italy

George Tsegas Laboratory of Environmental Quality and Geospatial Applications, Department of Marine Sciences, University of the Aegean, Mytilene, Lesvos, Greece; Laboratory of Heat Transfer and Environmental Engineering, Aristotle University, Thessaloniki, Greece

Enrico Turrini Department of Industrial and Mechanical Engineering, University of Brescia, Brescia, Italy

Rilka Valcheva Department of Meteorological Forecasts and Information Services, National Institute of Meteorology and Hydrology, Sofia, Bulgaria

Kris Vanherle Transport & Mobility Leuven, Leuven, Belgium

Petros Vasilakos School of Civil and Environmental Engineering, Georgia Institute of Technology, Atlanta, GA, USA

Willem W. Verstraeten Royal Meteorological Institute of Belgium (KMI), Ukkel, Belgium

Marta G. Vivanco Atmospheric Pollution Unit, CIEMAT, Avda. Complutense, Madrid, Spain

Evgeni Vladimirov Sofia University "St. Kliment Ohridski", Sofia, Bulgaria; BULATSA, Sofia, Bulgaria

Annika Vogel Institute for Energy and Climate Research - Troposphere (IEK-8), Forschungszentum Jülich, Jülich, Germany;
Rhenish Institute for Environmental Research (RIU) at the University of Cologne, Cologne, Germany

Marialuisa Volta Department of Industrial and Mechanical Engineering, University of Brescia, Brescia, Italy

Vivien Voss Meteorological Institute, CEN, University of Hamburg, Hamburg, Germany

Michael Weger Leibniz Institute for Tropospheric Research (TROPOS), Leipzig, Germany

Johannes Werhahn Institute for Meteorology and Climate Research (IMK-IFU), Karlsruhe Institute of Technology (KIT), Karlsruhe, Garmisch-Partenkirchen, Germany

Christian Winkler Institute of Transport Research, German Aerospace Center (DLR), Berlin, Germany

Ralf Wolke Leibniz Institute for Tropospheric Research (TROPOS), Department Modelling of Atmospheric Processes, Leipzig, Germany

Junhua Zhang Air Quality Research Division, Environment and Climate Change Canada (ECCC), Toronto, Canada

Shunliu Zhao Carleton University, Ottawa, Canada

Qiong Zheng Air Quality Research Division, Environment and Climate Change Canada (ECCC), Toronto, Canada

Iñaki Zuazo Faculty of Engineering Bilbao, University of the Basque Country (UPV/EHU), Bilbao, Spain

Aerosols in the Atmosphere

Role of Organic Aerosol Chemistry Schemes on Particulate Matter Modeling in Europe

Jianhui Jiang, Sebnem Aksoyoglu, Giancarlo Ciarelli, and André S. H. Prévôt

Abstract Organic aerosols (OA) contribute to 20–90% of the particulate matter (PM) concentration worldwide. To investigate the effects of OA schemes on PM modeling, we conducted whole-year (2010) simulations in Europe using the regional air quality model CAMx v6.50 with three different OA schemes: (1) an updated version of the traditional Odum 2-product model SOAP2.1, (2) the standard volatility basis set (VBS) algorithm, and (3) a modified VBS scheme which applies 3 times of POA emissions to offset the influence of missing semi-volatile organic compound (SVOC) emissions and enables aging of secondary condensable gases from biomass burning (referred as VBSNEW). The modeled OA concentration by SOAP was significantly higher than OA by VBS over land especially in the eastern Europe, while VBS led to higher OA only over the Mediterranean sea. The higher OA–SOAP mainly came from the primary organic aerosol (POA), which was 0.4 $\mu g\, m^{-3}$ higher than POA–VBS on average. However, the SOA–VBS was higher than SOA–SOAP in most of the areas except for the northeastern Europe, where the modeled OA concentration was strongly influenced by the boundary conditions. The VBSNEW increased the domain average OA by 26% and 63% compared to SOAP and VBS, respectively. Both POA and SOA were increased by VBSNEW, especially in winter when biomass burning is the dominant OA source. Comparison with observed $PM_{2.5}$ in 432 AIRBASE stations in Europe showed that VBSNEW led to lowest mean bias (MB) and root-mean-square error (RMSE), which reduced MB by 1.3 and 0.7 $\mu g\, m^{-3}$ compared to VBS and SOAP.

J. Jiang (✉) · S. Aksoyoglu · A. S. H. Prévôt
Laboratory of Atmospheric Chemistry, Paul Scherrer Institute, 5232 Villigen, Switzerland
e-mail: jianhui.jiang@psi.ch

S. Aksoyoglu
e-mail: sebnem.aksoyoglu@psi.ch

A. S. H. Prévôt
e-mail: andre.prevot@psi.ch

G. Ciarelli
Department of Chemical Engineering, Carnegie Mellon University, Pittsburgh, PA, USA
e-mail: ciarelli@andrew.cmu.edu

© The Author(s), under exclusive license to Springer-Verlag GmbH, DE, part of Springer Nature 2021

C. Mensink and V. Matthias (eds.), *Air Pollution Modeling and its Application XXVII*, Springer Proceedings in Complexity, https://doi.org/10.1007/978-3-662-63760-9_1

1 Introduction

Organic aerosols (OA) constitute 20–90% of particulate matter (PM) concentration worldwide (Jimenez et al., 2009). Traditional OA chemistry schemes in the chemical transport models (CTM) tend to underestimate secondary organic aerosols (SOA), which are generated from oxidation of a wide range of anthropogenic and biogenic precursors (Hallquist et al., 2009). With the evolution of understanding the SOA formation processes, the OA chemistry schemes are constantly being improved. The traditional OA schemes were mostly based on the "2-product model" (Odum et al., 1996) assuming that the primary organic aerosols (POA) are non-volatile and chemically inert, while the POA was found mostly semi-volatile and the vapor phase can undergo oxidation (Robinson et al., 2007). The volatility basis set (VBS) approach was then developed and implemented in CTMs to improve the situation (Donahue et al., 2006; Koo et al., 2014). It distributes OA species into volatility bins equally spaced in a logarithmic scale and allows further reaction and volatility changes of the OA species, which could better describe the atmospheric processes of OA. However, the performance of the CTMs with VBS largely depend on its parameterization. Some studies show that the default VBS parameterization does not really improve the model performance for OA compared to the traditional chemistry scheme (Ciarelli et al., 2016; Meroni et al., 2017). Meanwhile, the traditional OA schemes based on the Odum approach were also improved. For instance, the Secondary Organic Aerosol Partitioning (SOAP) scheme of CAMx (Comprehensive Air Quality Model with extensions) was updated with a new set of SOA parameters based on the wall-loss corrected aerosol yield data, addition of an anthropogenic intermediate volatility organic compound (IVOC) precursor, and inclusion of photolytic loss of SOA in the latest version, SOAP2.1 (Ramboll, 2018). In this study, we applied the regional model CAMx in Europe, and compared the performance of CAMx with three different OA schemes including the new SOAP2.1, default VBS and VBS with updated parameterization on OA and $PM_{2.5}$ simulation.

2 Method

We conducted whole-year (2010) simulations in Europe using the air quality model CAMx version 6.5. The model domain follows a regular latitude–longitude projection with increments of 0.25° and 0.4° in latitude and longitude, respectively. The total coverage extends from 17° W to 39.8° E and from 32° N to 70° N. There are 14 terrain-following vertical layers ranging from 50 to 8000 m asl. Three simulations with different OA chemistry schemes were performed and compared: (1) **SOAP**, the 2-product approach SOAP2.1 including updates on SOA simulation, (2) **VBS**, the standard VBS algorithm with default parameterization (Koo et al., 2014), and (3) **VBSNEW**, a modified VBS scheme which applies 3 times of POA emissions to offset the influence of missing semi-volatile organic compound (SVOC) emissions

and enables aging of secondary condensable gases from biomass burning (Jiang et al., 2019).

The inputs of meteorological parameters and anthropogenic emissions were obtained from the EURODELTA-Trends database (Colette et al., 2017). As important SOA precursors, the IVOC emissions were calculated as 4.5 times of POA for biomass burning (Ciarelli et al., 2017) and 1.5 times of POA for other anthropogenic sources (Robinson et al., 2007). The same IVOC emission inputs were adopted for all the three simulations. The biogenic emissions of isoprene, monoterpenes, sesquiterpenes and soil-NO were generated using the Model of Emissions of Gases and Aerosol from Nature (MEGAN) version 2.1 (Guenther et al., 2012). The initial and boundary conditions were obtained from the global model data MOZART-4/GEOS-5 (Horowitz et al., 2003), with a time resolution of 6 h. The modeled results were compared with hourly measurements extracted from the European Environment Agency database AirBase v7.

3 Results and Discussion

Different OA schemes lead to significant differences on modeled POA and SOA (Fig. 1). The modeled OA by SOAP was higher than the default VBS over land. The higher OA-SOAP mostly came from the POA, which is treated as inert in SOAP but volatile and undergoing aging processes in VBS. The domain average POA-SOAP was nearly 1.9 times (0.4 $\mu g\ m^{-3}$) higher than POA-VBS. However, the VBS produced higher SOA than SOAP in most of the domain especially in northern Italy and over the Mediterranean Sea, with the maximum difference up to 1.3 $\mu g\ m^{-3}$

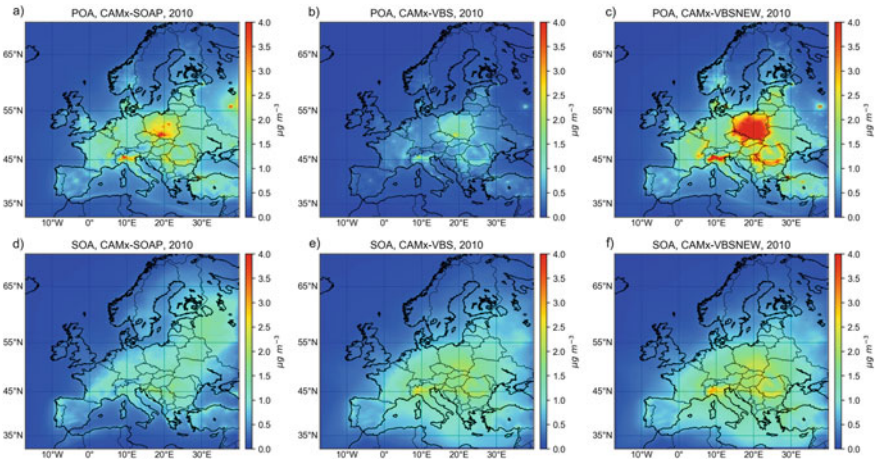

Fig. 1 Annual mean concentration of POA (**a**–**c**) and SOA (**d**–**f**) modeled by SOAP, VBS and VBSNEW

Table 1 Comparison between measured and modeled $PM_{2.5}$ by different OA schemes. MB: mean bias; ME: mean error; RMSE: root-mean-square error; MFB: mean fractional bias; MFE: mean fractional error; r: correlation coefficients

OA scheme	MB ($\mu g\ m^{-3}$)	ME ($\mu g\ m^{-3}$)	RMSE ($\mu g\ m^{-3}$)	MFB (%)	MFE (%)	r(−)
SOAP	−2.2	4.1	6.8	−13	27	0.59
VBS	−2.8	4.3	7.0	−17	29	0.58
VBSNEW	−1.5	3.8	6.3	−9	26	0.64

in Milan. The VBSNEW with updated VBS parameterizations led to the highest domain average OA among the three cases, which was 26% and 63% higher than SOAP and VBS respectively. The increase was even higher in winter when biomass burning is the dominant OA source, by 60% and 110% relative to SOAP and VBS, respectively. Both POA (12% higher than SOAP) and SOA (9% higher than VBS) concentrations were increased by using VBSNEW. Despite the missing OA observational data during the specific simulation period, comparison with the literature values of POA/SOA ratio in Europe indicates that the modeled composition of OA components by VBSNEW is closer to observations than the other two cases (Crippa et al., 2014).

To investigate the influence of OA on particulate matter simulations, we compared the modeled $PM_{2.5}$ concentrations by different OA schemes with observations of 432 AIRBASE stations (Table 1). VBSNEW shows the highest agreement between modeled and measured $PM_{2.5}$, which reduced the mean bias by 0.7 and 1.3 $\mu g\ m^{-3}$ compared to the SOAP and VBS cases. The largest improvement was predicted in Poland, where the mean fractional bias (MFB) using VBSNEW was 15 and 20% lower than that using SOAP and VBS.

4 Conclusion

We conducted whole-year (2010) simulations of air quality in Europe using three different OA chemistry schemes. The updated 2-product approach SOAP produces higher OA than the default VBS scheme due to higher POA, while the VBSNEW with updated VBS parameterization lead to highest OA (both POA and SOA). The increased OA by VBSNEW also leads to a better agreement between modeled and measured $PM_{2.5}$ in Europe. It reduces the mean bias between modeled $PM_{2.5}$ and observations at the 432 AIRBASE stations by 0.7 and 1.3 $\mu g\ m^{-3}$ compared to SOAP and VBS.

Acknowledgements We thank Ramboll for their continuous support in CAMx modeling, EURODELTA-Trends project for some of the model input data. We thank Swiss Federal Office of Environment (FOEN) for financial support.

References

Ciarelli, G., Aksoyoglu, S., Crippa, M., et al. (2016). Evaluation of European air quality modelled by CAMx including the volatility basis set scheme. *Atmospheric Chemistry and Physics, 2016*, 10313–10332.

Ciarelli, G., Aksoyoglu, S., El Haddad, I., et al. (2017). Modelling winter organic aerosol at the European scale with CAMx: Evaluation and source apportionment with a VBS parameterization based on novel wood burning smog chamber experiments. *Atmospheric Chemistry and Physics, 17*, 7653–7669.

Colette, A., Andersson, C., Manders, A., et al. (2017). EURODELTA-Trends, a multi-model experiment of air quality hindcast in Europe over 1990–2010. *Geoscientific Model Development, 10*, 3255–3276.

Crippa, M., Canonaco, F., Lanz, V. A., et al. (2014). Organic aerosol components derived from 25 AMS data sets across Europe using a consistent ME-2 based source apportionment approach. *Atmospheric Chemistry and Physics, 14*, 6159–6176.

Donahue, N. M., Robinson, A. L., Stanier, C. O., et al. (2006). Coupled partitioning, dilution, and chemical aging of semivolatile organics. *Environmental Science & Technology, 40*, 2635–2643.

Guenther, A. B., Jiang, X., Heald, C. L., et al. (2012). The model of emissions of gases and aerosols from nature version 2.1 (MEGAN2.1): An extended and updated framework for modeling biogenic emissions. *Geoscientific Model Development, 5*, 1471–1492.

Hallquist, M., Wenger, J. C., Baltensperger, U., et al. (2009). The formation, properties and impact of secondary organic aerosol: Current and emerging issues. *Atmospheric Chemistry and Physics, 9*, 5155–5236.

Hildebrandt, L., Engelhart, G. J., & Mohr, C., et al. (2010). Aged organic aerosol in the Eastern Mediterranean: The Finokalia aerosol measurement experiment-2008. *Atmospheric Chemistry and Physics, 10*, 4167–4186.

Horowitz, L. W., Walters, S., & Mauzerall, D. L., et al. (2003). A global simulation of tropospheric ozone and related tracers: Description and evaluation of MOZART, version 2. *Journal of Geophysical Research-Atmospheres, 108*, D24, 4784.

Jiang, J., Aksoyoglu, S., El-Haddad, I., et al. (2019). Sources of organic aerosols in Europe: A modelling study using CAMx with modified volatility basis set scheme. *Atmospheric Chemistry and Physics, 2019*(19), 15247–15270.

Jimenez, J. L., Canagaratna, M. R., Donahue, N. M., et al. (2009). Evolution of organic aerosols in the atmosphere. *Science, 326*, 1525–1529.

Koo, B., Knipping, E., & Yarwood, G. (2014). 1.5-Dimensional volatility basis set approach for modeling organic aerosol in CAMx and CMAQ. *Atmospheric Environment, 95*, 158–164.

Meroni, A., Pirovano, G., Gilardoni, S., et al. (2017). Investigating the role of chemical and physical processes on organic aerosol modelling with CAMx in the Po Valley during a winter episode. *Atmospheric Environment, 171*, 126–142.

Odum, J. R., Hoffmann, T., Bowman, F., et al. (1996). Gas/particle partitioning and secondary organic aerosol yields. *Environmental Science & Technology, 30*, 2580–2585.

Ramboll. (2018). *User's guide: The comprehensive air quality model with extensions (CAMx) version 6.5.*

Robinson, A. L., Donahue, N. M., Shrivastava, M. K., et al. (2007). Rethinking organic aerosols: Semivolatile emissions and photochemical aging. *Science, 315*, 1259–1262.

Questions and Answers

Questioner: Volker Matthias

Question: Did you also evaluate the correlation coefficient and what are the results for those?

Answer: Yes, we did. The correlation coefficients between measured and modeled $PM_{2.5}$ by SOAP, VBS and VBSNEW are 0.59, 0.58, and 0.64 respectively (Table). The VBSNEW slightly improves the correlation between measured and modeled $PM_{2.5}$.

Questioner: Annica Ekman

Question: How you looked at the impact on aerosol size distribution?

Answer: We selected the static two-mode coarse/fine (CF) scheme in the CAMx model, which has two size modes for particles, i.e. fine ($\leq$2.5 μm) and coarse (>2.5 μm). All the organic and inorganic aerosols are considered as "fine" in this study.

Questioner: George Tsegas

Question: Observed SOA/OA in the Finokalia station may have been influenced by a sharp increase in biomass burning in SE Europe after 2010. Maybe an update emission inventory would improve bias in this area.

Answer: The measurements indicated that OA in Finokalia is dominated by the highly aged SOA (Hildebrandt et al., 2010). We agree that the underestimated SOA/OA in Finokalia could partially come from high uncertainties of biomass burning emissions, especially since the wildfire emissions were not included in this study. Meanwhile, we think the underestimated monoterpene emissions (main precursors of biogenic SOA) by MEGAN could be the main reason for the underestimated SOA/OA ratio in Finokalia.

Questioner: Matthias Karl

Question: (1) How does the VBS of the biomass burning compounds compare to the VBS of the biogenic SOA? Is it more or less volatile (in the VBS-NEW)? (2) Is the parameterization of the VBS for biomass burning compounds derived from laboratory experiments?

Answer: (1) The VBS schemes of biomass burning and biogenic sources are with completely different precursors. For biomass burning, we considered SOA generated from POA, IVOC/SVOC, toluene, xylene and benzene, while biogenic SOA is formed from oxidation of isoprene, monoterpenes, and sesquiterpenes. The biogenic SOA species are more volatile than the biomass burning SOA. (2) Yes, the parameterization of the VBS for biomass burning was modified based on recent chamber experimental data. More detailed can be found in Ciarelli et al. (2017).

Questioner: Bok H. Baek

Question: Have considered to apply VBS to on-road mobile emission sectors?

Answer: The VBS scheme contains already the on-road mobile emission sectors (i.e. gasoline and diesel vehicles) in the current version of CAMx.

Biogenic Emissions and Urban Air Quality

Marie Luise Luttkus, Ralf Wolke, Bernd Heinold, Andreas Tilgner, Laurent Poulain, and Hartmut Herrmann

Abstract Trees emit a species-specific mixture of biogenic volatile organic compounds (BVOCs) like isoprene, monoterpenes and sesquiterpenes. These highly reactive BVOCs are quickly degraded by OH- NO_3- and O_3 radicals and hence, alter the atmospheric composition. Under high NO_x conditions their chemical degradation causes the formation of ground-level ozone. Furthermore, due to progressing chemical reactions BVOCs become less volatile and form secondary organic aerosol (SOA), which is one of the main components of $PM_{2.5}$. In this way, BVOCs can have negative effects on air quality and thus on human health and the ecosystem through their influence on NO_x, O_3 and $PM_{2.5}$ concentrations. However, since BVOC emission is trees species-specific, this influence depends on the composition of the tree population. Air quality may even improve due to a selection of specific tree species. Studies with different land use datasets are performed with the model system COSMO-MUSCAT for Germany and May 2014. The consideration of isoprene, sesquiterpene, HOMs and the reaction of monoterpene with NO_3 results in a doubling of organic matter (OM) concentration compared to the original SORGAM mechanism at higher temperatures.

Keywords BVOCs · SOA · Air quality · Land use

1 Introduction

Trees have a great CO_2 uptake and storage potential. Planting trees could play a key role in climate mitigation options (Bastin et al., 2019). For urban areas trees are also used for climate adaption strategies as they lower the ambient air temperature

M. L. Luttkus (✉) · R. Wolke · B. Heinold
Leibniz Institute for Tropospheric Research, Department Modelling of Atmospheric Processes, Permoserstraße 15, 04318 Leipzig, Germany
e-mail: luttkus@tropos.de

A. Tilgner · L. Poulain · H. Herrmann
Leibniz Institute for Tropospheric Research, Atmospheric Chemistry Department (ACD), Permoserstraße 15, 04318 Leipzig, Germany

© The Author(s), under exclusive license to Springer-Verlag GmbH, DE, part of Springer Nature 2021

C. Mensink and V. Matthias (eds.), *Air Pollution Modeling and its Application XXVII*, Springer Proceedings in Complexity, https://doi.org/10.1007/978-3-662-63760-9_2

and thereby reduce the urban head island effect (Schubert & Grossmann-Clarke, 2013). The emission of trees (BVOCs) and their influence on air quality are much more complex and could be both positive or negative (Popkin, 2019). The chemical degradation of isoprene by OH radicals under high NO_x conditions will lead to the formation of ground level ozone. In general, the oxidation of BVOCs will reduce their volatility and they start to condense onto existing particles or even create new particles which leads to the formation of SOA, a major constituent of $PM_{2.5}$ (Schneidemesser et al., 2015). Due to tree species-specific emission profiles different tree species are likely to have modified impacts on air quality. Therefore, more tree species-specific information is needed for climate mitigation and adaption strategies.

2 Model Setup

The influence of two different land use (LU) datasets is studied with the model system COSMO-MUSCAT (Wolke et al., 2012). The MUltiScale Chemistry Aerosol Transport model MUSCAT has been developed at the Leibniz Institute for Tropospheric Research (TROPOS). It is coupled to COSMO, which is the numerical weather prediction model of the German weather service DWD and works as the meteorological driver for MUSCAT. The first LU dataset used is the novel maps for tree species in Europe (Köble & Seufert, 2001) with 138 LU classes including 116 tree species. The second one is generated out of the first one. Here the 138 LU classes are transformed into 10 LU classes: water, mudflats, sand, mixed land use (agriculture), meadows, heath, bushes, mixed forest (broadleaved trees), conifer forest (coniferous trees) and urban area. The resolution for the modeled domain Germany (N2) is 7 × 7 km. The initial boundary values are generated from the European model run (N1), which has a resolution of 28 × 28 km. For the initialization of the N1 boundary values ECMWF-IFS CAMS data are used. In MUSCAT several modules can be chosen for emissions, chemistry, aerosol formation and dynamics. The treatment of biogenic emissions is realized by the parametrization from Steinbrecher et al. (2009). Anthropogenic emission inventories are taken from MACC 2010 for Europe and from UBA (federal environmental agency) for Germany. For the chemistry treatment RACM-MIM2-ext. is used (Karl et al, 2006; Stockwell et al., 1997). The SOA module is based on SOARGAM (Schell et al., 2001) and was updated by reactions for monoterpenes with NO_3 (Griffin et al., 1999), isoprene (Ng et al., 2008; Kroll & Seinfeld, 2008), sesquiterpenes (Hoffmann et al., 1997; Karl et al., 2009) and highly oxidized multifunctional organic molecules HOMs (Jokinen et al., 2015; Richters et al., 2016; Berndt et al., 2016a, 2016b). The modeling period is May 2014 and the simulations are compared with measurements from Melpitz.

3 Model Results

The BVOC emissions are higher and spread throughout the whole forest area for the 10 LU classes. Monoterpene (α-pinine and limonene together) and sesquiterpene show similar distributions but differ in the emission strength, depending on the linked tree species. Isoprene on the contrary shows a much more distinct emission pattern. For the model domain N2 the dominant isoprene emitting trees are oaks (Quercus rubra, Quercus robur) which are more prominent in the western part of the domain and only a view spots in the eastern part (north of Berlin, 4 areas in Poland and 4 smaller regions in the Czech Republic). That is where the difference between the two LU datasets (10_LU–138_LU) shows the greatest negative values while all the rest is positive (Fig. 1a). This demonstrates a wide spatial redistributed isoprene concentration between the two LU datasets. The main isoprene degradation agents are OH radicals. Their concentration correlates directly with the isoprene emission, showing the exact opposite picture than the isoprene emission plot, but with a minor intensity (Fig. 1b). Another effect is the increased ozone concentration in the west of the 138_LU model run (negative difference values), where the isoprene emission is higher than for the 10_LU classes and lower in the east (positive difference values), where the emission is observed only in a view regions (Fig. 1c).

The highest monoterpene emissions are reached for coniferous forests in Brandenburg for the 10_LU. For the 138_LU the dominant tree species in this region is Pinus Sylvestris which has a lower biomass density (BMD 700 g m^{-3}) than the generalized LU class conifer forest (1000 g m^{-3}) resulting in lower emissions. The only tree species with a higher sesquiterpene emission potential than 0.1 are birches (a view spots in Poland). An increase or decrease in sesquiterpene emissions can otherwise only be realised by a change in BMD. For Brandenburg, there is a decrease in BMD and in the low mountain range there is an increase in BMD due to the main tree species spruce (1400 g m^{-3}). A higher monoterpene emission is not accomplished here due to the fact that spruce trees have a lower monoterpene emission potential. For nearly the whole model domain monoterpene emissions are stronger for the 10_LU. Monoterpenes are mainly oxidized by NO_3 radicals which results in a reduction of NO_3 radicals for the 10_LU. The reaction of monoterpenes with NO_3 radicals has one

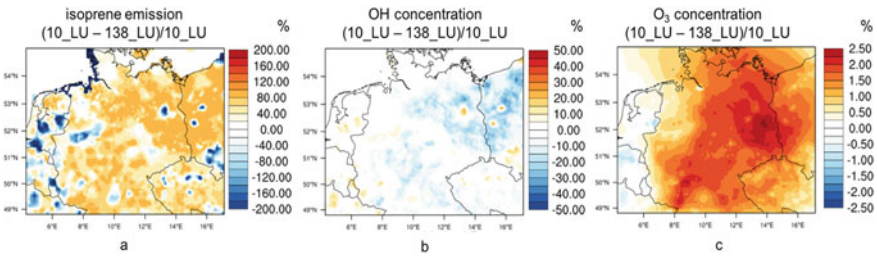

Fig. 1 Mean relative difference between the 10 and 138 LU classes model runs for isoprene emission (**a**), OH concentration (**b**) and O_3 concentration (**c**) for May 2014

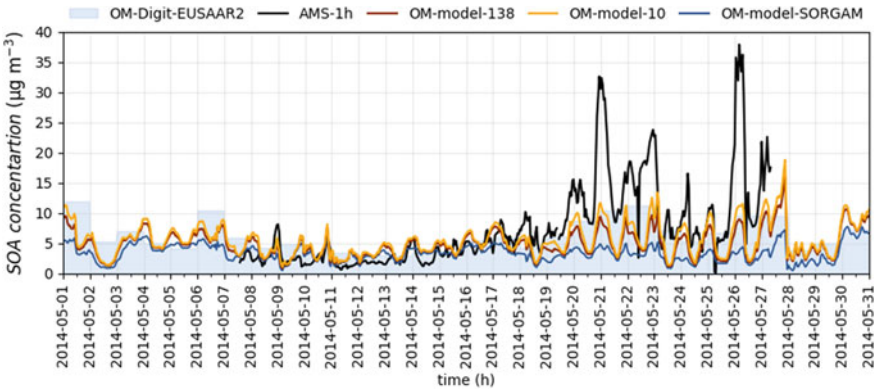

Fig. 2 Organic matter (OM) measured and modeled for Melpitz May 2014

of the greatest SOA forming potential. Consequently, the maximum SOA concentration for both LU datasets are reached in Brandenburg, where the monoterpene emissions are the utmost. Anthropogenic SOA products play a minor role (10–20%) compared to biogenic sources (80–90%). Roughly 30–40% of the monthly average for May consists of monoterpene NO_3 reaction SOA products which is the dominating product throughout the whole model domain.

Melpitz is situated in northern Saxony close to the border to Brandenburg. Brandenburg's vegetation is characterized by pine trees. That is also true for the surroundings of Melpitz but the main LU is agriculture. For temperatures lower than 20 °C all model runs predict similar organic matter (OM) for Melpitz (Fig. 2). But for higher temperatures the updated SORGAM mechanism produces approximately twice as much OM as the original one. However, the measurements show still two or even three times higher OM peaks. Low wind velocities, warm temperatures and enhanced solar radiation favour high ozone, NO_x and SOA concentrations. In that case, up to 90% of SOA is of biogenic origin with a total of 65% being from the reaction of α-pinine with NO_3. At temperatures below 20° and higher wind velocities the overall SOA concentration is reduced but the anthropogenic SOA part is increased and reaches up to 40%. The comparison between measurements and the model run with the 10 LU classes gives the best results for Melpitz.

4 Conclusion

BVOC emissions are greatly influenced by land use which effects the atmospheric composition. Isoprene emitting trees (oaks: Quercus robur, Quercus rubra) increase the ground level ozone concentration, reduce the OH radical concentration and produce only little SOA. Monoterpenes (conifers) are linked to NO_3 radicals and have the greatest SOA formation potential which results in the major SOA constituent.

Associated with specific meteorological conditions (low wind velocities, warm temperatures, high solar radiation) these effects can result in impaired air quality.

Acknowledgements M.L.L. wants to thank the Ph.D. scholarship program of the German Federal Environment Foundation (Deutsche Bundesstiftung Umwelt, DBU) for its funding (AZ 20016/452).

References

Banzhaf, E., & Kollai, H. (2018). Land use/Land cover for Leipzig, Germany, for 2012 by an object-based image analysis (OBIA). *PANGAEA*.

Bastin, J. F., et al. (2019). The global tree restoration potential. *Science, 365*(6448), 76–79.

Berndt, T., et al. (2016a). Highly Oxidized Second-Generation Products from the Gas-Phase Reaction of OH Radicals with Isoprene. *The Journal of Physical Chemistry A, 120*(51), 10150–10159.

Berndt, T., et al. (2016b). Hydroxyl radical-induced formation of highly oxidized organic compounds. *Nature Communications, 7*, 13677.

Griffin, R. J., et al. (1999). Organic aerosol formation from the oxidation of biogenic hydrocarbons. *Journal of Geophysical Research: Atmospheres, 104*(3), 3555–3567.

Hoffmann, T., et al. (1997). Formation of Organic Aerosols from the Oxidation of Biogenic Hydrocarbons. *Journal of Atmospheric Chemistry, 26*(2), 189–222.

Jokinen, T., et al. (2015). Production of extremely low volatile organic compounds from biogenic emissions: Measured yields and atmospheric implications. *Proceedings of the National Academy of Sciences of the United States of America, 112*(23), 7123–7128.

Karl, M., et al. (2006). Product study of the reaction of OH radicals with isoprene in the atmosphere simulation chamber SAPHIR. *Journal of Atmospheric Chemistry, 55*(2), 167–187.

Karl, M., et al. (2009). Formation of secondary organic aerosol from isoprene oxidation over Europe. *Atmospheric Chemistry and Physics, 9*(18), 7003–7030.

Köble, R., & Seufert, G. (2001). Novel maps for forest tree species in Europe. *Proceedings of the 8th European Symposium on the Physico-Chemical Behaviour of Air Pollutants: "A Changing Atmosphere!"*, Torino, Italy, 17–20 September 2001.

Kroll, J. H., & Seinfeld, J. H. (2008). Formation and evolution of low-volatility organics in the atmosphere. *Atmospheric Environment, 42*(16), 3593–3624.

Ng, N. L., et al. (2008). Secondary organic aerosol (SOA) formation from reaction of isoprene with nitrate radicals (NO_3). *Atmospheric Chemistry and Physics, 8*(14), 4117–4140.

Popkin, G. (2019). The forest question. *Nature, 565*, 280–282.

Richters, S., et al. (2016). Highly Oxidized RO_2 Radicals and Consecutive Products from the Ozonolysis of Three Sesquiterpenes. *Environmental Science and Technology, 50*(5), 2354–2362.

Schell, B., et al. (2001). Modeling the formation of secondary organic aerosol within a comprehensive air quality model system. *Journal of Geophysical Research: Atmospheres, 106*(22), 28275–28293.

Schubert, S., & Grossmann-Clarke, S. (2013). The influence of green urban areas and roof albedos on air temperatures during Extreme Heat Events in Berlin, Germany. *Meteorologische Zeitschrift, 22*(2), 131–143.

Steinbrecher, R., et al. (2009). Intra- and inter-annual variability of VOC emissions from natural and semi-natural vegetation in Europe and neighboring countries. *Atmospheric Environment, 43*(7), 1380–1391.

Stockwell, W. R., et al. (1997). A new mechanism for regional atmospheric chemistry modeling. *Journal of Geophysical Research: Atmospheres, 102*(22), 25847–25879.

Von Schneidemesser, E., et al. (2015). Chemistry and the Linkages between Air Quality and Climate Change. *Chemical Reviews, 115*(10), 3856–3897.

Wolke, R., et al. (2012). Influence of grid resolution and meteorological forcing on simulated European air quality: A sensitivity study with the model system COSMO-MUSCAT. *Atmospheric Environment, 53*, 110–130.

Questions and Answers

Questioner: Pius Lee

Question: Your study was focused on scenarios in May 2014 when the trees are in blooming stages. Your conclusions on SOA production and ozone concentrations were interesting but not quite the peak production for summers (July/August) where air quality is often worse than May. Do you have summer scenarios and/or campaigns?

Answer: The periode May 2014 was chosen for evaluation purposes as for this time periode there are AMS, ACSM and filter measurements available for the Melpitz field site. The results already show a great improvement with the extended SORGAM module especially for warmer temperatures. It is planned to further extend the simulations for the entire summer 2014 and to compare the simulations with another campaigne, the F-BEACH campaign at Waldstein in July 2014. However, this will require further changes in the chemistry and SOA mechanisms, which are currently under development. The new mechanisms will than be used for the urban setup of Leipzig and the rather hot and dry summer of 2018 and 2019 will be modeled and analyzed.

Questioner: Joachim Fallmann

Question: What efforts are planned to answer the question of what would be the best/right tree in terms of urban air quality (Resolution, urban scheme, model configuration …)?

Answer: As first step a new chemistry mechanism is beeing developed for better treatment of anthropogenic and biogenic VOCs, and associated therewith the SOA module. Therin the tree species specific monoterpene split will be addressed more detailed in terms of reaction constants. Simulations of test sceniarios are planed with diffent tree species under diverse environmental conditions (NO_x emissions, temperature, radiation, wind, …). For the urban setup of Leipzig a resolution of up to 200 m and a double-canyon effect parametrization has already been realized. For more details see “High-resolution air-quality modeling in urban areas—A case study for the City of Leipzig” from Bernd Heinold. The city of Leipzig provided data for forests (in percent of area), street and park trees (exact location but no area information) on tree species basis. In 2018, a Land use/Land cover dataset was published for Leipzig by object-based image analysis for 2012 which contains area information for artificial surfaces, agriculture, grass, trees (>5 m diameter) and young

trees/shrubs (Banzhaf & Kollai, 2018). With these information a tree species based map for Leipzig will be generated and urban simulations will be performed. For air quality mitigation potential of the different tree species the findings of the test scenarios will be used for future air quality assessment, where the actual existing tree species distribution is used and additional trees will be added. The influence of the additional trees will then be further analyzed for different future scenarios (NO_x emissions, meteorological parameters).

Global Simulations of Ice Nuclei Particles Derived from Organics and Inorganics Particles

M. Chatziparaschos, N. Daskalakis, S. Myriokefalitakis, G. Fanourgakis, and M. Kanakidou

Abstract Aerosol-cloud interactions are one of the major sources of uncertainty in climate projections. Ice Nuclei Particles (INP) significantly affect the radiative properties, cloud lifetime and precipitation rates due to their ability to form ice at temperatures higher than those of homogeneous ice nucleation. The majority of related studies investigate INP that originates from K-feldspar mineral desert dust particles and marine organic particles. In the present study we further investigate the contribution of terrestrial bio-aerosols to INP concentration via immersion freezing using the global 3-D chemistry transport model TM4-ECPL. The available and potential INP concentrations in the atmosphere at ambient and given temperature, respectively, are derived from model simulated dust, marine organics, and terrestrial bacteria, fungi and pollen using experimentally-deduced parameterizations of ice-active surface site density for each type of aerosol acting as INP. It is found that INP from desert dust dominates the concentration of INP over the entire Northern Hemisphere, terrestrial bio-aerosols contribute to INP concentration mainly close to the emission sources, while marine organics are important contributors to INP over remote oceans depending on marine biota, which varies seasonally.

M. Chatziparaschos · G. Fanourgakis · M. Kanakidou (✉)
Environmental Chemical Processes Laboratory, Department of Chemistry, University of Crete, 70013 Heraklion, Greece
e-mail: mariak@uoc.gr

N. Daskalakis · M. Kanakidou
Laboratory for Modeling and Observation of the Earth System (LAMOS), Institute of Environmental Physics (IUP), University of Bremen, Bremen, Germany

S. Myriokefalitakis
Institute for Environmental Research and Sustainable Development, National Observatory of Athens, Lofos Koufou, Penteli, Athens, Greece

© The Author(s), under exclusive license to Springer-Verlag GmbH, DE, part of Springer Nature 2021

C. Mensink and V. Matthias (eds.), *Air Pollution Modeling and its Application XXVII*, Springer Proceedings in Complexity, https://doi.org/10.1007/978-3-662-63760-9_3

1 Introduction

The radiative properties and microphysics of clouds are particularly sensitive to aerosol concentration, composition and size. Aerosol particles serve either as Cloud Condensation Nuclei (CCN) to form liquid cloud droplets via activation processes (Fanourgakis et al. 2019), or as INP to form ice (DeMott et al. 2010). Inside clouds, heterogeneous ice nucleation triggered by INP occurs at much higher temperatures than homogeneous freezing (DeMott et al. 2010). Aerosols may thus affect cloud properties and precipitation rates and the radiative balance of the atmosphere. Mineral dust globally dominates the aerosol mass concentration in the atmosphere, while measurements of hygroscopic growth indicate very low solubility of dust particles. In the present study, we use the well documented global 3-dimensional chemistry—transport model (CTM) TM4-ECPL to derive dust and bioaerosols distributions for the year 2010. We then apply experimentally derived parameterizations of INP from various sources to estimate the resulting INP concentrations at different locations.

2 Methods

2.1 The Global Model

The TM4-ECPL model is driven by the ERA interim meteorological fields assimilated by the European Centre for Medium-Range Weather Forecasts (ECMWF) meteorological model. It has a horizontal resolution of 3° x 2° (longitude x latitude) with 34 vertical levels from surface up to 0.1 hPa (about 65 km). The model considers lognormal aerosol distributions in the fine and coarse modes and allows the hygroscopic growth of particles as well as their wet removal and gravitational settling. Dust emissions are calculated online accounting for both fine and coarse modes with mass median radii (lognormal standard deviation) of 0.34 μm (1.59) and 1.75 μm (2.00), respectively, and K-feldspar emissions are derived from dust emissions and soil mineralogy. Bioaerosol emissions of bacteria, fungal spores and pollen are also calculated on line in the model based on land cover/vegetation type and meteorology and considering monodisperse particles of 1 μm, 3 μm and 30 μm diameter, respectively. Further details and references are provided in Myriokefalitakis et al. (2017). INP concentrations are calculated from experimentally derived parameterization combined with singular approximation (Vali et al. 2015).

2.2 Calculation of Potential INP Concentrations

Assuming that particles are externally mixed, parameterizations derived from laboratory studies are used to calculate the INP concentrations relevant to each aerosol species. The K-feldspar in the insoluble part of dust is considered as a potential contributor to INP. The probability of a particle to act as INP follows the Poisson distribution. INP concentration from dust is then calculated as suggested by Vergara-Temprado et al. (2017) and adapted for TM4-ECPL by Chatziparaschos et al. (2018):

$$INP_{dust_i} = N_{dust_i} * \left(1 - e^{-n_s(T)*S_i}\right) * F_i \tag{1}$$

where N_{dust_i} is the number of total insoluble dust particles, S_i is the surface of the particles in mode i (accumulation or coarse mode), F_i is the fraction of Feldspar in each model grid and $n_s(T)$ the active sites density. It is here assumed that all Feldspars have the same ice nuclei efficiency.

Wilson et al. (2015) express the spectrum of active sites density per unit mass of total organic carbon contained in insoluble marine organics as a function of temperature. A factor of 1.8 is used for the conversion of marine organic aerosols to organic carbon. The number of marine INP is calculated by using Eq. 2, where $n_m(T)$ is the active sites density per unit mass of total organic carbon and S_i is the spherical surface of marine particles in mode i.

$$INPs_{marine} = n_m(T) * S_i * TOC_{marine} \tag{2}$$

The parameterization of INP concentrations derived from terrestrial bioaerosols in this study uses the ice active density $n_s(T)$ as suggested by McCluskey et al. (2018). We implement the same probability as shown in Eq. 1 excluding the factor F_i.

3 Results

Annual mean potential INP concentrations are depicted in Fig. 1 for particles that can activate at −15 °C, temperature that is representative for mixed phase clouds glaciation (Vergara-Temprado et al. 2017). Those derived from mineral dust (Fig. 1a) maximize close to the major dust sources in North Africa (Sahara) and Asia (Gobi), with secondary regional maxima in South America (Patagonia) and Australia. Additionally, the comparison of potential INP concentrations from particles of various origins as shown in Fig. 1a–d, reveals that INP from dust are significantly more abundant (over two orders of magnitude) than INP from other bioaerosols at low and mid latitudes (Fig. 1). In the South Hemisphere potential INP from marine organics dominate (Fig. 1b), with the largest concentrations calculated to occur over the Southern

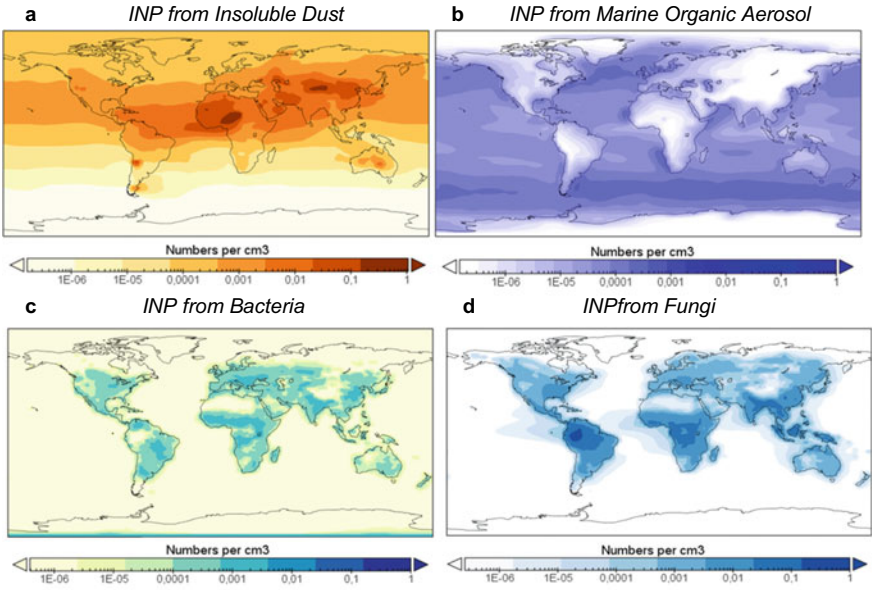

Fig. 1 Annual mean distributions of ice-nucleating particles number concentrations at 825 hPa, that can activate at –15 °C (reference temperature used for INP measurements) based on feldspar (**a**), marine organics (**b**), fungi (**c**) and bacteria (**d**)

Ocean, the North Atlantic and the North Pacific Oceans. Marine INP are also potentially important in coastal regions where biological activity in ocean waters and wind speeds are high. INP from terrestrial bioaerosols (insoluble fractions of fungi and bacteria; Fig. 1c, d) dominate close to the emission sources. The distribution of their concentrations is strongly affected by the leaf area index and the ecosystem distribution. Thus, over several land areas, INP from bio-aerosols are comparable in number with those from dust. This reveals the potentially important contribution of terrestrial bio aerosols to the total INP concentration.

Acknowledgements This work has been supported by the project "Panhellenic infrastructure for Atmospheric Composition and climate change" (MIS 5021516) which is implemented under the Action "Reinforcement of the Research and Innovation Infrastructure", funded by the Operational Programme "Competitiveness, Entrepreneurship and Innovation" (NSRF 2014–2020) and co-financed by Greece and the European Union (European Regional Development Fund).

References

Boose, Y., et al. (2016). Heterogeneous ice nucleation on dust particles sourced from nine deserts worldwide – Part 1: Immersion freezing. *Atmospheric Chemistry and Physics, 16*, 15075–15095. https://doi.org/10.5194/acp-16-15075-2016

Chatziparaschos, M., et al. (2018). Global atmospheric simulations of ice nuclei particles from marine organic aerosols and dust. *In Proceedings of the 14th International Conference on Meteorology, Climatology and Atmospheric Physics (COMECAP2018),* Alexandroupolis, Greece, 15–17 October 2018, https://www.researchgate.net/publication/330320408

DeMott, P. J., et al. (2010). Predicting global atmospheric ice nuclei distributions and their impacts on climate. *PNAS, 107*(25), 11217–11222. https://doi.org/10.1073/pnas.0910818107

Fanourgakis, G. S., et al. (2019). Evaluation of global simulations of aerosol particle number and cloud condensation nuclei, and implications for cloud droplet formation. *Atmospheric chemistry and physics, 19*(13), 8591–8617 https://doi.org/10.5194/acp-19-8591-2019

McCluskey, C. S., et al. (2018). Marine and terrestrial organic ice-nucleating particles in pristine marine to continentally influenced Northeast Atlantic air masses. *Journal of Geophysical Research: Atmospheres, 123*(11), 6196–6212. https://doi.org/10.1029/2017JD028033

Myriokefalitakis, S., et al. (2017). The contribution of bioaerosols to the organic carbon budget of the atmosphere. *Biogeosciences, 373.* https://doi.org/10.1007/978-3-319-35095-0

Murray, B.J., et al. (2012). Ice nucleation by particles immersed in supercooled cloud droplets. *Chemical Society Reviews, 41*, 6519–6554. https://doi.org/10.1039/C2CS35200A

Vali, G., et al. (2015). "Technical note: a proposal for ice nucleation terminology." *Atmospheric Chemistry and Physics 15*(18), 10263–70. https://doi.org/10.5194/acp-15-10263-2015

Vergara-Temprado, J., et al. (2017). Contribution of feldspar and marine organic aerosols to global ice nucleating particle concentrations. *Atmospheric Chemistry and Physics, 17*, 3637–3658. https://doi.org/10.5194/acp-17-3637-2017

Wilson, T. W., et al. (2015). A marine biogenic source of atmospheric ice-nucleating particles. *Nature, 525*(7568), 234–238. https://doi.org/10.1038/nature14986

Questions and Answers

Questioner: Annica Ekman

Question: When including bioaerosols as INP the bias (negative) at −16 °C was reduced but it looked like you instead got a positive bias at −4 °C. Do you know where this bias comes from? Is it a specific region?

Answer: We evaluated our approach by comparing the calculated global distributions of INP with observations from the BACCHUS database. For this, we used the temperature at which the INP concentrations were measured to calculate both n_m and n_s. Then these parameters were used to determine INP concentrations using monthly average concentrations of precursor aerosol particles calculated by TM4-ECPL. When we considered dust and marine organics as the only precursors of INP, the model appeared to underestimate (negative bias) the observations between −18 °C and −12 °C but it showed a good agreement at low temperatures. When considering that terrestrial bioaerosols are also acting as INP, the calculated INP values were evenly distributed across of the 1:1 correlation line over the whole

range of temperature, with only an overestimation (positive bias) in high temperatures (−4 °C), which can be due to an overestimation of the active sites density n_s of terrestrial bioaerosols, or of the fraction of terrestrial bioaerosols that have the potential to act as INP. More data and relevant parameters of higher accuracy are needed to improve model predictions. Note also that Bacteria (typeII) are more active to nuclei ice at higher temperatures than the other IN sources Murray et al. (2012).

Estimating Aerosol Loads and Aerosol-Cloud-Interaction in the 1980s and Today

Roland Schrödner, Christa Genz, Bernd Heinold, Holger Baars, and Ralf Wolke

Abstract In order to estimate the CCN number concentration during the highly polluted mid 1980s, the aerosol mass, number, and composition in Germany were simulated for 1985 and 2013 using the regional chemistry-transport-model COSMO-MUSCAT (Wolke et al. (2012) Atmospheric environment. 53:110–130). The emissions of the year 1985 were estimated by scaling the present-day emission fields with constant factors, which were derived from the mean concentration reduction of total particulate matter, SO_2, NH_3, and soot. The resulting CCN fields were provided for high resolution ICON-LEM simulations as part of the project HD(CP)^2 (High definition clouds and precipitation for advancing climate prediction). The model results were compared to observations from the two HD(CP)^2 campaigns that took place in 2013 as well as the satellite-based aerosol optical thickness. Despite the fact, that emissions of the 1980s are very uncertain, the modelled AOD is in good agreement with observations. The modelled mean CCN number concentration in 1985 is a factor of 2–4 higher than in 2013.

R. Schrödner (✉) · C. Genz · B. Heinold · H. Baars · R. Wolke
Leibniz Institute for Tropospheric Research (TROPOS), 04318 Leipzig, Germany
e-mail: roland.schroedner@tropos.de

C. Genz
e-mail: christa.genz@uni-leipzig.de

B. Heinold
e-mail: bernd.heinold@tropos.de

H. Baars
e-mail: holger.baars@tropos.de

R. Wolke
e-mail: ralf.wolke@tropos.de

© The Author(s), under exclusive license to Springer-Verlag GmbH, DE, part of Springer Nature 2021

C. Mensink and V. Matthias (eds.), *Air Pollution Modeling and its Application XXVII*, Springer Proceedings in Complexity, https://doi.org/10.1007/978-3-662-63760-9_4

1 Introduction and Motivation

Due to reduction of emissions the ambient aerosol mass and number in Europe was strongly decreased since the 1980s (Smith et al., 2011). Today, both mass and number concentrations of aerosol particles are substantially smaller. This is likely also the case for particles in the CCN size range. Therefore, microphysical and macroscopic properties of clouds might have changed. The HD(CP)^2 project (High Definition Clouds and Precipitation for Climate Prediction) amongst others aimed at analysing the effect of the emission reduction on cloud properties. For this purpose, CCN concentrations over Germany for the year 1985 and 2013 were estimated using aerosol-chemistry transport simulations conducted with COSMO-MUSCAT. The spatially and temporally varying CCN fields were then fed into the new-generation large-domain large-eddy model ICON-LEM (Dipankar, 2015) and used in sensitivity simulations. The present abstract describes the results from the aerosol-chemistry-transport simulations.

2 Methods

Model. In order to derive CCN (cloud condensation nuclei) concentrations, the multi-scale model system COSMO-MUSCAT is used. It consists of two online-coupled model codes: the aerosol-chemistry-transport model MUSCAT (Multi-Scale Chemistry Aerosol Transport, Wolke et al., 2012), which calculates the dispersion and chemical processing for several gas phase and aerosol species based on meteorological fields provided every time step by the forecast model of the German Weather Service (DWD) COSMO (Consortium for Small-scale Modeling, Schättler et al., 2019).

Setup. COSMO-MUSCAT is applied for the time period of two intense measurement campaigns that took place in Germany in 2013 (HOPE (HD(CP)^2 Observational Prototype Experiment) from 26 to March to 19 June and HOPE-Melpitz from 01 to 30 September; see Macke et al., 2017). The model domain with a horizontal resolution of $0.0625 \times 0.0625°$ covers Germany except for the Alps. The meteorological boundary conditions were derived from reanalysis data. The emissions of anthropogenic primary aerosol particles and precursors of secondary aerosols is prescribed using emission fields from the European Monitoring and Evaluation Programme (EMEP, 2009; http://www.emep.int/). In addition to the simulations for the year 2013, a "peak aerosol" scenario was developed to simulate mid 1980s aerosol conditions and derive CCN concentrations (referred to as "1985"). In order to avoid uncertainty due to meteorological conditions, the re-analysis data of the year 2013 were used to drive the meteorology of 1985 scenario. The countrywide annual emissions of SO_2, soot, and particulate matter in 1985 were extrapolated from data of West Germany (available also before 1990) and East Germany (available

Table 1 Annual emissions over Germany for the 2013 (observed) and 1985 (extrapolated) in Mt and scaling factors

	1985	2013	Ratio 1985/2013
Dust (incl. soot)	2.65	0.35	7.7
SO_2	7.73	0.41	18.9
NH_3	0.86	0.74	1.2

Data source Umweltbundesamt

from 1990) provided by the German Environment Agency (ger.: Umweltbundesamt, UBA). These were compared to the 2013 annual emissions and scaling factors were calculated (see Table 1). Finally, for the 1985 simulation, the anthropogenic emission datasets were scaled with these factors.

3 Results and Discussion

The modelled aerosol masses, aerosol optical thickness (AOT) and CCN concentrations were compared to available in-situ, remote sensing and satellite observations (see also Genz et al., 2020; Costa-Surós et al., 2020). The AOT retrieved from the satellite-based AVHRR (Advanced Very High Resolution Radiometer, Zhao and NOAA CDR Program, 2017) instrument is the only available dataset that gives observables to compare with for the year 1985. However, the data set only includes retrievals over water surfaces, therefore only over the North Sea and Baltic Sea, modelled AOT could be compared to observations. Overall, the model agreed well to the observed mean AOT values of the considered time periods for both the present day and peak aerosol scenario.

The scaling factors for the emission of aerosol and their precursor did not transfer into similar factors of the modelled concentrations. Figure 1 shows the domain and time mean profiles of the mass of different aerosol constituents for 1985 and 2013 in the spring period (March–June). It can be seen that the strong emission reduction of SO_2 (factor of 19) lead to factor of ~5 decrease in ammonium sulfate concentrations in the boundary layer. However, ammonium nitrate is modelled to have increased slightly (up to a factor of 2). This is because today less sulfate is available for the formation of ammonium sulfate, but still the ammonia emissions have not changed much since the 1980s.

The modelled aerosol was then transferred into CCN number concentrations by first converting the aerosol species mass into a number size distribution for every aerosol constituent and then applying the activation parameterization by Abdul-Razzak and Ghan (2000) to these number size distributions. Figure 2 compares the derived mean CCN profile at the measurement station Melpitz, Germany, for a constant supersaturation of 0.2% to CCN number concentration retrieved with the PollyXT lidar (Engelmann et al., 2016). The observed CCN number concentration

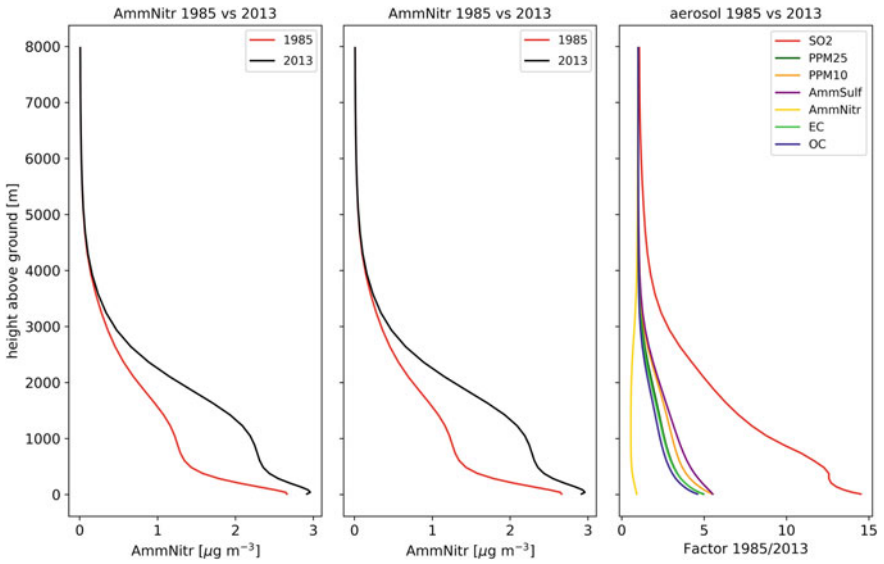

Fig. 1 Domain and time mean vertical profiles of the mass concentrations of ammonium nitrate (left), ammonium sulfate (right) for 2013 (black line) and 1985 (red line), as well as scaling factors between the 1985 and 2013 profiles for different aerosol constituents and SO_2

is overestimated by up to a factor of 2, which is in the range of known uncertainty of this lidar product (see Mamouri & Ansmann, 2016). However, the modelled CCN number concentration is far outside of present-day observations, indicating significantly higher CCN concentrations in the highly polluted 1980s over Europe. Locally, CCN concentrations could have been more than a factor of 5 higher than today. On the domain and time average the difference in CCN number concentration in the boundary layer between 1985 and 2013 is a factor 2–3 for supersaturations between 0.1 and 0.7%.

4 Further Conclusions

For further details and comparisons, the interested reader is referred to the following studies. Genz et al. (2020) describe and evaluate the mass-to-number conversion and the activation parameterization. Costa-Surós et al. (2020) analyzed the ICON-LEM runs that utilized the spatially and temporally variant CCN fields provided by COSMO-MUSCAT and evaluated the aerosol optical depth and CCN number concentrations. The study could detect according differences in the number of cloud droplets between the 1985 and 2013 case. The rain water mass was slightly increased due to the large number of CCN in 1985, leaving more water as cloud water and

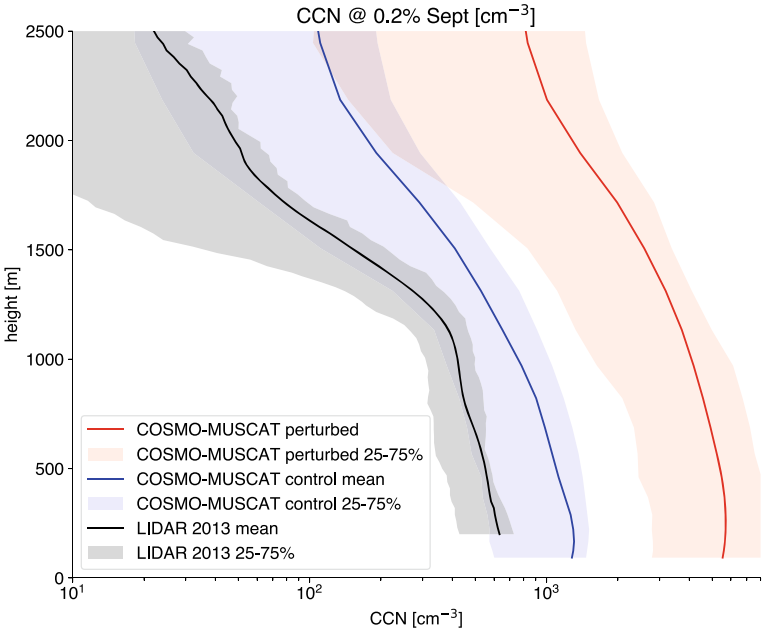

Fig. 2 Mean vertical CCN number concentration profile at Melpitz, Germany retreived with the PollyXT Lidar (black) for September 2013, and modelled with COSMO-MUSCAT for the same period in the 2013 (blue) and 1985 simulation (red). Shown is the median (thick lines) and the 25–75% percentiles (shaded area)

inhibiting precipitation by 2.6% for the investigated day. Overall, with the difference in cloud cover and top of atmosphere net solar radiation they could derive the radiative forcing of aerosol cloud interaction between the 1980s and present-day as -2.8 W m^{-2}.

Acknowledgements This work was funded by the Federal Ministry of Education and Research in Germany (BMBF) through the research programme "High Definition Clouds and Precipitation for Climate Prediction—HD(CP)2" (FKZ: 01LK1503F, 01LK1502I, 01LK1209C and 01LK1212C). We also acknowledge good cooperation and support from the German Weather Service (Deutscher Wetterdienst, DWD). Furthermore, the authors acknowledge support from ACTRIS under grant agreement no. 262 254 of the European Union Seventh Framework Programme (FP7/2007–2013).

References

Abdul-Razzak, H., & Ghan, J. (2000). *Journal of Geophysical Research, 105*, 6837–6844. https://doi.org/10.1029/1999JD901161

Costa-Surós, et al. (2020). *Atmospheric Chemistry and Physics,20*, 5657–5678. https://doi.org/10.5194/acp-20-5657-2020

Dipankar, A., et al. (2015). *Journal of Advance in Modeling Earth System, 7*. https://doi.org/10.1002/2015MS000431
Engelmann, R., et al. (2016). *Atmospheric Measurement Techniques, 9*, 1767–1784.
EMEP. (2009). *European monitoring and evaluation programme*. http://www.emep.int/
Genz, et al. (2020). *Atmospheric Chemistry and Physics*, *20*, 8787–8806. https://doi.org/10.5194/acp-20-8787-2020
Macke, A., et al. (2017). *Atmospheric Chemistry and Physics, 17*, 4887–4914. https://doi.org/10.5194/acp-17-4887-2017
Mamouri, R. E., & Ansmann, A. (2016). *Atmospheric Chemistry and Physics, 16*, 5905–5931.
Schättler, U., et al. (2019). *Deutscher wetterdienst, Offenbach*. http://www.cosmo-model.org
Smith, S. J., et al. (2011). *Atmospheric Chemistry and Physics, 11*, 1101–1116. https://doi.org/10.5194/acp-11-1101-2011
Wolke, R., et al. (2012). *Atmospheric Environment, 53*, 110–130.
Zhao, X., & NOAA CDR Program. (2017). *NOAA climate data record (CDR) of AVHRR daily and monthly aerosol optical thickness (AOT) over global oceans, Version 3.0*. https://doi.org/10.7289/V5BZ642P

Questions and Answers

Questioner: Golam Sarwar

Question: Nice presentation! Did you adjust VOC emissions between the two years?

Answer: No. Natural VOC emissions are not expected to have changed substantially in the ~30 years in Germany. The impact of land use change on biogenic VOC emissions is an interesting study topic. For the change of anthropogenic VOC emissions, there are no reliable estimates available.

Questioner: Annica Ekman

Question: Did you also change the boundary conditions for COSMO-MUSCAT? (To account for changes in long-range transport).

Answer: No. The aim of the study was to investigate the effect of changed emissions only. Therefore, the simulation for the year "1985" is actually the 2013-simulation with only changed emissions of SO_2, OC, EC, and NH_3, but otherwise.

Questioner: Volker Matthias

Question: Why did you keep the NOx emissions constant between 1985 and 2013? They decreased also significantly since the 1980s.

ANSWER: In the first place, we expected the effect of changed NO_x emissions on the CCN number concentration to be less important as the change SO_2 emissions and therefore decided to not consider changes in NO_x emissions so far. However, we will include such changes in a following study.

Characterisation of Light-Absorbing Particles in the Brussels Sub-urban Atmosphere and Implications for the Emission Scheme of a Regional Chemical Transport Model

Alexander Mangold, Quentin Laffineur, Veerle De Bock, Rafiq Hamdi, Nathalie Steenhuyzen, and Andy Delcloo

Abstract The Royal Meteorological Institute of Belgium (RMI) gathered ambient aerosol data in Brussels with a 7-wavelengths aethalometer and a 3 wavelengths integrating nephelometer. The amount of light-absorbing particles showed a clear daily and weekly cycle, with a sharp peak in the morning rush hour time and a broader peak in the evening. During weekends, the rush hour peak diminished. The spectral dependency of the absorption coefficient revealed peak contributions of traffic emissions to the amount of light-absorbing particles of up to 90%. Other sources (like wood burning from households) showed peak contributions of up to 35%. These percentages showed in addition a clear daily, weekly and seasonal cycle, with higher contributions of these other sources during night time, weekends and summer.

Keywords Aerosol absorption coefficient · Soot · Emission sources · Chemical transport modeling

A. Mangold · Q. Laffineur · V. De Bock · R. Hamdi · A. Delcloo (✉)
Royal Meteorological Institute of Belgium, Ukkel, Belgium
e-mail: Andy.Delcloo@meteo.be; Andy.Delcloo@ugent.be

A. Mangold
e-mail: Alexander.Mangold@meteo.be

Q. Laffineur
e-mail: Quentin.Laffineur@meteo.be

V. De Bock
e-mail: Veerle.Debock@meteo.be

R. Hamdi
e-mail: Rafiq.Hamdi@meteo.be

N. Steenhuyzen
University of Antwerp, Antwerp, Belgium

A. Delcloo
Department of Physics and Astronomy, University of Ghent, Brussels, Belgium

© The Author(s), under exclusive license to Springer-Verlag GmbH, DE, part of Springer Nature 2021

C. Mensink and V. Matthias (eds.), *Air Pollution Modeling and its Application XXVII*, Springer Proceedings in Complexity, https://doi.org/10.1007/978-3-662-63760-9_5

1 Introduction

The particle composition is important for air quality studies in the urban atmosphere. In particular, particles smaller than 1 μm are increasingly in the focus with respect to human health since they are inhalable deeply into the human lungs. A relevant part of such ultra-fine particles are light-absorbing particles. Important sources for such particles in the cities and residential areas are emissions from traffic (mainly soot), and emissions from wood-burning stoves in private households. The relative contributions of these sources to the atmospheric particle load are important to be known in order to be able to reduce hazardous emissions by specific measures. More precise information on the emissions is also necessary for chemical transport models in order to produce more reliable predictions of air quality. The spectral dependency of the aerosol absorption coefficient can be used to derive the relative contribution of fresh soot (thus traffic emissions) and other sources to the amount of light-absorbing aerosol. The spectral dependency of the aerosol scattering coefficient can be used to derive information on the dominant particle size. In addition, meteorological conditions have an important influence on air quality, e.g., by changes in the mixing layer height or atmospheric stability.

2 Methods

The Royal Meteorological Institute of Belgium (RMI) gathered ambient aerosol data in Brussels with a 7-wavelengths aethalometer (AE-31; Magee Sci., Slovenia) and a 3 wavelengths integrating nephelometer (TSI Inc., USA, model 3563). The aethalometer measured the aerosol absorption coefficient and derived the mass concentration of light-absorbing particles at 370, 470, 520, 590, 660, 880 and 950 nm. Five years of data (2014–2018) have been analyzed. The nephelometer measured the aerosol total scattering coefficient at 450, 550 and 700 nm. The respective Angstrøm Exponents can be derived from the spectral dependency of the absorption (Absorption Angstrøm Exponent; AAE) and scattering coefficient (Scattering Angstrøm Exponent; SAE), following the equations:

$$\mathrm{AAE} = -(\ln\,(\mathrm{abs}_{\lambda 1}/\mathrm{abs}_{\lambda 2})/\ln\,(\lambda_1/\lambda_2) \tag{1}$$

$$\mathrm{SAE} = -(\ln\,(\mathrm{sca}_{\lambda 1}/\mathrm{sca}_{\lambda 2})/\ln\,(\lambda_1/\lambda_2) \tag{2}$$

where λ_1 is the shorter wavelength of the two. Nephelometer data was available non-continuously during 2013–2017. The measurement site is located in the suburban, rather residential southern part of Brussels. The inlets are at 10 m height, on the flat roof of the Belgian Institute for Space Aeronomy, with non-obstructed air flow. Measurements are representative for the urban background. The boundary layer

height and atmospheric stability parameter are derived from a co-located ceilometer (Vaisala CL51, FIN) and an eddy-covariance system (Campbell Sci., UK).

Further, RMI uses the multi-scale chemical transport model CHIMERE (Vautard et al., 2001), coupled to the high resolution regional numerical weather prediction limited area model ALARO for the BENELUX domain. (Delcloo et al., 2017).

3 Results

Figure 1 (left) shows the average week for the aerosol absorption coefficient, representative of the amount of light-absorbing particles. Clearly to be seen is the sharp morning peak, indicating the contribution of traffic emissions during rush hours. The evening peak was broader instead. The morning peak was much less on Saturdays and quasi non-existing on Sundays. The AAE (Fig. 1, right) showed values decreasing to 1.2–1.1 during the rush hours and increasing to 1.4–1.5 during the evening and night. Fresh combustion soot usually has values of the AAE around 1.0 (Hansen, 2005). Values distinctly higher than 1.0 indicated the presence of compounds which absorb stronger at shorter wavelengths. The contribution of traffic-related soot was thus obvious during the rush hours. In the evening and night, and in particular during the weekend, other sources (probably from heating of buildings and wood-burning in private households) contributed relatively stronger.

The total aerosol scattering coefficient increased over night, with a maximum in early morning and decreased to a minimum in the early afternoon (not shown). The scattering coefficient correlates well with the amount of particulate matter (PM) because atmospheric aerosol is dominantly scattering (Seinfeld & Pandis, 1998). The pattern reflected thus the accumulation of aerosol during the shrinking mixing layer height, the rush hour emissions when the mixing layer is still relatively low, and the decrease of PM concentration during the day when the mixing layer height increases and less polluted air masses are mixed in. The SAE values (not shown; calculated with the scattering values at 450 and 700 nm) had minimum values around 1.2 in

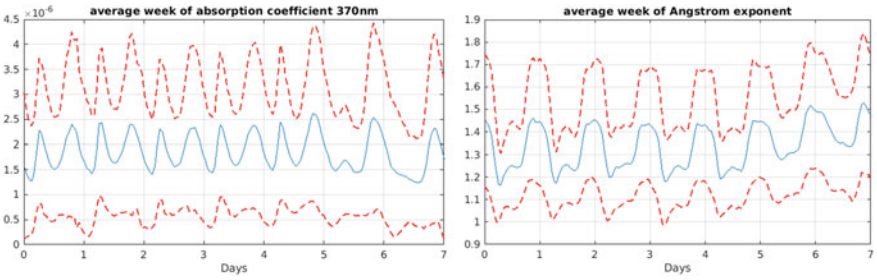

Fig. 1 Left: average week of the absorption coefficient (hourly means), example for 370 nm; right: average week of the absorption Angstrøm Exponent (hourly means), using 370 and 660 nm; broken lines represent standard deviations; day 0 is Monday

the morning, increased to 1.6 in the late afternoon and decreased in the following again. Values of the SAE distinctly larger than 1.0 indicated a dominant contribution of particles <1 μm to the aerosol population, and values below 1.0 indicated distinct contributions of coarse mode particles (>1 μm). The found pattern reflected thus a shift of the particle size distribution to larger sizes (indicating particle growth) during periods of decreasing mixing layer height, and that the fresh emissions over the day shifted the size distribution to smaller sizes.

With the help of the spectral dependency of the absorption coefficient, the fraction of traffic-related soot to the amount of light-absorbing particles could be derived. Under the assumption that fresh soot from traffic has an AAE of 1.0, that the absorption at 880 and 950 nm is mostly due to soot, and that in Brussels almost all soot comes from traffic, Eq. 1 can be inverted to get the fraction of soot-absorption at 370 nm (extrapolated from the absorption coefficients at 880 and 950 nm). The absorption measured at 370 nm which was higher than the extrapolated absorption could then be attributed to other sources than traffic-related soot. Respectively, the percentage of traffic-related soot can be calculated.

These percentages for typical daily cycles of a winter and a summer month are shown in Fig. 2. In winter, there was a clear daily cycle with the fraction of traffic-related soot to the overall amount of light-absorbing aerosol, peaking at 80% in the morning and another bit weaker peak, in the evening. Other sources, like heating, contributed during the night up to one third to the light-absorbing aerosol. In summer, the heating sources were less important and traffic-related soot contributed to 85 to 90% to the light-absorbing particles, with a peak corresponding to the rush hour periods. The patterns corresponded also well to the daily cycles given in Fig. 1.

These new updated schemes of aerosol characteristics will be integrated in the emission pre-processing tool of CHIMERE in order to take more accurately into account these daily specific cycles for Brussels.

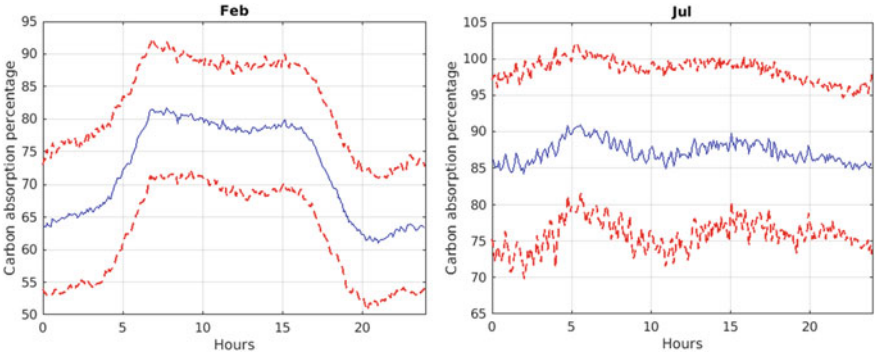

Fig. 2 Percentages (15 min intervals) of the contribution of traffic-related soot to the amount of light-absorbing particles; left: typical day for February; right for July; red lines give standard deviations

The boundary layer height and atmospheric stability parameter will be related to the aerosol properties. First results indicated that distinct, sharp increases of the absorption coefficient in the morning were connected to a decrease of the mixing layer height.

4 Conclusion

Our measurements showed that the amount of light-absorbing particles had a sharp morning and a broader evening peak. The morning peak was less pronounced on Saturdays and quasi non-existing on Sundays. The spectral dependency of the absorption coefficient revealed that during the day traffic-related soot dominated the light-absorbing aerosol and other sources like heating became more important during night. During the weekend, traffic-related soot was much less important. Traffic-related soot contributed with 65–80% to the light-absorbing aerosol during winter and with 85–90% during summer. The measurements of the scattering coefficient and its spectral dependency showed that sub-micron particles contributed dominantly to the Brussels sub-urban atmospheric aerosols. During night, particles tended to grow and with the fresh emission during the day, the size distribution shifted again to smaller sizes. We expect that the integration of these emissions in the CTM will significantly improve the model results.

Acknowledgements We are grateful for the support and financing of the Royal Meteorological institute of this research and the Belgian Institute for Space Aeronomy for providing the measurement platform.

References

Delcloo, A. W., Duchêne, F., Hamdi, R., Berckmans, J., Deckmyn, A., & Termonia, P. (2017). The impact of heat waves and urban heat island on the production of ozone concentrations under present and future climate conditions for the Belgian domain. In *Air pollution modeling and its application XXV. ITM 2016*. Springer Proceedings in Complexity. Springer. https://doi.org/10.1007/978-3-319-57645-9_30

Hansen, A. D. A. (2005). *The aethalometer* (p. 209). Magee Scientific Company.

Seinfeld, J. H., & Pandis, S. N., (1998).*Atmospheric chemistry and physics: From air pollution to climate change*. Wiley, ISBN 0-471-1781-2.

Vautard, R., Beekmann, M., Roux, J., & Gombert, D. (2001). Validation of a deterministic forecasting system for the ozone concentrations over Paris area. *Atmospheric Environment, 35*, 2449–2461.

Questions and Answers

Questioner 1: F. Lenartz

Question 1: Can the aethalometer provide you directly with an information about the particle size? How do you retrieve it?

Answer 1: It is not the aethalometer which can provide information on particle size. It is the nephelometer. As explained in the last paragraph of page 2, the Scattering Angstrøm Exponent gives an indication of particle size.

Questioner 2: Oriol Jorba

Question 2: Have you detected episodes Where AAE > 1.5–2 and if this correlates well with expected emissions of wood combustion?

Answer 2: Yes, periods with an AAE > 1.5–2 were detected. They occur preferentially during winter months and during night hours. Daily means of AAE reached values of 1.8 ± 0.3 during November and December 2018, for example. However, we have not yet performed a detailed analysis on the exact timing of these events. We also have no direct proof that it is wood combustion. For this, chemical analyses would be necessary. But the distinctly higher AAE > 1.5–2 indicates that a distinct part of the measured particles were not from traffic emissions but from heating sources.

Emission Modeling and Processing

Traffic Emissions 2040—Impact on Air Quality in Germany

Volker Matthias, Johannes Bieser, Markus Quante, Stefan Seum, and Christian Winkler

Abstract Traffic emissions in Central Europe were calculated for today and for future scenarios in 2040. For Germany, a sophisticated multi-model chain including transport models, fleet composition models and an up-to-date set of emission factors was embedded. The relationship between transport demand and emissions for several road types has then been applied to other Central European countries for calculating transport demand from total road traffic emissions in these countries. This allows for the construction of consistent and detailed future scenarios for 2040, taking into account modified transport demand and fleet composition. Three emission scenarios were modelled with the full model chain based on societal and legislative developments that are both, plausible and consistent. The traffic emission data was then, together with emissions for all other relevant sectors, fed into the CMAQ chemistry transport model. Concentrations of NO_2, O_3 and $PM_{2.5}$ have been calculated for summer and winter in the year 2010 and for three emission scenarios for 2040. All scenarios revealed an emission reduction in the order of 75–80% for NOx in 2040 compared to 2010. NO_2 concentrations caused by traffic emissions were reduced accordingly. Their contribution to overall NO_2 concentrations in Central Europe was halved in 2040.

V. Matthias (✉) · J. Bieser · M. Quante
Helmholtz-Zentrum Hereon, Max-Planck-Straße 1, 21502 Geesthacht, Germany
e-mail: volker.matthias@hereon.de

J. Bieser
e-mail: johannes.bieser@hereon.de

M. Quante
e-mail: markus.quante@hereon.de

S. Seum · C. Winkler
Institute of Transport Research, German Aerospace Center (DLR), Rutherfordstraße 2, 12489 Berlin, Germany
e-mail: stefan.seum@dlr.de

C. Winkler
e-mail: christian.winkler@dlr.de

© The Author(s), under exclusive license to Springer-Verlag GmbH, DE, part of Springer Nature 2021

C. Mensink and V. Matthias (eds.), *Air Pollution Modeling and its Application XXVII*, Springer Proceedings in Complexity, https://doi.org/10.1007/978-3-662-63760-9_6

Keywords Traffic emissions · Nitrogen dioxide concentrations · Future scenarios

1 Introduction

Traffic is still the dominant source of NO_x and a significant source of CO, VOCs and particulate matter in Europe. Although emissions have decreased substantially in the last 20–30 years, annual limit values for NO_2 are still exceeded in many European cities. In addition, NOx and VOC emissions contribute to ozone formation, secondary aerosol particle formation and to reactive nitrogen inputs into sensitive ecosystems. On the other hand, large efforts are made to reduce emissions of air pollutants from traffic through new exhaust gas cleaning and propulsion technologies.

In the German project Traffic Development and Environment ("Verkehrsentwicklung und Umwelt", VEU) a model chain was built up that includes traffic models, fleet composition developments, new driving technologies, emission factors and atmospheric chemistry transport models. This model chain was first used to calculate current day traffic emissions in Germany and then to develop consistent future scenarios for 2040. These scenarios were based on possible story lines for economic, societal and technological developments in Germany. The effects on air quality were studied for 2010 and 2040 with the COSMO-CLM/CMAQ model system established at Helmholtz-Zentrum Hereon.

2 Traffic Emissions

The traffic emission model chain has been applied to first calculate emissions in Germany in 2010 on three road types (urban, extra-urban, motorway) based on travelled kilometers and emission factors from the Handbook of Emission Factors (HBEFA), version 3.3, differentiated by vehicle type and age. Traffic emissions in other European countries were taken from European emission inventories (EMEP) and then split into travelled kilometers and average emissions factors based on the fleet composition in Germany. This was done for applying the same technology developments until 2040 for vehicles travelling in Central Europe and consequently deriving consistent future scenarios for traffic emissions.

Spatially resolved maps of traffic emissions in Europe for VOCs, $PM_{2.5}$, PM_{coarse}, CO and NO_x are shown in Fig. 1. They are split into processes leading to these emissions, namely combustion, cold starts, brake, tyre, road wear and evaporation. While NOx emissions are almost exclusively from combustion processes, PM emissions are dominated by brake, tyre and road wear. For VOCs, both evaporation and clod starts play an important role. CO emissions are mostly from incomplete combustion while driving, however, cold starts play an important role, as well.

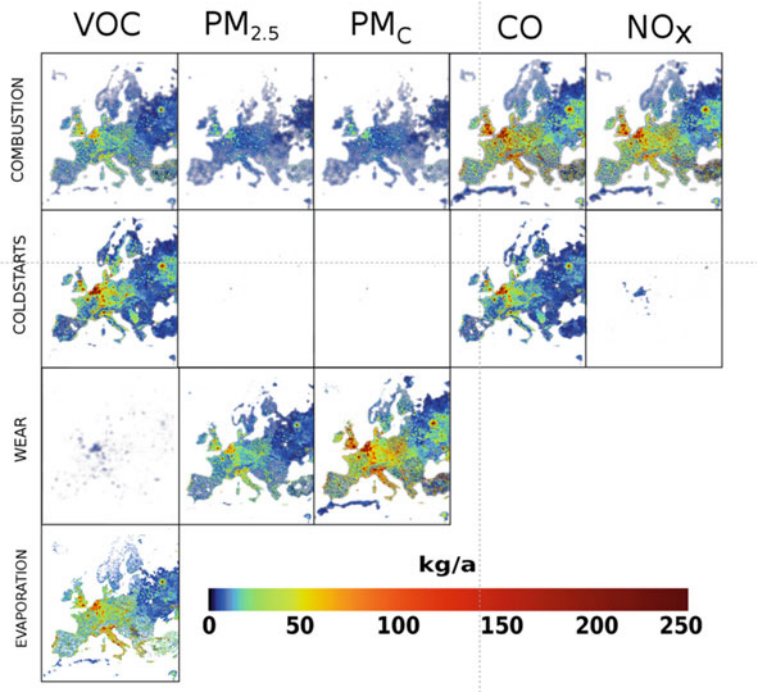

Fig. 1 Traffic emissions in Europe per grid cell of 24 × 24 km^2 in 2010 for the source categories combustion, coldstarts, brake, tyre, road wear and evaporation. VOC emissions were multiplied by a factor of 10 to fit to the same color scale as PM, CO and NOx

3 Atmospheric Concentration Patterns

Traffic emissions were fed into the SMOKE for Europe model system (Bieser et al, 2011) and combined with anthropogenic emissions from all other relevant sectors as well as biogenic emissions. Air quality simulations were performed with the COSMO-CLM/CMAQ model for a 6 × 6 km^2 grid comprising Central Europe (see Fig. 2) for 2010 and subsequently also for three traffic emission scenarios in 2040. Meteorological conditions in January and July 2010 were taken to represent winter and summer conditions, respectively.

3.1 Situation in 2010

Figure 2 shows the modelled NO_2 concentrations in January and July 2010 and the possible reductions without traffic. In large areas of Central Europe, the concentrations in January are higher than 25 μg/m^3 on a monthly average basis. About 40–50% of the NO_2 is caused by traffic emissions. In July, average concentrations

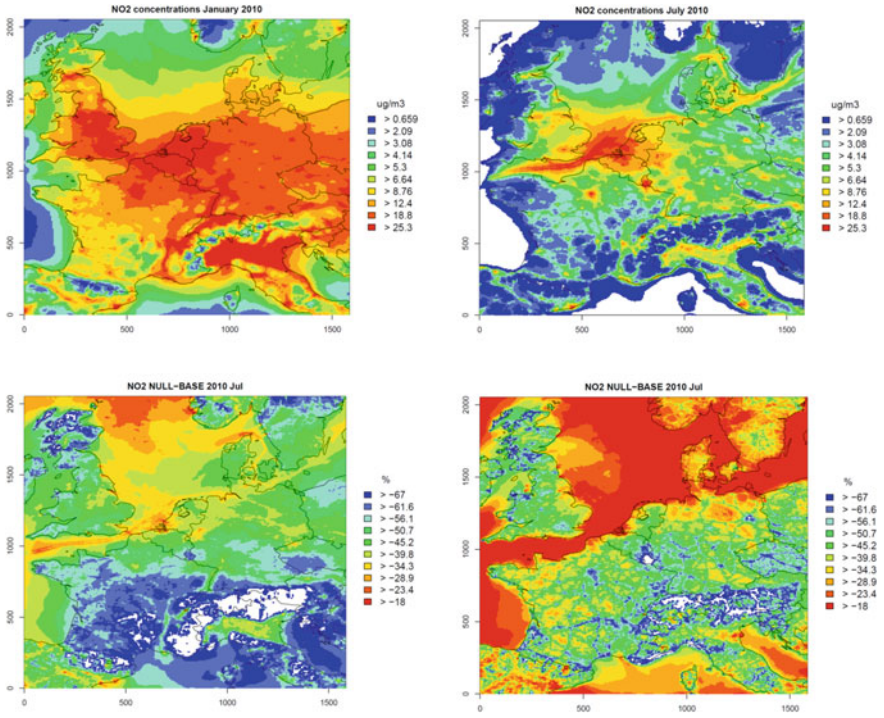

Fig. 2 Top: Modelled NO_2 concentrations in January (left) and July 2010 (right). Bottom: Relative concentration reduction without road traffic in January (left) and July 2010 (right). White areas denote values smaller than the lowest value in the color scale

are much lower. Values above 20 $\mu g/m^3$ are only reached in large cities and in the English Channel, where shipping emissions are a major source. In many regions, road traffic has a slightly lower share of approx. 35–45% in the total concentrations than in January. For reasons of space, results for other pollutants cannot be discussed here.

3.2 Future Scenarios

Three future scenarios were created for traffic emissions in 2040. The Reference scenario includes the developments in legislation, technology and fleet composition that can already be foreseen, today. In the Free Play scenario, regulations are less strict and prices for fuel and technologies steer the emission developments. In contrary to that, in the Regulated Shift scenario stricter regulations and incentives for new technologies and for using public transport lead to traffic emission reductions. In

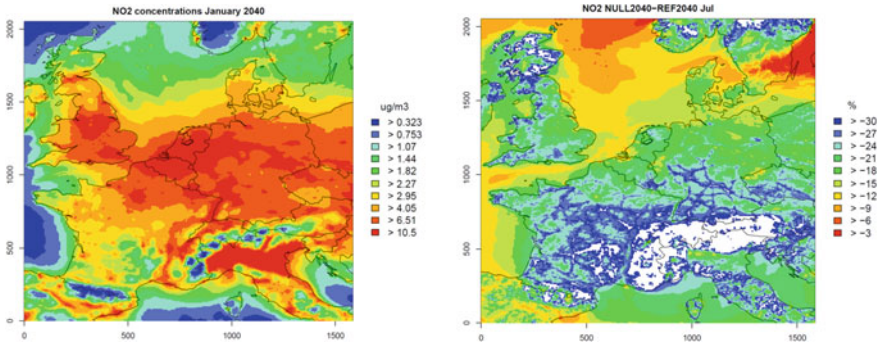

Fig. 3 Results for the Reference scenario 2040. NO_2 concentration in January (left) and relative concentration reductions without traffic (right). White areas denote values smaller than the lowest value in the color scale

all scenarios, other emissions were reduced as well according to the ECLIPSE CLE scenario (Amann et al, 2014).

Figure 3 shows results for NO_2 concentrations for January 2040 according to the Reference scenario and their relative reduction omitting traffic emissions. Compared to 2010, monthly average NO_2 concentrations would be below 10 $\mu g/m^3$ in large parts of Europe. Traffic emissions would contribute about 20% to the average concentrations, i.e. their overall importance would be much lower than in 2010. The results for the Free Play scenario are close to those in the Reference scenario. In the Regulated Shift scenario, NO_2 concentrations caused by road traffic would be further reduced to approx. 15% of the total concentrations.

4 Conclusion

Traffic emissions in Germany were calculated with a sophisticated model chain including models for transport, fleet composition and technology, and emission factors. Relationships between travelled distance and emissions were transferred to other European countries for the construction of consistent future scenarios. A complex atmospheric chemistry transport model system was applied for studying the impact of road traffic emissions on air quality including interactions with pollutants from other sources.

It could be shown that in 2010 traffic contributed around 40% to the average NO_2 concentrations in the most polluted areas in Central Europe. Following our scenarios for 2040, NO_2 concentrations will be reduced by more than 50% compared to 2010. Traffic will only contribute 20% to the future concentrations, which means that traffic emissions will exhibit larger reductions than other sectors.

Acknowledgements CMAQ is developed and maintained by US EPA. Its use by Hereon is gratefully acknowledged.

References

Amann, M., Borken-Kleefeld, J., Cofala, J., Hettelingh, J.-P., Heyes, C., Höglund-Isaksson, L., Holland, M., Kiesewetter, G., Klimont, Z., Rafaj, P., Posch, M., Sander, R., Schöpp, W., Wagner, F., & Winiwarter, W. (2014). *The Final Policy Scenarios of the EU Clean Air Policy Package.*

Bieser, J., Aulinger, A., Matthias, V., Quante, M., & Builtjes, P. (2011). SMOKE for Europe—Adaptation, modification and evaluation of a comprehensive emission model for Europe. *Geoscientific Model Development, 4*(1), 47–68.

Questions and Answers

Questioner: J. Fallmann

Question: How did you consider inland shipping in your modeling approach and in the scenarios?

Answer: Inland shipping is considered as an emission source based on the information provided in the EMEP emission inventory. There were no special activities on inland shipping emissions in VEU, however, we are working on emissions from inland navigation within the Clean Inland Shipping (CLINSH) project. The results will be available in the end of 2020.

Questioner: S. Aksoyoglu

Question: How did you deal with ship emissions for scenario calculations in 2040?

Answer: We have been working on ship emission scenarios for 2040 within the SHEBA project. We considered the development of the fleet, the uptake of new regulations like the nitrogen emission control area in 2021 and the global sulphur cap in 2020. For these simulations, we used the business as usual case from SHEBA, which show large reductions in emissions from ships caused by efficiency gains and the new regulations on NO_x and SO_2 emissions.

Questioner: B.H. Baek

Question: How did you apply averaged vehicle specific speed?

Answer: The emission factors in the traffic emission model are based on HBEFA emission factors. They distinguish between certain street and terrain types (e.g. driving uphill or downhill) as well as size and age of the vehicles. Vehicle speeds are averaged within these categories.

Biogenic VOC Emission Modeling for Spain: Adaptation of the National Forest Inventory as Input for MEGANv3

Eduardo Torre-Pascual, Estibaliz Sáez de Cámara, Gotzon Gangoiti, and Iñaki Zuazo

Abstract Biogenic Volatile Organic Compounds (BVOC) are well-known ozone and secondary organic aerosol precursors. Consequently, the estimation of their emissions is crucial for air quality modeling, and specifically for photochemical models. We have adapted the Spanish National Forest Inventory creating a new landcover database that can be used into the new Model of Emissions of Gases and Aerosols from Nature (MEGANv3) in order to improve air quality simulations in Spain. Preliminary results show that spatial distributions of emission potentials compared to the MEGANv3's default database are closer to reality.

Keywords Biogenic emissions · MEGAN3 · BVOC · Spanish forest · Emission potentials

1 Introduction

Tropospheric ozone EU thresholds set for protection of human health and ecosystems are largely and widely exceeded in peninsular Spain and the Balearic Islands (Querol et al., 2016). In the troposphere, ozone and a large range of secondary pollutants are produced from chemical reactions in which BVOC play a key role (Zenone et al., 2016). Therefore, the characteristics of both biogenic and anthropogenic emissions are required for air quality simulations. Vegetation in Spain covers around 80% of the

E. Torre-Pascual (✉) · E. Sáez de Cámara · G. Gangoiti · I. Zuazo
Faculty of Engineering Bilbao, University of the Basque Country (UPV/EHU), Plaza Ingeniero Torres Quevedo 1, 48013 Bilbao, Spain
e-mail: eduardo.delatorre@ehu.eus

E. Sáez de Cámara
e-mail: estibaliz.saezdecamara@ehu.eus

G. Gangoiti
e-mail: g.gangoiti@ehu.eus

I. Zuazo
e-mail: joseignacio.zuazo@ehu.eus

© The Author(s), under exclusive license to Springer-Verlag GmbH, DE, part of Springer Nature 2021

C. Mensink and V. Matthias (eds.), *Air Pollution Modeling and its Application XXVII*, Springer Proceedings in Complexity, https://doi.org/10.1007/978-3-662-63760-9_7

total area, and the emission of BVOC in the Iberian Peninsula is almost equal to the total amount emitted in Central Europe (Oderbolz et al., 2013). It is also important to highlight that tree-covered areas in Spain are characterised by a large variety of highly BVOC emitting species (Navazo et al., 2008). A high-spatial resolution vegetation inventory (including speciation of vegetation types) is needed because the reference emission factors vary strongly between species (Niinemets et al., 2011). In view of the above, we have developed a methodology to adapt the national forest inventory to the new MEGANv3 model. This methodology and preliminary results are presented in the next sections.

2 Methodology

The Model of Emissions of Gases and Aerosols from Nature (MEGAN) is the most widely used emission model to calculate BVOC (Sindelarova et al., 2014). Its last version (MEGAN3, 2019) includes several datasets to run the model and, for the first time, explicit species' distributions (ecotypes) are included, allowing MEGAN users to generate their own distribution of species without modifying the code. The Spanish National Forest Inventory (SNFI) provides up-to-date, extensive, and unique records of key information about forests and woodlands (MITECO, 2019).

This inventory has been adapted to the input format of MEGANv3 (Sect. 2.1) by applying GIS techniques to adjust spatial resolutions. The compatibility between MEGAN's and SNFI's species and the adaptation to specific requirements of MEGAN has also been established. These novel datasets have been used in the analysis of the BVOC emission potential distribution in peninsular Spain.

2.1 Spanish National Forest Inventory

The SNFI is a vegetation inventory that delivers a national estimate of species distribution in Spain every ten years. It gives exhaustive data of forestry land use by providing high-resolution vectorial maps: tree covered vectors have a minimum area of 2.5 ha and non-tree ones of 6.25 ha. Each vector includes information about growth form (tree, shrub, grass, and crop fractions) and ecotype information (three major species on tree-covered areas). Based on this inventory, 39.7% of the Spanish total area is covered by cultivatable lands or crops, 18.5% by trees, 11.0% by shrubs, and 9.1% by grass.

2.2 BVOC Emission Potentials Distribution

Emission potentials (EP) and their distribution have been calculated with the aim of integrating these results into the domains used for ozone episodes simulations in Northern Spain (Gangoiti et al., 2006; Valdenebro et al., 2011; Camara et al., 2018). Growth form fractions and predominant species fractions (ecotype) datasets have been rasterized to 3 arcsec resolution ($3'' \times 3''$) in lat-lon projection. Then, they have been aggregated to 30 arcsec for the adjustment to MEGANv3 input variables' spatial resolution ($30'' \times 30''$). This new landcover database is available at: https://doi.org/10.5281/zenodo.3580226. The domain showed in this paper covers the whole Iberian Peninsula with a grid spatial resolution of 9×9 km in Lambert Conformal projection. The "prep4cmaq" tool has been used to adjust spatial resolution of input variables to our domain, and the new "Emission Factor Processor" has been used to calculate the emission potential. Four family compounds EP have been calculated using highest confidence level of emission potentials ($J = 4$): Isoprene (ISOP), Pinene (MT-PIN), Sesquiterpenes (SQT) and Oxygenated VOC (OVOC).

3 Results

MEGAN's ecotype distribution, based on MEGAN2.1-CLM4 model (Guenther et al., 2012), shows large areas with the same ecotype, whereas the SNFI shows a much more detailed ecotype distribution, especially in the most vegetated areas of Northern Spain (Fig. 1).

Total mean potential values calculated for the Spanish territory and for the aforementioned four family compounds of BVOC are detailed in Table 1. EP distribution calculations for ISOP and MT-PIN with the newly created variables (based on SNFI) and MEGANv3's (based on default data) are presented for their comparison in Fig. 2.

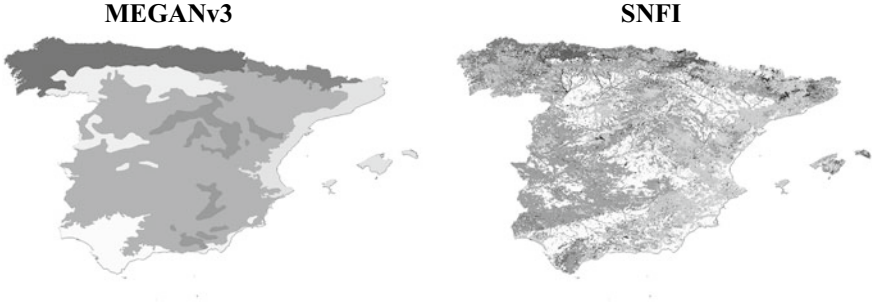

Fig. 1 Spanish ecotype distribution: MEGAN's dataset (left) and rasterized SNFI (right). Random colors of the gray scale for each map represent different ecotypes

Table 1 Mean EP calculated for the Spanish territory with SNFI and MEGANv3's default variables (kg/km^2 h)

Variable	MEGANv3	SNFI
MEAN EP ISOP	0.863	0.965
MEAN EP MT-PIN	0.110	0.087
MEAN EP SQT	0.034	0.014
MEAN EP OVOC	0.200	0.089

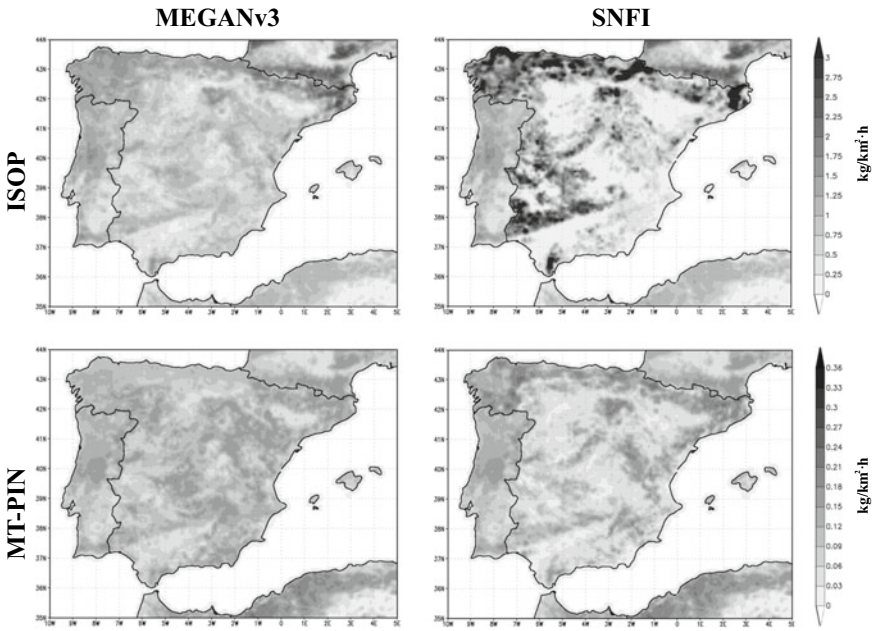

Fig. 2 Emission potentials distribution in Spain for ISOP and MT-PIN estimated by MEGAN (left panels) and using SNFI inventory (right panels)

There is a great deal of similarity between ISOP and MT-PIN mean values for the whole territory of Spain (Table 1). However, EP intensity varies considerably from one area to another (Fig. 2). Differences in EP rates of up to 300% are found in Northern Spain for ISOP and in the tree covered areas of the main mountain ranges of Spain (N-Eastern and Southern Spain). This higher resolution vegetation inventory SNFI leads presumably to better emission estimations (Oderbolz et al., 2013). Mean values for MT-PIN are also similar with remarkable differences in local scale. In the SNFI higher EP for MT-PIN are located in tree vegetated areas but, in contrast to ISOP, there are some areas with more intensity due to the presence of pine trees.

4 Conclusion

New BVOC emission potentials have been calculated in Spain introducing adapted data from the SNFI into the new MEGANv3 model. Important differences regarding intensity and spatial distribution of BVOC EP have been found. Differences in isoprene EP are as high as 300% in Northern, N-Eastern, and Southern Spain. The SNFI gives more detailed heterogeneous information regarding vegetation distribution data which improves BVOC emission calculations. This novel landcover datasets will help improving air quality simulations in Spain.

Acknowledgements This work has been developed under the UPV/EHU PIFG004-2017 PhD fellowship program: "Meteorología, Climatología y Dispersión de Contaminantes" IT1057-16, GIC 15-152. Authors wish to thank the Spanish Ministry for the Ecological Transition (MITECO) for providing the Spanish National Forest Inventory data and Prof. Alex Guenther for his kind support.

References

Gangoiti, G., Albizuri, A., Alonso, L., Navazo, M., Matabuena, M., Valdenebro, V., García, J. A., & Millán, M. M. (2006). Sub-continental transport mechanisms and pathways during two ozone episodes in Northern Spain. *Atmospheric Chemistry and Physics, 6*, 1469–1484.

Guenther, A. B., Jiang, X., Heald, C. L., Sakulyanontvittaya, T., Duhl, T., Emmons, L. K., & Wang, X. (2012). The model of emissions of gases and aerosols from nature version 2.1 (MEGAN2.1): An extended and updated framework for modeling biogenic emissions. *Geoscientific Model Development, 5*, 1471–1492.

Mapa Forestal de España (MFE50). (2019). Retrieved June 25, 2019. https://www.miteco.gob.es/es/biodiversidad/servicios/banco-datos-naturaleza/informacion-disponible/mfe50.aspx

MEGAN3. Biosphere atmosphere interactions group. (2019). Retrieved June 25, 2019. https://sites.google.com/uci.edu/bai/megan/versions/megan3

Navazo, M., Durana, N., Alonso, L., Gómez, M., García, J., Ilardia, J. L., Gangoiti, G., & Iza, J. (2008). High temporal resolution measurements of ozone precursors in a rural background station. A two-year study. *Environmental Monitoring and Assessment, 136*, 53–68.

Niinemets, Ü., Kuhn, U., Harley, P. C., Staudt, M., Arneth, A., Cescatti, A., Ciccioli, P., Copolovici, L., Geron, C., Guenther, A., Kesselmeier, J., Lerdau, M. T., Monson, R. K., & Peñuelas, J. (2011). Estimations of isoprenoid emission capacity from enclosure studies: Measurements, data processing, quality and standardized measurement protocols. *Biogeosciences, 8*, 2209–2246.

Oderbolz, D. C., Aksoyoglu, S., Keller, J., Barmpadimos, I., Steinbrecher, R., Skjøth, C. A., Plaß-Dülmer, C., & Prévôt, A. S. H. (2013). A comprehensive emission inventory of biogenic volatile organic compounds in Europe: Improved seasonality and land-cover. *Atmospheric Chemistry and Physics, 13*, 1689–1712.

Querol, X., Alastuey, A., Reche, C., Orio, A., Pallares, M., Reina, F., Dieguez, J. J., Mantilla, E., Escudero, M., Alonso, L., Gangoiti, G., & Millán, M. (2016). On the origin of the highest ozone episodes in Spain. *Science of the Total Environment, 572*, 379–389.

Sáez de Cámara, E., Gangoiti, G., Alonso, L., Valdenebro, V., Aksoyoglu, S., & Oikonomakis, E. (2018). Ozone source apportionment to quantify local-to-continental source contributions to episodic events in Northern Iberia. In C. Mensink, & G. Kallos (Eds.), *Air pollution modeling and its application XXV, springer proceedings in complexity* (pp. 361–365). Springer International Publishing.

Sindelarova, K., Granier, C., Bouarar, I., Guenther, A., Tilmes, S., Stavrakou, T., Müller, J.-F., Kuhn, U., Stefani, P., & Knorr, W. (2014). Global data set of biogenic VOC emissions calculated by the MEGAN model over the last 30 years. *Atmospheric Chemistry and Physics, 14*, 9317–9341.

Valdenebro, V., Gangoiti, G., Albizuri, A., Alonso, L., Navazo, M., García, J., Iza, J., & Millán, M. (2011). Build-up and decay of two ozone episodes through Northern Iberia and Southern France—An inter-regional transport analysis. *Atmospheric Environment, 45*, 1595–1603.

Zenone, T., Hendriks, C., Brilli, F., Fransen, E., Gioli, B., Portillo-Estrada, M., Schaap, M., & Ceulemans, R. (2016). Interaction between isoprene and ozone fluxes in a poplar plantation and its impact on air quality at the European level. *Scientific Reports, 6*, 32676.

Question and Answer

Questioner: Ari Karppinen (Finnish Meteorological Institute)

Question: Are these detailed inventories used already for pollen emission modeling?

Answer: We are looking forward to collaborating with pollen modellers. The high spatial resolution of this novel landcover datasets, together with the possibility of distributing growth forms down to genus or species level, could be of great applicability for both pollen and BVOC modeling.

Alteration of Vehicle Propellant Use and the Impact on CO_2 Emissions and NO_2 Concentrations in Gothenburg and Mölndal

Martina Frid, Marie Haeger-Eugensson, and David Rayner

Abstract Sweden has set the target of a fossil independent vehicle fleet in 2030, focusing on a transport system mainly driven by biofuel and electricity. This study investigates the potential of reducing GHG emissions and improving local air pollution, by altering propellant- and vehicle use. Based on literature studies, five individual- and two combined scenarios were created, with different amount of hybridization, electrification and a shift towards biodiesel, for four different vehicle categories. Emission factors, collected from HBEFA, were used for 2016 and 2030 to generate the total emissions, in Business As Usual (BAU) and the individual scenarios. For cases where emission factors were missing, new factors were created through literature studies and the relation between new and conventional propellant- and engine types. The geographical vehicle distribution and vehicle numbers were used to calculate total annual emissions, showing large improvements, in both CO_2 and NO_X, from 2016 to 2030 BAU with even further reduction in the scenarios. Dispersion simulations of NO_2 were conducted with The Air Pollution Model and the results showed large potential in improving the local air quality and reducing the population exposed to concentrations above the environmental target.

M. Frid (✉) · M. Haeger-Eugensson · D. Rayner
Department of Earth Science, University of Gothenburg, 413 20 Gothenburg, Sweden
e-mail: mifd@cowi.com

M. Haeger-Eugensson
e-mail: marie.haeger-eugensson@gu.se; mrhr@cowi.com

D. Rayner
e-mail: david.rayner@gu.com

M. Frid · M. Haeger-Eugensson
Section of Environmental Modeling and Sustainability Analyses, COWI, 402 41 Gothenburg, Sweden

© The Author(s), under exclusive license to Springer-Verlag GmbH, DE, part of Springer Nature 2021

C. Mensink and V. Matthias (eds.), *Air Pollution Modeling and its Application XXVII*, Springer Proceedings in Complexity, https://doi.org/10.1007/978-3-662-63760-9_8

1 Introduction

In 2013, the Swedish government office submitted the final report SOU 2013:84 "Fossilfrihet på väg" with the goal of reaching a fossil independent vehicle fleet in 2030. This is a step towards a long-term development of a sustainable and resource efficient energy system, including a net of zero greenhouse gas (GHG) emissions in 2050 (Governmental Official Investigations, 2013). In 2018 the 2030 target, for the transport sector, were set to a 70% GHG reduction in relation to the levels of 2010 (Swedish Transport Administration, n.d.). The governmental official investigation (2013) defined a fossil independent vehicle fleet, as a transport system where vehicles are mainly driven by biofuel or electricity. They argue that mixtures with high concentrations of renewable propellant should be considered as fossil independent, including propellant-hybrids and all diesel vehicles. Diesel (fossil and renewable) stands for more than 30% of the Swedish propellant use and it is predicted to increase (Trafikanalys, 2017). There are several advantages with bio-diesel, as a non-mineral diesel it can be derived from renewable and domestic resources, leading to a reduction of GHG emissions. Although NO_x emissions are somewhat more complicated. The source material affects the amount of emissions and several studies show that NO_x emissions generally increase by the use of biodiesel, in relation to fossil (da Silva et al., 2017; Atabani et al., 2012; McCormick et al., 2001). Today both Gothenburg and Mölndal exceed the environmental targets for NO_2, both for hourly and daily NO_2 concentrations (Environmental Administration, 2018), pointing to the importance of reducing both CO_2 and NO_x emissions.

2 Method

To investigate the impact of an altered vehicle fleet, a literature study where conducted to gain deeper knowledge of the predicted fleet composition in 2030, whereafter five base scenarios were created, affecting individual vehicle categories, and two combined scenarios, to show the total vehicle impact. Emission factors (EF) were collected from HBEFA 3.3, for all vehicle sub-categories under 2016 and 2030, although EF's did not exist for all vehicle types and new factors where therefore created. These EF's were based on literature studies, where the relation between emissions from conventional propellant types, more renewable propellants and hybrid engines, both regarding CO_2 and NO_x, were used, together with existing factors for 2030 and their distribution between the sub-categories. The geographical distribution and the number of vehicles were collected from the environmental administration database and the total annual emissions were calculated for CO_2 and NO_x under 2016 Business As Usual (BAU), 2030 BAU and each scenario. The total traffic NO_x emissions were used together with regional background NO_x concentrations and the individual temporal variability's, to run NO_2 dispersion simulations with The Air Pollution Model (TAPM). 2016 BAU were verified against measurements and as the

simulations were conducted separately for background- and traffic concentrations, the simulated traffic data were corrected, based the uncertainty in traffic numbers. The simulated NO_2 concentrations were thereafter analysed and an exposure study was conducted, with the information of population density in 100 × 100 m resolution, for 2015 and the predicted population increase in 2030.

3 Results and Discussion

3.1 Emission Calculations

To understand both the small- and large-scale effects of propellant alterations the total traffic CO_2, both fossil and renewable, were put in relation to total traffic NO_x emissions (Fig. 1). These results showed large reduction potential for both CO_2 and NO_x, where the individually largest CO_2 reduction could be obtained for Private Cars (PC-DPE) using biodiesel (35%), petrol driven plug-in hybrids (40%) and electricity (20%). This scenario gave a CO_2 reduction of 91% in relation to 2016 BAU (fossil diesel), although the NO_x emissions were slightly higher in relation to PC-Mix, with 20% biodiesel, 20% petrol and 37% petrol hybrids. These differences in emission could be connected to the difference in hybrid and diesel vehicle numbers, where the larger number of hybrid and diesel vehicles contributes to larger reduction in CO_2, but the high number of diesels also contributes to the lower reduction in NO_x emissions. Except for the use of biodiesel, only small improvements could be obtained by alterations for heavy vehicles, HGV-mix, UB-Mix and UB-E, where the later include only electric public transportations. The two combined scenarios showed the total largest improvement, where C-PE, including PC-DPE, HGV-Mix and UB-E, showed the largest CO_2 reduction, with the use of biodiesel, and slightly lower

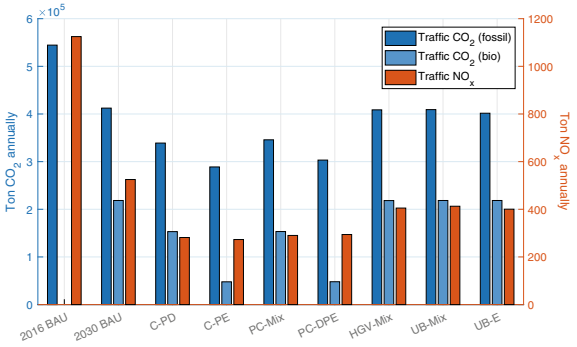

Fig. 1 Total annual traffic CO_2, with fossil- (dark blue) and renewable (light blue) diesel, together with total annual traffic NO_x emissions (orange), for the whole study area. The CO_2 bars represent individual scenarios, where total diesel use is either fossil or renewable

NO_x emissions. C-PD (including PC-Mix, HGV-Mix and UB-Mix) gave a 75% NO_x reduction whereas C-PE gave a 76% reduction, both in relation to 2016 BAU. The NO_x improvements in C-PE could be connected to the fully electrified public transportation, contributing to slightly larger NO_x improvements despite higher number of diesel cars.

3.2 Dispersion Simulations

The dispersion simulations showed, of the condition of today (2016), large areas with concentrations above the environmental target for NO_2 (60 $\mu g\ m^{-3}$), and the central areas above the environmental quality standards of 90 $\mu g\ m^{-3}$, both as the 98th percentile of hurly mean concentrations, in 2016 BAU. This was reduced to only include small areas in the central of Gothenburg in 2030 BAU (Fig. 2, top left). This improvement is, most likely, based on current emissions regulation and the main effect is caused by a shift towards Euro VI for heavy transport. With propellant alterations, these concentrations could be even further reduced (Fig. 2, bottom left). One hour with high average concentrations (27th of January 08:00–09:00,), were used to calculate the ratio between 2030 BAU and the combined scenario (Fig. 2, right). This showed an increased reduction with up to 35% at the most heavy trafficked road sections.

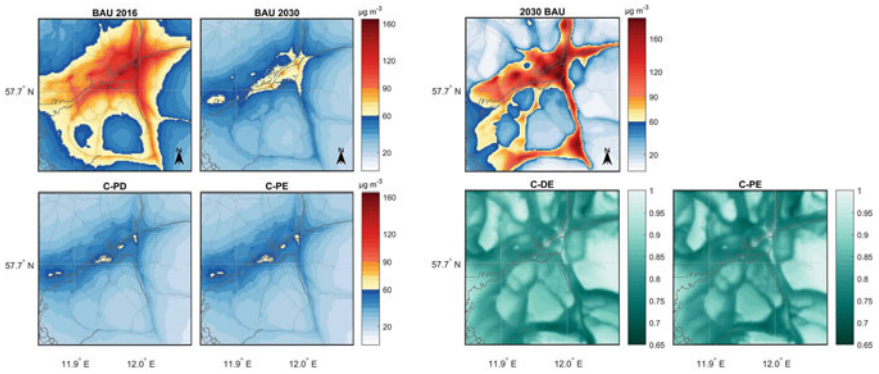

Fig. 2 The 98th percentile of hourly average NO_2 concentrations for 2016 BAU, 2030 BAU and the two combined scenarios (left) together with the NO_2 concentration for one hour with high concentrations (27th of January 08:00–09:00) 2030 BAU and the ratio of the two combined scenarios (right)

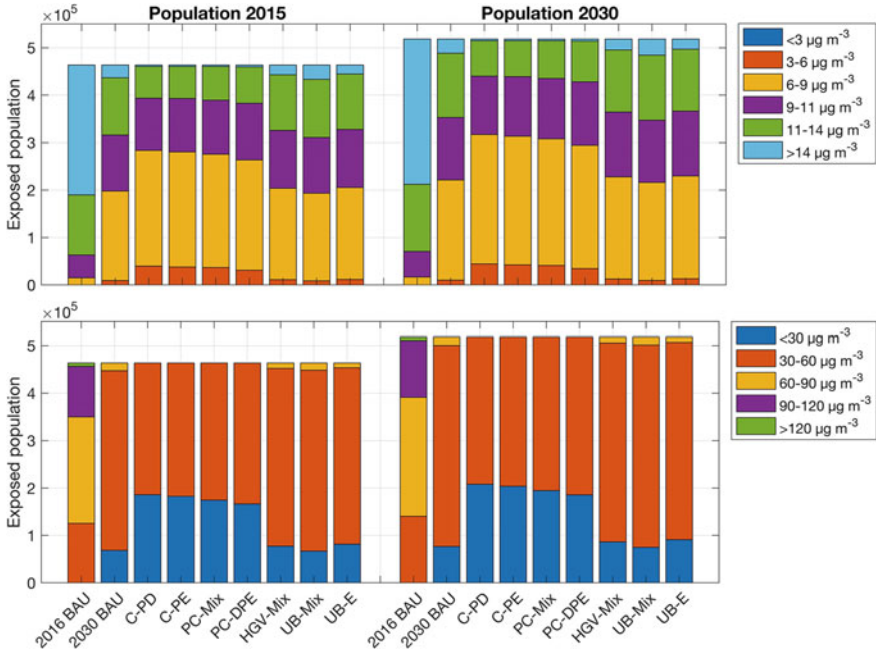

Fig. 3 Population exposed to annual average NO_2 concentrations (top) and the population exposed to hourly 98th percentile concentrations (bottom), for 2015 population (left) and the predicted 2030 population (right)

3.3 Population Exposure

In 2016 BAU, large numbers of the population were exposed to high NO_2 concentrations (Fig. 3). The region was more affected by short-term high concentrations and the population exposed were highly reduced in 2030 BAU. Further improvements could be obtained in the two combined- and the PC-scenarios, where only 21 and 197 of the 2030 predicted population were exposed, respectively, to concentrations above 60 $\mu g\ m^{-3}$.

4 Summary and Conclusion

Large emission improvements can be obtained by a shift towards renewable propellant types, but the use of biodiesel will not improve local air quality. A combination of alterations in all vehicle classes showed the largest reduction potential, where private cars stood for the largest individual contribution. We argue that the use of

petrol-driven hybrids and electrical vehicles can help to improve both GHG emissions and NO_2 concentrations, during a transition period towards better solutions, but that there is not one simple path, rather that several mitigation actions are needed, in all vehicle categories, both regarding propellant use and travel patterns.

References

Atabani, A. E., Silitonga, A. S., Badruddin, I. A., Mahlia, T., Masjuki, H., & Mekhilef, S. (2012). A comprehensive review on biodiesel as an alternative energy resource and its characteristics. *Renewable and Sustainable Energy Reviews, 16*(4), 2070–2093.

da Silva, M. A. V., da Ferreira, B. L. G., Costa Marques, L. G., Murta, A. L. S., & de Freitas, M. A. V. (2017). Comparative study of NO_x emissions of biodiesel-diesel blends from soybean, palm and waste frying oils using methyl and ethyl transesterification routes. *Fuel, 194*, 144–156.

Environmental Administration. (2018). *Luftkvaliteten i Göteborgsområdet Årsrapport 2017*. R 2018:10.

Governmental Official Investigations. (2013). *Fossilfrihet på väg del 1: Betänkande av utredningen om fossilfri fordonstrafik* (No. SOU 2013:84).

McCormick, R. L., Graboski, M. S., Alleman, T. L., & Herring, A. M. (2001). Impact of biodiesel source material and chemical structure on emissions of criteria pollutants from a heavy-duty engine. *Environmental Science Technology, 9*(35), 1742–1747.

Swedish Transport Administration. (n.d.). *Trafikverkets kunskapsunderlag och klimatscenario för energiefek- tivisering och begränsad klimatpåverkan.*

Trafikanalys. (2017). *Prognoser för fordonsflottans utveckling*. rapport 2017:8.

Regional and Intercontinental Modeling

Improvements of Chemical Transport Modeling Over the Last 40 Years—A Personal Journey

Peter Builtjes

Abstract Chemical transport modeling, 3-D Eulerian grid modeling, started around 1975. Its development, based on work by the authors' Ph.D.-students, is followed over the last 40 years. An attempt is made to analyse model improvement.

Keywords Chemical transport modeling · Model improvement

1 Introduction

Chemical transport models are in fact a mass-balance. They describe the fate of emissions into the atmosphere, resulting in concentrations and depositions: what goes up has to go down, with chemical transformations in between. The first publication concerning a 3-D Eulerian grid model described episodic ozone formation in the Los Angelos area, Reynolds et al. (1973). The science question which will be addressed in this paper is whether it can be proven that current models are better than the models in 1973. Better is defined in two ways: a better agreement with observations—more policy, application oriented, and better in the sense of containing more information, having better modules, process-descriptions inside the overall model, which is a more science aspect.

With increasing computer capacity, calculations over longer times, over larges areas became possible. Models started to address deposition, followed by modeling of aerosols. Current models try to include all processes relevant for the description of the "complete" chemical composition of the atmosphere. It is clear that processes in the models have been improved, but also emissions, meteorological descriptions have been improved as well. Also the number of observations have been increased, more sites as well as more species.

A sketch will be given of a way to give a clear answer to the question: How much better are current models relative to the models of 40/50 years ago?

P. Builtjes (✉)
Free University Berlin, Berlin, Germany

© The Author(s), under exclusive license to Springer-Verlag GmbH, DE, part of Springer Nature 2021

C. Mensink and V. Matthias (eds.), *Air Pollution Modeling and its Application XXVII*, Springer Proceedings in Complexity, https://doi.org/10.1007/978-3-662-63760-9_9

2 A Short History

Around 1960 there was growing attention to air pollution and atmospheric chemistry. Books appeared by Pasquill (1962), Junge (1963), Slade (1968). The times were changing, Dylan (1963). The first generation air pollution models, mainly Gaussian plume models, were in place around 1969, Steyn (2017). The year 1969 can also be seen as the first year of the ITM's. That is the reason to celebrate today 50 years of ITM's. My own start attending ITM's and giving presentations was in 1980 Builtjes et al. (1980). So, I can only cover about 40, not 50 years. As already stated, the first 3-D Eulerian grid model was developed at Caltech in the group of John Seinfeld, see Reynolds et al. (1973). This first model, the Urban Airshed Model-UAM—with the Carbon Bond Chemical Mechanism-CBM—formed also the starting point of the current LOTOS-EUROS model used by TNO and the Free University Berlin, and many other institutes.

3 Chemical Transport Modeling

Observations are essential to obtain information concerning the chemical composition of the atmosphere. However, just observations without any further analysis do not lead to knowledge. Observations are the eyes, modeling can be seen as the brains. Bruno Latour (2017) makes an intriguing difference in observations between matters of fact, f.e. temperature, and matters of concern, like climate change. Latour makes also a detailed analysis about the Gaia theory by Lovelock and its implications: Gaia is fighting back. At the moment you could also state: Youth is fighting back, Thunberg (2019).

Concerning observations, this does not mean that matters of fact, when they are reliable and of high quality, are not important, they are essential, Raes (2012). The book by Raes gives also, based on interviews by leading scientists active in modeling, an assessment of the interaction between modeling application and policy.

Concerning modeling, my preference has always been for 3-D Eulerian Grid modeling above Trajectory modeling. Next to the fact that trajectory models have difficulties in handling chemical transformations, 3-D Eulerian grid modeling has a much closer link with the general balance equations as the Navier–Stokes equation for the conservations of momentum and the Reynolds (turbulence) equation. Of great importance is the fact that 3-D Eulerian Grid modeling is mass-conserving.

Modeling has an applied, policy-oriented side, and a science side, which is also clear in the book by Raes (2012). This has also implications with respect how to define whether a model has improved, is a better model. In the applied, policy arena a model is better when it agrees better with observations, because in that case the model is considered suited for policy applications and emission-scenario studies. In this context it should also be mentioned that for policy the final purpose of the models

is not concentrations or deposition, but health effects and the protection of the ecosystem. In the science arena, a model is better when it has improved modules/process descriptions inside the model. The model is then more reliable, more up-to-date, state of the art.

Over the last years many activities have been carried out concerning model evaluation. Denis (2010) presented a new model evaluation framework. A distinction is made between 4 aspects; operational evaluation, diagnostic evaluation, dynamic evaluation and probabilistic evaluation. The first 2 evaluation aspects are more oriented to the applied side, the last 2 are more focussed on the science. An important activity is AQMEII: Air Quality Model Evaluation International Initiative of which many results are presented at recent ITM's, see f.e. Rao et al. (2012).

4 Highlights of Ph.D.-Studies Over the Last 30 Years

Mass-conservation has been from the beginning a key aspect of chemical transport modeling. Also from the beginning, two stumble-blocks have been present. The first one is non-linearity in the relation between emissions and concentrations and deposition, with its danger of being right—calculated concentrations in agreement with observations—for the wrong reason. The second one is the role of clouds on radiation and on chemistry. Both aspects will be addressed in the overview given here, which is based on the work of a number of Ph.D.-students, of which I was the first promoter.

An important philosophy in model improvement has always been that the model should be in balance. This means that an improvement in one module of the model should be not more sophisticated than the rest of the model, or its input. As an example: a very detailed VOC-chemistry module should be in balance with the information contained in the VOC-emission input data-base.

The Ph.D. research can be divided in the following areas:Studies on general model improvements, studies on aerosols, on deposition, on emissions and on satellite observations.

Model improvement has taken place concerning the role of clouds in tropospheric chemistry. Lelieveld (1990)-supervision by Paul Crutzen and Adolf Ebel—investigated the impact on O_3, NO_2 and SO_2 in cloudy and cloud free air. A detailed model study and comparison with observations have been performed by van Valk (1992). Dentener (1993)-supervision Paul Crutzen-modelled the influence of heterogeneous reactions on aerosols and in clouds on photo-chemistry. A striking result was that the improved module did not always lead to improved agreement with observations.

A study on aerosols with interaction by clouds was carried out by Roelofs (1992). Schaap (2003) incorporated an aerosol module in the LOTOS-model and made a detailed study of nitrate and compared model results with observations. Secondary inorganic aerosols-SIA—were modelled by Banzhaf (2014). Special attention was given to the non-linear relation between precursor emissions and SIA-concentrations.

Deposition studies were performed by Erisman (1992) concerning dry and wet deposition fluxes of SO_2, NO_x, and NH_3 based on observations and modeling, and by Duyzer (1995), an experimental study of dry deposition of nitrogen. Banzhaf (2014) made an improved module of cloud chemistry and wet deposition, Szinyei (2014) performed a model evaluation study for ozone dry deposition.

Emissions are an essential input to the models. In fact, as much attention should be given to the emission input as to the meteorological input. Unfortunately, many more scientists are working in the area of meteorology, and just a view in the area of emissions. Olivier (2002) gave an overview of the quality of global emissions, determining the uncertainty of emissions is a real challenge. Although most of the work by Mues (2013) was focussed on modeling air quality in a changing climate, she made an important contribution to emissions showing that including in an detailed way the time-variation of emissions clearly improves the model performance.

Satellite data are in potential an important contribution to the improvement of observations of chemical species. They have the advantage above ground-based observations that one instrument is used and they have a large spatial coverage, and form a large data-set. Ph.D.-studies showed the great potential of satellite data, but also made clear that these data, especially in the troposphere, have an inherent large uncertainty. Because observations are only possible under cloud-free conditions, the resulting bias should be considered in the further use of the data. Engelen (1996) studied the possibilities to measure ozone in the troposphere, Veefkind (1999) the same for aerosols. An attempt was made by Tuinder (2002) to use satellite data to obtain information about the OH-radical. This turned out to be too ambitious, but the study resulted in valuable information concerning the influence of clouds on the observations.

A special issue that is in most models still neglected, is the interaction between chemistry and turbulent mixing, a sub-grid scale phenomena that depends on the ratio between chemical and mixing time scales. Important contributions in this area have been made by Vila (1992) and Galmarini et al. (1997).

The studies mentioned above have, with contributions of many other studies, led to an in principle improved model. The question remains whether it can be shown that the current models agree better with observations than the models in 1975, and in case that is so, is that due to an improved model, or is it caused by improved emission input data, by improved meteorological descriptions, or more accurate observations, or simply more observations of more species, with a better spatial representativeness.

5 Model Improvement

The science question stated was: Can we, or how can we determine model improvement over the last 40/50 years. As an example modelled ozone concentration versus observed ozone. With the UAM in 1973, the correlation coefficient was around 0.7, with LOTOS-EUROS in 2019, it is about 07–0.8. Does this mean that there is no

model improvement? (Obviously, there are more statistical indexes, see AQMEII, this is just an example).

One can also state: Models have improved because there are better descriptions of dry and wet deposition, better chemistry including aerosols, improved modules for the impact of clouds on chemistry. Also the model input data have been improved; emission data have become more reliable. Meteorological data are available with finer grid resolution.

There is also a clear change from diagnostic to prognostic meteorology, and from off-line to online: coupling of meteorological and chemical processes. However, there seems to be no research that shows that these changes have led to model improvement in the sense of a better agreement between calculated and observed concentrations.

The fact that there are more observations for more species and more attention has been given to the spatial representativeness of observations has helped to improve the model evaluation process. More, and more detailed satellite data, like the recent TROPOMI-instrument, will also be of advantage. Faster and larger computers have made it possible that more model calculations over longer periods, with finer grid resolution and for more species can be made nowadays.

To investigate model improvement distinction should be made between improvement in input data like emissions, and real chemical transport model improvement. This improvement should be judged not on only concentrations, but also on the modelled dry and wet deposition. Unfortunately, only observations on wet deposition are available. This analysis of calculated dry and wet deposition together with concentrations- so to assess the mass-balance- is essential to avoid being right for the wrong reasons, and to avoid the temptation to tune the model to arrive at a better agreement between modelled and calculated concentrations. AQMEII—practice is to analyse concentrations and deposition simultaneously.

A sketch of a lay-out for a model improvement study could contain the following elements. A benchmark should be defined starting with a base-year, for example 1980—40 years ago. The benchmark should include the model of 1980, the emissions of 1980, the meteorology of 1980, the observations of 1980, resulting in the model performance in 1980. Then, the current model from 2019 should be taken, and again the emissions, meteorology, observations of 1980 should be used to perform model runs with the current model for the situation in 1980. Comparison between the results with the 1980 and with the 2019 model show then the real model improvement. Further studies can then be done using the 1980 model and the 2019 model for the current situation.

Experience shows that an improved, more detailed, more complicated model with more detailed modules does not lead automatically to a better model performance. The reason for this fact might be that the simpler models do contain the basic features in a correct way. Furthermore, the modeling will always contain inherent uncertainties in the modules, and in the input data emissions and meteorology. There is a limit in improving emissions, as a clear example, VOC-emissions will always have a substantial uncertainty. Concerning meteorology, the treatment of clouds and vertical

exchange, the stable boundary layer are still stumble blocks. Giving these uncertainties, an improved module for say, wet deposition will not necessarily improve the overall model results.

Two additional elements should be mentioned here: ensemble modeling and chemical data assimilation. Ensemble modeling, combining the results of several models, nearly always gives a better model performance for the ensemble than for any single models. This is due- in short- to cancelling out of errors in the single models, see f.e. Galmarini et al. (2012) and Solazzo et al. (2012). Chemical data assimilation is a mathematical method to combine, to integrate modeling and observations, see for example Eskes et al. (2012) and many other publications. The basic idea is that combining the knowledge in observations with the knowledge in modeling will lead to more than $1 + 1 = 2$. It might also improve the interaction between modeling people and observation people. With chemical data assimilation weaknesses/uncertainties in the model and its input can be detected, information can be obtained about the representativeness of observations. With chemical data assimilation satellite data can be made into "full" data-sets by combining satellite data with a chemical transport model. Chemical data assimilation is useful/essential for operational/application studies However, one should be careful to claim that data assimilation can improve "science", missing knowledge in a model cannot be found by data assimilation.

6 Conclusions

The results and assessment presented here lead to the conclusion that the current chemical transport models are better than 40/50 years ago because:

- The models contain more species, can perform calculations over longer time periods, over larger areas and with finer grid resolution
- The models contain improved modules
- There is currently much more model testing and evaluation, resulting in a more robust, solid model
- There is at the moment better interaction between meteorology people and air quality people then previously, which has led to meteorological input data with more attention for air quality aspects.

On the other hand, often the agreement between calculated and measured concentrations has not much improved, although—as stated above—the models have become more detailed and more complicated/sophisticated. The reason is that the older, more simpler models did already contain the basic features. And furthermore, there will always be an inherent uncertainty in the modules and in the input data, as in the emissions, that cannot be improved further. Also the major tumble blocks, clouds and non-linearity will form a barrier in further model improvement.

The major goal for the future is: Further understanding of atmospheric chemistry/air quality with the aim to help to improve the environment. And don't forget: The best is yet to come, Dylan (2017).

References

Banzhaf, S. (2014). *Modeling the fate of secondary inorganic aerosol and its precursors over Europe*. Ph.D.-study Free University Berlin, Germany.

Builtjes, P., et al. (1980). *Application of a photochemical dispersion model to the Netherlands and its surroundings*. 11th ITM, Amsterdam.

Denis, R., et al. (2010). A framework for evaluation of regional-scale numerical photochemical modeling systems. *Environmental Fluid Mechanics*. https://doi.org/10.1007/s10652-009-9163-2

Dentener, F. (1993). *Heterogeneous chemistry in the troposphere*. Ph.D.-study University Utrecht, the Netherlands.

Duyzer, J. (1995). *Dry deposition of nitrogen compounds to semi-natural ecosystems*. Ph.D.-study University Utrecht, the Netherlands.

Dylan, B. (1963). *The times they are a-changin'*.

Dylan, B. (2017). *Triplicate: The best is yet to come.*

Engelen, R. (1996). *Satellite observations of ozone*. Ph.D-study University Utrecht, the Netherlands.

Erisman, J. W. (1992). *Atmospheric deposition of acidifying compounds in the Netherlands*. Ph.D.-study University Utrecht, the Netherlands.

Eskes, H., et al. (2012). *Data assimilation and air quality forecasting*. 32th ITM, Utrecht, the Netherlands.

Galmarini, S. (1997). *Turbulent transport of nitrogen oxides in the atmospheric boundary layer*. Ph.D.-study University Utrecht, the Netherlands.

Galmarini, S., et al. (2012). Ensemble and Amet: Two systems and approaches to a harmonized, simplified and efficient assistance to air quality model developments and evaluation. *Atmospheric Environment*. https://doi.org/10.1016/j.atmosenv.2011.08.076

Junge, C. (1963). *Air chemistry and radioactivity*.

Latour, B. (2017). *Facing Gaia.*

Lelieveld, J. (1990). *The role of clouds in tropospheric chemistry*. Ph.D.-study University Utrecht, the Netherlands.

Mues, A. (2013). *Modeling air quality in a changing climate*. Ph.D.-study Free University Berlin, Germany.

Olivier, J. (2002). *On the quality of global emission inventories*. Ph.D.-study University Utrecht, the Netherlands.

Pasquill, F. (1962). *Atmospheric Diffusion.*

Raes, F. (2012). *Air and climate. Conversations about molecules and planets, with humans in between*. JRC7, 1278.

Rao, S. T., et al. (2012). *AQMEII: A two-continent effort for the evaluation of regional air quality models*. 32th ITM, Utrecht, the Netherlands.

Reynolds, S., Roth, P., & Seinfeld, J. (1973). Mathematical modeling of photochemical air pollution. *Atmospheric Environment, 7*.

Roelofs, G. J. (1992). *Aerosol and drop size dependent cloud chemistry*. Ph.D.-study University Utrecht, the Netherlands.

Schaap, M. (2003). *On the importance of aerosol nitrate in Europe*. Ph.D.-study University Utrecht, the Netherlands.

Slade, D. (1968). *Meteorology and Atomic Energy*, USAEC, Hep. NO TID-24190.

Solazzo, E., et al. (2012). Model evaluation and ensemble modeling for surface-level ozone in Europe and North America in the context of AQMEII. *Atmospheric Environment*. https://doi.org/10.1016/j.atmosenv.2012.01.003

Steyn, D. (2017). *The intellectual history of air pollution modeling as represented by the ITM meeting Series*. 35th ITM, Crete.

Szinyei, D. (2014). *Modeling and evaluation of ozone dry deposition*. Ph.D.-study Free University Berlin.

Thunberg, G. (2019). *No one is too small to make a difference.*

Tuinder, O. (2002). *Global distribution of OH Radical production in the troposphere based on satellite data.* Ph.D.-study University Utrecht, the Netherlands.
vanValk, P. (1992). *A model for cloud-chemistry: Simulations and observations.* Ph.D.-study University Utrecht, the Netherlands.
Veefkind, P. (1999). *Aerosol satellite remote sensing*. Ph.D.-study University Utrecht, the Netherlands.
Vila, J. (1992). *The influence of turbulence on chemical reactions in the atmospheric boundary layer*. Ph.D.-study University Utrecht, the Netherlands.

Questions and Answers

Questioner Name: Silvia Trini Castelli

Q: A colleague of us stated 20 years ago that models are affected by an intrinsic uncertainty, or error, around 30%. Do you think that we have a chance to go over it? Do you agree?

A: I agree that models will always have an inherent uncertainty, and that 30% is in fact not so bad. And as I stated, there is a limit in further model improvement. We should also not forget that observations have an inherent uncertainty also, not forgetting to include their spatial representativeness.

Questioner Name: Heinke Schluenzen

Q: Do you think that the bias of O_3 is also the same as 40 year ago? And as a remark: We might have to consider non-Gaussian error measures for very high resolution model result evaluation.

A: I did not look in other statistical measures, which I should have done. I think that the bias might has improved, but I don't have looked into these data. Using other statistical measures is a very good idea.

Questioner name: Bertrand Carissimo

Q: I was interested in your point that model improvement does not show in the statistical comparison with observations because I encounter this problem in my work on small scale modeling. So my suggestion is do we need also to improve the statistics? This is a serious remark as for example, with current statistics, a refined model that reproduces a realistic small feature at slightly the wrong place and wrong time will do worse than a larger scale model that does not reproduce the feature.

A: My first answer is that the focus should be on model improvement, not on improvement in statistics because that does not change the model results. I do agree that we should look into other statistical measures in addition to the conventional ones. See also the remark by Heinke Schluenzen.

Questioner name: Steven Hanna

Q: You say that the correlations between model predictions and observations of ozone have remained at about 0.7 for the past 40 years. But isn't it easy for an ozone model to have a good correlation because observed concentrations are usually high in the day and low at night? Even a bad model should be able to reproduce that behaviour.

A: I agree, any simple, but still basically correct model is able to model ozone right. My point is that I think that, due to inherent uncertainties, it will be impossible to have a model for ozone with a correlation of 0.9.

Questioner Name: B. Armand

Q: You say that observations do not lead to knowledge. I am not sure that everyone would agree with you. What do you think of Big Data?

A: My opinion is that just observations without further data-analysis or modeling do not lead to knowledge, this just lead to data. In case Big Data are seen as just many data, which are subsequently used to create algorithms without further thinking, this should in my opinion be avoided. It might even be dangerous and lead to misleading algorithms and correlations that give the wrong information.

Timely Update of Emission Inventories with the Use of Satellite Data

Jonilda Kushta, George K. Georgiou, and Jos Lelieveld

Abstract Cyprus is located in the eastern Mediterranean, an environmentally intriguing area that is subject to complex air pollution conditions, and has to be prepared for many climatic challenges. Air quality assessment and forecasting is an essential tool in strengthening the country's adaptation strategy, providing relevant information to sectors such as agriculture and tourism, helping reduce health related financial and human life costs, as well as establishing a core national priority axis for knowledge outreach to neighbouring countries. The use of current and next generation satellite information can open a new area in operational forecasting and scientific assessment of air quality and emissions in this complex region with past, current and projected societal, financial and geo-political influences. In this work we identify and elaborate on the discrepancies of emission inventories in the region and the use of satellite data for their timely update. Utilizing the EDGAR-HTAP emission inventories compiled by the Joint Research Center for the year 2010, we use a model-based methodology to update them based on satellite-derived trends. Initially we produce a model-based concentration-vertical column density (VCD) relation derived from sensitivity tests of NO_x emission fluxes in the WRF-Chem regional atmospheric model. Consequently, we translate the monthly trends obtained by satellite observations for the period 2010–2015 to produce updated emission inventories. Model simulations with the current and modified emission inventory are used to assess the discrepancies derived.

J. Kushta (✉) · G. K. Georgiou · J. Lelieveld
Climate and Atmosphere Research Center, The Cyprus Institute, Nicosia, Cyprus
e-mail: j.kushta@cyi.ac.cy

G. K. Georgiou
e-mail: g.georgiou@cyi.ac.cy

J. Lelieveld
e-mail: J.lelieveld@mpic.de

J. Lelieveld
Max Planck Institute for Chemistry, Mainz, Germany

© The Author(s), under exclusive license to Springer-Verlag GmbH, DE, part of Springer Nature 2021

C. Mensink and V. Matthias (eds.), *Air Pollution Modeling and its Application XXVII*, Springer Proceedings in Complexity, https://doi.org/10.1007/978-3-662-63760-9_10

1 Introduction

Modeling approaches, consisting of a mathematical representation of the physico-chemical processes that take place in the atmosphere, provide a versatile tool for air quality and impact assessment. The accuracy of the modeling systems however depends on the number and complexity of the atmospheric processes that they account for and the accuracy of the input data. Regarding the second challenge, pollutant emission fluxes have been recognized by several regional and global studies as a crucial parameter in the qualitatively and quantitatively efficient representation of air pollution features. Global anthropogenic emission inventories usually comprise of a compilation of national reported data (or, if missing, previous older estimates) usually developed at a frequency of 10 or more years. In the blank time-window between new estimates, emissions are dealt with as non-changing. There are regions, one of which the Eastern Mediterranean and Middle East, that under the pressure of unforeseen (in intensity and duration) financial and geo-political factors, do not adhere to projected emission change rates, in magnitude and sometimes even in sign (Lelieveld et al., 2015). Given the interlinked nature of regional industrial activities and financial (in)stability, modifications of the 'business as usual or as estimated' industrial and residential workload in one region affect other regions as well modifying their 'business as usual or as estimated' landscape. We propose the use of satellite information to overcome the non-frequent update of emission inventories given their spatially unbiased (from estimates and projections) representation and we investigate the importance of frequent localized emission revision for sensitive regions like the EMME.

2 Methodology

We utilize the Weather Research and Forecasting model coupled with chemistry (Grell et al., 2005) to apply the Lamsal et al. (2011) methodology regarding the identification of the relationship between NO_x emissions and NO_x vertical column density (VCD) in our area of interest. To achieve this objective two simulations are performed: one with the original EDGAR HTAP v2.2 global emissions as provided by the Joint Research Center (JRC) for the year 2010 (base case simulation thereafter referred to as WRF_{HTAP}) described in Janssens-Maenhout et al. (2015) and the second with a 30% perturbation in the emission fluxes of each grid cell (covering an area of $0.1^\circ \times 0.1^\circ$ degrees). The ratio between the difference in NO_x emissions ($\Delta E/E = 30\%$) and the resulting difference in modelled NO_x VCD ($\Delta\Omega/\Omega$) is defined as a factor (β) that describes in a linearized way the non-linear nature of the relationship between emissions and concentrations of NO_2 in the atmosphere. We propose the use of the inverse beta factor to the one in Lamsal et al. (2011) given that $\Delta E/E$ in the beta calculation procedure is a constant number and we keep it in the denominator position (instead of the numerator position of Lamsal et al.) and assess the differences in the

nominator $\Delta\Omega/\Omega$ being smaller or larger than the emission perturbation. Thus, when the beta factor is less than 1 ($\beta < 1$) the result denotes that an emission reduction of 30% causes—a less than—30% change in NO_x VCD indicating a more efficient NO_x loss, a result of higher OH levels in low-NO_x environments. When $\beta > 1$ enhanced NO_x levels supress OH levels resulting a relative increase in NO_2 columns larger than the perturbation in emissions (<30%).

Subsequently, the β factor can be used to update emission inventories based on emission trend analysis derived from satellite VCD. Emissions of year *y* can be thus derived from emissions of year *x* based on the changes of VCDs derived from satellite measurements between year *x* and *y*. We update the emissions of 2010, last available monthly EDGAR-HTAP emissions, to 2015, based on trend analysis derived from tropospheric NO_2 columns from the Ozone Monitoring Instrument onboard NASA's EOS Aura mission homogenized in the framework of the EU FP7 Quality Assurance for Essential Climate Variables project (Boersma et al., 2017).

The model domain extends from Northern Africa to Europe and eastward includes the whole Arabian Peninsula at a resolution of 50 km. After deriving 'new' updated emission fluxes for 2015 we compare NO_x and O_3 concentrations over EMME between simulations to investigate the magnitude of discrepancies in model results introduced by the emission inventories (and localized changes in those not accounted for in traditional approaches).

3 Results and Discussion

Winter and summer monthly averaged β factors (January and July 2015) are shown in Fig. 1. During winter months there is an overall horizontally smooth response of modelled VCD to the perturbation in emissions comprising of a change in VCD larger than of the emissions (>30%) and a resulting $\beta > 1$. This result could be a reflection of the limited photochemical activity during winter months over all domain as well as limited vertical mixing processes and a longer lifetime of NO_x in the atmosphere. During spring, fall and particularly in summer the β values have both >1 and <1

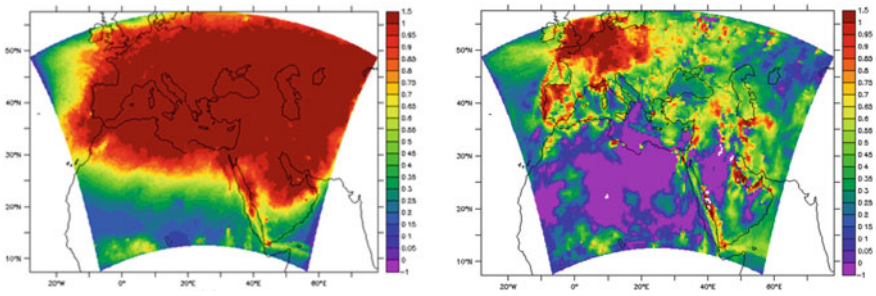

Fig. 1 Beta factor in January (left) and July (right)

values differentiating between the response of NO_2 VCD to NO_x emissions near NO_x sources and downwind distant regions, contrary to the less contrasted landscape of response during winter months. Distinctly over Central Europe, Gulf region and in proximity to other significant emission sources β is close to or larger than one while in the rest of domain it ranges between 0 and 1.

We apply the beta factors to derive an updated emission inventory at global scale (at monthly time scale)—with only the values within our model domain being modified. For reference we show in Fig. 2 how the beta factor mapped over the model domain is converted to a global variable with missing values in the rest of the world, resulting in emission differences in EDGAR-HTAP v2 mapping only where our initial study area (model domain) was set (Fig. 2a) to be compatible with the representation of the original emissions (Fig. 2b). Despite the figure depicting a global map the emissions have only changed in our area of study. The same base case simulation is then repeated with the modified emissions (thereafter WRF_{BETA}) and the differences between the ozone landscape in the original HTAP emission simulation $C_{O3\text{-}HTAP}$ and the modified emissions based on OMI trends $C_{O3\text{-}BETA}$ are depicted in Fig. 3.

We identify areas in Eastern Mediterranean that react to the modification of the emissions, such as Greece that after 2010 experienced a prolonged economic crisis

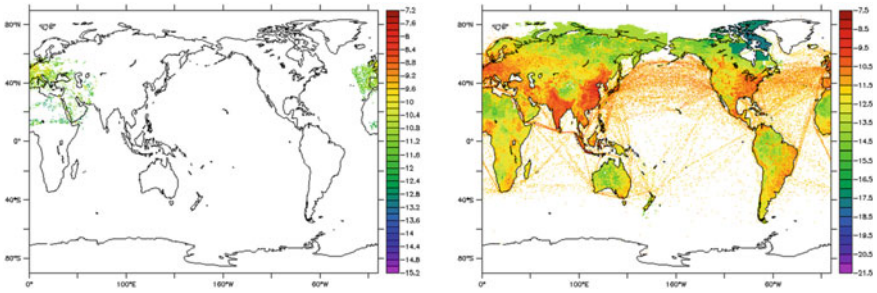

Fig. 2 Difference in emission fluxes of NO_x as derived from the satellite trends between 2010 and 2015 (left) and an original EDGAR-HTAP v2 representation of NO_x emissions (right)

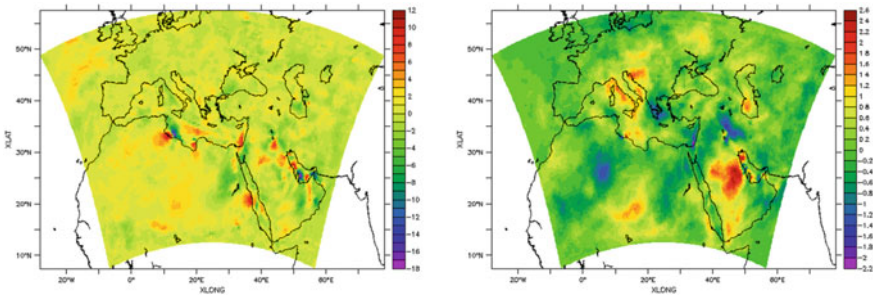

Fig. 3 NO_2 (left in %) and O_3 (right in $\mu g/m^3$) differences derived from differences in emission fluxes of NO_x as derived from the satellite trends between 2010 and 2015 expressed as C_{HTAP}-C_{BETA}

that led to a decline in both column and surface NO_2 levels Fig. 3 (left plot). Thus the use of the original emissions overestimate NO_2 values in this area. Changes in NO_x emission fluxes affected also secondary gaseous and aerosol pollutants such as ozone and fine particular matter as shown in Fig. 3 (right plot). Over Greece we see that the declining concentrations of NO_2 as a result of the reduction in local emissions of NO_x is associated with an increase in ozone due to reduced titration by NO. This behavior is also evident over Eastern Mediterranean coastal zone, west of Israel and Lebanon.

4 Conclusion

Satellite information on the columnar density of short-lived air pollutants like NO_x can prove useful in assessing the changes that occur in real life in the emission intensity of those as well as provide insight on missing sources and/or non-operational ones. The non-linear nature of the relationship between NO_x emissions and concentrations can be captured with a linear expression that, in turn, can be used to timely update emission inventories of year x to the year of interest y by deriving satellite VCD change rates. This approach can be extremely important for regions that experience unforeseen geopolitical and economic changes even in very abrupt time scales, leading to Nemissions deviating significantly from the reported, official spatiotemporal mapping.

Acknowledgements This work was made feasible with the use of the WRF-CHEM Pre-processing Tools for the Community (https://www2.acom.ucar.edu/wrf-chem/wrf-chem-tools-community) provided by the Atmospheric Chemistry Observations and Modeling Lab (ACOM) of NCAR. We acknowledge the use of the QA4ECV NO_2 datasets from http://temis.nl/qa4ecv/dois/no2_doi.html and emissions from https://edgar.jrc.ec.europa.eu/htap_v2/. This study received funding from the Government of Cyprus through the ESA Contract under the PECS (Plan for European Cooperating States) no. 4000124009/18NL/SC for the META-Sat project.

References

Boersma, K. F., et al. (2017). *QA4ECV NO_2tropospheric and stratospheric vertical column data from OMI (Version 1.1).* Royal Netherlands Meteorological Institute. https://doi.org/10.21944/qa4ecv-no2-omi-v1.1

Grell, et al. (2005). Fully coupled "online" chemistry within the WRF model. *Atmospheric Environment, 39*, 6957–6975. https://doi.org/10.1016/j.atmosenv.2005.04.027

Janssens-Maenhout, G., et al. (2015). HTAP_v2.2: A mosaic of regional and global emission grid maps for 2008 and 2010 to study hemispheric transport of air pollution. *Atmospheric Chemistry and Physics, 15*, 11411–11432. https://doi.org/10.5194/acp-15-11411-2015

Lamsal, et al. (2011). Application of satellite observations for timely updates to global anthropogenic NO_x emission inventories. *Geophysical Research Letters, 28*, L05810.

Lelieveld, J., et al. (2015). Abrupt recent trend changes in atmospheric nitrogen dioxide over the Middle East. *Science Advances, 1*, e1500498. https://doi.org/10.1126/sciadv.1500498

Questions and Answers

Questioner: Pius Lee

Question: Thank you for forward looking setting eyeballs on TROPOMI with finer temporal resolution. Perhaps in future advances even much more finer spatial resolution data. However very fine spatial resolved data may also give misleading information from transported attributions. How those new advances reconcile well with ship track emissions? Would meteorological measurements from Sentinel help?

Answer: Shipping emissions usually are located in clean background environments, however the validity of the methodology with higher spatial resolution satellite data remains to be assessed. Meteorological data might prove useful to separate emission source impact from transport of pollution.

Questioner: George Tsegas

Question: The 1 km emission inventory for Cyprus does not contain full information for the occupied areas on the north. Do you expect that this lack of information could introduce additional uncertainties at the corresponding grid cell?

Answer: With this method only grid cells with values above a certain threshold are updated. Missing data remain such. However, there are tools to not only update the change in emissions but also the absolute magnitude based on satellite information which is planned to be performed by our group.

Questioner: Marc Guevara

Question: Did you evaluate your timely update of emissions methodology against existing emission inventory and how can you derive sector-dependent beta factors using your methodology?

Answer: We have not produced past emission inventory to evaluate the methodology. For sector-based beta, this is a complicated issue because satellites see all vertical information without differentiating emission sources and possibly necessitates the use of other satellite products (pollutants) to be used as proxies for specific sectors.

Modeling Atmospheric Composition in the Summertime Arctic: Transport of North American Biomass Burning Pollutants and Their Impact on the Arctic Marine Boundary Layer Clouds

Wanmin Gong, Stephen Beagley, Roya Ghahreman, Ayodeji Akingunola, and Paul A. Makar

Abstract Cases of the transport of NA biomass burning plumes into the Canadian Arctic were identified based on existing model simulations, using the Environment and Climate Change Canada's on-line air quality forecast model (GEM-MACH). Analysis shows that, in one case, the pollutants from wild fires in northern Canada were first transported northwards rising against the polar dome then eastwards descending into the study area in the Canadian Arctic archipelago as the polar dome weakened and retreated out of the region. Precipitation associated with the uplifting of the air mass over the polar dome was responsible for scavenging aerosols in the initial fire plume but CO, unaffected by wet scavenging, remained in the air mass and hence impacted the study area. In another case, the study area is shown to be affected by the transport of an air mass up Baffin Bay within the marine boundary layer influenced by both biomass burning in northern Canada and anthropogenic pollution of eastern North America. Model simulations were also conducted using the fully coupled version of GEM-MACH to investigate the impact of biomass burning aerosols on the Arctic marine boundary layer clouds. The study shows that, during the transient period, there is an enhancement in average droplet number concentration and decrease in average droplet diameter of liquid water clouds in the Arctic due to the influence of northern Canada's biomass burning aerosols.

W. Gong (✉) · S. Beagley · R. Ghahreman · A. Akingunola · P. A. Makar
Air Quality Research Division, Science and Technology Branch, Environment and Climate Change Canada, Toronto, ON, Canada
e-mail: Wanmin.gong@ec.gc.ca

S. Beagley
e-mail: Stephen.beagley@ec.gc.ca

R. Ghahreman
e-mail: roga.ghahreman@ec.gc.ca

A. Akingunola
e-mail: Ayodeji.akingunola@ec.gc.ca

P. A. Makar
e-mail: paul.makar@ec.gc.ca

© Crown 2021

C. Mensink and V. Matthias (eds.), *Air Pollution Modeling and its Application XXVII*, Springer Proceedings in Complexity, https://doi.org/10.1007/978-3-662-63760-9_11

Keywords Arctic atmospheric composition · Transport of biomass burning pollutants · Aerosol-cloud interaction

1 Introduction

The Arctic is recognized as one of the key areas of the globe in terms of its sensitivity to climate change. The Arctic environment is undergoing rapid changes in recent years including rising temperature, melting sea ice, lengthening of warm seasons, and changing circulation patterns. There is a growing interest in better understanding the processes affecting the Arctic climate. Past Arctic air pollution research has been largely focused on the winter-spring transition period when the Arctic haze is prevalent. The summertime Arctic is generally characterised by a relatively clean lower atmosphere due to the slower transport from the lower latitudes and more efficient wet deposition. However, it has become evident that North American (NA) boreal forest fire plumes can be transported into the Arctic during summer, which will have an impact on the local radiation balance given the availability of shortwave radiation, high surface albedo, and the persistent presence of strongly reflective low-level stratus cloud decks in the Arctic summer.

In this study, based on model simulations of a recent summer field campaign carried out over the Canadian Arctic archipelago, using the Environment and Climate Change Canada's on-line air quality forecast model GEM-MACH (Gong et al., 2018), several cases of the transport of NA biomass burning plumes into the study region were identified. Analysis based on model back-trajectories were carried out to examine the transport mechanisms and the processing of the fire plumes en-route to the Arctic. Model simulations were also conducted using a fully-coupled version of GEM-MACH to investigate the impact of biomass burning aerosols on the formation and characteristics of marine boundary layer clouds.

2 Transport Cases During the 2014 NETCARE Field Campaign

Figure 1 shows two cases (flights) during the 2014 NETCARE Polar-6 campaign based at Resolute, Nunavut (Abbatt et al., 2019). Both flights were conducted during the second half of the Polar-6 campaign (July 17–21, 2014) when the study area was under an upper-level low experiencing several frontal systems, which brought in relatively warm and moist air from lower latitudes and the influence of wildfire plumes. In the first case (July 17 flight), both measurements and model simulation show a layer of relatively polluted air at ~1 km above the surface with elevated concentrations in CO and various aerosol components (Fig. 1a). Not included in the figure are the results from the repeated model simulation without the North American wild fire emissions where the modelled elevated CO peak disappeared while it made

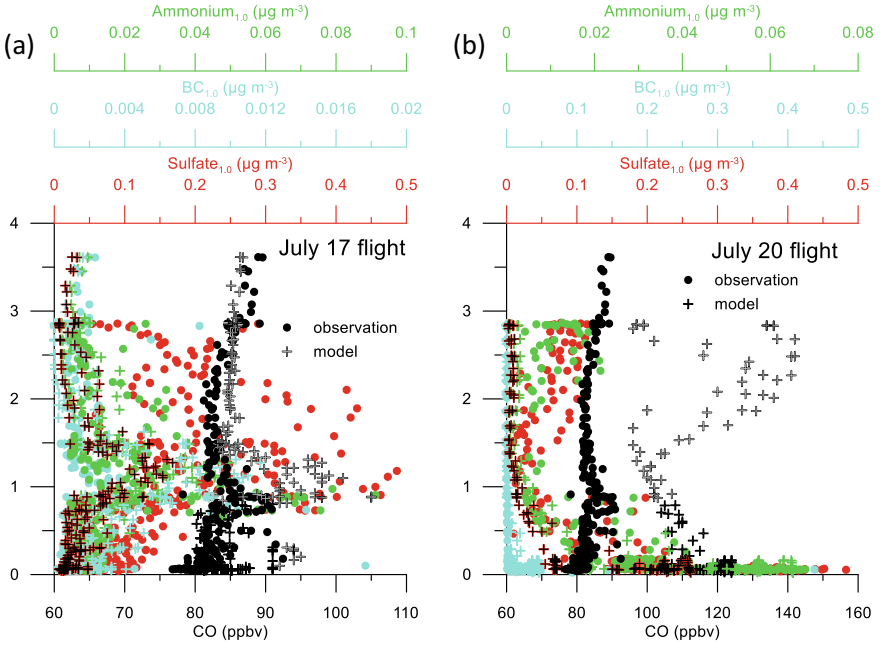

Fig. 1 Measurement and modelled CO and aerosol components for two Polar-6 flights during the 2014 NETCARE campaign: **a** July 17, 2014; **b** July 20, 2014

no changes in the modelled aerosol components during this flight. In the second case (July 20 flight; Fig. 1b), both measurements and model show relatively polluted air close to the surface. The model simulated high concentrations of CO and aerosol components were reduced (but not eliminated) when the NA wild fire emissions were excluded (not shown).

Based on CO and CO_2 measurements onboard polar 6 during the 2014 NETCARE campaign and 10-day kinematic back trajectories analysis, Bozem et al. (2019) determined a polar dome boundary to be located at ~73.5 N with strongest gradient in potential temperature between 299 and 305.5 K, separating air masses within the polar dome from those outside. Figure 2 shows the virtual potential temperature and

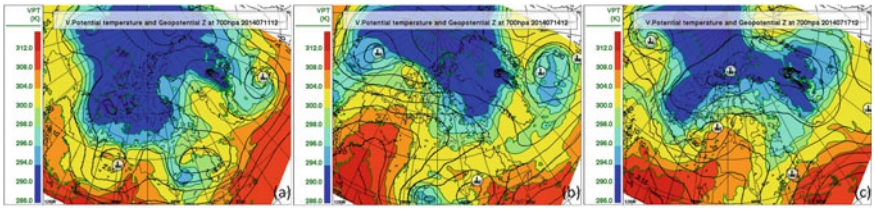

Fig. 2 Modelled virtual potential temperature and geopotential height at 700 hpa from GEM-MACH at 12 UTC on July 11, 14, and 17, 2014, respectively

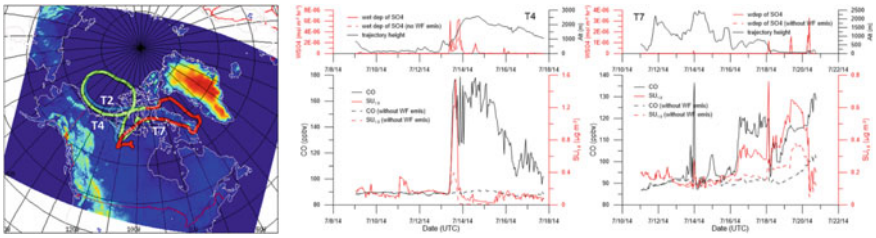

Fig. 3 Left panel: horizontal paths of three back trajectories (T2, T4, and T7; see text for description); right panel: time series of tracers (CO and $SU_{1.0}$), bottom, and wet deposition flux (WSO_4) of sulfate as well as the trajectory height, top, extracted along trajectory T4 and T7

geopotential height at 700 hpa simulated by GEM-MACH during the study period. Sharp gradient in virtual potential temperature is found between 290 and 300 K, which seems to define the cold polar air mass (or polar dome) in this case. The polar dome so defined is seen over the central Arctic extending to Canadian archipelago during the first period of the field campaign (July 4–12, 2014), isolating the study area from transport from lower latitudes. By mid July, the polar dome seemed to weaken and retreat out of the Canadian archipelago with a series of low-pressure systems moving through the study region from the west.

Back trajectories arriving at measurement locations and times corresponding to the elevated and surface based plumes in Fig. 1 were computed using a Lagrangian particle dispersion and trajectory model (MLDP, D'Amours et al., 2015) and hourly GEM-MACH wind fields. Figure 3a shows horizontal locations of three back trajectory paths: trajectories "T2" and "T4" are associated with the observed and modelled plumes on the July 17 flight (see Fig. 1a); trajectory "T7" is associated with the near-surface plume observed and modelled on the July 20 flight (see Fig. 1b). For the two flights, the air mass arrived at the measurement locations via quite different routes. For the July 17 case, the trajectories traced back to east of Great Bear Lake (Northwest Territories) 5 days prior, then tracking northward initially and ascending rapidly to 3 km (coinciding with the polar dome boundary as indicated in Fig. 2b), before turning around over the Beaufort Sea and traveling eastwards and slowly descending to flight location (at ~1 km). Plotted in Fig. 3b are time series of modelled tracer concentrations (CO and particulate sulfate at 1 μm size cut, $SU_{1.0}$), extracted along the trajectories (T4 and T7). The T4 tracer time series shows a sharp increase in CO and $SU_{1.0}$ as the trajectory moving north and ascending. The sharp increase is absent (particularly for CO) when wild fire emissions were turned off in model simulation. The CO concentration decreases gradually with time due to dispersion, while $SU_{1.0}$ concentration decreases sharply following the initial sudden enhancement. The rapid decrease in $SU_{1.0}$ concentration along the trajectory coincides with the wet removal events shown in the WSO_4 time series, indicating that the precipitation associated with the uplifting against the polar dome is responsible for the decease in $SU_{1.0}$ concentration along the trajectory. In the case of the July 20 flight, the back trajec-

tory route and time series indicate that the relatively polluted air mass affecting the study area was transported along Baffin Bay at low altitudes influenced by both NA wildfire emissions and anthropogenic emissions in eastern North America.

3 Impact of NA Wildfire Pollutants on Arctic Low-Level Clouds

The role of aerosols and the impact of NA wildfire pollutants on Arctic low-level clouds were examined by using a fully-coupled version of GEM-MACH which includes the representation of on-line aerosol effects on radiation and cloud microphysics (Makar et al., 2015a, 2015b; Gong et al., 2015). Model simulations using the fully coupled GEM-MACH were conducted with and without the NA wild fire emissions. The analysis here focuses on the second period of the 2014 NETCARE polar-6 campaign when the study area was influenced by transport from lower latitudes outside the polar dome. Figure 4 shows the probability distributions of modelled cloud droplet number concentration (CDNC) and cloud droplet mass-mean diameter (MMD). The statistical analysis was conducted over an area within 50–130° W and north of 70° N on grids with modelled cloud liquid water content (LWC) >0.01 g/kg. The CDNC distribution shifts to smaller number concentrations without the NA wildfire emission and, correspondingly, the MMD distribution shifts to larger sizes. In other words, the impact of NA wildfire pollutants on the Arctic liquid clouds is an overall enhancement in CDNC and reduction in droplet size. Included in Table 1 are summary statistics on selected cloud microphysics and aerosol parameters. The enhancement in CDNC is consistent with the increase in aerosol number concentrations in the >100 nm (N100) and >50 nm (N50) size ranges, due to the NA biomass burning. Despite the large impact on CDNC and MMD from NA biomass burning, the impact on bulk LWC is less significant.

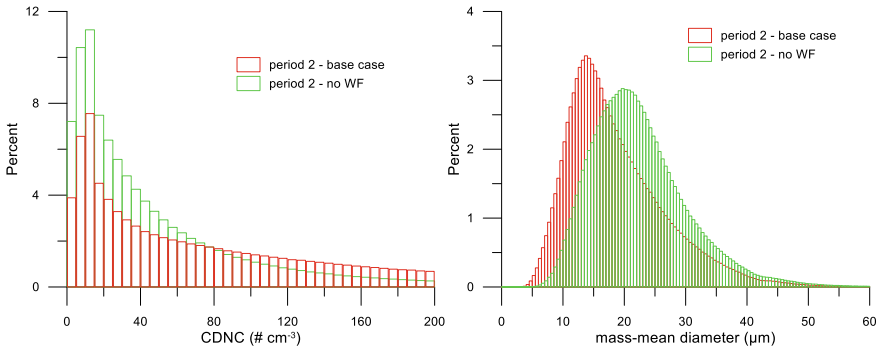

Fig. 4 Probability distributions of modelled CDNC and MMD, with and without the NA wildfire emissions, for the period of July 17–21, 2014 over the analysis area (see text for description)

Table 1 Cloud and aerosol summary statistics for the period July 17–21, 2014 (values in parenthesis are from measurements reported in Leaitch et al. (2016))

	With NA WF			Without NA WF		
	Mean	Median	5 | 95 percentile	Mean	Median	5 | 95 percentile
CD NC (#/cm^3)	140.2 (73)	75.8 (52)	5.9 (13) | 500.3 (228)	60.3	31.7	3.8 | 203.4
LWC (g/m^3)	0.26 (0.12)	0.18 (0.12)	0.02 (0.025) | 0.85 (0.26)	0.23	0.15	0.02 | 0.69
MMD (μm)	18.9 (15.0)	16.9 (14.5)	8.7 (9.1) | 34.5 (21.4)	22.8	21.4	11.8 | 37.3
N50 (#/cm^3)	250.3 (126)	92.4 (68)	2.5 (29) | 1043.7 (334)	57.4	22.9	1.7 | 202.7
N100 (#/cm^3)	86.4 (81)	42.6 (31)	0.6 (13.8) | 322.6 (274)	16.2	6.8	0.4 | 65.4

Table 1 also includes (in parenthesis) corresponding summary statistics from Leaitch et al. (2016) based on measurements taken on the Polar-6 flights. Qualitative agreement between model and measurement can be found: for example, both model and measurement indicate the activation of aerosol particles smaller than 100 nm. However, the model seems to over-predict CDNC and LWC significantly. Further investigation is underway.

References

Abbatt, J. P. D., et al. (2019). Overview paper: New insights into aerosol and climate in the Arctic. *Atmospheric Chemistry and Physics, 19*, 2527–2560. https://doi.org/10.5194/acp-19-2527-2019

Bozem, H., et al. (2019). Characterization of transport regimes and the Polar Dome during Arctic spring and summer using in-situ aircraft measurements. *Atmospheric Chemistry and Physics, Discussions* (in review).https://doi.org/10.5194/acp-2019-70

D'Amours, R., et al. (2015). The Canadian meteorological centre's atmospheric transport and dispersion modeling suite. *Atmosphere-Ocean, 53*(2), 176–199. https://doi.org/10.1080/07055900.2014.1000260

Gong, W., et al. (2015). Modeling aerosol cloud meteorology interaction: A case study with a fully coupled air quality model GEM-MACH. *Atmospheric Environment, 115*, 695–715. https://doi.org/10.1016/j.atmosenv.2015.05.062

Gong, W., et al. (2018). Modeling regional air quality in the Canadian Arctic: Simulation of an Arctic summer field campaign. In C. Mensink & G. Kallos (Eds.), *'Air Pollution Modeling and Its Application XXV', edit* (pp. 401–406). Springer.

Leaitch, W. R., et al. (2016). Effects of 20–100 nm particles on liquid clouds in the clean summertime Arctic. *Atmospheric Chemistry and Physics, 16*, 11107–11124. https://doi.org/10.5194/acp-16-11107-2016

Makar, P. A., et al. (2015a). Feedbacks between air pollution and weather, part 1: Effects on weather. *Atmospheric Environment, 115*, 442–469.

Makar, P. A., et al. (2015b). Feedbacks between air pollution and weather, part 2: Effects on chemistry. *Atmospheric Environment, 115*, 499–526.

Questions and Answers

Questioner: Heinke Schlunzen

Question: Did you simulate soot and compare deposition of soot?

Answer: We do include soot (modelled as black carbon) in our simulations including black carbon from biomass burning. Black carbon deposition is also calculated, but we have not looked at this yet in this study. One important source of aerosols (particularly for summer Arctic) is wind-blown dust, which is not yet represented in our model.

Effect of Aerosol Nitrate Photolysis on Wintertime Air Quality

Golam Sarwar, Daiwen Kang, and Rohit Mathur

Abstract Recent field and laboratory studies suggest that aerosol nitrate can undergo photolysis over the marine environment to generate gaseous nitrous acid and nitrogen dioxide. In this study, we examine the effect of aerosol nitrate photolysis on air quality using the hemispheric Community Multiscale Air Quality (CMAQ) model. Consistent with other air quality models, CMAQ currently does not contain the photolysis of aerosol nitrate. We add the photolysis of aerosol nitrate to the CMAQ model using recently published rate expression developed based on laboratory experiments and apply the photolysis of aerosol nitrate only over marine environments. Simulations are performed without and with the photolysis of aerosol nitrate over the Northern Hemisphere. Model results suggest that the photolysis of aerosol nitrate decreases annual mean surface aerosol nitrate over the ocean by ~60%, enhances annual mean surface nitrous acid by ~60%, and enhances annual mean surface ozone by ~17%. Enhanced ozone over marine environment is transported to land areas which increases annual mean surface ozone by 1–7 ppbv over large land-based areas. Simulated nitrous acid with the photolysis of aerosol nitrate agree better with observed data. Simulated ozone with the photolysis of aerosol nitrate reduces mean bias in cooler months but increases the bias in warmer months compared to observations in the United States and Japan.

Keywords Aerosol nitrate · Photolysis · Nitrous acid · Nitrogen dioxide · Ozone

G. Sarwar (✉) · D. Kang · R. Mathur
Center for Environmental Measurement & Modeling, U.S. Environmental Protection Agency, RTP, NC, USA
e-mail: sarwar.golam@epa.gov

D. Kang
e-mail: kang.daiwen@epa.gov

R. Mathur
e-mail: mathur.rohit@epa.gov

This is a U.S. government work and not under copyright protection in the U.S.; foreign copyright protection may apply 2021

C. Mensink and V. Matthias (eds.), *Air Pollution Modeling and its Application XXVII*, Springer Proceedings in Complexity, https://doi.org/10.1007/978-3-662-63760-9_12

1 Introduction

Ye et al. (2016) recently suggested that particulate nitrate (pNO_3) can undergo photolysis over marine environments to produce nitrous acid (HONO) and nitrogen dioxide (NO_2). They conducted aircraft measurements of gaseous and aerosol species over the North Atlantic Ocean during July 2013 and performed box model simulation using measured chemical species and known atmospheric chemistry to predict atmospheric HONO concentrations. The box model with known atmospheric chemistry could not predict observed high HONO concentrations over the marine environment. When they introduced the photolysis of pNO_3, the box model successfully reproduced observed HONO concentrations. They also performed laboratory chamber experiments involving ambient aerosol samples and detected HONO and NO_2 from the photolysis of pNO_3. Here, we examine the potential impact of modeled pNO_3 photolysis over marine environments on air quality.

2 Method

We use the hemispheric Community Multiscale Air Quality (CMAQ) model (Mathur et al., 2017) using a horizontal resolution of 108-km and 44 vertical layers. Vukovich et al. (2018) previously developed 2016 hemispheric emissions for the CMAQ model which we use in this study. The Weather Research and Forecasting (WRFv3.8) (Skamarock, 2008) model was used to prepare meteorological fields for the CMAQ model. Similar to all other air quality models, the current CMAQ model (5.3) does not contain photolysis of pNO_3. We incorporate the photolysis of pNO_3 with the following reaction using the photolysis rate suggested by Ye et al. (2017):

$$pNO_3 = 0.67 \times HONO + 0.33 \times NO_2 \quad (1)$$

We performed two model simulations for 2016. One simulation uses the Carbon Bond chemical mechanism (CB6r3) (Emery et al., 2015) without the photolysis of pNO_3 while the other simulation uses CB6r3 with the photolysis of pNO_3. Differences in the results between the two simulations are attributed to the photolysis of pNO_3.

3 Results and Discussion

Predicted pNO_3 concentrations are compared with observed data from the Clean Air Status and Trends Network (CASTNET) in the U.S. Monthly mean bias (MB) for both simulations at CASTNET sites ranged within ± 0.2 $\mu g/m^3$. Thus, CMAQ predicted pNO_3 concentrations are in reasonable agreement with observed data. Reed (2017)

reported mean observed night-time HONO levels of ~0.6 pptv and a daytime peak level of ~3.5 pptv at the Cape Verde Atlantic Observatory (CVAO). The simulation without the photolysis of pNO_3 predicts night-time HONO levels of ~0.1 pptv and a daytime peak value of only ~0.35 pptv. Thus, the simulation without the photolysis of pNO_3 substantially underestimates both the night and day-time observed HONO at CVAO. In contrast, the simulation including the photolysis of pNO_3 predicts night-time values of ~1.2 pptv and a day-time peak value of ~5.7 pptv. Thus, simulated HONO levels with the photolysis of pNO_3 compare better with the observed data from the CVAO site. However, it tends to overpredicts the observed data.

The simulation with the photolysis of pNO_3 increases ozone (O_3) levels not only over the ocean but also over land. It increases annual mean surface O_3 over the ocean from 20.5 to 23.9 ppbv. The spatial distribution of the annual mean surface O_3 without and with enhancements for the photolysis of pNO_3 are shown in Fig. 1. The simulation without the photolysis of pNO_3 predicts higher concentrations of O_3 over land and lower concentrations over the ocean. The simulation with the photolysis of pNO_3 enhances O_3 by 1–10 ppbv over the oceanic areas and 1–7 ppbv over the land areas. It enhances O_3 to a greater extent over the western United States than over the eastern United States.

Simulated O_3 levels are compared to observed data from the CASTNET sites in the United States in Table 1. The simulation without the photolysis of pNO_3 underestimates observed data in cooler months and overestimates the concentrations in warmer months. The simulation with the photolysis of pNO_3 improves the predictions in cooler months but deteriorates the comparison in warmer months. Similarly, the simulation with the photolysis of pNO_3 improves the predictions in cooler months when compared to observations from Japan (Acid Deposition Monitoring Network in East Asia, www.eanet.asia/eanet) (Table 2) but deteriorates the comparison in warmer months.

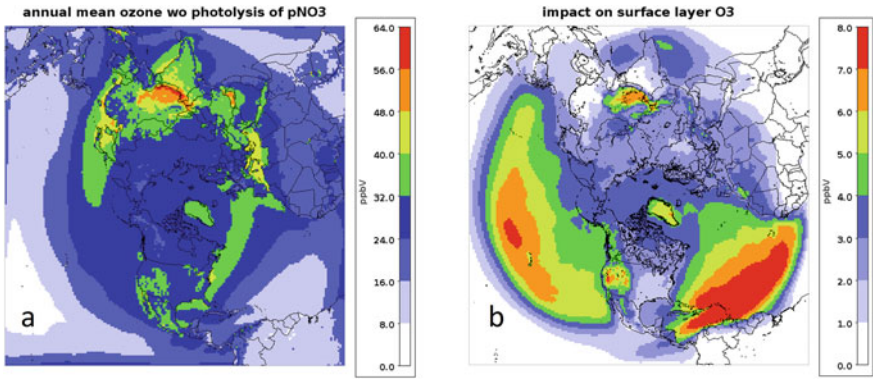

Fig. 1 **a** Simulated annual mean O_3 without the photolysis of pNO_3 and **b** annual mean enhancements due to the the photolysis of pNO_3

Table 1 A comparison of monthly mean bias of daily maximum O_3 at CASTNET sites

Month	Mean bias without the photolysis of pNO_3 (ppbv)	Mean bias with the photolysis of pNO_3 (ppbv)
1	−1.5	+0.5
2	−3.0	−1.4
3	−3.5	−0.1
4	−4.3	+0.1
5	−4.3	+0.3
6	−2.5	+3.0
7	+4.0	+7.0
8	+5.0	+8.0
9	+4.5	+9.0
10	+0.1	+3.5
11	−3.5	+0.1
12	−0.1	+3.0

Table 2 A comparison of monthly mean O_3 with observed data from Japan

Month	Observed data (ppbv)	Simulation without photolysis of pNO_3 (ppbv)	Simulation with photolysis of pNO_3 (ppbv)
1	43.0	36.0	37.6
2	45.4	39.3	40.9
3	51.9	42.3	45.4
4	55.7	42.2	47.3
5	51.1	41.8	46.6
6	40.4	37.6	41.7
7	29.3	33.1	35.3
8	29.1	32.4	35.0
9	32.4	31.1	33.4
10	40.4	32.4	34.8
11	41.4	35.0	38.0
12	37.1	34.6	37.3

4 Conclusion

We examined the impact of the photolysis of pNO_3 over marine environments on air quality using the hemispheric CMAQ model. It enhances HONO which compares better with limited observed data over marine environments. It increases O_3 over seawater as well as over land. Enhanced O_3 levels agree better with observed data in cooler months but the agreement worsens in warmer months. Ye et al. (2017)

suggested that photolysis of pNO_3 can occur not only over the marine environments but also over other areas which we plan to examine in a future study.

Disclaimer The views expressed in this paper are those of the authors and do not necessarily represent the view or policies of the U.S. Environmental Protection Agency.

References

Emery, et al. (2015). *Improvements to CAMx snow cover treatments and carbon bond chemical mechanism for winter ozone*. Final Report prepared for Utah Department of Environmental Quality, Salt Lake City, UT. Prepared by Ramboll Environ, Novato, CA, August 2015.

Mathur, et al. (2017). Extending the community multiscale air quality (CMAQ) modeling system to hemispheric scales: Process considerations and initial applications. *Atmospheric Chemistry and Physics, 17*, 1–25.

Reed, et al. (2017). Evidence for renoxification in the tropical marine boundary layer. *Atmospheric Chemistry and Physics, 17*, 4081–4092.

Skamarock, W. C. (2008). *A description of the advanced research WRF version 3*. NCAR Tech Note NCAR/TN 475 STR, 2008, 125 pp. [Available from UCAR Communications, P.O. Box 3000, Boulder, CO 80307].

Vukovich, J. M. et al. (2018). Development of 2016 hemispheric emissions for CMAQ. In *The 17th annual CMAS models-3 user's conference*, October, Chapel Hill, NC, October 22–24, 2018.

Ye, et al. (2016). Rapid recyling of reactive nitrogen in the marine boundary layer. *Nature, 532*, 489–491.

Ye, et al. (2017). Photolysis of particulate nitrate as a source of HONO and NOx. *Environment Science & Technology, 51*, 6849–6856.

Questions and Answers

Questioner: B. H. Baek

Question: Have you considered including isoprene emissions from ocean as an ozone-precursor?

Answer: Isoprene emissions from oceans were not considered in this study. The impacts of isoprene emissions from oceans on ozone are expected to be small.

Questioner: Ted Russel

Question: Have you considered differentiating between aqueous and solid aerosol nitrate photolysis?

Answer: In this study, all fine-mode aerosol nitrate was considered for photolysis. Aerosol nitrate was not differentiated between aqueous and solid phase.

Improved Estimation of Background Ozone and Emission Impacts Using Chemical Transport Modeling and Data Fusion

T. Nash Skipper, M. Talat Odman, Yongtao Hu, Petros Vasilakos, and Armistead G. Russell

Abstract As ozone air quality standards are tightened, the portion of the standard taken up by background ozone (BGO) increases. BGO is the ozone that would be observed in the absence of anthropogenic emissions. BGO can be a major, sometimes dominant, contribution to overall ozone. BGO originates from noncontrollable sources (e.g., wildfires, stratosphere-troposphere exchange, non-domestic pollution) and can vary significantly by region, elevation, and season, leading to high uncertainty in BGO contributions. In this work, US BGO is first quantified using a chemical transport model, specifically the Community Multiscale Air Quality (CMAQ) model, with US anthropogenic emissions set to zero. A method of adjusting for model bias in the estimation of BGO is developed that fuses model results with observations. This method uses observational and modelled data to develop functions of space, time, and meteorology that relate CMAQ-simulated base case (using estimated emissions) and CMAQ-modelled US BGO (no US anthropogenic emissions) to the observations. Separate adjustment factors are developed for locally formed and background ozone. This allows for calculating both an adjusted US BGO and the amount of ozone formed from anthropogenic emissions that better align with observations and elucidation of the key influences and sources of bias for these two sources of ozone. The effects of boundary conditions on BGO estimates and model bias is also examined. Application of this adjustment factor method improves agreement between BGO estimated with two different sets of boundary conditions from $r = 0.58$ for the original modelled values to $r = 0.85$ for the adjusted values.

Keywords Ozone · Background ozone · Data fusion

T. N. Skipper (✉) · M. T. Odman · Y. Hu · P. Vasilakos · A. G. Russell
School of Civil and Environmental Engineering, Georgia Institute of Technology, Atlanta, GA 30332, USA
e-mail: tskipper33@gatech.edu

© The Author(s), under exclusive license to Springer-Verlag GmbH, DE, part of Springer Nature 2021

C. Mensink and V. Matthias (eds.), *Air Pollution Modeling and its Application XXVII*, Springer Proceedings in Complexity, https://doi.org/10.1007/978-3-662-63760-9_13

1 Introduction

Ozone is a major air pollutant that has adverse impacts on human health and ecosystems. A complication to its control is that ozone is not emitted directly but rather is formed through a series of photochemical reactions involving precursor species. In the United States (US), the air quality standard for ozone was lowered in 2015 from 75 to 70 ppb. As the standard becomes lower, the portion of the standard taken up by background ozone (BGO) increases. BGO is ozone that originates from noncontrollable sources (e.g., wildfires, stratosphere-troposphere exchange, non-domestic pollution). BGO can be a major, sometimes dominant, contribution to overall ozone. BGO is typically quantified using a chemical transport model, but as a hypothetical quantity, model predictions of BGO cannot be directly evaluated through comparison to observations. In the US, remote monitoring sites (e.g. Trinidad Head, California and Mt. Bachelor, Oregon) that are not heavily influenced by anthropogenic sources can provide some insight into the US BGO, but such monitoring sites are limited in number and spatial distribution and are never totally isolated from US emission impacts. Different models provide different estimates of BGO. Differences can arise due to the biases inherent to each model. The current uncertainty in US BGO estimates is about $\pm$ 10 ppb for seasonal means with higher uncertainty on individual days (Jaffe et al., 2018). Understanding and quantifying BGO is an important aspect of air quality management, and it will become increasingly important as air quality standards are further strengthened in the future. Narrowing the range of the uncertainty in BGO estimates can provide additional knowledge to air quality planning agencies that can help them design the most effective ozone reduction strategies. In this work, a method for estimation of BGO through the blending of modelled and observed ozone is developed. This method results in improved estimates of BGO that better align with observations and that have decreased uncertainty compared to BGO estimated by modeling alone.

2 Methods

CMAQ simulations were conducted for 2017 for a domain covering the contiguous United States and parts of Mexico, Canada, and the Caribbean at 36 km resolution. Two simulations include all anthropogenic emissions (base case simulations). One base case simulation uses the CMAQ default profile static boundary conditions; the other uses dynamic boundary conditions derived from a Hemispheric CMAQ (HCMAQ) simulation. Two more simulations in which US anthropogenic emissions are removed but emissions from other countries are included (background case) are conducted with each set of boundary conditions. The base case maximum daily 8-h (MDA8) ozone is separated into background and US anthropogenic components. The background component is the average ozone from the background case occurring

during the same 8-h time period as the base case MDA8 ozone and is obtained directly from the background case simulations. The US anthropogenic component is the difference of the base and background case ozone. The model error attributable to both components is estimated by regression with observed ozone. The estimate of model error takes the form of a correction factor for each component that is a function of space, time, and meteorology. The variables included in the regression factor are as follows: deviation of daily mean temperature from annual mean (ΔT), absolute value of longitude and latitude normalized by 180 and 90° respectively (X and Y), elevation in km (Z), day of year (d) transformed to a sinusoidal form, daily mean cloud cover fraction (CLD), and daily mean relative humidity (RH). Separate adjustment factors are developed for background and US anthropogenic ozone for both sets of boundary conditions. The adjustment factors are then applied to the modeled results to develop improved estimates of background and locally formed ozone.

3 Results and Discussion

In the base and background cases, the HCMAQ boundary conditions result in higher ozone concentrations compared to the static boundary conditions, but the US anthropogenic component is mostly consistent between the two cases (Figs. 1 and 2). Most of the difference between the two sets of boundary conditions is due to the modelled

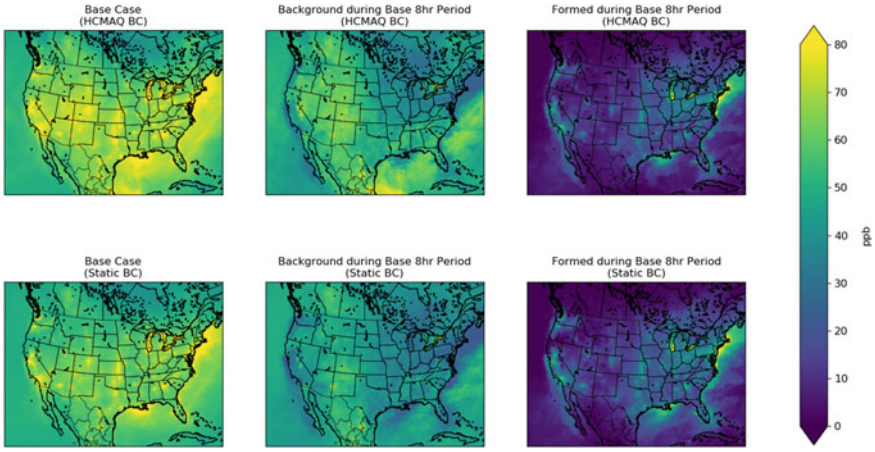

Fig. 1 Mean of the ten highest base case MDA8 ozone concentrations, mean BGO on the same ten days, and the difference between the two which represents the amount formed from US anthropogenic emissions

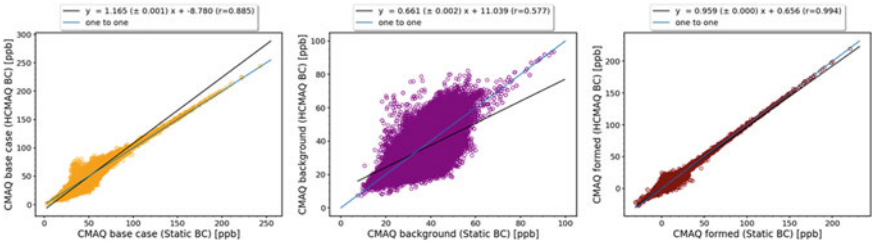

Fig. 2 Comparison of base case, background, and locally formed ozone for Static and HCMAQ BC cases

background. The following are the adjustment factors for each set of boundary conditions obtained through regression with observed ozone:

Static

$$[O_3] = [O_3]_{bg}*(0.8747 + 0.0006*\Delta T - 0.2984*X + 0.6220*Y - 0.0146*Z + 0.0830*\sin(d*2\pi/365) - 0.0370*\cos(d*2\pi/365) - 0.0743*CLD - 0.1200*RH) + [O_3]_{formed}*(1.2532 + 0.0096*\Delta T + 0.6687*X - 0.7253*Y + 0.1621*Z - 0.0044*\sin(d*2\pi/365) + 0.1622*\cos(d*2\pi/365) - 0.5132*CLD - 0.6628*RH)$$
$(R^2 = 0.53)$

HCMAQ

$$[O_3] = [O_3]_{bg}*(0.5953 - 0.0024*\Delta T - 0.1121*X + 1.2859*Y - 0.0371*Z + 0.2525*\sin(d*2\pi/365) + 0.0376*\cos(d*2\pi/365) - 0.0809*CLD - 0.1372*RH) + [O_3]_{formed}*(1.4888 - 0.0006*\Delta T + 0.3484*X - 0.9320*Y + 0.1594*Z - 0.1446*\sin(d*2\pi/365) + 0.1085*\cos(d*2\pi/365) - 0.5443*CLD - 0.6949*RH)$$
$(R^2 = 0.53)$

Adjusted BGO estimates are obtained by setting the locally formed ozone to zero in the regression equation for each boundary condition case. The adjusted estimates show improved correlation between the BGO values for each set of boundary conditions. The correlation is improved from 0.58 for the original modelled values to 0.85 for the adjusted values (Fig. 3). Decreased variability in BGO estimated using different boundary conditions indicates that the uncertainty in the estimates is reduced. This method shows promise as a method of reducing the variability of BGO estimates obtained by different models, and in reducing the uncertainty in US BGO estimates. It can also be applied to results obtained from an ensemble of models.

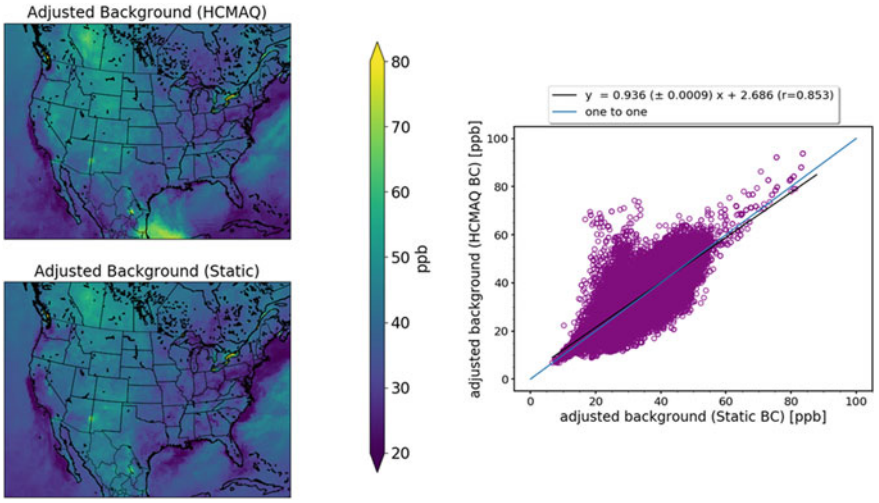

Fig. 3 Comparison of adjusted BGO for Static and HCMAQ BC cases. The spatial plot shows the mean across the ten days with the highest ozone. The scatter plot shows the comparison at observation locations for the entire year

Acknowledgements We would like to thank US EPA for providing boundary conditions from a Hemispheric CMAQ simulation. We would also like to acknowledge support from the Phillips 66 Company and NASA as part of their HAQAST program.

References

Jaffe, D. A., Cooper, O. R., Fiore, A. M., Henderson, B. H., Tonnesen, G. S., Russell, A. G., Henze, D. K., Langford, A. O., Lin, M, & Moore, T. (2018). Scientific assessment of background ozone over the U.S.: Implications for air quality management. *Elementa: Science of the Anthropocene*, *6*, 56. https://doi.org/10.1525/elementa.309

Zhang, L., Jacob, D. J., Downey, N. V., Wood, D. A., Blewitt, D., Carouge, C. C., van Donkelaar, A., Jones, D. B. A., Murray, L. T., & Wang, Y. (2011). Improved estimate of the policy-relevant background ozone in the United States using the GEOS-Chem global model with 1/2° × 2/3° horizontal resolution over North America. *Atmospheric Environment, 45*, 6769–6776. https://doi.org/10.1016/j.atmosenv.2011.07.054

Questions and Answers

Questioner: Pius Lee.

Question: Can you give an explanation about the sample size of around 397,000? It seems a little small for me in representativeness of the vast variabilities of background influence and multiple year variabilities, wet/dry years, wildfire active/inactive years.

Answer: The sample size of about 397,000 is the total number of model-observation pairs that we have available for the 2017 annual simulation. We could increase the sample size by extending to a multi-year simulation, and we do have plans to extend this work at least to 2016 in addition to what we have done here.

Questioner: Peter Builtjes.

Question: Did you model or estimate the natural background of ozone, without any anthropogenic emissions?

Answer: We did not model the natural background ozone. Others (e.g. Zhang et al., 2011) have modeled the natural background and have found that it is on average approximately 20 ppb over the US, though it does vary seasonally and geographically.

Questioner: Saravanan Arunachalam.

Question: When you used the hemispheric CMAQ boundary conditions from EPA, did you use hourly boundary conditions or some temporal means?

Answer: We used hourly boundary conditions from the hemispheric CMAQ simulation.

Same Model (CAMx6.50), Same Year (2010), Two Different European Projects: How Similar Are the Results?

Sebnem Aksoyoglu, Jianhui Jiang, Emmanouil Oikonomakis, and André S. H. Prévôt

Abstract The European air quality in 2010 was simulated by the regional air quality model CAMx in two different projects: Eurodelta-Trends (EDT) and PSI-Project. We used the same model version CAMx v6.50 and the same parameterization in both projects but with different domain resolution and input data. In this study, we investigated (i) how different are the results for ozone, $PM_{2.5}$ and its components and (ii) which parameter/input is more critical for each pollutant. Our analyses suggested that the differences mainly originated from the boundary conditions, biogenic emissions and the vertical distribution of anthropogenic emissions. The most sensitive species to inputs were ozone and secondary organic aerosols (SOA). The difference in ozone concentrations was mainly due to the difference in boundary conditions. On the other hand, the difference in the annual $PM_{2.5}$ concentrations originated mainly from SOA, due to different biogenic emissions used in the two projects. Concentrations of secondary inorganic aerosols (SIA) were comparable with small differences due to the different resolutions and vertical distribution of emissions. Although their generation was not the same, the meteorological data were similar in both projects and effects of small differences were not significant for the annual concentrations of pollutants.

Keywords CAMx · Biogenic emissions · Ozone · Secondary organic aerosols · Eurodelta-Trends · Boundary conditions

S. Aksoyoglu (✉) · J. Jiang · E. Oikonomakis · A. S. H. Prévôt
Laboratory of Atmospheric Chemistry, Paul Scherrer Institute (PSI), 5232 Villigen, Switzerland
e-mail: sebnem.aksoyoglu@psi.ch

J. Jiang
e-mail: jianhui.jiang@psi.ch

E. Oikonomakis
e-mail: emmanouil.oikonomakis@psi.ch

A. S. H. Prévôt
e-mail: andre.prevot@psi.ch

© The Author(s), under exclusive license to Springer-Verlag GmbH, DE, part of Springer Nature 2021

C. Mensink and V. Matthias (eds.), *Air Pollution Modeling and its Application XXVII*, Springer Proceedings in Complexity, https://doi.org/10.1007/978-3-662-63760-9_14

1 Introduction

Several intercomparison exercises of regional-scale chemical transport models (CTM) have been reported in recent years (Bessagnet et al., 2016; Colette et al., 2017; Im et al., 2015). In such model intercomparison studies, different models are usually applied using common input data on the same domain and the differences are expected to come mainly from the models. In this paper, we analyze the opposite situation- same model, different input data- to identify the most critical inputs which might lead to different results depending on how they are prepared. The main aim of this paper is to estimate which pollutant is more sensitive to which input parameter for further improvement of the air quality simulations.

2 Method

The European air quality in 2010 was simulated using the regional chemical transport model CAMx v6.50 (www.camx.com) in both Eurodelta-Trends (EDT) (Colette et al., 2017) and PSI projects (Oikonomakis et al., 2018). The model domain, horizontal resolution and input data were different in these projects (see Table 1). Meteorology, boundary conditions, anthropogenic emissions, horizontal domain and resolution were prescribed in the EDT project. In the PSI-project, we prepared meteorology, boundary conditions and anthropogenic emissions using the CAMx preprocessors as well as our own methods as described in Oikonomakis et al. (2018). On the other hand, we used the same model parameterization in both cases. The gas-phase chemical mechanism was CB6r2 and secondary organic aerosol (SOA) formation was calculated using the SOAP2 module. Two-mode fine/coarse scheme was applied to represent particle size distribution.

Table 1 Differences between the two projects

Inputs	EDT	PSI
Model domain	17° W–39.8° E, 32°–70° N	15° W–35° E, 35°–70° N
Horizontal resolution	0.25° × 0.4°	0.125° × 0.250°
Meteorology	WRF3.3.1, regridded	WRF3.7.1
Boundary conditions	Monthly climatological data	MOZART, 6-h
Biogenic emissions	MEGAN 2.1	PSI-model
Anthropogenic emissions	GAINS, TNO-MACC	TNO-MACC III
Vertical distribution of emissions	Different layers	First layer

3 Results and Discussion

The effect of different horizontal resolution used by two projects is visible from the spatial distribution of NO_x emissions (Fig. 1). Analyses of meteorological parameters used in EDT and PSI projects revealed relatively small differences due to different procedures used to generate them. The effects of such small differences were not significant for the annual concentrations of pollutants.

The annual ozone mixing ratios in the EDT project were significantly higher mainly in the western and southern part of the model domain (Fig. 2). Replacing the EDT boundary conditions with data from MOZART global model led to lower values improving the model performance. On the other hand, higher isoprene emissions produced by MEGAN in the EDT project caused a small difference on ozone over central Europe.

In case of $PM_{2.5}$ concentrations, different boundary conditions caused a difference in fine crustal particle concentrations in northern Africa (Fig. 3). The main difference

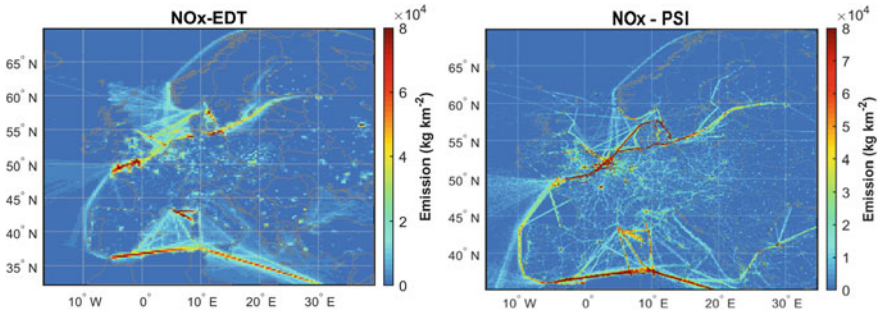

Fig. 1 Annual emissions of NO_x in 2010 used in EDT (left) and PSI (right) projects. The model domains and horizontal resolutions are different

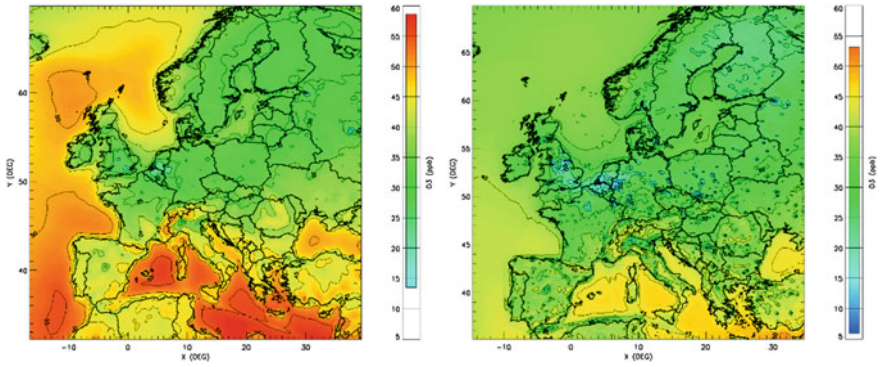

Fig. 2 Annual ozone (ppb) modeled in EDT (left) and PSI (right) projects

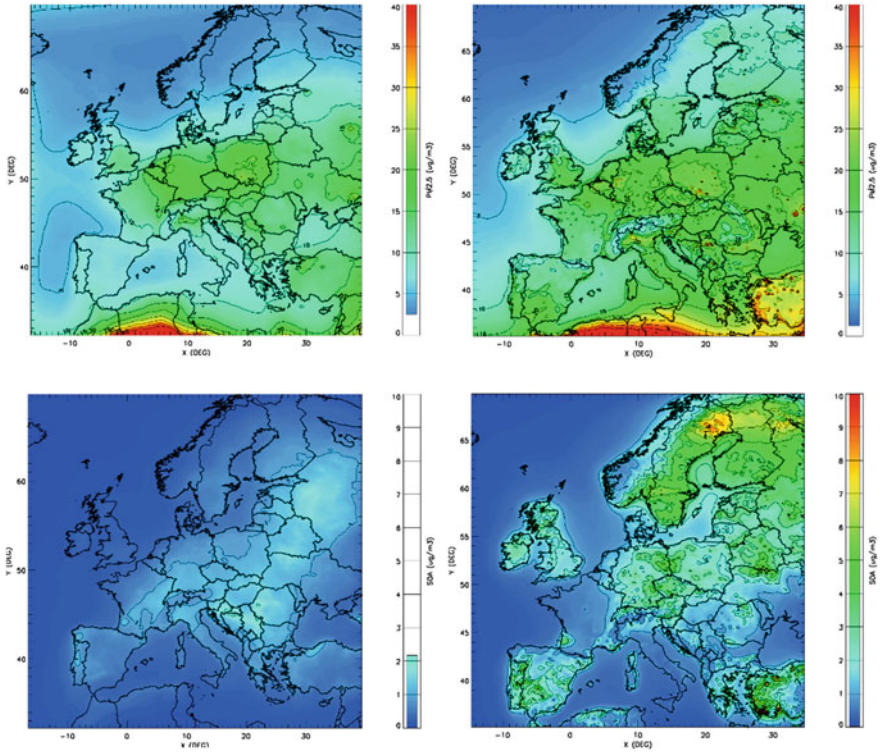

Fig. 3 Annual $PM_{2.5}$ (top) and SOA (bottom) modeled in EDT (left) and PSI (right) projects ($\mu g\ m^{-3}$)

over Europe was due to higher SOA in the PSI domain resulted from larger monoterpene emissions calculated by the PSI biogenic emission model (Jiang et al., 2019). Concentrations of secondary inorganic aerosols (SIA) were comparable with small differences due to the different resolutions and vertical distribution of emissions.

4 Conclusion

The comparison of CAMx results for 2010 from two different European projects (EDT and PSI projects) with the same parameterization but with different input data and different domain resolution suggested the following: (i) ozone was sensitive to boundary conditions over the western and southern part of the domain and to a lesser extent, to isoprene emissions over the European continent, (ii) the difference in the annual $PM_{2.5}$ concentrations originated mainly from SOA, due to different biogenic emissions used in the two projects (higher monoterpene emissions in the PSI domain led to higher SOA and therefore higher $PM_{2.5}$), (iii) concentrations of secondary

inorganic aerosols (SIA) were comparable with small differences due to the different resolutions and vertical distribution of emissions, (iv) the meteorological data were similar in both projects and small differences did not affect the annual concentrations of pollutants.

Acknowledgements We would like to thank the Eurodelta-Trends team, TNO, NCAR and ECMWF for providing various input data. We are grateful to Ramboll for their continuous support. Simulations were performed at the Swiss National Supercomputing Center (CSCS). Our thanks extend to Swiss Federal Office of Environment (FOEN) for financial support.

References

Bessagnet, B., Pirovano, G., Mircea, M., et al. (2016). Presentation of the EURODELTA III intercomparison exercise—Evaluation of the chemistry transport models' performance on criteria pollutants and joint analysis with meteorology. *Atmospheric Chemistry and Physics, 16*, 12667–12701. https://doi.org/10.5194/acp-16-12667-2016

Colette, A., Andersson, C., Manders, A., et al. (2017). EURODELTA-Trends, a multi-model experiment of air quality hindcast in Europe over 1990–2010. *Geoscientific Model Development, 10*, 3255–3276. https://doi.org/10.5194/gmd-10-3255-2017

Im, U., Bianconi, R., Solazzo, E., et al. (2015). Evaluation of operational on-line-coupled regional air quality models over Europe and North America in the context of AQMEII phase 2. Part I: Ozone. *Atmospheric Environment, 115*, 404–420. https://doi.org/10.1016/j.atmosenv.2014.09.042

Jiang, J., Aksoyoglu, S., Ciarelli, G., et al. (2019). Effects of two different biogenic emission models on modelled ozone and aerosol concentrations in Europe. *Atmospheric Chemistry and Physics, 19*, 3747–3768. https://doi.org/10.5194/acp-19-3747-2019

Oikonomakis, E., Aksoyoglu, S., Ciarelli, G., Baltensperger, U., & Prévôt, A. S. H. (2018). Low modeled ozone production suggests underestimation of precursor emissions (especially NO_x) in Europe. *Atmospheric Chemistry and Physics, 18*, 2175–2198. https://doi.org/10.5194/acp-18-2175-2018

Questions and Answers

Questioner: Renske Timmermans

Question: Did you also have a look whether the different distribution of the emissions (shipping emissions in layer 2 vs. layer 1) have an impact on ozone? Could it be also a cause of the differences?

Answer: Yes, we compared two simulations with different vertical distribution of emissions. A small, local effect was found for point source emissions, especially for SO_2 from SNAP1 sources; concentrations were lower in the first layer when emissions were distributed vertically within the first 4–5 layers. In case of ship emissions, on the other hand, there was no significant difference when they were released to the second layer.

Questioner: Andrey Vlasenko

Question: What is the impact of resolution on the accuracy of your results in your experiment?

Answer: In this study, the horizontal resolutions of the two domains were $0.25^{o} \times 0.4°$ and $0.125° \times 0.250°$. A small effect of resolution could be seen locally around the polluted areas, especially those with high NO_x emissions such as Benelux and northern Italy. In the domain with relatively higher resolution, ozone concentrations were slightly lower due to more titration with NO while $PM_{2.5}$ concentrations were slightly higher in the polluted regions. The effect of resolution was less significant than the effects of input data in this study.

SMART Modeling Suite: Assessment of the Turbulence Parameterisation for the Simulation of Atmospheric Circulation and Dispersion

Andrea Bisignano and Silvia Trini Castelli

Abstract An assessment of turbulence closure and parameterisation in the meteo-dispersive modeling suite SMART is proposed, investigating some critical issues.

1 Introduction

In the frame of the development of the SMART (Spray—Moloch Atmospheric Regional Tool) modeling suite, we evaluate and test the turbulence closure in MOLOCH meteorological model and the parameterisation for the wind velocity standard deviations derived by it and used in SPRAY Lagrangian particle model. After having assessed the MOLOCH turbulence closure, based on measurements in two sites in north and south Italy, and in different meteorological conditions, two alternative standard-deviation parameterisations implemented in the interfacing code ARAMIS (Atmospheric Regional Algorithm for Moloch Interfaced to Spray) are compared. Critical issues are considered and addressed.

The effect on the pollutant dispersion using the different turbulence parameterisations is seen performing SPRAY model numerical experiments, with releases in different conditions. The sensitivity of the simulations to the turbulence parameterisation is considered, comparing the plume pattern and the ground-level concentrations.

A. Bisignano (✉)
Department of Civil, Environmental and Mechanical Engineering, University of Trento, Trento, Italy
e-mail: andrea.bisignano@unitn.it

S. T. Castelli
Institute of Atmospheric Sciences and Climate, National Research Council, Torino, Italy

© The Author(s), under exclusive license to Springer-Verlag GmbH, DE, part of Springer Nature 2021

C. Mensink and V. Matthias (eds.), *Air Pollution Modeling and its Application XXVII*, Springer Proceedings in Complexity, https://doi.org/10.1007/978-3-662-63760-9_15

2 The Parameterisations and the Simulations

We tested two different formulations to compute the wind velocity standard deviations needed by SPRAY Lagrangian particle dispersion model. The first is a K-closure (K-TH) and it is based on the eddy-viscosity concept, determining the turbulent Reynolds stresses as proportional to the mean-velocity gradients:

$$\sigma_u^2 = -2K_{mx}\frac{\partial \overline{u}}{\partial x} + \frac{2}{3}E, \sigma_v^2 = -2K_{my}\frac{\partial \overline{v}}{\partial y} + \frac{2}{3}E, \sigma_z^2 = -2K_{mz}\frac{\partial \overline{w}}{\partial z} + \frac{2}{3}E \quad (1)$$

where σ_i $(i = u, v, w)$ are the wind velocity standard deviations, K_{mi} are the diffusion coefficients and E is the turbulent kinetic energy (t.k.e.).

The term $\frac{2}{3}E$ in addition to the classical formulation of the eddy-viscosity is necessary to make the expression applicable to the normal stresses (Rodi, 1980). In fact, the sum of the first parts containing the velocity gradients would be zero because of the continuity equation. The additional term assures that the normal stresses are positive quantities and that their sum is equal to 2E, as by definition of the t.k.e.

The second (MY82) is adopted from Mellor-Yamada (1982) closure, largely used in meteorological models. It determines the wind velocity variances as directly proportional to the t.k.e.:

$$\sigma_u^2 = \left(\frac{1-\gamma_1}{2}\right)q^2, \sigma_v^2 = \sigma_u^2, \sigma_w^2 = \gamma_1 q^2 \quad (2)$$

where $q^2 = 2E$ and $\gamma_1 = 0.22$ is an empirical constant.

The main difference between the two formulations, K-TH and MY82, depend then on the use of the wind-velocity gradients in K-TH, while in MY82 the variances depend uniquely on the t.k.e. E.

In Trini Castelli et al. (2019), the turbulence closure in the MOLOCH meteorological model has been thoroughly assessed for several different atmospheric conditions against observations collected in two sites, Torino in north-west Italy and Lecce in south-east Italy. Here we consider MOLOCH simulations made at 500 m grid resolution in Torino site (observed data at 25 m, in the inertial sublayer) for two days, characterized by strong (SW, on 13.02.2007) and low (LW, on 01.10.2007) wind speeds, respectively. In Fig. 1 the t.k.e. as reproduced by MOLOCH model is plotted and compared to the observations. In both cases, the agreement between predictions and observations is fair.

3 Results and Discussion

In Fig. 2 a comparison between the wind velocity standard deviations as calculated by K-TH and MY82 parameterisation in shown. Minimum and maximum threshold values of 0.2 and 2.5 m/s are assigned in ARAMIS code for SPRAY simulations.

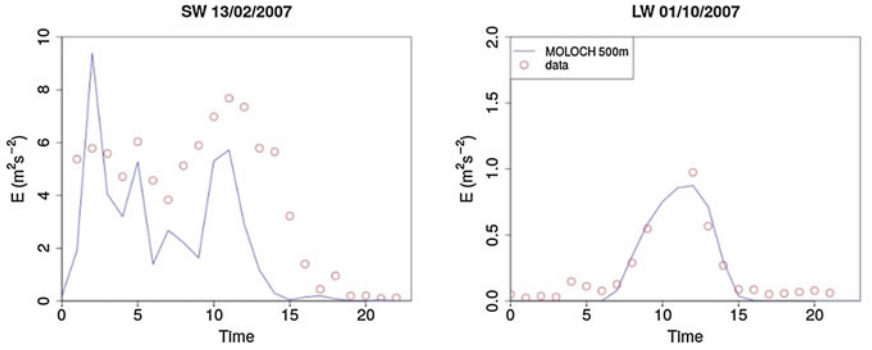

Fig. 1 Turbulent kinetic energy observed (red circles) and predicted by MOLOCH model (blue line), for a case of strong wind (left) and low wind (right) speeds

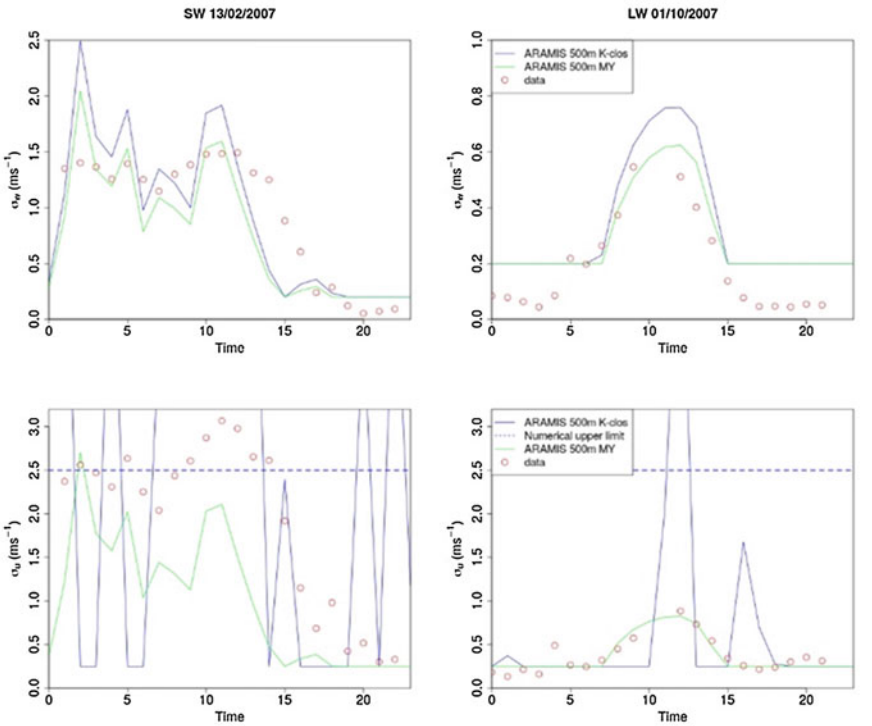

Fig. 2 Vertical (top) and horizontal (bottom) wind velocity standard deviation, observed (red circles) and calculated with K_TH (blue line) and MY (green line) parameterisation, for strong wind (left) and low wind (right) speeds

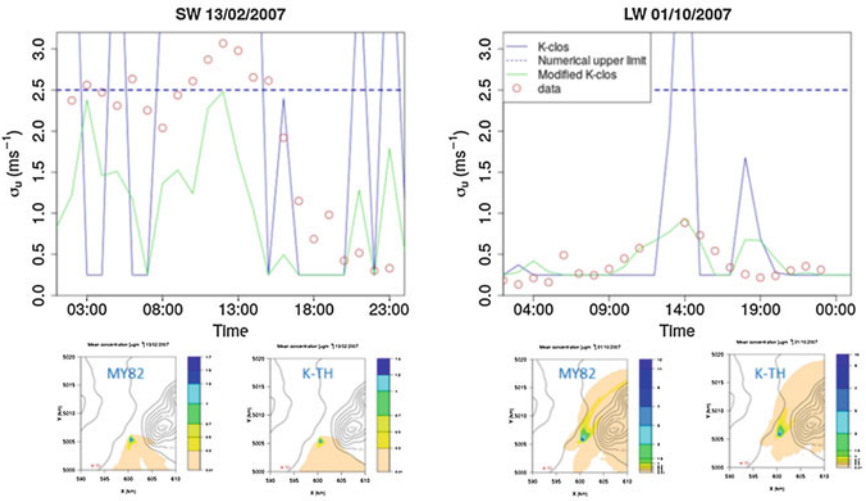

Fig. 3 Horizontal wind velocity standard deviation, observed (red circles) and calculated with K_TH (blue line, Eq. 1) and K-TH corrected (green line, Eq. 4) parameterisation, for strong wind (left) and low wind (right) speeds, and relative SPRAY concentration fields (bottom)

While for σ_w the agreement with the observations is fair, with some overestimation in K-TH case, the σ_u in K-TH is largely fluctuating and shows unreliable values.

We checked the terms in Eq. 1 and verified that when the horizontal velocity gradients take absolute values around the unit, their product with the diffusion coefficients assumes largely fluctuating values, leading to non-sensible values of the standard deviation. The horizontal diffusivity in MOLOCH model is based on a mixing length proportional to the horizontal grid spacing. Thus the dependency on the numerical resolution may overcome the physical representation. It can become critical using such diffusion coefficients together with the horizontal velocity gradients resulting from the typical grid resolutions of regional models. To assess this issue, we applied a correction to the horizontal diffusion coefficients based on the vertical coefficient, considering typical relationship between the horizontal and vertical wind velocity variances in the surface layer, as in Eq. (3) (from Stull, 1988)

$$\left[\left(\sigma_u^2\right)^2 + \left(\sigma_v^2\right)^2\right]^{1/4} \Big/ u_* = c_H \quad \text{and} \quad \left(\sigma_u^2\right)^{1/2} \Big/ u_* = c_V \tag{3}$$

The horizontal diffusivity is thus corrected as follows, here using a value from literature for $c_H / c_V = 2.1$:

$$K_{m\_x,y} = \left[\frac{c_H}{c_V} K_{mz} \frac{\partial \overline{w}}{\partial z} + \frac{1}{3} E \left(2 - \frac{c_H}{c_V}\right)\right] \Big/ \left(\frac{\partial \overline{u}}{\partial x} + \frac{\partial \overline{v}}{\partial y}\right) \tag{4}$$

In Fig. 3 the corrected formulation is compared to the original one and shows a clear improvement in the representativeness of the wind velocity standard deviation. The results indicate that the generic formulation for the horizontal variances in Eq. 1 can be revisited with this type of corrections, in order to make it applicable to the typical configuration and resolution of the fields output by a regional model. Yet, more extensive investigation is needed to achieve final conclusions. The concentration fields from SPRAY using the two parameterisations show some difference close to the release point, but not major ones, indicating the robustness of the simulations.

References

Mellor, G. L., & Yamada, T. (1982). Development of a turbulence closure model for geophysical fluid problems. *Reviews of Geophysics and Space Physics, 20*, 851–875.

Rodi, W. (1980). *Turbulence models and their application in hydraulics—A state of the art review*. Book Publication of International Association for Hydraulic Reasearch.

Stull, R. B. (1988). An introduction to boundary layer meteorology. Kluwer Academic Publishers, Dordrecht, Boston and London, p. 666

Trini Castelli, S., Bisignano, A., Donateo, A., Landi, T., Martano, P., & Malguzzi P. (2020). Evaluation of the turbulence parameterisation in the MOLOCH meteorological model. *Quarterly Journal of the Royal Meteorological Society*.

Questions and Answers

Questioner: Stefano Alessandrini.

Question: Since Mellor-Yamada closure is working quite well on your dataset, why did you develop an additional model?

Answer: From past studies with RAMS model, we verified that when using Mellor-Yamada closure, the turbulent kinetic energy and the related diffusivity were generally underestimated. This affected the plume dispersion in the SPRAY model, often inducing a reduced spread of it with respect to the observed one. For this reason, already in RAMS we implemented alternative closure schemes. In MOLOCH an E-l based turbulence closure is included. In this work, we focused on the wind velocity standard deviations needed in input to SPRAY and calculated based on the output from the meteorological model. In order to check what we here define as the K-closure formula, what we used of the Mellor-Yamada closure was just the proportionality expressed between the variances and the turbulent kinetic energy, not the full Mellor-Yamada scheme. Thus, the good agreement between the predicted and observed values is given by the turbulent kinetic energy output from MOLOCH. The K-theory closure parameterize the turbulence effects through the molecular diffusion analogy and thus using an eddy viscosity model. With respect to Mellor-Yamada formulation

for the wind velocity variances, it explicitly includes the velocity gradients, which can be crucial quantities in describing the turbulence, especially in complex terrain.

Analysis of the Zero-Out Method of Source Apportionment for Air Quality Modeling in Spain

Mark R. Theobald, Marta G. Vivanco, Victoria Gil, Juan Luis Garrido, and Fernando Martín

Abstract The zero-out method of source apportionment was applied to air pollutant concentrations (ozone, nitrogen dioxide and particulate matter) from an air quality simulation for Spain and the suitability of the method was analysed.

Keywords Air pollution · Air quality models · Source apportionment

1 Introduction

Methods of source apportionment are frequently applied to estimate the contribution of individual emission sources or source sectors to atmospheric pollutant concentrations. These methods can be based on the combination of measurements and models using techniques such as chemical mass balance or positive matrix factorisation or based purely on model simulations using approaches such as emission reduction potential or tagging (Mircea et al., 2019). All source apportionment methods have advantages and disadvantages and some are more suitable for certain applications than others. Thunis et al. (2019) define four properties of the methods: unambiguity, additivity, linearity and dynamicity. For example, measurement-based methods can be ambiguous if the concentrations are influenced by multiple sources and linearity can be problem for many of the methods when applied to secondary pollutants such as ozone or secondary particulate matter. One of the most used model-based methods is the emission reduction potential or brute-force method, in which the contribution of an emission source or geographic source area or sector is estimated by comparing simulations with and without an emission reduction. This method is called the "zero-out" method when the emission reduction is 100% (i.e. all emissions removed for the source). Brute-force methods can lack linearity and additivity when applied to secondary pollutants, although the errors can be reduced by only applying small emission reductions (<50%). However, in this case the results are only valid for the range of emission reductions applied. Although the zero-out method is not ideally

M. R. Theobald (✉) · M. G. Vivanco · V. Gil · J. L. Garrido · F. Martín
Atmospheric Pollution Unit, CIEMAT, Avda. Complutense, 40, 28040 Madrid, Spain
e-mail: mark.theobald@externos.ciemat.es

© The Author(s), under exclusive license to Springer-Verlag GmbH, DE, part of Springer Nature 2021

C. Mensink and V. Matthias (eds.), *Air Pollution Modeling and its Application XXVII*, Springer Proceedings in Complexity, https://doi.org/10.1007/978-3-662-63760-9_16

suited for secondary pollutants, it is instructive to test this assumption and analyse the linearity and additivity of this source apportionment method for a real case study. In this work, the zero-out method was applied to estimate source apportionment for ozone (O_3), nitrogen dioxide (NO_2) and particulate matter ($PM_{2.5}$ and PM_{10}) for an annual air quality simulation for Spain.

2 Materials and Methods

The chemistry transport model CHIMERE (v2013, Menut et al., 2014) was used to simulate hourly atmospheric pollutant concentrations for 2016 for a domain with a grid-resolution of 0.15° covering southwest Europe. Concentrations at the domain boundaries were taken from the global models LMDz-INCA and LMDz-AERO/GOCART for the gaseous and aerosol species, respectively and meteorological data were taken from the IFS model of the ECMWF rescaled to 0.15°. Emissions data were the result of a spatial and temporal disaggregation of emissions from EMEP and from the Spanish Ministry for the Ecological Transition. Nine simulations were carried out: one simulation with all sources (base case) and eight simulations with emissions from a particular source sector/region reduced to zero. The source sectors/regions used were: boundary conditions, international shipping, biogenic, dust and anthropogenic emissions from Spain, France, Portugal and the rest of Europe (within the domain).

The contributions of all sectors/regions to the hourly pollutant concentrations were summed at the locations of air quality stations in Spain and compared with the concentrations from the base case simulation. The additivity of the zero-out method at these locations was assessed using two criteria:

Criterion 1: The hourly concentrations calculated by adding the contributions from sectors/regions are not negative

Criterion 2:The concentration calculated by adding the contributions from sectors/regions differs less than 5% from the concentration of the base case

Criterion 2 could be applied to all hourly concentrations but to simplify the analyses for this preliminary study it was only applied to the concentration metrics used in assessing exceedances of European limit values (Table 1). The threshold used here was arbitrarily set to 5% to represent summed contributions that were similar to those of the base case but other thresholds should be assessed in future work.

Table 1 Concentration metrics used in the study

Pollutant	Metric	Used for assessing
O_3	26th highest maximum daily 8-h mean	If limit value (120 $\mu g\ m^{-3}$) is exceeded more than 25 times
NO_2	19th highest hourly concentration	If limit value (200 $\mu g\ m^{-3}$) is exceeded more than 18 times
	Annual mean	If limit value (40 $\mu g\ m^{-3}$) is exceeded
$PM_{2.5}$	Annual mean	If limit value (25 $\mu g\ m^{-3}$) is exceeded
PM_{10}	36th highest daily mean concentration	If limit value (50 $\mu g\ m^{-3}$) is exceeded more than 35 times
	Annual mean	If limit value (40 $\mu g\ m^{-3}$) is exceeded

3 Results and Discussion

3.1 Ozone

Figure 1 shows the criteria met for the modelled ozone concentrations at the locations of the air quality monitoring stations. Concentrations did not meet criterion 1 (i.e. negative summed contributions) for about half of the locations, mostly those designated as urban and suburban stations. This strong non-linearity is most likely due to the proximity of large anthropogenic sources of precursor emissions leading to negative summed contributions at night. Modelled concentrations did not meet criterion 2 at only 14 locations, all of which are situated on the southern and south-eastern coasts and the island of Ibiza. These locations are influenced by a variety of biogenic and anthropogenic precursor emissions, including those from international shipping. The locations that did not meet either criterion are also situated in these regions. The explanations for this non-linearity and non-additivity will be explored in future work, although this preliminary analysis suggests that this can occur when ozone is formed from precursors that originate from various source types. In these

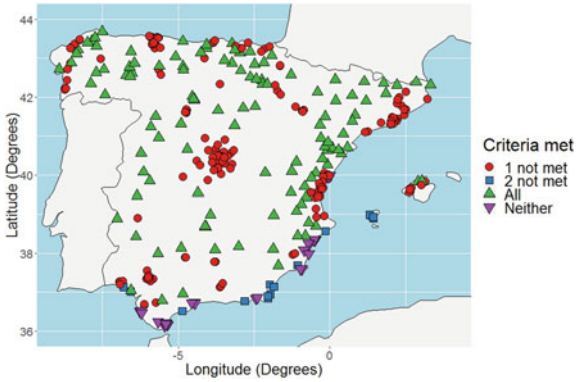

Fig. 1 Locations that meet the criteria (or not) for the 26th highest maximum 8-h mean O_3 concentration

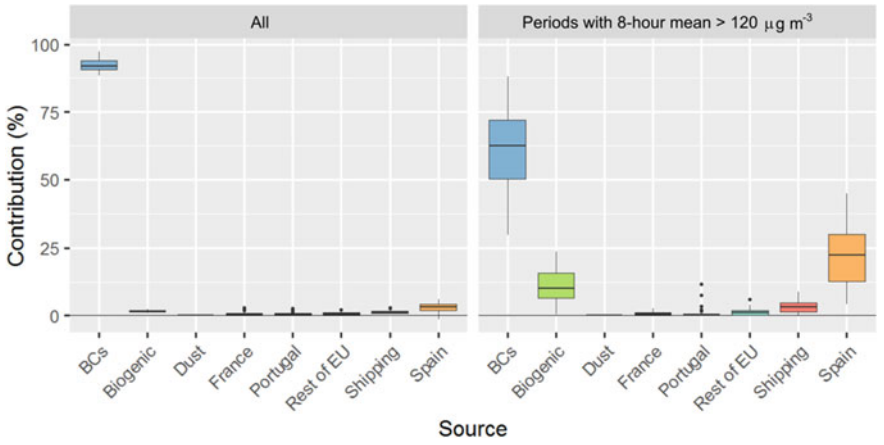

Fig. 2 Integrated source contributions for hourly O_3 concentrations (left) and periods for which the 8-h mean was greater than 120 $\mu g\ m^{-3}$ (right) at the locations meeting both criteria. BCs: Boundary Concentrations

cases the removal of any of the sources would restrict the formation of ozone and so their contributions would be counted more than once. Approximately a third of the locations met both criteria. These mostly rural locations are situated far from large anthropogenic precursor emission sources. Due to the approximately linear and additive results at these locations, it is possible to estimate the source apportionment for these sites using the zero-out method. Integrating the hourly concentrations for each source contribution shows that the boundary concentrations contribute between 88 and 97% of the ozone throughout the year (Fig. 2), suggesting that the vast majority of the modelled ozone at these locations originates from the ozone and precursors entering the modeling domain.

However, if the same analysis is done only for the periods when the 8-h mean exceeds 120 $\mu g\ m^{-3}$, the contribution of the boundary concentrations is reduced to between 30 and 88% and the importance of the biogenic and domestic anthropogenic emissions is evident, with contributions of up to 24% and 45%, respectively for these periods with high concentrations. In future work the robustness of these results will be assessed using simulations with smaller emission reductions.

3.2 Nitrogen Dioxide and Particulate Matter

Table 2 shows that the summed contributions for NO_2 and particulate matter do not meet both criteria at any of the sites. In the case of NO_2, neither criterion is met at most of the sites, with the exception of sites close to large anthropogenic NO_x sources (e.g. cities, ports, industrial sites etc.), for which only the first criterion (no negative concentrations) is met. The failure to meet the 5% difference criterion at

Table 2 Summary of the results for nitrogen dioxide, particulate matter and ozone

Pollutant	Metric	Number of sites meeting criteria			
		Criterion 1 only	Criterion 2 only	Both	Neither
NO_2	19th highest hourly concentration	103	1	0	332
	Annual mean	103	23	0	310
$PM_{2.5}$	Annual mean	82	0	0	2
PM_{10}	36th highest daily mean concentration	221	0	0	7
	Annual mean	221	0	0	7
O_3	26th highest maximum daily 8-h mean	14	182	124	26

most of the sites is due to the summed contributions giving larger concentrations than the base case (up to 80% in some cases). Similarly for $PM_{2.5}$ and PM_{10}, the 5% difference criterion was not met at nearly all of the locations studied, again due to the contributions giving larger concentrations than the base case (up to 93% in some cases). The reasons for this non-additivity when the zero-out method is applied to NO_2 and PM concentrations will be explored in future work.

4 Conclusions

- The sum of the contributions compared to the base scenario for ozone is very similar for peak concentrations at more than a third of the air quality monitoring stations in Spain
- The largest contribution to ozone concentrations in Spain is from the global background
- However, domestic (and biogenic) emissions of precursors contribute significantly to peak concentrations
- Interactions of sources leads to the sum of contributions to be substantially different to the base scenario and/or negative values at many sites
- The sum of the contributions is substantially larger than the base scenario at all sites in Spain for NO_2 and particulate matter.

Acknowledgements This work has received financial support from the Spanish Ministry of Science, Innovation and Universities through the project Retos-AIRE (RTI2018-099138-B-I00). The authors would also like to thank the Spanish Ministry for the Ecological Transition for the air quality observations, emissions, and additional financial support, the European Centre for Medium-Range Weather Forecasts (ECMWF) for providing the IFS data, the Spanish meteorological agency (AEMET) for the meteorological observations and access to the IFS data, EMEP/CEIP for the emissions data and the supercomputing team at CIEMAT.

References

Menut, L., Bessagnet, B., Khvorostyanov, D., Beekmann, M., Blond, N., Colette, A., & Mailler, S. (2014). CHIMERE 2013: A model for regional atmospheric composition modelling. *Geoscientific Model Development, 6*(4), 981–1028.

Mircea, M., Calori, G., Pirovano, G., & Belis, C. A. (2019). European guide on air pollution source apportionment (SA) for estimating particulate matter (PM) source contributions with source oriented models (SMs) and combined use of SMs and Receptor Models (RMs), JRC report (in press)

Thunis, P., Clappier, A., Tarrasón, L., Cuvelier, C., Monteiro, A., Pisoni, E., ... & Guerreiro, C. (2019). Source apportionment to support air quality planning: Strengths and weaknesses of existing approaches. *Environment International, 130*, 104825.

Questions and Answers

Questioner: Matthias Karl.

Question: A criteria for the addition of contributions from different sources of ozone impacts was set to 5%. Does this mean that an error of 5% in the addition of O_3 contributions is acceptable?

Answer: We used a value of 5% to indicate situations where the sum of the contributions was similar to the base case simulation. However, in this preliminary analysis, the value was chosen arbitrarily and the effect of using other thresholds should be assessed in future work.

Questioner: Eduardo de la Torre.

Question: Are you considering employing different emission inventories? For example, analysing North African of French emissions in depth.

Answer: We have not considered using other emission inventories although it would be one way to assess the robustness of our analyses in the future.

Spatio-Temporal Modeling of Grass and Birch Pollen in Belgium

Andy Delcloo, Willem W. Verstraeten, Rostislav Kouznetsov, Nicolas Bruffaerts, Sébastien Dujardin, Marijke Hendrickx, and Mikhail Sofiev

Abstract The contribution of biogenic aerosols such as pollen to air pollution effects on the human wellbeing is substantial. Recently there is a global increase in the burden of allergic respiratory diseases. In Europe, a quarter of the population suffers from pollinosis, whereas in some countries the prevalence is over 40%. To date, pollen of various trees and grasses in Belgium are monitored by the Belgian Scientific Institute for Public Health (Sciensano) at five stations on a daily basis. This sampling is rather general and cannot retrieve the spatial representativeness of the airborne pollen into enough detail for individual use. Chemistry Transport Models (CTM's) are able to quantify the spatial and temporal distributions of airborne pollen at different

Andy W. Delcloo and Willem W. Verstraeten are equal contribution of authors.

A. Delcloo (✉) · W. W. Verstraeten
Royal Meteorological Institute of Belgium (KMI), Ukkel, Belgium
e-mail: Andy.Delcloo@meteo.be

W. W. Verstraeten
e-mail: Willem.Verstraeten@meteo.be

A. Delcloo
Department of Physics and Astronomy, University of Ghent, Brussels, Belgium

R. Kouznetsov · M. Sofiev
Finnish Meteorological Institute (FMI), Helsinki, Finland
e-mail: Rostislav.Kouznetsov@fmi.fi

M. Sofiev
e-mail: Mikhail.Sofiev@fmi.fi

N. Bruffaerts · M. Hendrickx
Belgian Scientific Institute of Public Health (SCIENSANO), Elsene, Belgium
e-mail: Nicolas.Bruffaerts@sciensano.be

M. Hendrickx
e-mail: Marijke.Hendrickx@sciensano.be

S. Dujardin
Department of Geography, University of Namur, Namur, Belgium
e-mail: Sebastien.Dujardin@unamur.be

© The Author(s), under exclusive license to Springer-Verlag GmbH, DE, part of Springer Nature 2021

C. Mensink and V. Matthias (eds.), *Air Pollution Modeling and its Application XXVII*, Springer Proceedings in Complexity, https://doi.org/10.1007/978-3-662-63760-9_17

scales and frequencies. Moreover, CTM's are useful for short-term forecasting of the intensities of pollen levels. Here we show the results of the modelled spatio-temporal distributions of grass and birch pollen over Belgium for 2008 using SILAM driven by ECMWF meteorological data, an updated MACCIII birch tree areal fraction map based on local information, and a grass pollen emission map showing the spatial distribution of the potential grass pollen sources updated with Copernicus grassland data.

Keywords CTM · Pollen · Birch · Grass · Pollinosis · SILAM · Health

1 Introduction

Anthropogenic emissions affect the human health substantially causing six million premature and more deaths worldwide in 2015 (Landrigan et al., 2017). Pollen are biogenic emissions of aerosols that also have a large impact on the human well-being. There is an increase in the burden of allergic respiratory diseases worldwide and especially in industrialized regions. By increasing the immune reaction and by intensified biogenic emissions, air pollution both influences the amount of allergens and the number of persons with allergy.

In most countries airborne pollen of various trees and grasses are monitored on some selected locations, implying that there is no continuous info on pollen levels over time and space. Chemistry Transport Models (CTM's) can both quantify and forecast the spatial and temporal distribution of airborne pollen levels. Here we use the CTM SILAM (System for Integrated modeLling of Atmospheric coMposition) (Sofiev et al., 2013) to obtain spatio-temporal data on airborne grass and birch pollen levels over Belgium, evaluated with reference data from monitoring stations.

2 Data and Methods

CTM's can model the dispersion of pollen since airborne pollen are biogenic aerosols with a diameter of typically 5–50 times larger than conventional atmospheric aerosols. SILAM simulates the presence of pollen in the air based on processes such as wind advection, turbulent mixing, dry and wet deposition (Kouznetsov & Sofiev, 2012).

Prior to modeling pollen levels in the lower atmosphere, all the possible pollen emission sources must be provided. Therefore, a detailed and timely map of vegetation fractions must be obtained. For birches, recently a new version of a map with birch fractions was proposed for Belgium by Verstraeten et al. (2019) on 0.1° horizontal resolution based on forestry inventory plots from Flanders and the Walloon region. For grasses, a MACCIII map was applied as preliminary spatial source of

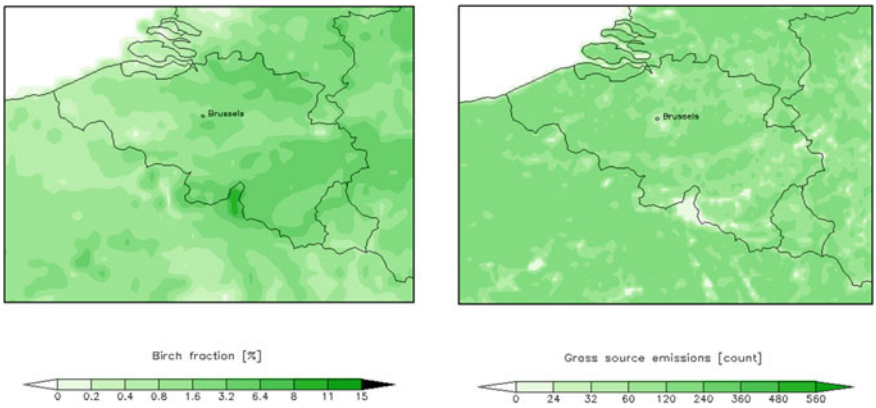

Fig. 1 The MACIII map with the areal fractions of birches (left panel, %) for the Belgian territory and the spatial distribution of grass pollen sources (right panel, amount of pollen, up to 560 and more)

grass pollen as illustrated in Fig. 1 (Sofiev, 2017). The reference map for areal birch fractions is also shown (Sofiev, 2017; Sofiev et al., 2013).

We then used the Copernicus grassland dataset on 100 m resolution to update the primary emission map of grass pollen in SILAM on a 0.05° horizontal resolution. Once the pollen sources are properly located, a temperature degree days approach or the thermal time flowering model (Sofiev et al., 2006) was applied to determine the time of flowering. It assumes that the flowering is driven by the sum of ambient temperature during a certain period in time with different thresholds for birches (season March–May) and for grasses (May–September) (Linkosalo et al., 2010; Sofiev, 2017; Sofiev et al., 2013) with a slightly modified methodology. Meteorological varying conditions such as wind speed, relative humidity and precipitation rate will affect the pollen release at the surface, transport and deposition. SILAM is driven by ECMWF ERA5 reanalysis meteorological data (grid-cell of 0.25° × 0.25°) for the birch and grass seasons of 2008. The modelled birch and grass pollen levels are evaluated using observations of pollen data taken from the Belgian Aerobiological Surveillance Network from Sciensano. In 2008 Sciensano monitored pollen concentrations at four stations (De Haan, Antwerp, Brussels, Charleroi; see for more details Verstraeten et al., 2019) on daily basis.

3 Results and Discussions

The original grass pollen sources map used in SILAM by Sofiev (2017) shows little variation in pollen amounts (Fig. 1, right panel). Locations without forests or urban land-use areas, contain grass sources. In the updated version (Fig. 2, right panel) areas with higher values pop up in the north, west and southeast of Belgium. For the

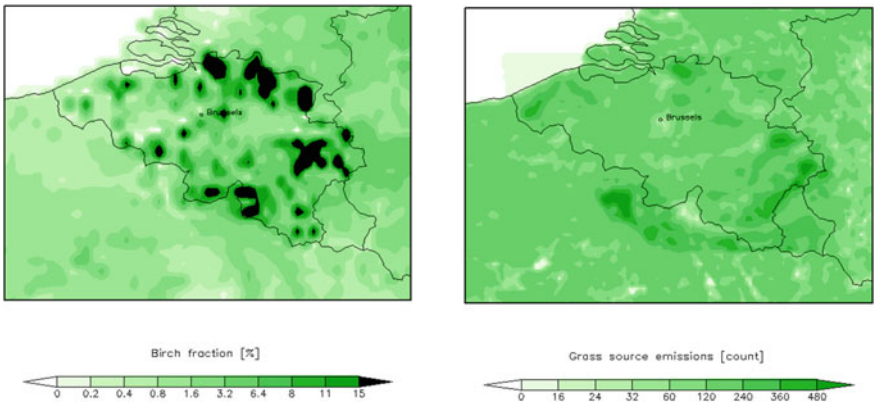

Fig. 2 Left panel, the updated birch fraction map for the Belgian territory using Flemish and Walloon forest inventory data; Right panel, a preliminary updated version of the grass pollen emission sources by combining Copernicus grassland data with the original set (pollen counts, up to 480 and more)

birch map (left panel) generally low fractions are given, with only some locations with more than 8% (Delcloo et al., 2018; Verstraeten et al., 2019).

The SILAM modelled and observed seasonal variations of birch (March–May) and grass airborne pollen (May–September) levels near the surface for 2008 for Brussels are shown in Fig. 3. The modelled time series are based on the updated spatial distributions of grass and birch pollen sources as shown in Fig. 2.

The modelled pollen levels are close to the observed pollen levels with R^2 values of 0.51 for birch pollen and 0.66 for grass pollen levels. Reducing the grass pollen time series to the period May–August 2008 decreases the R^2 value to 0.63, and to 0.58 for May–July (excluding the many zero values in August–September). Apart

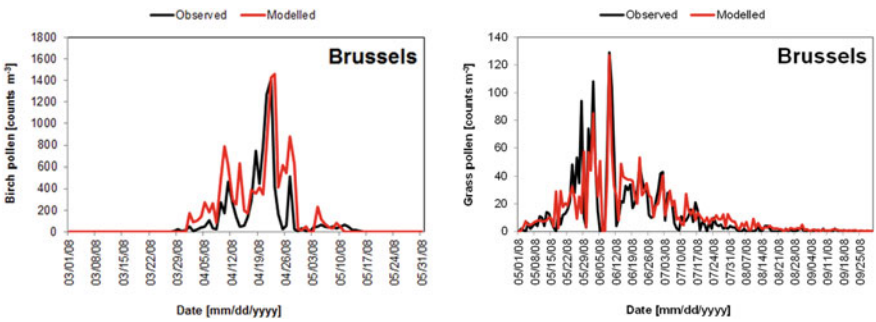

Fig. 3 Left panel, time series of observed (in black, Sciensano) and modelled (in red, SILAM) airborne birch pollen counts for the pollen season of 2008 (March–May) at Brussels using the updated birch tree fraction map (Verstraeten et al., 2019); Right panel, a preliminary time series of observed and modelled airborne pollen for grasses at Brussels (May–September) by combing the Copernicus grassland and the original data

from updating the spatial distribution of pollen emissions sources (the amount of grassland and birch fraction), also the inter-seasonal variations in the emissions of pollen (Siljamo et al., 2013) should be considered. These inter-seasonal differences in pollen amounts can be very important, especially for trees which present typical production cycles due to mast seeding (Hoebeke et al., 2018; Verstraeten et al., 2019). Moreover, the start and ends of the pollen season is often based on general climatology lacking spatio-temporal details. So there is room for further improvements in future work.

4 Conclusions

Using the CTM SILAM we simulated airborne pollen levels of grass and birch species in Belgium by ingesting updated vegetation maps containing pollen emissions sources into the model. The areal birch tree fractions are based on the most recent Flemish and Walloon forest inventory data, the grasslands are taken from Copernicus datasets. The modelled pollen concentrations were evaluated with observation from the Belgian Aerobiology surveillance network for 2008. The preliminary results are promising.

Acknowledgements This research was partly funded by the Belgian Science Policy Office (BELSPO) in the frame of the Belgian Research Action through Interdisciplinary Networks Brain (BRAIN.be) programme – project RespirIT (BR/154/A1/RespirIT) and partly funded by the Royal Meteorological Institute of Belgium.

References

Delcloo, A. W., Verstraeten, W. W., Dujardin, S., Hoebeke, L., Bruffaerts, N., Hendrickx, M., Hamdi, R., & Sofiev M. (2018). Spatio-temporal monitoring and modelling of birch pollen levels in Belgium, ITM 2018, 14 - 18 May 2018, Ottawa, Canada. Air Pollution Modeling and its Application XXVI. https://doi.org/10.1007/978-3-030-22055-6_12

Hoebeke, L., Bruffaerts, N., Verstraeten, C., et al. (2018). Thirty-four years of pollen monitoring: An evaluation of the temporal variation of pollen seasons in Belgium. *Aerobiologia.* https://doi.org/10.1007/s10453-017-9503-5

Kouznetsov, R., & Sofiev, M. (2012). A methodology for evaluation of vertical dispersion and dry deposition of atmospheric aerosols. *Journal of Geophysical Research, 117*. https://doi.org/10.1029/2011JD016366

Landrigan, P. J. et al. (2017). The Lancet Commission on pollution and health. Published online October 19, 2017. https://doi.org/10.1016/S0140-6736(17)32345-0

Linkosalo, T., Ranta, H., Oksanen, A., Siljamo, P., Luomajoki, A., Kukkonen, J., & Sofiev, M. (2010). A double-threshold temperature sum model for predicting the flowering duration and relative intensity of *Betula pendula* and *B. pubescens. Agricultural and Forest Meteorology, 150*(12), 6–11. https://doi.org/10.1016/j.agrformet.2010.08.007

Siljamo, P., Sofiev, M., Filatova, E., et al. (2013). A numerical model of birch pollen emission and dispersion in the atmosphere. Model evaluation and sensitivity analysis. *International Journal of Biometeorology, 57*, 125–136. https://doi.org/10.1007/s00484-012-0539-5

Sofiev, M., Siljamo, P., Ranta, H., Linkosalo, T., Jaeger, S., Rasmussen, A., Rantio-Lehtimaki, A., Severova, E., & Kukkonen, J. (2013). A numerical model of birch pollen emission and dispersion in the atmosphere. Description of the emission module. *Int Journal of Biometeorology, 57*, 45–58. https://doi.org/10.1007/s00484-012-0532-z

Sofiev, M. (2017). On impact of transport conditions on variability of the seasonal pollen index. *Aerobiologia, 33*, 167–179. https://doi.org/10.1007/s10453-016-9459-x

Sofiev, M., Siljamo, P., Ranta, H., & Rantio-Lehtimäki, A. (2006). Towards numerical forecasting of long-range air transport of birch pollen: Theoretical considerations and a feasibility study. *International Journal of Biometeorology, 50*, 392–402. https://doi.org/10.1007/s00484-006-0027-x

Verstraeten, W. W., Dujardin, S., Hoebeke, L., Bruffaerts, N., Kouznetsov, K., Dendoncker, N., Hamdi, R., Linard, C., Hendrickx, M., Sofiev, S., & Delcloo, A. W. (2019). Spatio-temporal monitoring and modelling of birch pollen levels in Belgium. *Aerobiologia, 35*(4), 703–717. https://doi.org/10.1007/s10453-019-09607-w

Multi-compartment Chemistry Transport Models

Johannes Bieser and Martin Otto Paul Ramacher

Abstract There exists a large range of pollutants of global concern for whom the ocean is a key part in their environmental cycle. Namely, mercury (Hg) and several persistent organic pollutants (POPs) which are subject to international treaties (e.g. Minamata Convention, Stockholm Convention) are actively exchanged between atmosphere and ocean and subsequently accumulated in the marine food web. Thus, modeling their environmental fate requires a numerical representation of atmospheric and marine physics and chemistry. Additionally, in the marine environment interactions with biota and detritus are an important factor leading to a multi-disciplinary biogeochemical research field involving chemistry, meteorology, oceanography, and biology. However, the chemistry transport modeling research community is still virtually limited to atmospheric transport and transformation of pollutants. The ocean is typically treated as a boundary condition and only few coupled hydrodynamic models have been developed so far.

Keywords Numerical modeling · Chemistry transport · Multi compartment · Air-sea exchange · Bioaccumulation

1 Introduction

Chemistry transport models (CTMs) historically developed from meteorological models with passive tracers. About 4 decades ago, in the late 80ties and early 1990ties of the last millennium several CTMs with active photochemistry were developed (Savonis, 1995; Simpson, 1993; Zlatev et al., 1993). The first models were developed with the aim to investigate high ozone concentrations (summer smog) and acidification (winter smog). Ever since, these models have been improved and enhanced to implement additional species and physicochemical processes in the atmosphere.

J. Bieser (✉) · M. O. P. Ramacher
Department of Chemical Transport Modeling, Helmholtz-Zentrum Hereon, Institute of Coastal Research, Max-Planck-Strasse 1, 21502 Geesthacht, Germany
e-mail: johannes.bieser@hzg.de

© The Author(s), under exclusive license to Springer-Verlag GmbH, DE, part of Springer Nature 2021

C. Mensink and V. Matthias (eds.), *Air Pollution Modeling and its Application XXVII*, Springer Proceedings in Complexity, https://doi.org/10.1007/978-3-662-63760-9_18

Today, typically include bi-directional exchange processes with other compartments in order to capture the cycling of pollutants in the atmosphere (Bash et al., 2013). Starting with simple parametrizations like instantaneous re-emissions or two layer exchange models, there has been a development towards fully coupled multi-compartments models for pollutants that cycle between different compartments (Bieser & Schrum, 2015; Soerensen et al., 2010).

2 Mercury

Mercury is a toxic substance of anthropogenic origin. Every year around 2000 tons of Hg are emitted into the atmosphere, mostly (97%) from anthropogenic sources. Gaseous elemental mercury has a lifetime of 1.2–1.6 years and thus is transported on a global scale. Since pre-industrial times the mercury burden has increased sevenfold in the atmosphere and threefold in the global ocean (Lamborg et al., 2014). Mercury is a unique heavy metal, as it exists as gaseous elemental mercury in its natural form and is thus transported on a global scale. As residence time of mercury in the environment has been estimated in the order of several thousand years (Amos et al., 2013) even with decreasing emissions there will be elevated level of mercury in the environment for years to come.

In the aqueous environment, mercury can be transformed to highly toxic methyl mercury species that accumulated along the food chain and pose a direct threat to human health and food safety. In order to understand the impact of changing external drivers (e.g. emission reductions, climate change, food web composition, anthropogenic marine particles) on the cycling and bio-availability of mercury in the environment it is necessary to develop fully coupled multi-compartment models that are able to simulate the behavior of mercury in different compartments as well as their cycling between them.

Similarly, there is a large collection of persistent organic pollutants including a range of legacy pollutants that have already be banned and new upcoming replacement chemicals which can be actively exchanged between atmosphere, ocean, and ecosystem.

3 Model and Domain

Here we show results from the coupled atmosphere–ocean-ecosystem modeling system ECOSMO-CMAQ (Bieser et al., submitted). The model consists of the atmospheric CTM CMAQ (Byun & Schere, 2006; Zhu et al., 2015) coupled to the ocean-ecosystem model ECOSMO (Daewel & Schrum, 2013). The model was setup for a domain covering the North- and Baltic Sea in northern Europe and was run for a period of 60 years. Here we show average concentrations of major Hg species in atmosphere, ocean, and biota (Fig. 1). It can be seen, that the system exhibits a high

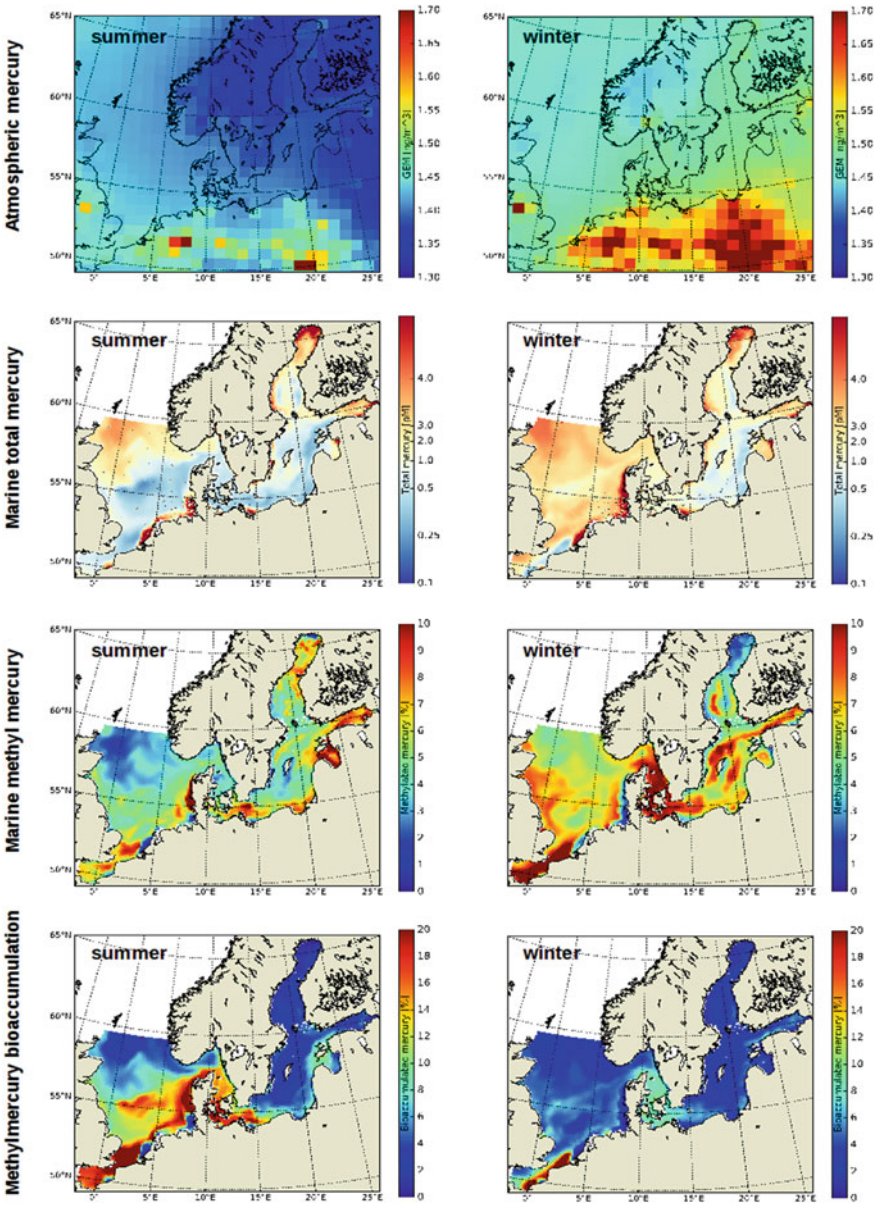

Fig. 1 Average mercury concentrations for summer (left) and winter (right) in different compartments **a** atmosphere, **b** ocean total Hg, **c** ocean methylated Hg, **d** Mercury accumulation in lower trophic levels

level of variability and that there is a non-linear relationship between compartments and species.

Atmospheric mercury concentrations are determined by local sources and show a distinct annual cycle due to emissions and planetary boundary layer height (Fig. 1a). In the ocean, elevated mercury concentrations can be found at the coast (due to riverine inflow) and in upwelling regions (Fig. 1b). The main sources for mercury in the North- and Baltic Sea are atmospheric deposition (8.5 t/a) and riverine inflow (4 t/a). In the ocean, Hg undergoes a complex biochemical red-ox cycle, including photolytic, abiotic and biotic reactions. Elemental mercury evades back into the atmosphere with a net release of 10 t/a per year, making the domain, on average, a net sink for mercury. However, because of low atmospheric concentrations and high biological activity, during summer the ocean can become a source for mercury at times.

In the marine environment Hg can form methylmercury (MeHg), a dangerous neurotoxin. This process was thought to occur only in sediments and in the water column under anoxic conditions. However, it was found that the majority of methylmercury in the marine environment is formed by bacteria related to the remineralization of organic matter in oxic waters. Figure 1c depicts the marine methyl mercury distribution which can be seen to follow frontal systems of high biological activity and leads to higher concentrations in anoxic and upwelling regions.

Depending on chemical speciation and particle partitioning methyl mercury accumulates in phytoplankton. Observed biomagnification factors from water to the lowest trophic level range from 10^3 to 10^6. Unlike inorganic Hg, methylmercury is then further accumulated along the food chain (Fig. 1d).

4 Conclusions

Here we presented first results of a multi compartment model for mercury and methyl mercury that includes atmosphere, ocean, and ecosystem. We show that due to different processes each of these compartments and species exhibits distinct spatio-temporal distribution patterns necessitating the development of complex models in order to predict the impact of changing drivers on the cycling, transformation, and bioaccumulation of mercury in the food chain.

References

Amos, H. M., Jacob, D. J., Streets, D. G., & Sunderland, E. M. (2013). Legacy impacts of all-time anthropogenic emissions on the global mercury cycle Global Biogeochm. *Cycles, 27*(2), 410–421.

Bash, J. O., Cooter, E. J., Dennis, R. L., Walker, J. T., & Pleim, J. E. (2013). Evaluation of a regional air-quality model with bidirectional NH_3 exchange coupled to an agroecosystem model. *Biogeosciences, 10*, 1635–1645.

Bieser, J., Kuss, J., Daewel, U., & Schrum, C. (2020). MECOSMO v2.3—A novel coupled multi-compartment chemistry transport model for mercruy cycling (submitted)

Bieser, J., & Schrum, C. (2015). Impact of marine mercury cycling on coastal atmospheric mercury concentrations in the North- and Baltic Sea region. *Elementa 2016*, 000111.

Byun, D., & Schere, K. L. (2006). Review of the governing equations, computational algorithms, and other components of the models-3 community multiscale air quality (CMAQ) modeling system. *Applied Mechanics Reviews, 59*, 51–77. https://doi.org/10.1115/1.2128636

Daewel, U., & Schrum, C. (2013). Simulating long-term dynamics of the coupled North Sea and Baltic Sea ecosystem with ECOSMO II: Model description and validation. *Journal of Marine Systems, 119–120*, 30–49.

Lamborg, C. H., Hammerschmidt, C. R., Bowman, K. L., Swarr, G. J., Munson, K. M., Ohnemus, D. C., Lam, P. J., Heimbürger, L.-E., Rijkenberg, M. J. A., & Saito, M. A. (2014). A global ocean inventory of anthropogenic mercury based on water column measurements. *Nature, 512*, 65–68.

Savonis, M. J. (1995). The CMAQ Program: Realizing ISTEA's Promise. *Public Roads, 58*(4), Federal Highway Administration. ISSN: 0033-3735. https://www.fhwa.dot.gov/publications/publicroads/

Simpson, D. (1993). Photochemical model calculations over Europe for two extended summer periods: 1985 and 1989. Model results and comparison with observations. *Atmospheric Environment. Part A. General Topics, 27*(6), 921–943. ISSN 0960-1686. https://doi.org/10.1016/0960-1686(93)90009-N

Soerensen, A. L., Sunderland, E. M., Holmes, C. D., Jacob, D. J., Yantosca, R. M., Skov, H., Christensen, J. H., Strode, S. A., & Mason, R. P. (2010). An improved global model for air-sea exchange of mercury: High concentrations over the North Atlantic. *Environmental Science and Technology, 44*(22), 8574–8580.

Zhu, J., Wang, T., Bieser, J., & Matthias, V. (2015). Source attribution and process analysis for atmospheric mercury in eastern China simulated by CMAQ-Hg. *Atmospheric Chemistry and Physics, 15*(15), 8767–8779.

Zlatev, Z., Christensen, J., & Elissen, A. (1993). Studying high ozone concentrations by using the Danish Eulerian model. *Atmospheric Environment. Part A. General Topics, 27*(6), 845–865, ISSN 0960-1686. https://doi.org/10.1016/0960-1686(93)90006-K

Climate Change Projections for Bulgaria According to RCP45 Scenario Until 2099

Rilka Valcheva

Abstract The ICTP regional climate model RegCM4 is used to simulate future climate over Bulgaria and the Balkan Peninsula with horizontal grid resolution of 20 km. The boundary conditions are provided from Hadley Centre Global Environment Model version 2—Earth System (HadGEM2-ES) according to RCP4.5 scenario. The results are presented for the two future periods 2021–2050 and 2071–2099 relative to the reference period 1975–2004 on spatial maps of annual and seasonal mean temperature and precipitation.

Keywords Climate change · RegCM4 · RCP4.5 · HadGEM2-ES

1 Introduction

This study is focusing on regional climate modeling with 20 km resolution over the Balkan Peninsula domain and Bulgaria. The main aim of this work is to provide climate change projections of temperature and precipitation for Bulgaria by using RCP4.5 scenario (Thomson et al., 2011) by the end of the twenty first century.

2 Data and Experiment Design

The ICTP regional climate model RegCM4.4.5 is used to simulate future climate in Bulgaria and the Balkan Peninsula. The model resolution is 20 km and the boundary conditions are provided from HadGEM2-ES model (Hadley Centre Global Environment Model version 2—Earth System) (Collins et al., 2011) which has 38 vertical levels and lat/lon grid 1.25° × 1.875°, according to RCP4.5 scenario (Thomson et al., 2011). The results are presented for near future (2021–2050) and far future

R. Valcheva (✉)
Department of Meteorological Forecasts and Information Services, National Institute of Meteorology and Hydrology, 66 Tsarigradsko Shose Blvd., 1784 Sofia, Bulgaria
e-mail: Rilka.Valcheva@meteo.bg

© The Author(s), under exclusive license to Springer-Verlag GmbH, DE, part of Springer Nature 2021

C. Mensink and V. Matthias (eds.), *Air Pollution Modeling and its Application XXVII*, Springer Proceedings in Complexity, https://doi.org/10.1007/978-3-662-63760-9_19

(2071–2099) periods relative to the reference period (1975–2004) on spatial maps of annual and seasonal mean temperature and precipitation. For validation purposes, the results from the reference run 1975–2004 are compared with observational CRU TS3.23 (Harris & Jones, 2015) data sets with horizontal grid resolution 0.5° × 0.5°. It is calculated the deviation of the model from measured climatic data (bias) of temperature and precipitation. The mean bias values are defined as the spatial average of differences between the simulated (RegCM) and observed (CRU) data sets over Bulgaria.

The ICTP RegCM4 model (Giorgi et al., 2012) has the dynamical core of the fifth-generation Mesoscale Model (MM5) from the National Centre for Atmospheric Research (NCAR) and Pennsylvania State University. RegCM4 is a hydrostatic, compressible, sigma-p vertical coordinate model run on an Arakawa B-grid. It is used the radiation scheme of the Community Climate Model 3 (CCM3). For convective precipitation parametrization it is used Grell scheme with Arakawa-Schubert closure assumption. The sub-grid explicit moisture scheme (SUBEX) is used for large-scale non-convective precipitation. The biosphere–atmosphere transfer scheme (BATS) is used for simulating land surface processes and the planetary boundary layer is modelled based on the scheme of Holtslag.

The domain is centred at 24° E–42° N, with a grid size of 20 km and 128 × 96 grid points, which correspond to 2560 × 1920 km^2. The topography of the integration domains (after removing the buffer zones of 12 points from each side) used in the present study can be seen in Fig. 1.

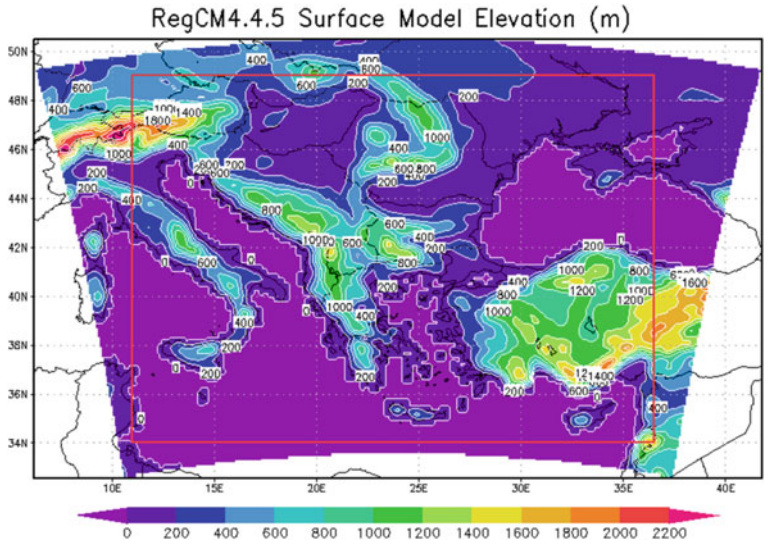

Fig. 1 Model domain (11.0° E–36.5° E, 34° N–49° N) and topography (m) at a grid spacing of 20 km using RegCM4.4.5-HadGEM2-ES over Balkan Peninsula and Bulgaria. The box shows the interior domain marked with red line, which is not directly affected by the lateral buffer zone

3 Results

The results obtained by downscaling from HadGEM2-ES global model by using regional climate model RegCM4 for the reference period 1975–2004 are compared with CRU TS3.23 data sets for the territory of Bulgaria (Tables 1 and 2).

The mean biases for spring and autumn are lower than 0.5 °C, cold in spring and warm in autumn. In summer and winter the model shows warm temperature biases (1.9 °C and 1.1 °C, respectively). Considering the annual mean temperature the model shows a positive bias (0.7 °C) for the territory of Bulgaria.

In case of precipitation, the model shows overestimation in all seasons except the summer season. Considering annual rainfall the RegCM4_HadGEM2-ES model shows 67% more precipitation for the territory of Bulgaria compared with CRU TS3.23 data sets.

The results from future simulations for the two future periods (2021–2050 and 2071–2099) relative to the reference period (1975–2004) are summarized in Fig. 2 on spatial maps of annual and seasonal mean temperature and precipitation. Annual temperature raising is between 1.5 °C and 2.3 °C in the first period and up to 3.5 °C in the second for the entire domain. Considering the annual rainfall amounts, it is noted ±5% change in precipitation for the continental parts of the domain for both periods and up to 25% increase in precipitation over the Black Sea for the period 2071–2099. In the first period (2021–2050) the highest warming is shown in the summer

Table 1 Seasonal and annual mean temperature (°C) for Bulgaria from simulations with RegCM4_HadGEM2-ES compared with observational CRU data sets and mean BIAS for the period 1975–2004

Temp (°C)	RegCM4	CRU	BIAS
Winter	2.504	1.035	1.136
Spring	10.171	10.525	−0.455
Summer	22.838	20.948	1.918
Autumn	12.352	11.866	0.248
Annual	11.966	11.094	0.712

Table 2 Seasonal and annual precipitation (mm/day) for Bulgaria from simulations with RegCM4_HadGEM2-ES compared with observational CRU data sets and mean BIAS for the period 1975–2004

PREC mm/d	RegCM4	CRU	BIAS
Winter	3.059	1.512	1.604
Spring	3.050	1.750	1.480
Summer	1.486	1.711	−0.09
Autumn	2.946	1.615	1.412
Annual	2.636	1.647	1.099

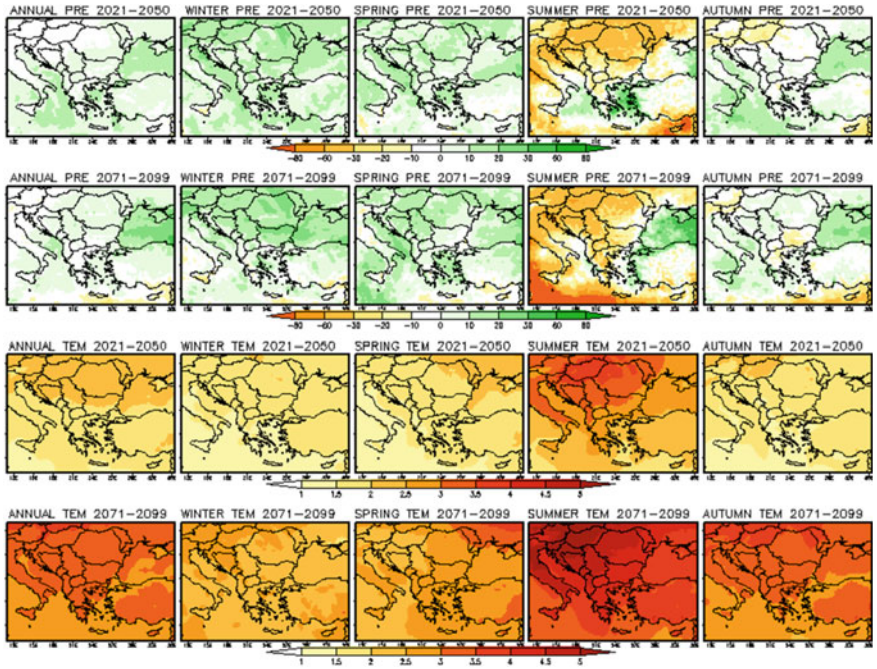

Fig. 2 Simulated annual and seasonal mean changes of precipitation (mm/d) (first two rows) and temperature (in °C) (second two rows) for near future 2021–2050 and far future 2071–2099 periods by using RegCM4.4.5_HadGEM2-ES model according to RCP45 scenario (reference period: 1975–2004)

period between 2.5 °C and 3 °C. In the other seasons the evaluated temperatures are slightly lower, between 1.5 °C and 2 °C. In case of precipitation, there would be a decrease in summer rainfall between 20 and 40% and in autumn between 10 and 20% in the north-western and south-eastern parts of the domain. In the second period (2071–2099) there would be an increase between 2 °C and 2.5 °C in winter temperature and between 2.5 °C and 3.5 °C in spring and autumn temperatures. It can be expected an increase up to 5 °C in summer temperature in the north and north-western parts of domain. There would be an increase in winter precipitation up to 20%, especially in the north parts of Bulgaria and in spring with about 10%. There would be a decrease between 30 and 60% in summer precipitation except the Black Sea region. For Bulgaria, a decrease in autumn precipitation can be expected with about 10% and a decrease in summer precipitation with about 30%.

4 Conclusion

Considering annual mean temperature and precipitation the RegCM4 model forced with boundary conditions provided from HadGEM2-ES global model shows warm temperature bias (0.7 °C) and 67% more precipitation for the territory of Bulgaria for the period 1975–2004.

According to the outputs obtained from the projections by the end of the twenty first century the model simulation projects warmer conditions throughout the whole year, less precipitation in summer and autumn, and more precipitation in winter and spring.

Acknowledgements This work has been carried out in the framework of the National Science Program "Environmental Protection and Reduction of Risks of Adverse Events and Natural Disasters", approved by the Resolution of the Council of Ministers № 577/17.08.2018 and supported by the Ministry of Education and Science (MES) of Bulgaria (Agreement № D01-230/06.12.2018). This study has been also funded by the Bulgarian National Science Fund (DN-14/3 13.12.2017).

References

Collins, W. J., Bellouin, N., Doutriaux-Boucher, M., Gedney, N., Halloran, P., Hinton, T., Hughes, J., Jones, C. D., Joshi, M., Liddicoat, S., Martin, G., O'Connor, F., Rae, J., Senior, C., Sitch, S., Totterdell, I., Wiltshire, A., & Woodward, S. (2011). Development and evaluation of an Earth-system model—HadGEM2. Geoscientific Model Development Discussion, *4*, 997–1062.https://doi.org/10.5194/gmdd-4-997-2011

Giorgi, F., Coppola, E., Solmon, F., Mariotti, L., Sylla, M. B., Bi, X., Elguindi, N., Diro, G. T., Nair, V., Giuliani, G., Turuncoglu, U. U., Cozzini, S., Güttler, I., O'Brien, T. A., Tawfik, A. B., Shalaby, A., Zakey, A. S., Steiner, A. L., Stordal, F., Sloan, L. C., & Brankovic, C. (2012). RegCM4: Model description and preliminary tests over multiple CORDEX domains. *Climate Research, 52*(1), 7–29. https://doi.org/10.3354/cr01018

Harris, I. C., & Jones, P. D. (2015). CRU TS3.23: Climatic Research Unit (CRU) Time-Series (TS) Version 3.23 of high resolution gridded data of month-by-month variation in climate (Jan. 1901- Dec. 2014). Centre for Environmental Data Analysis, 09 November 2015. https://doi.org/10.5285/4c7fdfa6-f176-4c58-acee-683d5e9d2ed5

Thomson, A., Calvin, K., Smith, S., Kyle, P., Volke, A., Patel, P., Delgado-Arias, S., Bond-Lamberty, B., Wise, M., Clarke, L., & Edmonds, J. (2011). RCP4.5: A pathway for stabilization of radiative forcing by 2100. *Climatic Change, 109*, 77–94. https://doi.org/10.1007/s10584-011-0151-4

Data Assimilation and Air Quality Forecasting

Interpreting Measurements from Air Quality Sensor Networks: Data Assimilation and Physical Modeling

F. Barmpas, George Tsegas, Nicolas Moussiopoulos, and Eleftherios Chourdakis

Abstract The Interreg Balkan-Med AIRTHINGS project exploits rapid developments in sensor technology and numerical air quality modeling, in order to provide reliable regulatory air quality assessment services. For this purpose, inexpensive air quality measuring sensors provide real-time air quality data in selected cities of five Balkan countries. The Internet of Things measuring sensor network is deployed over urban hotspots and areas of high population density implementing peer-to-peer connectivity. The sensor data stream combines real-time information on pollutant concentrations, meteorological parameters and error-correction feedback. At the same time, the mesoscale modeling system MEMO/MARS-aero and the two-way coupled meso-micro MEMICO scheme are also deployed in the urban- and neighbourhood scales, respectively. A combination of data fusion and data assimilation methods is employed to incorporate emission data, real-time sensor measurements and sensor error management in the dispersion modeling system. An advanced spatial and temporal analysis algorithm is applied, whereby outlier measurements due to accumulated error can be quickly distinguished from actual concentration extremes and either discarded or corrected. Model results are further analysed off-line to detect diurnal, seasonal or spatial pollution patterns. In line with the provisions of the Interreg Balkan-Med program, the combined data are freely available through an Open Data Platforms.

F. Barmpas (✉) · G. Tsegas · N. Moussiopoulos · E. Chourdakis
Laboratory of Heat Transfer and Environmental Engineering,
Aristotle University, 54124 Thessaloniki, Greece
e-mail: fotisb@auth.gr

G. Tsegas
e-mail: gtsegas@auth.gr

N. Moussiopoulos
e-mail: moussio@eng.auth.gr

E. Chourdakis
e-mail: chourdakis@auth.gr

© The Author(s), under exclusive license to Springer-Verlag GmbH, DE, part of Springer Nature 2021

C. Mensink and V. Matthias (eds.), *Air Pollution Modeling and its Application XXVII*,
Springer Proceedings in Complexity, https://doi.org/10.1007/978-3-662-63760-9_20

1 Introduction

The aim of this work is to focus on the exploitation of rapid developments in technology in order to combine low-cost innovative air pollution sensors with advanced air quality modeling tools, thus providing regulatory assessment services and supporting the evaluation of mitigation measures. For this purpose, air quality measuring sensors are used in selected cities of five Balkan countries, to provide real time air quality data.

A continuous quality testing and data assimilation process integrates emission data and real-time sensor measurements in an operational atmospheric modeling system based on the MEMO/MARS-aero and MIMO numerical models. The dispersion modeling tools incorporate and complement the sensor data on pollutant levels with predictions of high temporal and spatial resolution, covering the selected urban areas, so as to highlight pollution hot spots. A continuous quality-testing and data assimilation process ensures that data flows from the sensor network are appropriately integrated in both on-line and off-line simulations of concentration fields. This information is used to identify and quantify source contributions in the areas of interest, particularly during periods of exceedances above EU limit values, in this way supporting the evaluation of the efficiency of proposed mitigation plans.

2 Methodology

Mesoscale models can typically simulate atmospheric flows in the 20–500 km scale, providing reliable 3D meteorological fields to be used in pollutant transport, diffusion and chemical transformation calculations in and around urban areas. In the case of the AIRTHINGS target cities, an Operational Air Quality System (AQMS) is deployed, based on a modeling core consisting of the coupled mesoscale MEMO and MARS-aero chemical dispersion models (Moussiopoulos et al., 2010, 2012). These models however, by themselves are not capable of resolving urban canopy effects or explicitly taking into account obstacle geometries. Figure 1 illustrates the concept of quantifying the so-called concentration increments, each representing contributions from sources and processes at a specific spatial scale.

In order to provide additional information on finer spatial scales over the application areas, the two-way coupling scheme MEMICO (Tsegas et al., 2015) has been applied for coupling the mesoscale model MEMO and the microscale model MIMO (Ehrhard et al., 2000), employing a collection of interpolating metamodels. In the two-way coupling scheme, a three-dimensional spatial interpolation scheme, a spatial adjustment of values within the surface layer, and the formulation of the lateral boundary conditions to introduce the interpolated values into the microscale model are utilized.

The third component of the modeling system deployed over the target areas is an advanced operational data assimilation (DA) system (denoted AQMS + DA), which

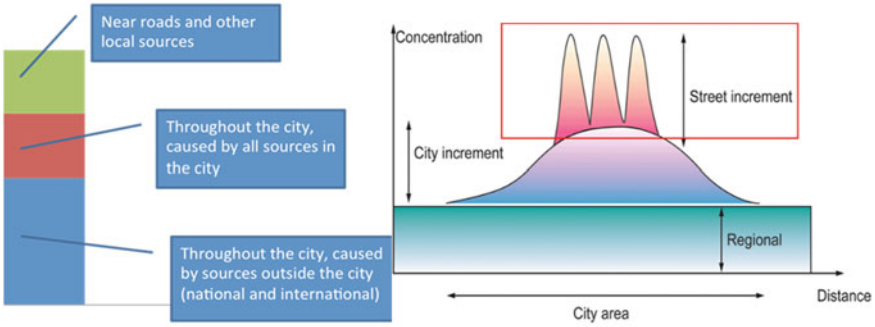

Fig. 1 Estimation of concentration increments in different spatial scales

incorporates the data and control streams from the sensor networks. In this way, additional information is incorporated on the forecast results from sensors denoted as "traffic stations", on spatial scales not normally resolved by the MEMO/MARS-aero system. Additionally, the accuracy of the mesoscale calculation themselves is improved by assimilated data from sensors located away from streets, chimneys of heating systems, denoted as "background stations".

3 Operational Phase

The combined operation of the AQMS + DA system during the operational deployment of the system can be described as a sequence of eight steps. Steps 1–8 are repeated on a 5- or 10-min frequency, or whenever a new packet of sensor data becomes available. During this period, additional iterations of steps 4–8 could be performed internally, in order to improve/correct the accuracy of the last available data.

1. *Transfer of concentration data*: this encompasses all the low-level operations necessary for communicating with the station monitoring software, checking the availability of new data, format conversions and handling of errors. Data received includes time-stamps and location/GPS data (in case of mobile sensors).
2. *Trimebase checking, rejection of out-of-sequence data*: in this stage, the time-stamps of the received data are checked and out-of-order data rejected. Mobile sensor location data are also checked and invalid locations (e.g. outside the fine computational grid) are be rejected.
3. *Sanity checking*: during this step, more sophisticated checks are performed: concentrations and their derivatives are checked against predefined (per-species) hard bounds. Data from stations with unjustifiably high spatial variability are selectively rejected.

4. *Classification of sensor and normalisation of data*: each data source (sensor, station) is classified, according to its location and area of coverage as "traffic station", "background station" and "rural station". For stationary equipment, this classification is done once in the beginning of the assimilation. Data from the classified stations are "normalised" in order to remove as much of the systematic/drift error as possible, on the basis of "offset corrections" that calculated at each assimilation cycle (step 8), as residuals between calculated calculations and concentration from nearby stations. A machine-learning algorithm is responsible for updating the corrective factors in the offset calculation.
5. *Calculation of numerical tendencies (forcing terms)*: difference terms indicating the necessary corrections to the calculated concentration are calculated to be applied in one or more computational cells of MARS-aero after an appropriate spatial and temporal "spreading" (step 6)
6. *Spatial "smearing" of tendencies*: depending on the spatial classification of each assimilated observation, an appropriate spatial and temporal scaling is applied prior to the final introduction of corrections in the MARS-aero dynamical equations: "rural" measurements affect several neighbour MARS-aero cells through a Gaussian spread function. For "background" stations, a smaller spread is applied. For "traffic"-hotspot measurements, the corrective term is not introduced directly in the mesoscale model, but incorporated in the finer-scale model MEMICO in proportion to the ratio of the station area of coverage (i.e. area of the nearest street segment which lies within each computational cell).
7. *Incorporation of tendencies in the dynamical terms and step integration*: the dynamical equations are time-stepped by the numerical solver as usual, but including the additional corrective terms.
8. *Extraction of normalisation terms/data*: during this step, the last available measurements are compared to the corresponding calculated concentrations and a potential drift/offset correction is calculated for the observations using a multilinear empirical equation. The equation factors are updated by a machine-learning algorithm using as convergence criteria (1) the minimization of total prediction error over all the sensors and over a specific period of time (2) the minimization of monotonic components (drift) in the measurements over the course of 24- or 48-h periods.

Model results are further processed off-line to detect diurnal, seasonal or spatial pollution patterns. This information can be used to identify and quantify source contributions in areas of interest, particularly during periods of exceedances above EU limit values, thus providing support for the evaluation of the efficiency of proposed mitigation plans. During the preliminary stage of the project, the AQMS + DA is operating using synthetic datasets simulating the data flow from deployed sensors, as well as anonymized data in collaboration with the SmartAQnet project. The first operational phase of the AIRTHINGS project will involve the deployment of AQMS + DA system for the on-line assimilation of actual data streams from ten

stationary mini-sensors, installed at a number of urban hotspots in the city of Thessaloniki. Additional data streams from mobile sensors are expected to be added over the course of the project.

4 Conclusion

The methodological approach of the presented work focuses on the utilization of latest developments both in sensor technology and numerical air quality modeling, aiming to provide end products able to support regulatory assessment and environmental information services. A peer-to-peer network of air quality measuring devices is deployed in six urban areas in the Balkan region in order to provide real time air quality data over areas of high population and emissions density. The coupled mesoscale modeling system MEMO/MARS-aero and the mesoscale-microscale MEMICO two-way coupling methodology implement the physical modeling core of an Air Quality Management System deployed in the respective study areas. An advanced data assimilation platform aims to alleviate issues typically related to the accuracy and consistency of data provided by networks of inexpensive sensors. In effect, the dynamical core of the modeling tools provides the means to evaluate, integrate and complement the sensor data on pollutant levels in predictions of high temporal and spatial resolution in order to highlight pollution and exposure in urban hot spots.

Acknowledgements The "AIRTHINGS" Project is co-funded by the European Union and national funds of the participating countries.

References

Ehrhard, J., Khatib, I. A., Winkler, C., Kunz, R., Moussiopoulos, N., & Ernst, G. (2000). The microscale model MIMO: Development and assessment. *Journal of Wind Engineering and Industrial Aerodynamics, 85*, 163–176.

Moussiopoulos, N., Douros, I., Tsegas, G., Kleanthous, S., & Chourdakis, E. (2010). An air quality management system for Cyprus. *Global Nest Journal, 12*, 92–98.

Moussiopoulos, N., Douros, I., Tsegas, G., Kleanthous, S., & Chourdakis, E. (2012). An air quality management system for policy support in Cyprus, Hindawi Publishing Corporation. *Advances in Meteorology*.https://doi.org/10.1155/2012/959280

Tsegas, G., Moussiopoulos, N., Barmpas, F., Akylas, V., & Douros, I. (2015). An integrated numerical methodology for describing multiscale interactions on atmospheric flow and pollutant dispersion in the urban atmospheric boundary layer. *Journal of Wind Engineering and Industrial Aerodynamics, 144*, 191–201. ISSN 0167-6105https://doi.org/10.1016/j.jweia.2015.05.006

Need and Potential Benefits of Improving Aloft Air Pollution Characterization: A Modeling Perspective

Rohit Mathur, Christian Hogrefe, James Szykman, Gayle Hagler, Amir Hakami, and Shunliu Zhao

Abstract Using process tendencies derived from the Community Multiscale Air Quality (CMAQ) model in conjunction with inferences from widespread surface measurements, we demonstrate that the amount of O_3 entrained in the morning to the surface is an indicator of non-local (or background) pollution at a location and that continuous aloft residual-layer O_3 measurements would provide a direct quantitative measure of this non-local contribution. We discuss how continuous aloft air pollution measurements can cost-effectively be achieved through leveraging recent technological advances to provide for the first time a complete regional view of nocturnal aloft O_3. Calculations with the CMAQ-adjoint model further demonstrate that such measurements would be 3–4 times more effective than surface measurements in characterizing the surface-level daily maximum 8-h average ozone. Preliminary results from chemical data "nudging" experiments demonstrate the additional benefits of assimilating aloft O_3 information in improving next day air quality forecasts.

1 Introduction

Changing amounts of non-local (or background) air pollution contributions is cited as a key challenge for many regions in demonstrating compliance with the air quality standards, but feasible strategies to characterize the space and time variations in these non-local contributions have been lacking (Mathur et al., 2017). Ground-level O_3 mixing ratios at any given location result from of an *in-situ* component dictated by local source-sink balance and a *background* component representing non-local O_3 transported to that location. Though airmasses are transported to a location throughout the day, long-range transport occurs efficiently in the nocturnal residual layer and in the free troposphere, suggesting that characterization of air

R. Mathur (✉) · C. Hogrefe · J. Szykman · G. Hagler
National Exposure Research Laboratory, US Environmental Protection Agency, 109 T.W. Alexander Dr., Research Triangle Park, NC 27711, USA
e-mail: Mathur.Rohit@epa.gov

A. Hakami · S. Zhao
Carleton University, Ottawa, Canada

This is a U.S. government work and not under copyright protection in the U.S.; foreign copyright protection may apply 2021

C. Mensink and V. Matthias (eds.), *Air Pollution Modeling and its Application XXVII*, Springer Proceedings in Complexity, https://doi.org/10.1007/978-3-662-63760-9_21

pollution aloft is essential for quantifying the non-local or background pollution contributions at a location.

2 Variations in Surface and Aloft O_3

Limited available measurements have suggested relationships between ground-level O_3 and its nocturnal aloft values and are illustrated in Fig. 1 which presents timeseries of O_3 measured at the surface and at two altitudes on a tall tower (Aneja et al., 2000) in Auburn, NC. As can be seen, nocturnal long-range transport results in higher values in the aloft residual layer which are largely decoupled from surface O_3 values. The O_3 rich air from aloft entrains to the surface with the break-up of the nocturnal inversion, providing a starting background value on which the in-situ chemical production builds, eventually leading to vertically well mixed O_3 by mid-day as indicated by similar magnitudes of O_3 mixing ratios at all three levels.

Figure 2a, b present summer average O_3 tendencies, i.e., rate of change (expressed in ppb/hr), measured at the AQS and CASTNET monitoring network sites across the continental U.S. In contrast to O_3 mixing ratios which typically peak around early

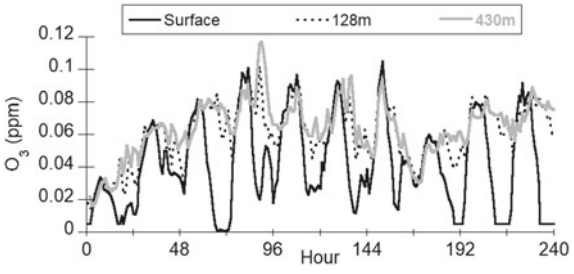

Fig. 1 Measured variations in O_3 mixing ratios at different altitudes at Auburn, NC during June 1996

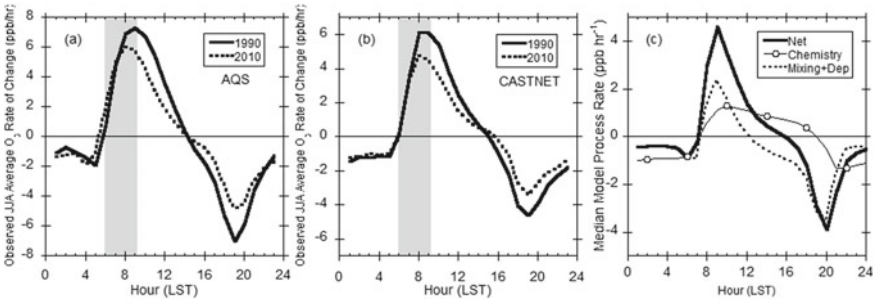

Fig. 2 Diurnal O_3 tendency: **a** observed average at the AQS sites, **b** observed average at the CASTNET sites, and **c** median model values across all continental U.S. land cells

to mid-afternoon, the ground-level O_3 tendency is highest in the morning and peaks around 9:00 am local time; similar diurnal variations in modeled O_3 tendency are illustrated in Fig. 2c. Process rates inferred from CMAQ calculations further show that while chemical production contributes to accumulation of O_3 at the surface, the net vertical O_3 flux at the surface is dictated by the turbulent mixing responding to the evolution of the planetary boundary layer and dry deposition at the earth's surface. More importantly, this vertical flux is the dominant contributor to the net increasing O_3 tendency during the morning, further suggesting the prominent contribution of O_3 trapped in the nocturnal residual layer aloft to daytime ground-level values. Also illustrated in Fig. 2a, b are changes in mean O_3 tendencies across monitoring locations in the U.S. over two decades. Over the 1990–2010 period significant changes in O_3 precursor emissions have occurred which result not only in reduced magnitude of daytime tendencies due to a reduction in local O_3 chemical production, but also reductions in the morning entrainment rates, suggesting changes in the aloft O_3 reservoir across the region.

It can thus be postulated that improved model characterization of O_3 (and other pollutants) in the residual layer will provide greater confidence in the model's ability to represent regional transport and also the surface background values that arise from the entrainment of the aloft nocturnal pollution reservoir every morning. This idea is further confirmed through detailed backward sensitivity calculations with the CMAQ-adjoint model (Hakami et al., 2007). Figure 3 shows the sensitivity of the daily maximum 8-h average O_3 ($DM8O_3$) across the southeastern U.S. to O_3 at different altitudes expressed as percent of total sensitivity integrated through the model depth. The figure shows that $DM8O_3$ at the surface is most sensitive to O_3 distributions between 200 and 2000 m, reflecting the prominent role of transport aloft on surface O_3. It may be noted that O_3 removal at the surface due to titration by NO_x emissions and dry deposition result in the comparatively smaller sensitivity to surface

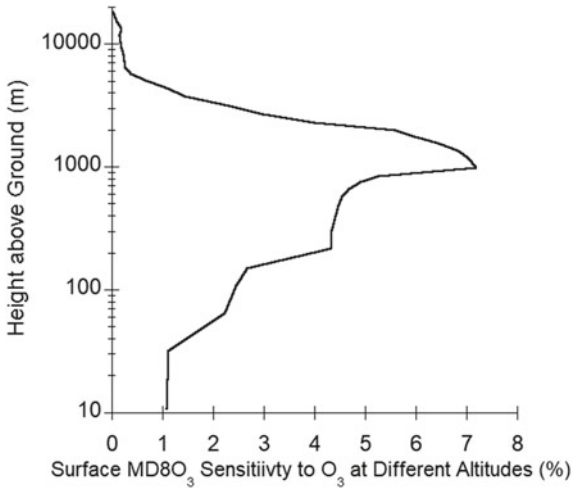

Fig. 3 Sensitivity of $DM8O_3$ across the southeastern U.S. to O_3 at different altitudes expressed as percent of total sensitivity integrated through the model depth. Adapted from Mathur et al., (2018)

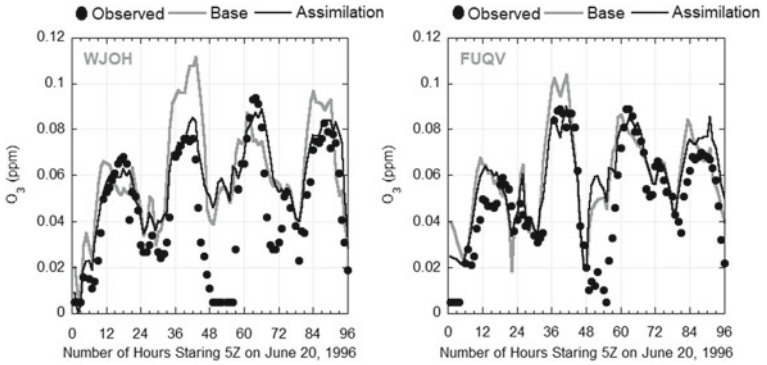

Fig. 4 Impact of assimilating aloft O_3 measurements at Auburn, NC on surface O_3 at downwind sites

O_3. Surface DM8O_3 shows the highest sensitivity to O_3 at 1–2 km, representative of the nominal daytime boundary layer height, where pollution lofted from the surface undergoes efficient lateral transport.

3 Impact of Assimilating Aloft O_3

To further explore the benefits of aloft O_3 characterization in improving model skill we conducted simple data assimilation experiments with the limited aloft measurements from the tower in Auburn, NC during 1996. We included a data-nudging technique in the Multiscale Air Quality Simulation Platform (MAQSIP; Mathur et al., 2005). Model values at layers corresponding to aloft measurements at 128 and 430 m were continuously nudged to the corresponding O_3 measurements in a 40 km area of influence. Figure 4 presents comparisons of the simulations without (Base) and with (Assimilation) this nudging, with observed surface O_3 at two sites downwind of the Auburn tower location. As can be seen from these comparisons, the improvements in model characterization of aloft O_3 resulting from the assimilation of aloft measurements helps improve the predicted variations in surface level O_3 and rectify both overestimation and underestimation of peak O_3 on different days. Consequently, assimilation of such information could dramatically improve next-day air quality forecasting.

4 A Possible Aloft Monitoring Strategy

Both the preliminary assimilation experiments and the adjoint model sensitivities point to the need for improved characterization of O_3 and other pollutant distributions

aloft, especially nocturnally, to better characterize regional pollutant transport and to quantify the spatial and temporal variability in background pollution levels. A possible strategy for such measurements could include *in-situ* measurements on tall broadcasting towers. As illustrated in Fig. 3, $DM8O_3$ is 3–4 times more sensitive to O_3 at 400–500 m than that at the surface. To estimate an optimal distribution of such monitoring locations we examined e-folding distances for modeled O_3 distributions. To estimate the e-folding distance for a given model altitude, we calculated the correlation between the synoptic component of the 0700 UTC O_3 time series at a grid point with that at each of the other grid points. For each location we then examined the relationship between this correlation and the distance between the points. The distance at which this correlation dropped below 0.37 was inferred as the e-folding distance for that location. The e-folding distance is thus an indicator of spatial correlation in the O_3 field. Analysis of summertime CMAQ simulated nocturnal O_3 at 400–500 m altitude across the contiguous U.S. indicates that these O_3 distributions typically have an e-folding distance of >200 km (Mathur et al., 2018). The proliferation of tall broadcasting masts (>400 m height) across the country and availability of high accuracy, autonomous, low-cost sensor packages (estimated at ~$5000) suggest that a cost-effective network for aloft pollution monitoring (with site separation of ~200 km) could be deployed, that would for the first time provide continuous aloft O_3 (and in the future other pollutant) measurements yielding an observed characterization of regional nocturnal pollution transport and furnish key information for quantifying background air pollution.

Acknowledgements The views expressed in this paper are those of the authors and do not necessarily represent the view or policies of the U.S. Environmental Protection Agency.

References

Aneja, V. P., Mathur, R., Arya, S. P., Li, Y., Murray, G. C., & Manuszak, T. L. (2000). Coupling the vertical distribution of ozone in the atmospheric boundary layer. *Environmental Science and Technology, 34*, 2324–2329.

Hakami, A., Henze, D. K., Seinfeld, J. H., Singh, K., Sandu, A., Kim, S., Byun, D., & Li, Q. (2007). The adjoint of CMAQ. *Environmental Science and Technology, 41*, 7807–7817.

Mathur, R., Shankar, U., Hanna, A. F., Odman, M. T., McHenry, J. N., Coats, C. J., Alapaty, K., Xiu, A., Arunachalam, S., Olerud, D. T., Byun, D. W., Schere, K. L., Binkowski, F. S., Ching, J. K. S., Dennis, R. L., Pierce, T. E., Pleim, J. E., Roselle, S. J., Young, J. O. (2005). Multiscale air quality simulation platform (MAQSIP): Initial applications and performance for tropospheric ozone and particulate matter. *Journal of Geophysical Research Atmosphere, 110*. https://doi.org/10.1029/2004JD004918

Mathur, R., Xing, J., Gilliam, R., Sarwar, G., Hogrefe, C., Pleim, J., Pouliot, G., Roselle, S., Spero, T. L., Wong, D. C., & Young, J. (2017). Extending the Community Multiscale Air Quality (CMAQ) modeling system to hemispheric scales: Overview of process considerations and initial applications. *Atmospheric Chemistry and Physics, 17*, 12449–12474. https://doi.org/10.5194/acp-17-12449-2017

Mathur, R., Hogrefe, C., Hakami, A., Zhao, S., Szykman, J., & Hagler, G. (2018). A call for an aloft air quality monitoring network: Need, feasibility and potential value. *Environmental Science and Technology, 52*, 10903–10908. https://doi.org/10.1021/acs.est.8b02496

Optimal Interpolation Based Data Fusion Techniques to Improve Deterministic Air Quality Forecast

Claudio Carnevale, Elena De Angelis, Giovanna Finzi, Enrico Turrini, and Marialuisa Volta

Abstract In the past decades, PM10 levels became one of the major environmental problems affecting humanity. The EU directive (2008/50/EC) recommends member states to ensure that (1) timely information about actual or near future exceedances of pollutants threshold values are provided to the public and that (2) it is up to regulatory agencies defining both short and long term emission control plans. In this frame, deterministic air quality forecasting models play a key role, due to their ability to predict air quality concentration on a daily basis. Unfortunately, these models are often affected by PM10 underestimation especially in high concentration areas, where their forecast of critical episodes (i.e. exceedance of 50 $\mu g/m^3$ daily threshold) has lower accuracy. To overcome this issue, several computationally expensive data assimilation techniques have been implemented in the last years. In this work, the use of fast and cheap computational techniques has been introduced and evaluated. All these techniques are based on the off-line correction of the chemical transport model output at time t, based on the measured data and the propagation of this correction up to 3 days. The propagation of the correction is a function of the results of the 3 previous days. The methodology has been tested on Lombardy region, a domain located in the Po valley, affected by high PM10 levels and frequent daily exceedances. The results show a great increase in the performance of the system, in particular for 1 day forecasts, with a strong improvement in the system ability to capture PM10 critical events.

C. Carnevale · E. De Angelis · G. Finzi · E. Turrini (✉) · M. Volta
Department of Industrial and Mechanical Engineering, University of Brescia, Brescia, Italy
e-mail: enrico.turrini@unibs.it

C. Carnevale
e-mail: claudio.carnevale@unibs.it

E. De Angelis
e-mail: e.deangelis@unibs.it

G. Finzi
e-mail: giovanna.finzi@unibs.it

M. Volta
e-mail: marialuisa.volta@unibs.it

© The Author(s), under exclusive license to Springer-Verlag GmbH, DE, part of Springer Nature 2021

C. Mensink and V. Matthias (eds.), *Air Pollution Modeling and its Application XXVII*, Springer Proceedings in Complexity, https://doi.org/10.1007/978-3-662-63760-9_22

Keywords Air quality forecast · CTM re-analysis · Optimal interpolation

1 Introduction

In the past decades, the control of PM10 has become one of the most relevant environmental problems causing the death of 9 million people worldwide (Landrigan et al., 2018).

Because of these health risks, the European Commission issued a directive (2008/50/EC) recommending the member states to (1) promptly inform the population about present or expected PM threshold exceedances and (2) to develop short and long term pollution control plans. To help environmental authorities in building these plans, Decision Support Systems have been developed (Relvas et al., 2017). A key component of these systems is the air quality forecasting model needed to compute the pollutant concentrations before critical levels occur.

One of the approaches commonly implemented to perform the forecast consists in the use of deterministic chemical transport model performing physical and chemical phenomena involved in the formation, accumulation and removal of pollutant in atmosphere (Honore et al., 2007; Manders et al., 2009). In order to make the results of CTMs more accurate, the integration of the available measurement data using Data Assimilation techniques are often implemented in the forecasting system. These techniques are usually quite computationally expensive and invasive of the CTM code.

This work presents the use of an optimal interpolation based data fusion technique to perform the re-analysis of CTM results for the forecast of daily PM10 mean. The presented technique is relatively simple to implement and does not need changes to be made in the CTM code. The results of methodology application are presented for Lombardy region, Italy.

2 Methodology

Let $PM10_{CTM}$ (t) be the PM10 concentration computed through the CTM model at time t and $PM10_{OI}(t) = PM10_{CTM}$ (t) + $C_{OI}(t)$ the estimated PM10 concentration after the correction $C_{OI}(t)$ due to the optimal interpolation technique (Carnevale et al., 2015). Unfortunately, in order to apply optimal interpolation at time t to obtain $C_{OI}(t)$, the measurements at time t are needed, and this makes this approach not applicable for forecast application.

The presented methodology is based on the estimation of an approximation $C_{OI}(t)$ of $C_{OI}(t)$ on the basis of the previous correction $C_{OI}(t-1)$, …, $C_{OI}(t-n)$.

In particular, the estimation has been performed following two main approaches: (i) the weighted mean approach and (ii) the least square one. The following subsections will explain the features of the two approaches.

2.1 Weighted Mean Approach

In this approach, the correction is computed as the weighted mean of the two previous available corrections Eq. (1).

$$\hat{C}_{OI}(t) = \alpha C_{OI}(t-1) + (1-\alpha) C_{OI}(t-2) \tag{1}$$

This very simple approach is based on the assumption that the value of the error on the results of the CTM at time t is strongly related to the errors at previous times. It can be easily noticed that for $\alpha = 1$ the value of the estimated correction at time t is equal to the correction at time $t - 1$ (persistent model) and for $\alpha = 0.5$ the estimation is the arithmetic mean of the two previous corrections.

One of the crucial aspects of this approach is related to the choice of the parameter α.

2.2 Least-Square Error Approach

In this approach, the correction is computed applying the least square technique to the previous corrections:

$$\hat{C}_{OI}(t) = \alpha_0 + \sum_{i=1}^{n} \alpha_i C_{OI}(t-i) \tag{2}$$

where α_0 and α_i, $i = 1, \ldots, n$ are computed applying the least square technique to the correction at time t-1 (dependent variable) and the n previous corrections at time t-i (independent variables). So, the estimation of the correction on time t is computed using the best least square linear model of order n, estimated on the basis of the previous corrections.

3 Case Study

The methodology has been evaluated for the daily PM10 forecast for a Northern Italy domain, an area often characterized by critical episodes and high concentration levels.

The simulations for the whole year 2011 have been computed through CAMx deterministic model, using meteorological data computed by WRF model. The integration of the CAMx results with the measurements has been implemented by means of optimal interpolation using the data of 104 PM10 stations from the Lombardy

regional network. In order to correctly evaluate the performance of the methodology, a Monte Carlo approach has been followed. In fact, 100 tests have been performed, randomly selecting 20% of the stations for the validation phase and using the remaining 80% for the optimal interpolation. Figures 1 and 2 present the forecasting results in terms of boxplot. Two groups of tests have been performed: (i) weighted mean tests, with α ranging from 0 to 1 with a 0.1 step width and (ii) least-square tests, with $n = 2$ and $n = 3$.

These results are always better with respect to the forecast performed with only CAMx model. This is particularly highlighted by the value of NMAE (Fig. 2). There is a general increasing in the performances for α going from 0 to 1 in the weighted mean tests, and similar behaviour for the least square approaches, where $n = 2$ test shows slightly better results.

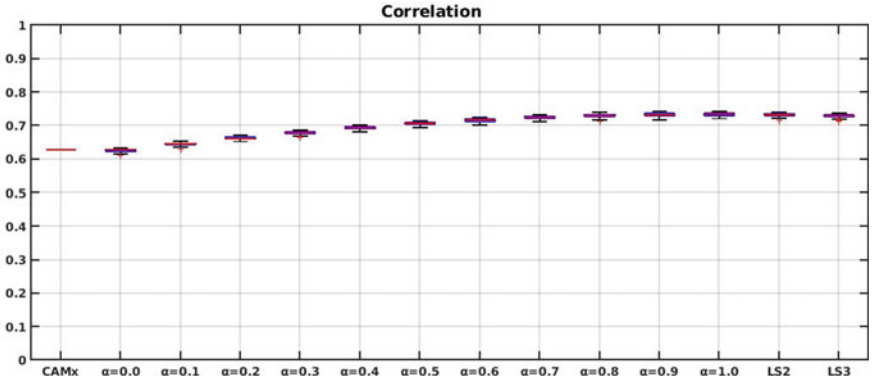

Fig. 1 Performances of the Monte Carlo analysis on the presented methodology—correlation coefficient, 1 day ahead

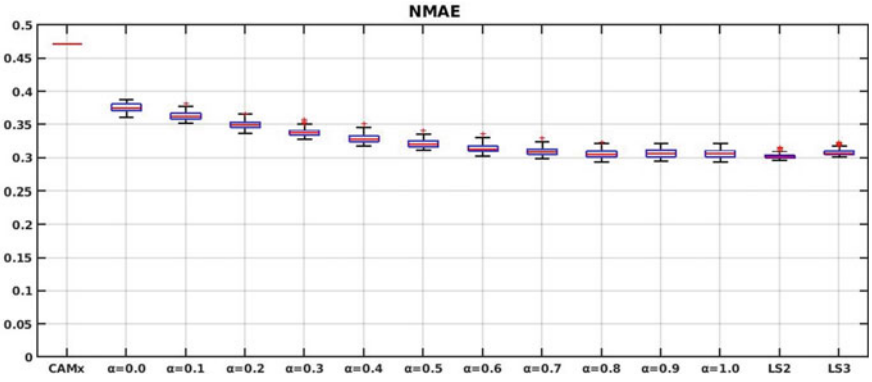

Fig. 2 Performances of the Monte Carlo analysis on the presented methodology—normalised mean absolute error, 1 day ahead

4 Conclusion

The paper presents a methodology for the integration between model results and measurement data for forecasting applications. The methodology is based on the estimation of CTM results correction through optimal interpolation based on the previous days corrections. Two different approaches have been tested: (i) a simple, weighted mean approach based on the last 2 computed corrections and (ii) a more complex least-square approach based on the estimation of the linear regression coefficient linking the last correction occurrences. In both these cases the computation is fast and does not need any change in the CTM model code. The methodology greatly increases the performances of the CTM model forecasts, with a higher correlation coefficient and lower normalised mean absolute error.

References

Carnevale, C., Finzi, G., Pederzoli, A., Pisoni, E., Thunis, P., Turrini, E., Volta, M. (2015). A methodology for the evaluation of re-analyzed PM10 concentration fields: a case study over the PO Valley. *Air Quality, Atmosphere and Health, 8*(6), 533–544.

Honore, C., Menut, L., Bessagnet, B., Meleux, F., Rouil, L., Vautard, R., Poisson, N., & Peuch, V. (2007). PREV'AIR: A platform for air quality monitoring and forecasting. *Development in Environmental Science, 6*, 292–300.

Landrigan, P. J., Fuller, R., Acosta, N. J. R., Adeyi, O., Arnold, R., Basu, N. N., Balde´, A. B., Bertollini, R., Bose-O'Reilly, S., Boufford, J. I., Breysse, P. N., Chiles, T., Mahidol, C., Coll-Seck, A. M., Cropper, M. L., Fobil, J., Fuster, V., Greenstone, M., Haines, A. … Zhong, M. (2018). The lancet commission on pollution and health. *The Lancet, 391*(10119), 462–512.

Manders, A., Schaap, M., & Hoogerbrugge, R. (2009). Testing the capability of the chemistry transport model LOTOTS-EUROS to forecast PM10 levels in the Netherlands. *Atmospheric Environment, 43*(26), 4050–4059.

Relvas, H., Miranda, A. I., Carnevale, C., Maffeis, G., Turrini, E., & Volta, M. (2017). Optimal air quality policies and health: A multi-objective nonlinear approach. *Environmental Science and Pollution Research, 24*(15), 13687–13699.

Questions and Answers

Questioner: Ulas Im.

Question: Would your result change if you change horizontal resolution?

Answer: This is possible. The topic will be analyzed in the future developments of the work.

Questioner: Pavel Kishcha.

Question: Effects of short term phenomena, such as dust intrusions and temperature inversions on PM10 cannot be predicted by the statistical approach to model updating using PM10 measurements from the previous days. Would it be better to use hourly PM10 form available measuring sites?

Answer: Hourly PM10 measurements can of course improve the results, but unfortunately the only available data from monitoring stations for the domain studied are daily mean concentrations.

Eigenmode-Based Parameter Perturbation for Stochastic Chemistry Transport Modeling

Annika Vogel and Hendrik Elbern

Abstract Efficient and reliable uncertainty quantification in air quality modeling has become increasingly important for the assessment of atmospheric chemical forecasts. However, current algorithms for estimating parameter uncertainties in atmospheric models do not account for intrinsic correlations within these high-dimensional systems. Using spatial correlations of model parameters, an eigenmode-based approach for efficient perturbation of uncertain parameters is developed. By substituting the parameter perturbations into an uncorrelated subspace, the degrees of freedom of the problem can be lowered significantly. An application to isoprene emissions in a regional chemical transport model is selected to demonstrate the opportunities of eigenmode-based parameter perturbation. Required covariances of these highly variable parameters are estimated from a sensitivity analysis of various input uncertainties. Preliminary results indicate high spatial correlations of regional isoprene emissions. By considering these large correlations, leading uncertainties can be described by a few principal directions only, allowing for an efficient modeling of uncertainties.

Keywords Uncertainty estimation · Stochastic chemistry transport modeling · Model parameter · Eigenmode analysis · Isoprene emissions

1 Introduction

Efficient and reliable uncertainty quantification for air quality forecasts has become increasingly important for validating our system understanding. Unlike in numerical weather prediction, only few approaches for unceratintiy estimation by ensembles have been applied to air quality models (see Zhang et al., 2012 for an overview). These

A. Vogel (✉) · H. Elbern
Institute for Energy and Climate Research - Troposphere (IEK-8), Forschungszentum Jülich, Jülich, Germany
e-mail: av@eurad.uni-koeln.de

Rhenish Institute for Environmental Research (RIU) at the University of Cologne, Cologne, Germany

© The Author(s), under exclusive license to Springer-Verlag GmbH, DE, part of Springer Nature 2021

C. Mensink and V. Matthias (eds.), *Air Pollution Modeling and its Application XXVII*, Springer Proceedings in Complexity, https://doi.org/10.1007/978-3-662-63760-9_23

include multi-model ensembles, different meteorological input, boundary conditions and parameterization schemes, as well as combinations of those (e.g. Delle Monarche et al., 2008; Garaud & Mallet, 2010).

Additionally, uncertainties in input parameters like emissions are treated by random pertrubations of each parameter – either uniformly for the whole parameter field or at each location separtely. In the latter case, the resulting large number of degrees of freedom cannot be covered by small sets of forecasts as it is enforced by computational reasons. Given these contraints, the presented approach identifies and exploits spatial correlations for computationally efficient parameter perturbation.

The method is implemented in the regional chemical transport model EURAD-IM (EURopean Air pollution Dispersion—Inverse Model, e.g. Elbern et al., 2007) for stochastic treatment of biogenic emissions. In this model framework, biogenic emissions are simulated with MEGAN 2.1 (Guenther et al., 2012) considering terrestrial emissions of 19 compound classes. Local emissions of each class are dependent on various meteorological parameters as well as vegetation fraction and leaf area index. For EURAD-IM, meteorological fields are forecasted with the numerical weather prediction model WRF (Skamarock et al., 2005).

2 Method

Applying the Karhunen-Loève expansion (e.g. Xiu, 2010), a stochastic process $x(\omega, s)$ can be described by a series of deterministic functions and stochastic coefficients:

$$x(\omega, s) - \bar{x}(s) = \sum_{i=1}^{\infty} \sqrt{\lambda_i}\ \varphi_i(s) Y_i(\omega) \tag{1}$$

where the deterministic functions are given by the eigenvalues λ_i and eigenvectors $\varphi_i(s)$ of the covariances of $x(\omega, s)$:

$$\int_S C(s,t)\ \varphi_i(t) dt = \lambda_i\ \varphi_i\ (s) \tag{2}$$

Arranging the eigenvalues in decreasing order, the first eigenvectors have the highest contribution to the stochastic process (Eq. 1). The higher the correlations, the faster is the decrease of the eigenvalues because of a low number of independent contributions (Eq. 2). Thus, a high dimensional stochastic process can be approximated by a finite series of principal components given by the leading eigenvalues and their corresponding eigenvectors.

The stochastic coefficients $Y_i(\omega)$ are random numbers perturbing the stochastic process around its mean $\bar{x}(s)$ according to the covariances $C(s,t)$. This renders the covaricance matrix crucrial for the stochastic behaviour of the processes considered.

Applying this approach to biogenic emissions of isoprene, a simple method to determine covariances is given by estimating sensitivities to input uncertatinties. Given various dependencies of simulated biogenic emissions, related sensitivities may be approximated using different model options. For this study, sensitivities to six input options are considered: global meteorological input, land use informaton, land surface schemes, boundary layer schemes, cloud microphysics schemes, radiation schemes – where each input sensitivity is determined from the reference and one alternative selection. Generally, every combination of the six input options could be choosen which would lead to 64 possible combinations. Here, a subset of 32 combinations is performed to estimate related covariances of isorpene emissions.

3 Results

The method is applied to a case study focusing on the Po valley in nothern Italy on 12.07.2012. The forecasts of WRF and EURAD-IM were initialized at 11.07.2012 at 00 UTC and nested to a horizontal resolution of 1 km in this region. The time intervall of interest is 00–10 UTC on 12.07.2012. In order to ensure the comparability of isoprene emissions over this time interval, factors of emissions relative to reference emissions at each time are defined as stochasitc parameter. For the covariance matrix, sensitivities are averaged over the whole intervall assuming roughly constant amplification factors during this time (similar to the approach of Elbern et al., 2007).

Figure 1 shows the leading eigenvalues resulting from the eigenmode analysis for isoprene emissions. The fast decrease of eigenvalues displays a high correlation of these emissions. More specifically, isoprene emissions over the whole domain are dominated by the four leading eigenmodes. Especially high importance is attributed to the first mode, which is almost one order of magnitute larger than the remaning ones.

The eigenvectors corresponding to the leading eigenvalues of isoprene emissions are shown in Fig. 2. The patters of the eigenvectors show that the leading modes are related to sensitivities to land use information and land surface parameterization which are found to be the dominating sources of unceratinties in this case. The dominant contribution of the first eigenmode is caused by especially high sensitivitiy to unceratinties in land use information because isoprene is almost exclusively emitted by broadleaf trees.

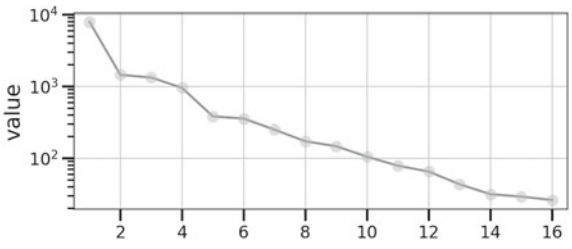

Fig. 1 Decrease of leading eigenvalues (logarithmic scale)

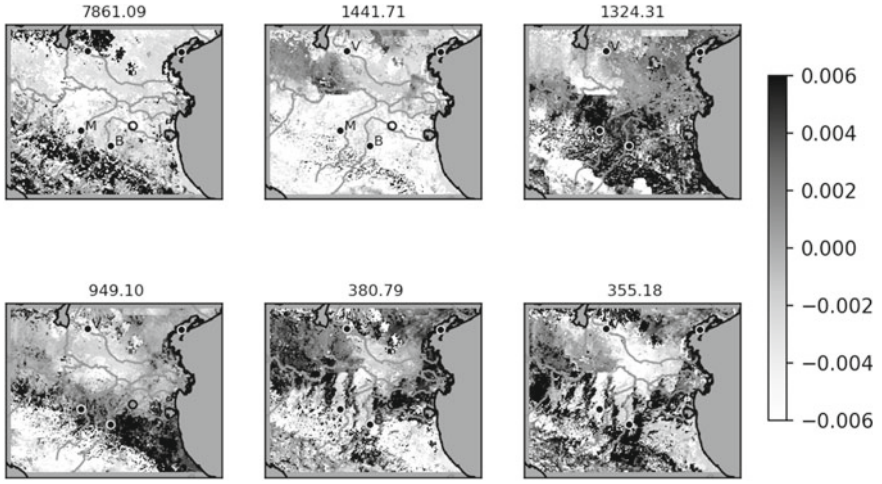

Fig. 2 Eigenvectors of the leading eigenvalues from covarianes of isoprene emissions. The eigenvectors are normalized to unit lenght. Related eigenvalues are given on top of each eigenvector map

4 Conclusion

In this study, an eigenmode-based approach for computationally efficient parameter perturbation is presented. By substituting the perturbations into an uncorrelated subspace, the degrees of freedom of the problem can be lowered significantly. The application to isoprene emissions demonstrates high spatial correlations in the regional domain. The leading eigenmodes indicate that the uncertatinties in biogenic emissions are dominated by a few principal components, which are mainly related to sensitivities to land use information.

While the eigenvalues provide the importance of the leading uncertatinties, the eigenvectors point into directions of coupled uncertainies. These information is used in the Karhunen-Loève expansion for an optimal approximation of the stochastic process. Translating this to uncertatinty estimation of model parameters, an ensemble of forecasts is created via different sets of stochastic coefficients. The optimiality of the approximation enables an efficient ensemble generation focusing on the leading uncertatinties of the parameters. This motivates the application to different types of model parameters in chemical transport models and numerical weather prediction systems alike.

Acknowledgements This work has been funded by the Helmholtz Climate Initiative REKLIM, a joint research project of the Helmholtz Association of German research centers (HGF) under grant: REKLIM-2009-07-16. The authors gratefully acknowledge the computing time granted through JARA-HPC on the supercomputer JURECA (Jülich Supercomputing Centre, 2018) at Forschungszentrum Jülich.

References

Delle Monarch, L., Wilczak, J., McKeen, S., Grell, G., Pagowski, M., Peckham, S., Stull, R., McHenry, J., & McQueen, J. (2008). A Kalman-filter bias correction method applied to deterministic, ensemble averaged and probabilistic forecasts of surface ozone. *Tellus, 60B*, 238–249.

Elbern, H., Strunk, A., Schmidt, H., & Talagrand, O. (2007). Emission rate and chemical state estimation by 4-dimensional variational inversion. *Atmospheric Chemistry and Physics, 7*, 3749–3769.

Garaud, D., & Mallet, V. (2010). Automatic generation of large ensembles for air quality forecasting using the Polyphemus system. *Geoscientific Model Development, 3*, 69–85.

Guenther, A. B., Jiang, X., Heald, C. L., Sakulyanontvittaya, T., Duhl, T., Emmons, L. K., & Wang, X. (2012). The Model of Emissions of Gases and Aerosols from Mature version 2.1 (MEGAN2.1): An extended and updated framework for modeling biogenic emissions. *Geoscientific Model Development, 5*(6), 1471–1492.

Jülich Supercomputing Centre. (2018). JURECA: Modular supercomputer at Jülich Supercomputing Centre. *Journal of Large-Scale Research Facilities, 4*, A132.

Skamarock, W. C., Klemp, J. B., Dudhia, J., Gill, D. O., Barker, D. M., Wang, W., & Powers, J. G. (2005). A description of the advanced research wrf version 2. *NCAR technical note.*

Xiu, D. (2010). *Numerical methods for stochastic computations: A spectral method approach.* Princeton University Press.

Zhang, Y., Bocquet, M., Mallet, V., Seigneur, C., & Baklanov, A. (2012). Real-time air quality forecasting, part II: State of the science, current research needs, and future prospects. *Atmospheric Environment, 60*, 656–676.

Questions and Answers

Questioner: Ulas Im

Question: What are the implication of the work on modeled O_3 levels?

Answer: The effect of uncertainties in isoprene emissions to O_3 concentrations depends on the regime of O_3 production. Most regions of high isoprene emissions – e.g. like the Apennine Mountains – can be attributed to the low NO_x regime. Thus, O_3 production is not highly sensitive to uncertainties in local VOC concentrations induced by varying isoprene emissions in this case. In some local areas, the ensemble exhibits significant effects in terms of 5–10% standard deviation in O_3 concentrations. These effects are found at location of either exceptionally high absolute differences in isoprene emissions north of Verona or increased NO_x levels in the north-western part of the Po valley.

Evolution of the Performance of the Canadian Operational Regional Air Quality Deterministic Prediction System from 2010 to 2019

Michael Moran, Junhua Zhang, Radenko Pavlovic, Verica Savic-Jovcic, Sylvain Ménard, Hugo Landry, Qiong Zheng, Alexandru Lupu, Samuel Gilbert, Si Jun Peng, and Patrick M. Manseau

Abstract The GEM-MACH air quality model has been used by Environment and Climate Change Canada in its operational Regional Air Quality Deterministic Prediction System (RAQDPS) since November 2009. The RAQDPS is run twice daily to produce 48-h forecasts of hourly surface O_3, NO_2, and $PM_{2.5}$ concentration fields over North America. In the past decade there have been 20 upgrades of varying magnitude made to the RAQDPS, and it is now possible to examine the evolution of RAQDPS performance skill over the near-decadal period from January 2010 to June 2019. A set of quality-controlled near-real-time hourly measurements of O_3, NO_2, and $PM_{2.5}$ surface concentrations for North America has been used for this evaluation. Results of three selected analyses that focus on time trends in performance skill are presented in this study along with a discussion of the impacts of some of the major model upgrades.

Keywords GEM-MACH · Ozone forecasts · $PM_{2.5}$ forecasts · Performance evaluation · RAQDPS · Air quality forecasts

M. Moran (✉) · J. Zhang · V. Savic-Jovcic · Q. Zheng · A. Lupu
Air Quality Research Division, Environment and Climate Change Canada (ECCC), Toronto, Canada
e-mail: mike.moran@ec.gc.ca

J. Zhang
e-mail: junhua.zhang@ec.gc.ca

R. Pavlovic · S. J. Peng · P. M. Manseau
Air Quality Policy-Issue Response Section, Canadian Meteorological Centre, ECCC, Montreal, Canada

S. Ménard
Numerical Weather Prediction Section, ECCC, Montreal, QC, Canada

H. Landry · S. Gilbert
Scientific Application Development Section, ECCC, Montreal, QC, Canada

© Crown 2021

C. Mensink and V. Matthias (eds.), *Air Pollution Modeling and its Application XXVII*, Springer Proceedings in Complexity, https://doi.org/10.1007/978-3-662-63760-9_24

1 Introduction

Environment and Climate Change Canada (ECCC) has run an operational, continental-scale Regional Air Quality Deterministic Prediction System (RAQDPS) for North America since 2001. The first version of the RAQDPS employed an off-line chemical transport model (CTM) and was run on a 21-km horizontal grid to predict surface ozone. The meteorological driver that was used was the ECCC operational Global Environmental Multi-scale (GEM) numerical weather prediction model. $PM_{2.5}$ was added as a predictand to the system in 2003, and in Nov. 2009 the off-line CTM was replaced by the GEM-MACH (GEM–Modeling Air quality and CHemistry) on-line CTM, which had improved representations of gas-phase, aqueous-phase, and aerosol chemistry and used a new, continental-scale 15-km grid (Anselmo et al., 2010; Moran et al., 2011b). The RAQDPS is now run routinely twice daily on a 10-km grid to produce 48-h forecasts of hourly O_3, NO_2, and $PM_{2.5}$ surface concentration fields over North America. These three species are the chemical indicators needed by Canada's national Air Quality Health Index (Stieb et al., 2008).

Since 2009 there have been 20 upgrades of varying magnitude made to the GEM-MACH-based version of the RAQDPS to improve forecast skill and also to adjust to changes in ECCC's computer system hardware and software. For example, in 2009 the RAQDPS grid had 15-km horizontal grid spacing and 58 vertical levels extending from the surface to 0.1 hPa, whereas the current grid has 10-km horizontal grid spacing and 84 vertical levels over the same depth. The input emissions files for the RAQDPS have also been updated seven times since 2009. Table 1 lists the

Table 1 Major updates to the operational RAQDPS over the period from 2009–2019. See Moran and Ménard (2019) for more details about these versions and other versions

Version	Release date	Short description
001	Nov. 2009	First version (Emission Inventories: 2006 CA, 2005 US, 1999 MX)
004	Oct. 2011	New emissions (EIs: 2006 CA, projected 2012 US, 1999 MX)
007	Oct. 2012	New model version, new grid (15 km → 10 km, 58 → 80 levels)
009	Feb. 2013	3 model bug fixes, including one to near-surface vertical diffusion
013	Jun. 2015	New emissions (EIs: 2010 CA, 2011 US, 1999 MX)
016	Sep. 2016	New model code, new vertical discretization (non-staggered → staggered)
020	Sep. 2018	New emissions (EIs: 2013 CA, projected 2017 US, 2008 MX)
021	Jul. 2019	New model code, new vertical discretization (80 → 84 levels)

seven most important upgrades made over this period, three of which involved major updates to the input emissions. Other significant changes included improvements and bug fixes to the model code, the introduction of a finer horizontal grid (10 km), and several modifications to the vertical discretization.

Given this sequence of upgrades, it is of interest to examine the time evolution of the performance skill of RAQDPS forecasts of O_3, NO_2, and $PM_{2.5}$ surface concentrations across North America for the entire 9.5-year period from Jan. 2010 to June 2019. The next two sections describe the evaluation methodology and discuss selected time series of performance scores and the links between changes to the RAQDPS and changes in forecast performance. Note that model performance after June 2019 (not shown) will be impacted by the upgrade to version 021.

2 Evaluation Methodology

RAQDPS performance is monitored routinely at ECCC using hourly surface measurements of a handful of chemical species, in particular O_3, NO_2, and $PM_{2.5}$, made by stations belonging to multiple North American air-chemistry networks that report their measurements in near real time (NRT) to either the U.S. AIRNow datasharing website (see http://airnow.gov) or the ECCC Automatic Data Extraction [ADE] circuit (mainly Canadian National Air Pollution Surveillance [NAPS] network stations). For this retrospective study a large set of data pairs of NRT hourly measurements of O_3, NO_2, and $PM_{2.5}$ surface concentrations and corresponding RAQDPS surface concentration forecasts at station locations for the entire 9.5-year period was first extracted from the RAQDPS forecast evaluation archive. Only the first 12 h of each 48-h forecast were considered to avoid multiple forecasts for the same hour. The RAQDPS values correspond to forecasts made by the model version that was operational at the time (see Table 1).

While some data filtering is performed in NRT by both AIRNow and ADE, we performed additional filtering of the retrospective data set. For example, some stations have calibration data reported as actual measurements. To screen out such unrepresentative values, cutoff thresholds of 0 and 150 ppbv, 0 and 150 ppbv, and 0 and 200 $\mu g\ m^{-3}$ were applied to O_3, NO_2, and $PM_{2.5}$ hourly observations, respectively. This filtering removed less than 0.1% of all available hourly data over the 9.5-year period.

Table 2 summarizes the number of NRT stations and their location for the "network" of AQ networks that was considered. O_3, NO_2, and $PM_{2.5}$ measurements at up to 1311, 376, and 897 North American stations, respectively, were available during the 2010–2018 period. For O_3 and $PM_{2.5}$, the largest number of stations are located in the eastern U.S. (relative to the 100°W meridian) followed by the western U.S. Two other features of the measurement data should be mentioned. First, whereas Canadian AQ stations and U.S. NO_2 and $PM_{2.5}$ stations operate year-round, many U.S. O_3 stations only operate during the "ozone season" from May to September. And second, while the number of O_3 stations remained stable for this period, about

Table 2 Number of measurement stations by pollutant and region. Numbers in parentheses give the percentage of stations in that region

Pollutant	Western Canada	Western U.S	Eastern Canada	Eastern U.S	Total
O_3	84 (6)	313 (24)	136 (10)	778 (60)	1311
NO_2	90 (24)	259 (29)	93 (25)	93 (25)	376
$PM_{2.5}$	96 (11)	313 (24)	121 (13)	421 (47)	897

300 more $PM_{2.5}$ stations (50%) and 240 NO_2 stations (175%) were added to the NRT data feeds (cf. Moran et al., 2011a). In particular, NRT NO_2 measurements for the U.S. only became available from AIRNow in 2012.

3 Results and Discussion

Many analyses of this large evaluation data set are possible. Results of three selected analyses that focus on performance-skill time trends are presented in this section.

Figure 1 shows time series of domain-wide seasonal correlation coefficient (R) and root mean square error (RMSE) for the three forecast species O_3, NO_2, and $PM_{2.5}$

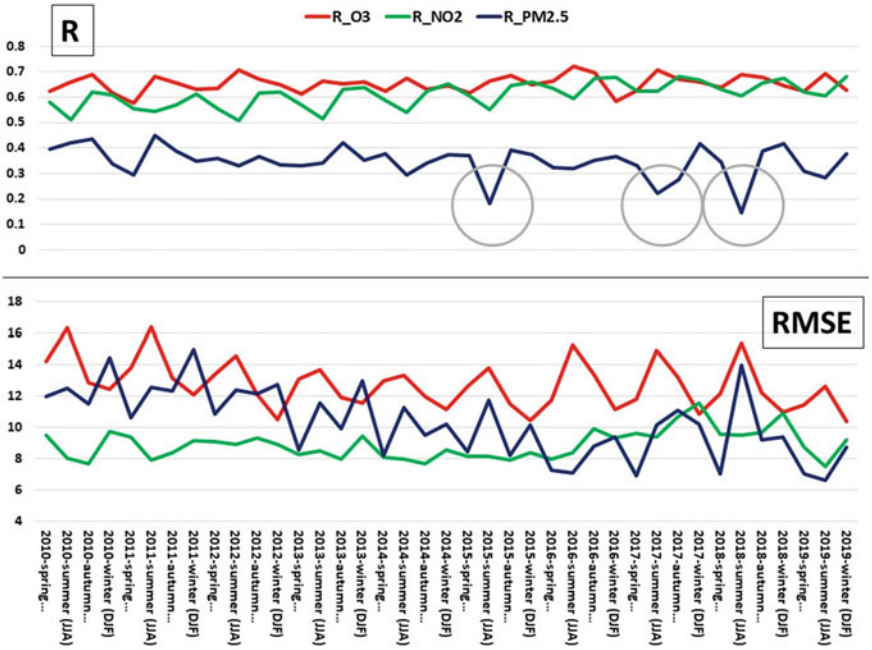

Fig. 1 Time series of seasonal correlation coefficient (R) and root mean square error (RMSE) for surface O_3 (red), NO_2 (green) and $PM_{2.5}$ (blue) for all available North American NRT measurement stations for the period Jan. 2010–June 2019, where winter is defined to be December to February

for the 2010–2019 period. The seasonal R scores for O_3 and NO_2 shown in the upper panel of this figure are similar and both of these time series exhibit some overall improvement with time (i.e., a trend towards higher R values). This is the hoped-for result since proposed RAQDPS upgrades are only accepted if they are shown to have at least equal forecast skill to the existing operational version that they are intended to replace. There is also a suggestion that there is a degree of anticorrelation to the seasonal R scores for O_3 and NO_2, with O_3 tending to have the highest (i.e., best) R scores in the summer whereas R scores for NO_2 are generally highest in the winter.

The seasonal R scores for $PM_{2.5}$, on the other hand, are lower than those for O_3 and NO_2 and they do not show any improvement with time. In fact there are some pronounced decreases in these scores (marked by circles) for the summers of 2015, 2017, and 2018. At least one factor contributing to these decreases was the occurrence of severe wildfire seasons in western North America in these three years with accompanying higher PM levels (Chen et al., 2019; Munoz-Alpizar et al., 2017). Since the RAQDPS does not account for wildfire emissions, it will underestimate PM levels in areas impacted by wildfire smoke, leading to poorer correlations. Note that there are corresponding peaks in $PM_{2.5}$ RMSE for these three summers in the lower panel of Fig. 1, consistent with model $PM_{2.5}$ underpredictions in areas impacted by wildfire smoke. Due to the impact of wildfires on $PM_{2.5}$ concentrations even in some Canadian cities in recent years, a special version of the RAQDPS called FireWork that includes NRT wildfire emissions is now being run operationally during the Canadian wildfire season (Chen et al., 2019; Pavlovic et al., 2016).

It is worth noting that the domain-wide seasonal RMSE time series for $PM_{2.5}$ does display an overall improvement (i.e., downward trend to lower values) from 2010 to 2019. This is also true of the RMSE time series for O_3, at least for the first half of the period. For NO_2, on the other hand, seasonal RMSE scores started to increase beginning in the second half of 2016. Two likely contributing factors are the introduction of a new RAQDPS upgrade (016) in Sept. 2016 (see Table 1), which included a change to the vertical discretization that effectively decreased the thickness of the lowest model layer, and the continued reliance on the 2011 U.S. emissions inventory despite large decreases in U.S. NO_x emissions that are known to have occurred after 2011 (Moran et al., 2018). It can also be seen that RMSE seasonal values for O_3 and $PM_{2.5}$ exhibit a distinct annual cycle. RMSE scores for O_3 are generally highest (i.e., worst) in the summer whereas those for $PM_{2.5}$ tend to peak in the winter.

Figure 2 shows the corresponding domain-wide time trends in seasonal mean bias (MB) the 2010–2019 period. Seasonal MB values increased somewhat for O_3 and NO_2 over this period whereas seasonal MB values for $PM_{2.5}$ decreased. There is also an annual cycle evident, particularly for O_3, which tends to have positive MB values (overpredictions) in the summer and negative values (underpredictions) in the winter. Seasonal $PM_{2.5}$ underpredictions were also more pronounced for the same three recent summers noted above in the discussion of Fig. 1.

The seasons in which six major upgrades listed in Table 1 were made to the RAQDPS are also indicated in Fig. 2. Three of these upgrades involved major changes to the input emissions files and the other three introduced significant changes to

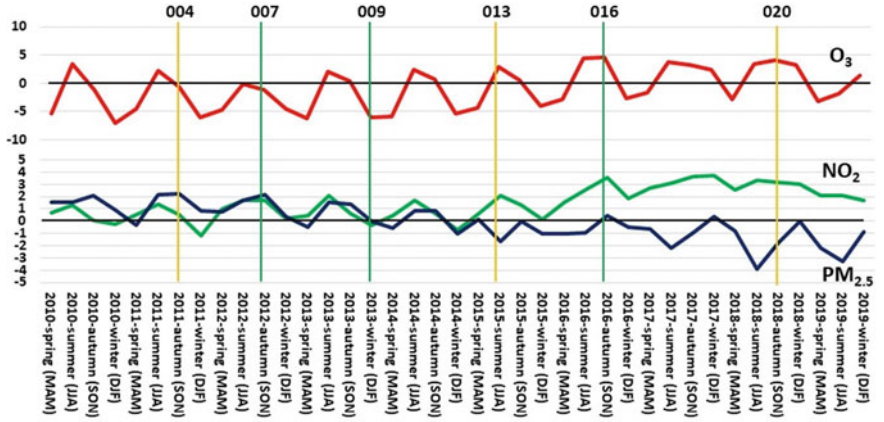

Fig. 2 Time series of seasonal mean bias (MB) for surface O_3 (upper panel, red, ppbv) and NO_2 (lower panel, green, ppbv) and $PM_{2.5}$ (blue, $\mu g\, m^{-3}$) for all available North American NRT measurement stations for the period Jan. 2010–June 2019. Vertical bars indicate the seasons in which major RAQDPS upgrades were introduced, where the number above each vertical bar indicates the version number of the upgrade and the colour of the bar indicates the type of upgrade: emissions-focused (orange) or model-focused (green)

the modelling system itself, including both the model code and the model grid. Some of the changes to MB scores in this figure appear to be associated with these upgrades. Interestingly, the first three of these upgrades (in 2011, 2012, and 2013) did not appear to have noticeable impacts on the seasonal MB scores but arguably did improve O_3 and $PM_{2.5}$ RMSE scores (see Fig. 1). The fourth upgrade (013), in mid 2015, implemented new emissions files based on newer inventories (Moran et al., 2015) and appears to have impacted seasonal MB scores for all three forecast species. The fifth upgrade (016) introduced major changes to the modelling system itself, including to the GEM and GEM-MACH model codes and to the vertical discretization, where a non-staggered vertical grid was replaced with a staggered grid (see Moran et al., 2018). Seasonal MB values increased for NO_2 and decreased for $PM_{2.5}$ after this upgrade. Finally, another major change to the input emissions was implemented in the sixth upgrade (020) that reflected the large decreases in North American SO_2, NO_x, and VOC emissions that have occurred over the last decade (Moran et al., 2018). Figure 2 suggests that MB values decreased for all three species in response to this upgrade, though by different response pathways: MB scores for NO_2 decreased directly due to reductions in NO_2 emissions; for O_3 they decreased due to reductions in precursor emissions (NO_x and VOCs); and for $PM_{2.5}$ they decreased due to decreased SO_2 emissions and hence reduced particle sulphate levels.

Lastly, Fig. 3 provides an analysis of the time variation of regional R scores for hourly $PM_{2.5}$ forecasts for two geographic regions, western Canada and eastern Canada, for the 2010–2019 period. Each of the 10 rectangles in the panel for each region shows the variation of monthly R scores by hour of day and month of year for a

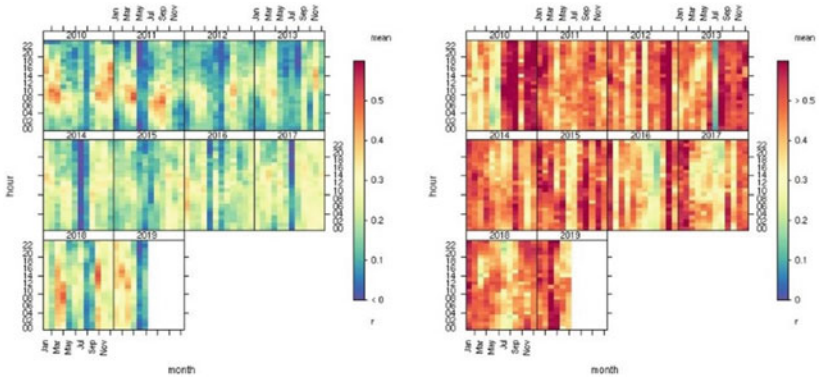

Fig. 3 Variation of regional correlation coefficient R for hourly surface $PM_{2.5}$ forecasts by year (rectangles), month (x-axis), and hour of day (y-axis; local time) for western Canada (lefthand panel) and eastern Canada (righthand panel) for the period Jan. 2010–June 2019. The 100°W meridian separates these regions

particular year. For example, the top left rectangle of the righthand panel (for eastern Canada) shows an analysis of RAQDPS hourly $PM_{2.5}$ forecasts by month for 2010. A sudden jump in R scores is evident between June and July, but interestingly there is no corresponding improvement in western Canada (lefthand panel). For the first half of 2010, R scores tend to be higher later in the day in eastern Canada whereas in western Canada the highest scores occur midday. Moving from individual rectangles to multiple rectangles, a comparison of multiple rectangles within a panel allows interannual variations and trends in performance to be examined for a region. For example, there appears to be an overall improvement in R scores in later years for western Canada but not for eastern Canada.

It is also clear from Fig. 3 that the R scores for hourly $PM_{2.5}$ are considerably higher for eastern Canada versus western Canada. R scores for western Canada are also lower for the summer than for other periods, possibly due to the neglect of wildfire emissions. However, this feature is also present for eastern Canada, although to a lesser extent.

4 Conclusions

The analyses of performance-skill time trends presented in Sect. 3 suggest a number of conclusions. First, overall model skill appears to have improved modestly over the near-decadal period from January 2010 to June 2019 due to a series of model upgrades. Two confounding factors are the changing chemical environment in North America caused by changes in regional and national emissions and the difficulty in accessing up-to-date emissions inventories. Second, the time trend analysis suggests that while emissions are very important model inputs, some modelling system

changes have also had significant impacts on forecast skill. Third, $PM_{2.5}$ continues to be the hardest pollutant to predict, in large part because of its inherent complexity as a hybrid primary-secondary pollutant with numerous sources, but also because the RAQDPS does not include wildfire emissions, an important seasonal source of both primary $PM_{2.5}$ and its precursors. And fourth, there are annual cycles in seasonal forecast skill for each pollutant for most objective scores that are as large or larger than the time trends in model performance. The presence of these seasonal variations can provide guidance on the parts of the modelling system where further improvements may be possible.

References

Anselmo, D., Moran, M. D., Ménard, S., Bouchet, V., Makar, P., Gong, W., Kallaur, A., Beaulieu, P. A., Landry, H., Stroud, C., Huang, P., Gong, S., & Talbot, D. (2010) A new Canadian air quality forecast model: GEM-MACH15.In 12th AMS Conference on Atmospheric Chemistry, January 17–21, Atlanta, Georgia, American Meteorological Society, p. 6. See http://ams.confex.com/ams/pdfpapers/165388.pdf

Chen, J., Anderson, K., Pavlovic, R., Moran, M. D., Englefield, P., Thompson, D. K., Munoz-Alpizar, R., & Landry, H. (2019). The FireWork v2.0 air quality forecast system with biomass burning emissions from the Canadian Forest Fire Emissions Prediction System v2.03. *Geoscientific Model Development, 12*, 3283–3310. https://doi.org/10.5194/gmd-12-3283-2019

Moran, M. D., Chen, J., Ménard, S., Pavlovic, R., Landry, H., Beaulieu, P. A., Gilbert, S., Makar, P. A., Gong, W., Stroud, C., Kallaur, A., Robichaud, A., Gong, S., & Anselmo, D. (2011a). Two years of operational AQ forecasting with GEM-MACH15: A look back and a look ahead. In *10th CMAS Conference*, 24–26 October, Chapel Hill, North Carolina, p 7. See http://www.cmascenter.org/conference/2011/abstracts/moran_two_years_2011.pdf

Moran, M. D., Makar, P. A., Ménard, S., Pavlovic, R., Sassi, M., Beaulieu, P. A., Anselmo, D., Mooney, C. J., Gong, W., Stroud, C., Gong, S., & Zhang, J. (2011b). Improvements to wintertime particulate-matter forecasting with GEM-MACH15. In D. G. Steyn & S. Trini Castelli (Eds.), *Air pollution modelling and its application XXI* v Springer, Dordrecht.

Moran, M. D., & Ménard, S. (2019). Regional Air Quality Deterministic Prediction System (RAQDPS): Update from version 020.2 to version 021. Canadian Meteorological Centre Tech. Note, Montreal, July, p. 49. http://collaboration.cmc.ec.gc.ca/cmc/cmoi/product_guide/docs/tech_notes/technote_raqdps-021_20190703_e.pdf. Accessed on December 30, 2019.

Moran, M., Pavlovic, R., & Anselmo, D. (2018). Regional Air Quality Deterministic Prediction System (RAQDPS): Update from version 019 to version 020. Canadian Meteorological Centre Tech. Note, Sept., Montreal, 48 pp, http://collaboration.cmc.ec.gc.ca/cmc/CMOI/product_guide/docs/tech_notes/technote_raqdps-v20_20180918_e.pdf. Accessed on December 30, 2019.

Moran, M., Zheng, Q., Zhang, J., & Pavlovic, R. (2015). RAQDPS version 013: Upgrades to the CMC operational regional air quality deterministic prediction system released in June 2015. Canadian Meteorological Centre Tech. Note, Montreal, Quebec, November, p 54. http://collaboration.cmc.ec.gc.ca/cmc/cmoi/product_guide/docs/lib/op_systems/doc_opchanges/Technical_Note_GEM-MACH10_v1.5.3+SET2.1.1_Emissions_9Nov2015.pdf. Accessed on December 30, 2019.

Munoz-Alpizar, R., Pavlovic, R., Moran, M. D., Chen, J., Gravel, S., Henderson, S. B., Ménard, S., Racine ,J., Duhamel, A., Gilbert, S., Beaulieu, P. A., Landry, H., Davignon, D., Cousineau, S., & Bouchet, V. (2017). Multi-year (2013–2016) $PM_{2.5}$ wildfire pollution exposure over North America as determined from operational air quality forecasts. *Atmosphere, 8*, 179, 24. https://doi.org/10.3390/atmos8090179

Pavlovic, R., Chen, J., Anderson, K., Moran, M. D., Beaulieu, P.-A., Davignon, D., & Cousineau, S. (2016). The FireWork air quality forecast system with near-real-time biomass burning emissions: Recent developments and evaluation of performance for the 2015 North American wildfire season. *Journal of the Air & Waste Management Association, 66*, 819–841. https://doi.org/10.1080/10962247.2016.1158214

Stieb, D. M., Burnett, R. T., Smith-Dorion, M., Orly, B., Shin, H. H., & Economou, V. (2008). A new multipollutant, no-threshold air quality health index based on short term associations observed in daily time-series analyses. *Journal of the Air & Waste Management Association, 58*, 435–450. https://doi.org/10.3155/1047-3289.58.3.435

Questions and Answers

Questioner: Saravanan Arunachalam

Question: The ozone diurnal plot showed lower model predictions than observations during nighttime for time means across the full domain. This is very impressive but the opposite of what most other models have shown. Can you explain this difference?

Answer: The diurnal variation of surface O_3 is determined by the complex interplay between, and the diurnal variations of, precursor emissions (especially NO), near-surface vertical diffusion, and dry deposition as well as the near-surface vertical discretization that is employed. The upcoming AQMEII-4 multi-model intercomparison study that will focus on removal processes may provide an answer.

Questioner: Saravanan Arunachalam

Question: Do your NO_2 observations in the U.S. include the "near-road" monitors?

Answer: We currently include all NRT U.S. measurements reported to AIRNow.

Questioner: Fotios Barmpas

Question: How do you explain the fact that model predictions for O_3 show differences in the peak concentrations compared to observations while model predictions for NO_2 do not?

Answer: NO_2 is a primary pollutant whose concentration is largely determined by the representation of local NO_x emissions and vertical mixing as well as photochemistry, whereas O_3 is a secondary pollutant for which more processes, including photochemistry, NO_x and VOC emissions, vertical mixing, horizontal transport, and dry deposition, play significant roles.

Questioner: Ulias Im

Question: Did you look to see if minimum and maximum O_3 levels changed during the modelled period and were you able to model this trend?

Answer: No, we did not do this but it is an excellent suggestion.

Questioner: Rostislav Kouznetsov

Question: You discard negative readings from observations. Measurement devices normally have a floating zero and non-negligible errors. Could a significant fraction of the discarded values actually be “observed zeroes”?

Answer: Yes, that is possible, but as noted the number of discarded values was only about 0.1% of the total available measurements.

Statistical Methods to Forecast Air Quality in Taipa Ambient and Taipa Residential of Macao

Man Tat Lei, Joana Monjardino, Luisa Mendes, David Gonçalves, and Francisco Ferreira

Abstract Air pollution is a major concern issue on Macao since the concentration levels of several of the most common pollutants are frequently above the internationally recommended values. The low air quality episodes impacts on human health paired with highly populated urban areas are important motivations to develop forecast methodologies in order to anticipate pollution episodes, allowing establishing warnings to the local community to take precautionary measures and avoid outdoor activities during this period. Using statistical methods (multiple linear regression (MLR) and classification and regression tree (CART) analysis) we were able to develop forecasting models for the main pollutants (NO_2, $PM_{2.5}$, and O_3) enabling us to know the next day concentrations with a good skill, translated by high coefficients of determination (0.82–0.90) on a 95% confidence level. The model development was based on six years of historical data, 2013 to 2018, consisting of surface and upper-air meteorological observations and surface air quality observations. The year of 2019 was used for model validation. From an initially large group of meteorological and air quality variables only a few were identified as significant dependent variables in the model. The selected meteorological variables included geopotential

M. T. Lei (✉) · L. Mendes
Department of Sciences and Environmental Engineering, NOVA School of Science and Technology, NOVA University Lisbon, Lisbon, Portugal
e-mail: lei.man.tat@usj.edu.mo; l.tat@campus.fct.unl.pt

L. Mendes
e-mail: lc.mendes@fct.unl.pt

J. Monjardino · F. Ferreira
Center for Environmental and Sustainability Research, NOVA School of Science and Technology, NOVA University Lisbon, Lisbon, Portugal
e-mail: jvm@fct.unl.pt

F. Ferreira
e-mail: ff@fct.unl.pt

M. T. Lei · D. Gonçalves
Institute of Science and Environment, University of Saint Joseph, Macau, China
e-mail: david.goncalves@usj.edu.mo

© The Author(s), under exclusive license to Springer-Verlag GmbH, DE, part of Springer Nature 2021

C. Mensink and V. Matthias (eds.), *Air Pollution Modeling and its Application XXVII*, Springer Proceedings in Complexity, https://doi.org/10.1007/978-3-662-63760-9_25

height, relative humidity and air temperature at different altitude levels and atmospheric stability characterization parameters. The air quality predictors used included recent past hourly levels of mean concentrations for NO_2 and $PM_{2.5}$ and maximum concentrations for O_3. The application of the obtained models provides the expected daily mean concentrations for NO_2 and $PM_{2.5}$ and maximum hourly concentrations O_3 for the next day in Taipa Ambient air quality monitoring stations. The described methodology is now operational, in Macao, since 2020.

1 Introduction

The World Health Organization has last update Air Quality Guidelines (AQG) in 2005, which sets the recommended threshold levels for each pollutant. Also, Macao has an air quality problem, in particular of high levels of nitrogen dioxide (NO_2), particulate matter ($PM_{2.5}$), and ozone (O_3), which often overstep the guidance values of AQG. In addition, there are a lot of studies that show that exposure to NO_2, $PM_{2.5}$, and O_3 have increased hospital admissions and emergency room visits and even led to death from heart or lung diseases in extreme cases (WHO, 2003). Thus, it is extremely important to develop a reliable air quality forecast for the concentration of NO_2, $PM_{2.5}$, and O_3 in Macao, which can alert the local population to take precautionary measures in case of a pollution episode (Neto et al., 2009). Figures 1, 2 and 3 showed the comparison of different air quality standards amongst WHO, EU, US, China, Macao, and Hong Kong for NO_2, $PM_{2.5}$, and O_3 (MEE, 2012; SMG, 2019; WHO Europe, 2006).

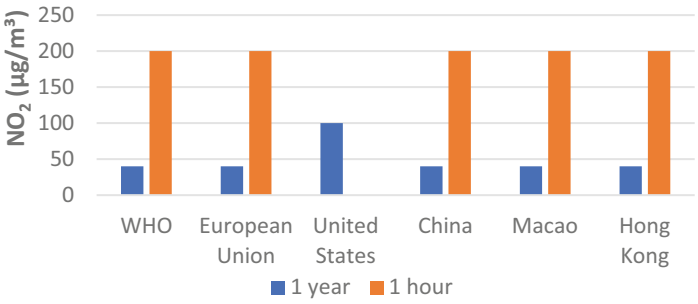

Fig. 1 Comparison of air quality standard for NO_2

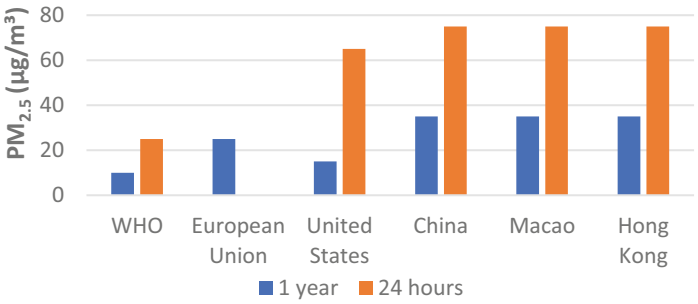

Fig. 2 Comparison of air quality standard for $PM_{2.5}$

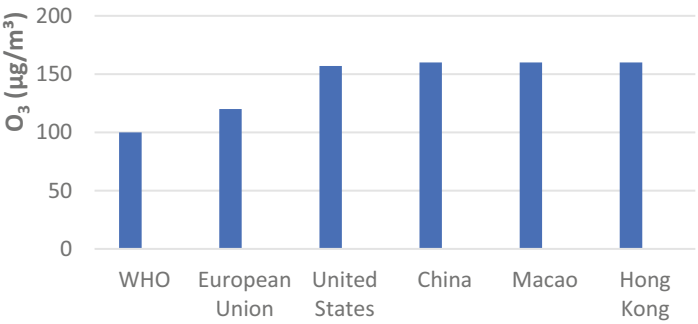

Fig. 3 Comparison of air quality standard for O_3

2 Methodology

To now the air quality for the next day was used statistical methods that were based on past data series analysis. For this paper was utilized multiple linear regression (MLR) and classification and regression tree (CART) analysis. As showed in previous work (Cassmassi, 1997), statistical models based on MLR and CART analysis were developed to forecast the average daily concentration for NO_2 and $PM_{2.5}$, and the maximum hourly O_3 levels for the next day, for the air quality monitoring stations of Taipa Ambient and Taipa Residential. Taipa Ambient is an ambient station, also a background representative station, which set the baseline for the levels of pollutant concentration. This station is located at Taipa Grande, the headquarter of Macao Meteorological and Geophysical Bureau (SMG). Taipa Residential is a high-density residential area station located in Taipa. This station is located at the Taipa Central Park, a leisure area for the local residents. A six-year period from 2013 to 2018 was selected as the period to develop the models, while the year of 2019 was selected for validation of the model.

Figure 4 shows the flowchart of the model development for the air quality forecast using statistical methods. The development of statistical model consists of collecting

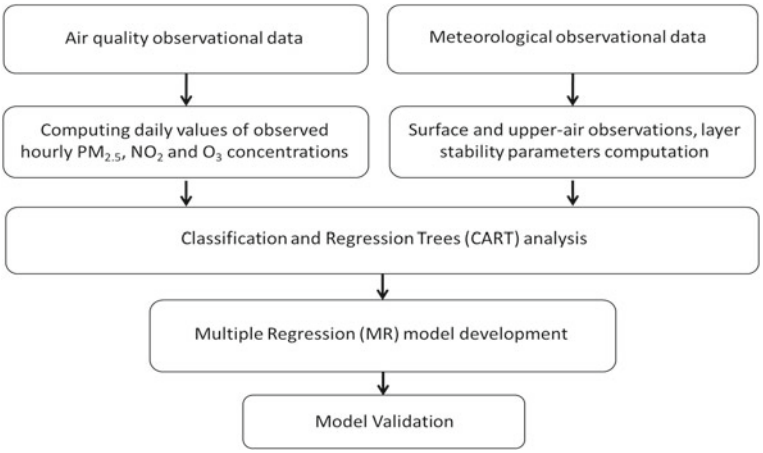

Fig. 4 Flowchart for the development of statistical air quality forecast models

the air quality data and meteorological data, followed by computing the hourly air quality data into the daily concentrations of NO_2, $PM_{2.5}$, and O_3. In addition, the meteorological data required to develop the statistical model would be extracted from different meteorological observations. These processed data would be analyzed by statistical methods such as multiple linear regression (MLR) and classification and regression trees (CART) analysis. The final procedure is to perform a model validation to ensure the accuracy of the next-day air quality forecast.

3 Results and Discussion

Table 1 provides the final list of meteorological and air quality parameters used as predictors, for each pollutant, in the obtained multiple regression models for the air quality air quality monitoring stations of Taipa Ambient and Taipa Residential. Table 1 shows $PM_{2.5}$ has a highly correlated relationship with past concentration

Table 1 Variables used in statistical model

Station	Pollutants	Variables used in equations
Taipa ambient	$PM_{2.5}$	PM_{25}_16D1, H_850, HRMD
	NO_2	NO_2_16D1, H_850, STB_925
	$O_{3\ MAX}$	$O_{3\ MAX}$_16D1, $O_{3\ MAX}$_23D1, H_850. HRMN
Taipa residential	$PM_{2.5}$	PM_{25}_16D1, TD_MD, TAR_925
	NO_2	NO_2_16D1, H_850, TD_MD
	$O_{3\ MAX}$	$O_{3\ MAX}$_16D1, $O_{3\ MAX}$_23D1, H_850, HRMN

levels (PM_{25}_16D1 as the average of the hourly values($\mu g/m^3$) between 16:00 of yesterday and 15:00 of today) for both Taipa Ambient and Taipa Residential air quality monitoring stations, geopotential height (m) at 850 hPa (H_850), and average relative air humidity (%) (HRMD) for Taipa Ambient, average dew point temperature (°C) (TD_MD), and air temperature (°C) at 925 hPa (TAR_925) for Taipa Residential. In addition, NO_2 has a highly correlated relationship with past concentration levels NO_2_16D1and geopotential height (m) at 850 hPa for both Taipa Ambient and Taipa Residential air quality monitoring stations, atmospheric stability (°C) at 925 hPa (STB_925) for Taipa Ambient, and average dew point temperature (°C) (TD_MD) for Taipa Residential. Furthermore, O_3 has a highly correlated relationship with past concentration levels $O_{3\,MAX}$_16D1, $O_{3\,MAX}$_23D1 (as the maximum hourly values ($\mu g/m^3$) between 00:00 and 23:00 of yesterday), geopotential height (m) at 850 hPa and minimum relative air humidity (%) (HRMN) for both Taipa Ambient and Taipa Residential air quality monitoring stations.

An example of one of the regression equations delivered is the following for next-day 24 h-average NO_2 at Taipa Ambient:

$$NO_2 = (0.914 \times NO_2\_16D1) + (0.004 \times H\_850) - (0.734 \times STB\_925) \quad (1)$$

Figure 5 shows the graph of the model validation for the MLR models of NO_2 concentrations in Taipa Ambient air quality monitoring station in 2019.

Table 2 shows the model performance indicators of $PM_{2.5}$, NO_2, and $O_{3\,MAX}$ for Taipa Ambient and Taipa Residential air quality monitoring stations. The model performance indicators include coefficient of determination (R^2), root mean square error (RMSE), mean absolute error (MAE), and BIAS. The results obtained from MLR and CART models perform a coefficient of determination between 0.86 and 0.87 for Taipa Ambient and between 0.78 and 0.88 for Taipa Residential. The air

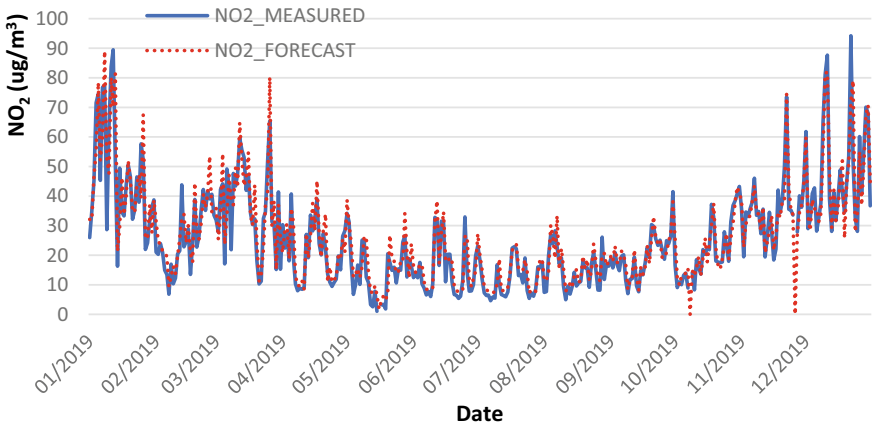

Fig. 5 Observed and predicted NO_2 concentrations value using MLR models in Taipa Ambient (2019)

Table 2 Model performance indicators

Station	Pollutant	Performance indicators				Model built using CART or MR	
		R^2	RMSE ($\mu g/m^3$)	MAE ($\mu g/m^3$)	BIAS ($\mu g/m^3$)	CART	MR
Taipa ambient	$PM_{2.5}$	0.86	4.8	3.1	0.2		✓
	NO_2	0.87	6.1	4.2	1.0		✓
	$O_{3\ MAX}$	0.86	23.7	14.7	−1.6	✓	✓
Taipa residential	$PM_{2.5}$	0.88	5.6	3.5	−0.1		✓
	NO_2	0.87	5.6	4.1	0.6		✓
	$O_{3\ MAX}$	0.78	20.9	12.7	1.3	✓	✓

quality forecast is at best forecasting the levels of NO_2 concentration in Taipa Ambient and is at best forecasting the levels of $PM_{2.5}$ concentration in Taipa Residential. All of the statistical models were built using MLR, while the models for the maximum hourly ozone were built using both MLR and CART.

The ambient station was better at predicting NO_2 while the residential station was better at predicting the maximum hourly concentration of O_3. Also, the developed models provide a better understanding of different air quality and meteorological variables and also the relationship between these variables. Furthermore, the variable that explained most of the variability is the 16D1 concentration for NO_2, $PM_{2.5}$, and O_3.

4 Conclusion

The work presented is an air quality forecast using statistical methods, based on a detailed analysis of both air quality and meteorological variables for NO_2, $PM_{2.5}$, and O_3. The final objective of this study is to develop a daily air quality forecast using statistical methods to predict the daily average of NO_2, $PM_{2.5}$, and maximum hourly O_3 levels for the next day, in the Taipa Ambient air quality monitoring station (background location) and the Taipa Residential air quality monitoring station (the high-density residential location). The models for NO_2, $PM_{2.5}$ and O_{3_MAX} used independent variables including the average of the hourly values between 16:00 of yesterday and 15:00 of today for NO_2, $PM_{2.5}$ and $O_{3\ MAX}$ respectively, the average of the hourly values between 00:00 and 23:00 of yesterday for $O_{3\ MAX}$, geopotential height at 850 hPa, atmospheric stability at 850 hPa and 925 hPa, air temperature at 925 hPa, average dew point temperature, minimum relative air humidity and average relative air humidity. The use of statistical models was successful in forecasting the average daily concentrations with MLR for NO_2 and $PM_{2.5}$ and MLR and CART analysis for the peak levels for maximum hourly O_3 for next day and be able to forecast the high concentration of pollution episodes, for both Taipa Ambient and Taipa Residential.

Acknowledgements The work developed was supported by The Macao Meteorological and Geophysical Bureau (SMG). The research work of CENSE is financed by Fundação para a Ciência e Tecnologia, I.P., Portugal (UID/AMB/04085/2019).

References

Cassmassi, J. C. (1997). Objective ozone forecasting in south coast Air Basin: Updating the objective prediction models for the late 1990's and Southern California ozone study (SCOS97-NARSTO) applications.

MEE. (2012). Ambient air quality standards. Retrieved from http://210.72.1.216:8080/gzaqi/Document/gjzlbz.pdf.

Neto, J., Torres, P., Ferreira, F., & Boavida, F. (2009). Lisbon air quality forecast using statistical methods. *International Journal of Environment and Pollution, 39*(3/4), 333. https://doi.org/10.1504/IJEP.2009.028695

SMG. (2019). Resumo anual sobre qualidade do ar em Macau—2019. Retrieved from https://cms.smg.gov.mo/uploads/sync/pdf/AIR_report/p_IQA_annual_report/IQA_2019.pdf.

WHO. (2003). Health aspects of air pollution with particulate matter, ozone and nitrogen dioxide. *Health Aspects of Air Pollution with Particulate Matter, Ozone and Nitrogen Dioxide*, (January), 98. https://doi.org/10.2105/AJPH.48.7.913.

WHO Europe. (2006). Air quality guidelines. Retrieved from http://202.171.253.71/www.euro.who.int/__data/assets/pdf_file/0005/78638/E90038.pdf.

Modeling Air Pollution in a Changing Climate

Impacts of Fine Particulate Matter and Climate Change on Human Health Over Europe—Present and Future Scenarios

Patricia Tarín-Carrasco, Ulas Im, Laura Palacios-Peña, and Pedro Jiménez-Guerrero

Abstract Nowadays, the evidence of the impacts of air pollution on human health is clear. A number of pollutants can damage our health but the most worrying is fine particulate matter ($PM_{2.5}$). This pollutant can damage different organs such as lungs, heart, brain; and can lead to premature death. Hence, this study tries to assess the present (1991–2010) and future (2031–2050, under the RCP8.5 scenario) cases of premature death due to Lung Cancer (LC), Chronic Obstructive Pulmonary Disease (COPD), Ischaemic Heart Disease (IHD) and Stroke in Europe due to exposure to ambient $PM_{2.5}$. WRF-Chem (Grell et al. in Atmospheric Environment 39:6957–6975, 2005) simulations over an Euro-CORDEX compliant simulation domain. The differences between these two scenarios provide the changes in future air quality. In order to isolate the climate change impact on air quality, (1) unchanged anthropogenic emissions from ACCMIP have been used; and (2) the population has been kept constant for the year 2010. The risk ratio (RR) and the base line mortalities for each pathology and different age ranges. Non-linear exposure–response functions for each risk ratio (RR) were obtained following (Lelieveld et al. in Nature 525:367–371, 2015) and (Liang et al. in Atmospheric Chemistry and Physics 18:10497–10520, 2018) methodologies. The results obtained in this differ from previous results using for linear exposure–response functions (e.g. Im et al. in Atmospheric Chemistry and Physics 18:5967–5989, 2018). Despite marked regional differences, overall, the pathologies included in this study will increase in the future period under a changing climate.

Keywords Climate change · Air pollution · Renewable energy · Human health · Mortality

P. Tarín-Carrasco · L. Palacios-Peña · P. Jiménez-Guerrero (✉)
Department of Physics, University of Murcia, 30100 Murcia, Spain
e-mail: pedro.jimenez@um.es

U. Im
Department of Environmental Science, Aarhus University, Frederiksborgvej 399, 4000 Roskilde, Denmark

P. Jiménez-Guerrero
Biomedical Research Institute of Murcia (IMIB-Arrixaca), 30120 Murcia, Spain

© The Author(s), under exclusive license to Springer-Verlag GmbH, DE, part of Springer Nature 2021

C. Mensink and V. Matthias (eds.), *Air Pollution Modeling and its Application XXVII*, Springer Proceedings in Complexity, https://doi.org/10.1007/978-3-662-63760-9_26

1 Introduction

The effects of air pollution on human health are numerous, even causing death. According to studies of World Health Organization (WHO), 9 out of 10 people breathe air of poor quality, this means that the population of the whole world is in danger due to this "invisible killer". Epidemiological studies shown that short and long-term exposures to some pollutants as Particulate Matter (PM) are associated with elevated rates of premature mortality (Liang et al., 2018). The different pollutants have various effects on health, nowadays one of the most harmful is PM (Burnett et al., 2018), causing from chronic diseases to premature death. In addition, these health damages have an impact on society, causing economic losses (Im et al., 2018). Recently studies show the large number of deaths due to this pollutant (e.g. Lelieveld et al., 2018, which estimates 790,000 deaths for the present period). In the future, due to climate change, a decrease of the dwellers wellness and increase of the premature mortality and chronic diseases is expected.

For all these reasons, this study focuses on the damages caused by PM on European population, in particular, the number of cases of deaths due to Lung Cancer (LC), Chronic Obstructive Pulmonary Disease (COPD), Ischemic Heart Disease (IHD) and cerebrovascular disease (CVD) trough non-linear functions and over three different regions (north, east and west of Europe).

2 Methodology

2.1 Exposure–Response Functions

Following Lelieveld et al. (2015) and Liang et al. (2018), the impacts of $PM_{2.5}$ on premature mortality has been estimated for each pathology and different group ages: 25–29, 30–34, 35–39, 40–44, 45–49, 50–54, 55–59, 60–64, 65–69, 70–74, 75–79, +80 and all ages. Firstly, premature mortality was calculated using the exposure–response function (Eq. 1) which is based on epidemiological relationships between air pollution concentration and mortality in each grid cell:

$$\Delta M = y_o[(RR - 1)/RR]Pop \tag{1}$$

where ΔM is premature mortality due to a disease, y_o is the baseline mortality rate for the different ages and European regions and *Pop* refers to the exposed population, y_o changes according mortality cause, age and European region and is set for the year 2010 and for both sexes. Risk Ratio (RR) value was determined for each pathology and age range the Monte Carlo method as in Eq. (2):

$$RR = 1 + \alpha\{1 - \exp[-\gamma(x - x_o)^{\delta}]\} \tag{2}$$

The upper and lower value was obtained representing the 95% confidence intervals. The parameters α, γ and δ change according to each disease and age range. X refers the $PM_{2.5}$ concentration in $\mu g\ m^{-3}$ and X_o the concentration below $PM_{2.5}$ have not risk for human health. α, γ, δ X_o were obtained from Global Burden Disease study 2010 (GBD2010). The gridded population data has been taken from the Socio Economic Data and Applications Center (SEDAC) of NASA (http://sedac.ciesin.columbia.edu) *Basic Demographic Characteristics, v4.11 (2010).* These data provide the population density by age and sex for the year 2010 consistent with national censuses and population registers with a resolution of 5 km^2 and were interpolated to the working grid.

2.2 Simulation WRF-Chem

Present and future simulations of air quality were used in order to check the possible changes in pathologies and diseases between due to climate change. The present reference period span 1991–2010; and the future enhanced forcing scenario, 2031–2050 under the RCP8.5 scenario. The differences between these two runs will provide the changes in future air quality. The WRF-Chem online-coupled meteorological/chemistry model (Grell et al., 2005) has been used in framework of the Spanish REPAIR and ACEX projects over the 0.44° Euro-CORDEX compliant domain.

In order to isolate the possible effects of climate change due entirely to air pollutants, unchanged anthropogenic emissions coming from ACCMIP are assumed. Moreover, that allows to anticipate the possible impacts if no mitigation strategies for regulatory pollutants are carried out. Natural emissions depend on climate conditions, and therefore vary in present and future simulations. Hence, the effects of climate change on air pollution follow the methodology, excluding possible changes in vegetation or land use. Also, the mortality in scenario where the use of renewable energy is 80% of the present is estimated.

3 Results and Discussion

Regarding the results, the different studied mortalities increase as the age range rises. Table 1 showed the estimation for the total mortality (LC, COPD, IHD and CVD) for all the studied regions for present, RCP8.5 and Renewable energy scenario. And is on east of Europe where we count with high number of mortality.

Over the north and centre Europe, the areas where more people live, total mortality will decrease on the future under climate change action, especially for IHD, the disease with more mortality cases found for both target periods. Over the west and east of Europe, the number of mortality cases will increase on the future due to climate

Table 1 Present, RCP8.5 and renewables total mortality (LC, COPD, IHD and CVD sum) estimation

	Present				RCP8.5				Renewables			
	west	center	east	EU	west	center	east	EU	west	center	east	EU
25–29	55	94	1732	1881	56	92	1729	1877	52	88	1584	1724
30–34	110	211	3052	3373	113	207	3049	3369	105	197	2797	3099
35–39	270	532	4400	5202	278	522	4396	5196	257	497	4028	4783
40–44	599	1434	7346	9380	616	1410	7342	9369	569	1342	6720	8631
45–49	1158	3080	13,228	17,465	1191	3031	13,200	17,422	1101	2892	12,058	16,051
50–54	1757	4823	22,551	29,130	1809	4741	22,506	29,056	1670	4510	20,453	26,633
55–59	2465	6679	33,878	43,022	2541	6557	33,835	42,933	2343	6221	30,725	39,289
60–64	3488	8823	40,281	52,592	3596	8644	40,243	52,483	3303	8171	36,418	47,892
65–69	4141	11,204	42,144	57,489	4275	10,975	42,176	57,426	3921	10,365	38,360	52,646
70–74	6047	16,737	52,309	75,093	6242	16,440	52,297	74,979	5738	15,535	46,085	67,357
75–79	5092	18,582	56,516	80,189	5288	18,239	56,623	80,149	4795	17,211	50,136	72,142
80plus	19,546	54,212	108,678	182,436	20,300	53,162	108,737	182,199	18,373	50,059	95,627	164,059
TOTAL	44,726	126,410	386,116	557,252	46,305	124,022	386,133	556,460	42,228	117,087	344,990	504,305

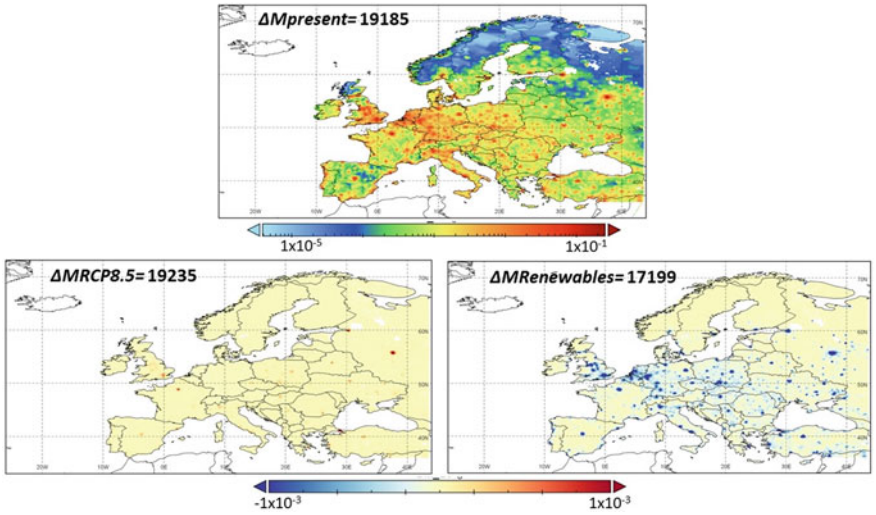

Fig. 1 Present mortality for LC for All Ages (top). Differences between RCP8.5 and present scenario (left-bottom) and differences between Renewables and Present scenario (right-bottom)

change penalty. Regarding to the renewables energy scenario, all the diseases studied will decrease on the future over all the studied regions.

Hotspots are located over around large European cities and central Europe as show Fig. 1. An increase of mortality cases due to LC caused by $PM_{2.5}$ is expected in the future scenario. LC mortality cases will be increased over western and eastern Europe. Conversely, for the renewables scenario, a decrease on the number of mortality cases over Europe is expected, especially in central and eastern Europe.

4 Conclusion

- The availability of detailed information about baseline mortality can help providing very detailed information about health issues.
- The different types of mortalities caused by $PM_{2.5}$ will increase in the future due to climate change penalty except IHD. This latter fact is conditioned by the high number of population which is living in central Europe, where mortality decreases.
- This climate penalty will affect mostly to western and eastern Europe by increasing mortality cases, while central Europe will benefit from a lower $PM_{2.5}$ concentration where mortality will decrease.
- Implementing renewable energies in the future will improve air quality and consequently, will positively impact the health of the population.

We should bear in mind the aging of European population and the increase of city dwellers, variables that have not been taken into account in this study in order just to isolate the effect of climate change alone in the health of European citizens.

Acknowledgements We acknowledge the project ACEX (CGL-2017-87921-R) of the Spanish Ministry of Economy and Competitiveness, the Fundación Biodiversidad of the Spanish Ministry for the Ecological Transition, and the FEDER European program, for support to conduct this research.

References

Burnett, R., Chena, H., Szyszkowicza, M., Fann, N., Hubbell, B., Pope, C. A., III., Apte, J. S., Brauer, M., Cohen, A., Weichenthal, S., Coggins, J., Di, Q., Brunekreef, B., Frostad, J., Lim, S. S., Kan, H., Walker, K. D., Thurston, G. D., Hayes, R. B., … Spadar, J. V. (2018). Global estimates of mortality associated with longterm exposure to outdoor fine particulate matter. *Proceedings of the National Academy of Sciences, 38*(115), 9592–9597.

Grell, G. A., Peckham, S. E., Schmitz, R., McKeen, S. A., Frost, G., Skamarock, W. C., & Eder, B. (2005). Fully coupled "online" chemistry within the WRF model. *Atmospheric Environment, 39*(37), 6957–6975.

Im, U., Brandt, J., Geels, C., Hansen, K., Christensen, J., Andersen, M., Solazzo, E., Kioutsioukis, I., Alyuz, U., Balzarini, A., Baro, R., Bellasio, R., Bianconi, R., Bieser, J., Colette, A., Curci, G., Farrow, A., Flemming, J., Fraser, A., … Galmarini, S. (2018). Assessment and economic valuation of air pollution impacts on human health over Europe and the United States as calculated by a multi-model ensemble in the framework of AQMEII3. *Atmospheric Chemistry and Physics, 18*(8), 5967–5989.

Lelieveld, J., Evans, J. S., Fnais, M., Giannadaki, D., & Pozzer, A. (2015). The contribution of outdoor air pollution sources to premature mortality on a global scale. *Nature, 525*, 367–371.

Lelieveld, J., Klingmüller, K., Pozzer, A., Pöschl, U., Fnais, M., Daiber, A., &, Münzel, T. (2018). Cardiovascular disease burden fromambient air pollution in Europe reassessed using novel hazard ratio functions. *European Heart Journal, 0*, 1–7.

Liang, C., West, J., Silva, R., Bian, H., Chin, M., Davila, Y., Dentener, F., Emmons, L., Flemming, J., Folberth, G., Henze, D., Im, U., Jonson, J., Keating, T., Kucsera, T., Lenzen, A., Lin, M., Lund, M., Pan, X., … Takemura, T. (2018). HTAP2 multi-model estimates of premature human mortality due to intercontinental transport of air pollution and emission sectors. *Atmospheric Chemistry and Physics, 18*(14), 10497–10520.

Questions and Answers

Questioner: Fabio Murena

Question: Do you plan to reduce the scale of 25 km in future work? In fact, most of the people live in urban areas, where spatial variability of pollutants is quite strong.

Answer: Yes, it is planned among our research objectives. As mentioned, a higher resolution could improve the precision over some spots on the domain as urban areas

or hotspots where high pollution levels are found. However, our current computational resources and the high computational cost of these online coupled simulations still does not allow us to run such a wide domain at lower resolution.

Questioner: Paul Makar.

Question: How much of the relativity small changes in human health impacts comparing current conditions to RCP85. Might be due to emissions decreases in RCP8.5 compared to current day emissions? E.g. overall 0.14/c decrease in mortality, while I've seen other studies where climate change makes health effects much worse. So, I was wondering if the RCP8.5 pollutant precursor emissions are lower than current day emissions, which might account for the 8.5 health effects being close to current day?

Answer: In this study, in order to isolate the possible effects of climate change due entirely to air pollutants, unchanged anthropogenic emissions coming from ACCMIP are assumed both for present and future scenarios. Thus, changes in pollutans are only caused by to meteorological changes under the RCP8.5 scenario and not due to a change in pollutant precursors in the future.

Air Quality Effects on Human Health and Ecology

Assessing the Impact of the Po Valley Air Quality Plan (Italy)

Elena De Angelis, Claudio Carnevale, Valeria Tolari, Enrico Turrini, and Marialuisa Volta

Abstract The Po Valley (Italy) is highly affected by air pollution and a large fraction of the population living in northern Italy is exposed to PM10 and PM2.5 concentrations that exceed both the European limit value and the stricter WHO air quality guidelines. For this reason, in 2017 four Regions (Piemonte, Lombardy, Veneto and Emilia Romagna) and the national Ministry of the Environment adopted a set of common measures, namely the "Po Valley air quality plan" (AQP). The main measures included in this plan consider emission reductions in road transport, residential heating and agriculture. The aim of this work is to apply the MAQ (Multidimensional Air Quality) model to assess the impacts of such measures on air quality, human health and greenhouse gases emissions in Lombardy and compare them to a cost-effective policy.

Keywords Integrated assessment modeling · Air pollution · Air quality plan

E. De Angelis (✉) · C. Carnevale · V. Tolari · E. Turrini · M. Volta
Department of Industrial and Mechanical Engineering, University of Brescia, Brescia, Italy
e-mail: e.deangelis@unibs.it

C. Carnevale
e-mail: claudio.carnevale@unibs.it

V. Tolari
e-mail: v.tolari@studenti.unibs.it

E. Turrini
e-mail: enrico.turrini@unibs.it

M. Volta
e-mail: marialuisa.volta@unibs.it

© The Author(s), under exclusive license to Springer-Verlag GmbH, DE, part of Springer Nature 2021

C. Mensink and V. Matthias (eds.), *Air Pollution Modeling and its Application XXVII*, Springer Proceedings in Complexity, https://doi.org/10.1007/978-3-662-63760-9_27

1 Introduction

In the past years, in Europe, several efforts have been undertaken at EU, national and regional level to limit population exposure to air pollution. The Po valley in Northern Italy is still a critical area because of high emissions and population density, in addition to a local climate that doesn't allow pollutants dispersion. In addition to the regional measures already in place, the AQP has been signed in 2017 by four regions (Piemonte, Lombardy, Veneto and Emilia Romagna) and the Ministry of Environment to identify common actions to reduce emissions mainly in road transport, residential heating and agriculture (MATTM, 2017). An effective air quality plan can be defined according to two different methodologies: scenario analysis and optimization approach. In the first case experts and stakeholders define a set of measures (e.g. from a source-apportionment study) and analyse the impacts using Chemical Transport Models, eventually modifying the technology application to achieve the required impacts. On the other hand, the multi-objective optimization (also cost-effectiveness or cost–benefit analysis) allows the decision makers to define the objectives (costs, air quality indexes) and to obtain a set of measures minimizing or maximizing them.

2 Materials and Methods

In this work, the Multi-dimensional Air Quality System (MAQ) is used (Turrini, 2018). MAQ is an Integrated Assessment Modeling tool that implements, through a set of models and databases, the DPSIR framework (EEA, 1999) and allows to identify the measures (*Response*) that directly abate precursors emissions (*Pressures*) or reduce the human activities (*Drivers*) causing a reduction of the air pollution level (*State*) which *Impacts* on human health, climate change, ecosystem and economy (Guariso et al., 2016). The MAQ model considers two different types of emission abatement measures: (1) end-of-pipe measures that abate the pollutants emissions before they are released in atmosphere, with no modification of the energy consumption (e.g. filters applied to cars) and (2) energy efficiency measures that modify the activity (drivers) causing pollution, changing the energy consumption. Such measures include both technological (e.g. substitution of fireplaces with gas boilers for domestic heating) and behavioural measures (e.g. active mobility).

The decision variables of the problem implemented in MAQ are the application rates of these measures. The model allows two different approaches: scenario analysis and optimization. In the scenario analysis the application rates of the measures are defined by the decision-maker and the impacts are then estimated by the system. The optimization approach can be a multi-objective optimization where one or more Air Quality Indexes and the policy implementation costs are minimized or a cost-effectiveness optimization where the policy implementation cost is fixed (constrained) and the air quality index is minimized. The formalization of the model is widely described by (Turrini et al., 2018). In this work MAQ system is used both

in scenario mode and optimization approach: the AQP scenario is compared to an efficient policy obtained by a cost-effectiveness optimization with a cost equal to the AQP.

3 Case Study

The methodology previously described is applied in Lombardy, a region in the Po valley. Two different policies are analysed and compared in the following:

1. AQP: the measures implemented are defined in the plan, no detailed quantitative information is provided, so a few hypotheses have been formulated in order to quantitatively assess the plan: (a) the reduction of biomass in residential heating is assumed equal to 25%, this energy demand is shifted to methane; (b) the application of energy efficiency measures in agriculture (biogas use, renewable energy in farms) is defined according to the Lombardy region air quality plan (Carnevale, 2018); (c) measures in the road traffic sector are applied to substitute EURO 0, 1, 2, 3 and 4 diesel cars with EURO 5 and 6; (d) Urea substitution in fertilization practice and low nitrogen feed are implemented with an application rate of respectively 10% and 50% (assumption based on a similar study (D'Elia, 2018). Measures are reported in Table 1.
2. The cost-effectiveness policy (optimal policy) is obtained using MAQ in an optimization approach and constraining the decision variables to 89.7 M€/yr cost, which is the cost estimated for the AQP by the model. The optimal policy includes end-of-pipe measures and energy efficiency measures.

In Fig. 1 the results are shown in the objective space, where the cost of the policy is represented on the horizontal axis and the Air Quality Index on the vertical axis, in this case the population weighted PM10 average concentration. The continuous line is the Pareto front representing the solutions of the multi-objective problem minimizing both the AQI and the costs, meaning the efficient policies. The base case (first point on the left) is the Current LEgislation scenario in 2020 (CLE2020) representing the application of the legislation in force in 2020 (at local, regional, national and

Table 1 Measures implemented in the AQP

SNAP1	Measure
Combustion in energy and transformation industries	• Energy efficiency measures in agriculture
Road transport	• Substitution of diesel car EURO 0, 1, 2, 3, 4 with EURO 5,6 diesel cars
Non-industrial combustion plants	• 25% of energy produced from biomass shifted to methane
Agriculture	• Urea substitution in fertilization practice • Low nitrogen feed for cattle

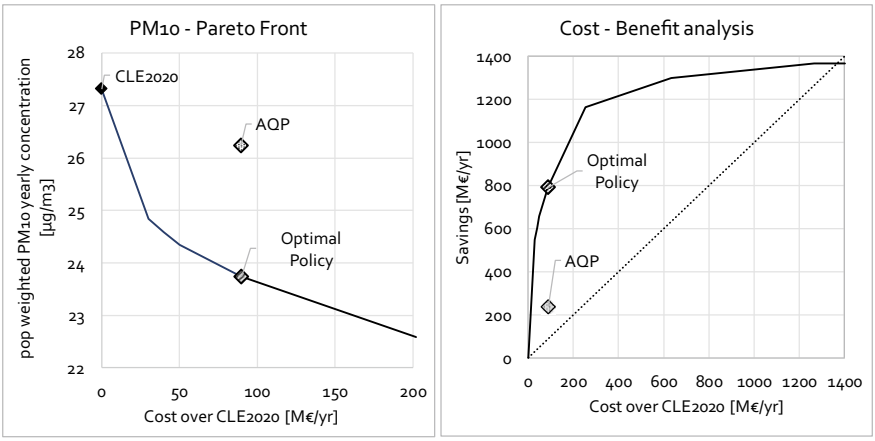

Fig. 1 Comparison of the AQP and the optimal policy in the objectives space (left) and cost–benefit analysis (right)

European level). In Fig. 1, on the right, the cost–benefit analysis is shown. On the vertical axis the savings in terms of fuel and health costs are represented. From both these figures it is clear that the optimal policies dominate the AQP scenario.

A comparison between the two policies in terms of health impacts, PM10 average concentrations (AQI) and CO_2 equivalent emission is shown in Table 2. The impacts, especially in terms of ΔAQI, and, accordingly, health savings, are clearly larger in the optimal policy compared to the AQP, as shown in Fig. 2 in terms of PM10 yearly concentration. The optimal policy is defined by measures in all the CORINAIR macro-sectors, in Table 3 only the measures in the macro-sectors considered by the AQP are reported.

4 Conclusion

This study highlights the differences between two decision approaches (scenario analysis and cost-effectiveness optimization) that can be applied to build an air quality plan. Strong assumptions have been made to quantify the AQP measures application because of a lack of detailed quantitative information in the plan, especially in road transport and residential heating where emission reductions have probably been over-estimated. Despite this, the AQP proves to be dominated by a policy built through a cost-effectiveness approach, mainly because it focuses only on four sectors and few measures. At the same cost, the optimal policy is a preferable way to achieve the EU Air Quality Directive objectives compared to the AQP.

Table 2 Impacts of the scenarios analyzed with respect to CLE2020 in terms of health, costs, air quality index and GHG emissions

Scenario	Cost over CLE2020 (M€/yr)	Health savings (M€/yr)	AQI ($\mu g/m^3$)	ΔAQI (%)	$CO_{2\ eq}$ (kt/yr)	$\Delta CO_{2\ eq}$ (%)
CLE2020	0.0	–	27.3	0	54,274	0
AQP	89.7	239	26.2	−4	54,557	+ 1
OPT Policy	89.7	793	23.7	−15	53,265	−2

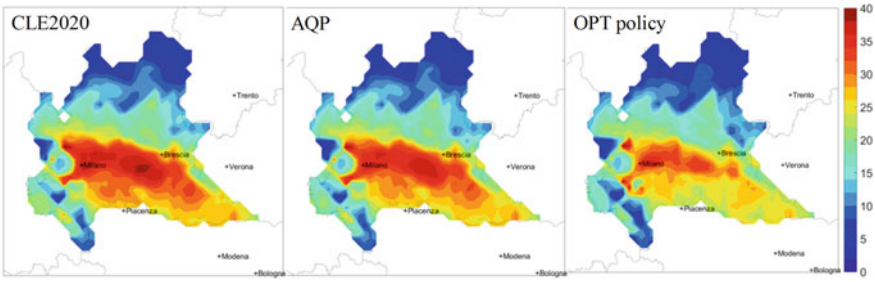

Fig. 2 PM10 yearly concentration in the CLE2020 scenario, AQP ant the optimal policy

Table 3 Main measures selected through the cost-effectiveness optimization approach

SNAP1	Measure
Combustion in energy and transformation industries	• Combustion modification on oil and gas boilers and furnaces
Road transport	• Optimization of urban good delivery
Non-industrial combustion plants	• New performance certification for stoves • Solar thermal plants in public buildings and new buildings
Agriculture	• Urea substitution in fertilization practice • Combination of low nitrogen feed, covered storage and other low ammonia applications (dairy cows and pig livestock)

References

Carnevale, C., et al. (2018). Assessing the economic and environmental sustainability of a regional air quality plan. *Sustainability (switzerland), 10*(10), 1–19.

D'Elia, I., et al. (2018). Evaluation of mitigation measures for air quality in Italy in 2020 and 2030. *Atmospheric Pollution Research. Elsevier, 9*(6), 977–988.

EEA (1999) Environmental indicators : Typology and overview *Technical report 25/1999.*

Guariso, G., Maione, M., & Volta, M. (2016). A decision framework for Integrated Assessment Modeling of air quality at regional and local scale. *Environmental Science & Policy Elsevier, 65*, 3–12.

MATTM (2017) *Nuovo accordo di programma per l'adozione coordinata e congiunta di misure per il miglioramento della qualità dell'aria nel bacino padano.* Available at: https://www.minambiente.it/pagina/qualita-dellaria (Accessed: June 11, 2019).

Turrini, E., et al. (2018). A non-linear optimization programming model for air quality planning including co-benefits for GHG emissions. *Science of the Total Environment Elsevier, 621*, 980–989.

Question and Answer

Questioner: Fabio Murena

Question: Which modification of the Air Quality Plan of Lombardy Region would you suggest?

Answer: The Po Basin Air quality plan focuses mainly on biomass burning (local space heaters) and road transport. Integrated Assessment Modeling in an optimization approach can be useful in defining efficient air quality plans, including end of pipe technologies and energy efficiency measures. In the Lombardy case study measures in livestock management, that is responsible for ammonia emissions, can be implemented as well as energy efficiency measures in residential buildings.

Innovative Atmospheric Dispersion Modelling in Support of Smart Farming Applications Within the Frame of the EU LIFE+ GAIA SENSE Project

F. Barmpas, George Tsegas, Nicolas Moussiopoulos, and E. Fragkou

Abstract Historically, the increased demand for food production was based on high use of fertilisers, pesticides and water as well as fossil fuels for the agricultural sector. The unsustainable use of these resources explains the negative effect of agriculture in major environmental issues like poor soil and water management, poor air quality and the greenhouse effect. The project LIFE+ GAIA Sense targets this environmental problem through the development and application of an innovative "Smart Farming" system that aims at reducing the consumption of natural resources and minimising environmental impact, while increasing crop production. One of the main objectives of the project is to evaluate the environmental impact of the GAIA Sense application in terms of air, soil and water pollution by implementing 18 demonstration campaigns across Greece, Spain and Portugal. A combined use of dispersion modelling and continuous measurements of several atmospheric pollutants is employed to assess the emission, dispersion and deposition of gases and particulates, taking advantage of collected meteorological data and soil moisture and temperature, as provided by the on-site GAIA sensors and meteorological stations. The atmospheric dispersion calculations follow a multiscale approach, based on a two-way coupled model system incorporating the mesoscale model MEMO/MARS-aero and the microscale model MIMO, in conjunction with a soil model for the simulation of water movement and solutes runoff and dispersion. A newly-developed physical

F. Barmpas · G. Tsegas (✉) · N. Moussiopoulos · E. Fragkou
Laboratory of Heat Transfer and Environmental Engineering,
Aristotle University, 54124 Thessaloniki, Greece
e-mail: gtsegas@auth.gr

F. Barmpas
e-mail: fotisb@auth.gr

N. Moussiopoulos
e-mail: moussio@auth.gr

E. Fragkou
e-mail: evfragkou@auth.gr

© The Author(s), under exclusive license to Springer-Verlag GmbH, DE, part of Springer Nature 2021

C. Mensink and V. Matthias (eds.), *Air Pollution Modeling and its Application XXVII*,
Springer Proceedings in Complexity, https://doi.org/10.1007/978-3-662-63760-9_28

submodel is used to simulate mass transport across the soil-atmosphere interface as well as provide season-dependent subscale parameterisations for different types of crop land coverage.

1 Introduction

Food security is closely linked to the agriculture economy sector for which sustainability is emerging as a critical condition for new technologies and methods. Sustainability in agriculture aims to ensure long term availability of the agricultural products in view of a changing environment but also to minimise environmental impacts on air, soil and water related to agricultural activities. In view of these problems, current agricultural methods, such as precision farming, embrace technological advances such as environmental assessment modelling, Remote Sensing, Geographic Information Systems (GIS) and Global Positioning Systems (GPS). Furthermore, environmental assessment tools, such as Life Cycle Assessment (LCA) and Cost Benefit Analysis (CBA), provide the scientifically relevant means to include environmental management into the agricultural processes.

In this frame, the GAIA Sense Smart Farming application has been developed as a resource efficiency tool for agricultural enterprises. Its main purpose is to monitor crops, collect high-resolution environmental data and offer advices about irrigation, fertilisation and pesticides based on soil, weather and plant nutrition data. This philosophy leads to an increase of resource efficiency promoting sustainable and circular economy, at the agricultural sector. The LIFE GAIA Sense project is implementing the circular economy concept through actions spanning the value chain, by minimising the inputs (chemicals and harmful compounds) which means less outputs and waste to process.

2 Methodology

GAIA Sense is an innovative "Smart Farming" (SF) solution that aims at reducing the consumption of natural resources, as a way to protect the environment and support Circular Economy models. Within the LIFE+ GAIA Sense project, a large SF infrastructure will be established and demonstrated in 18 applications across Greece, Spain and Portugal covering nine crops (olives, peaches, cotton, pistachio, potatoes, table tomatoes, industrial tomatoes, almonds, kiwi) in various terrain and microclimatic conditions. The project presents an innovative method, based on high-end technology, on how the farmer will be able to decide to either use or avoid inputs (irrigation, fertilisers, pesticides etc.) in a most efficient way, without risking the annual production. The GAIA Sense platform will be accessible and affordable to farmers either as individuals or collectively through Agricultural Cooperatives. At the core of the SF

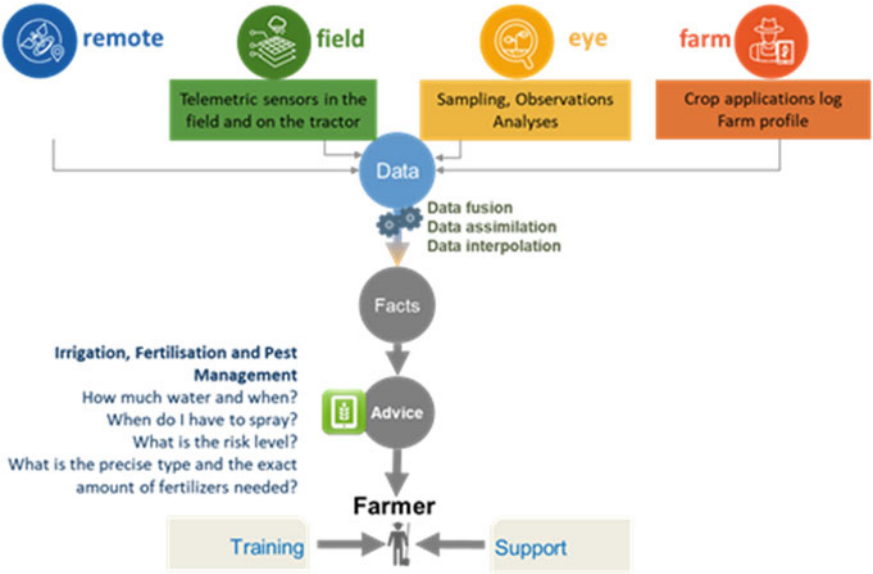

Fig. 1 GAIA sense—From data acquisition to agricultural advice

system, a data collection infrastructure is established, consisting of dense networks of meteorological/soil stations and traps (Fig. 1).

GAIA Sense consists of an infrastructure of IoT devices called GAIAtrons, a set of cloud computing services called GAIA Cloud and SF advisory services called GAIA SmartFarm. GAIAtrons are telemetric autonomous stations that collect data from sensors installed in the field and record atmospheric and soil parameters. GAIAtron Atmo is used to record climatic parameters, while GAIAtron Soil is used to collect soil parameters and control irrigation systems. At the heart of GAIA Sense is GAIA cloud platform, a set of computing services allowing not only the management of the IoT infrastructure but also the fusion and transformation of data into knowledge and finally to well-documented advices.

Through this cloud platform and with the use of novel assimilation techniques, the SF models are adjusted to the collected data in order to produce customised advice on agricultural practices, which is adapted to the needs of each selected crop and microclimate. After the application of the system, an infrastructure for the continuous monitoring and assessment of the environmental pollution is deployed, in order to measure the impact of SF on soil, water and air quality. These results, along with LCA and CBA outcomes, will be used to assess the economical and environmental efficiency of the GAIA Sense system and will allow for the development of a strategy to replicate and exploit the suggested solution.

3 Modelling Methodology for Assessing Air Quality Impacts

Within the frame of environmental impact assessment of the GAIA Sense solution, a novel multiscale modelling method for determining air pollution levels is developed. Air quality levels are largely influenced by scale-interaction processes, which have to be realistically described in numerical simulations. Wind flow over the cultivated and agricultural areas, which is closely associated with pollutant dispersion, is strongly influenced by atmospheric processes occurring at the next larger horizontal scale. The local pollutant concentration levels are influenced by regional scale processes, such as the atmospheric transport of pollutants emitted in surrounding cities and industrialised areas, which provide the background for the local scale over the agricultural areas. From a modelling point of view, these multiscale aspects have been historically addressed using independent modelling approaches, appropriate for each spatial scale. In such a scheme, dispersion modelling is realised in a uni-directional coupling approach where the coarse-scale model output provides initial and boundary conditions to the finer-scale model(s). The drawback of unidirectional coupling is that no information about the finer-grained physical processes is propagated back to the larger scale model(s). On the other hand, a full implementation of a bi-directional coupling between scales is hindered by the large computational cost of the finer-scale models, prohibiting any parallel execution with coarser-scale models.

Aiming to address the limitations which arise as a result of these disparities between the different modelling scales, a two-way scheme has been introduced for coupling the mesoscale model MEMO and the microscale model MIMO (Ehrhard et al., 2000), utilising a collection of interpolating metamodels. In the two-way MEMICO (Tsegas et al., 2015) coupling scheme, a three-dimensional spatial interpolation scheme, a spatial adjustment of values within the surface layer, and the formulation of the lateral boundary conditions to introduce the interpolated values into the microscale model are applied. Additionally, the physical parameters of the mesoscale model modified by the microscale simulations are realistically represented, in order to efficiently consider the feedback from the microscale simulations, and the horizontal resolution of MEMO is increased in several steps to approach the horizontal resolution of MIMO. For simulating pollutant chemistry and dispersion characteristics, the mesoscale dispersion model MARS-aero (Moussiopoulos et al., 2010, 2012) is applied at the same spatial resolution as the MEMO/MIMO model system, which downscales from a spatial resolution of 500 m for the entire selected area to 1 m for selected agricultural location. Specifically, an atmospheric dispersion model in conjunction with a mathematical model that simulates soil water movement and solutes fate will be used. To investigate the reliability of the simulation models, calibration, validation and evaluation using soil, meteorological and hydrological data will be performed. Specific subroutines will simulate atmospheric emissions, chemistry and deposition, nitrogen incorporating mineralisation, immobilisation, nitrification, denitrification, ammonium exchange, uptake and mass transport. In addition to the mathematical models, an LCA environmental impact assessment model will

be applied for the estimation of pollutants fate using international standards and eco-indicators.

As the accuracy of modelling estimates strongly depends on the availability of extensive and detailed input data, the influx of meteorological and soil moisture data from GAIAtrons and meteorological stations significantly boosts the accuracy and precision (i.e. forecasting skill) of the air quality modelling system. In order to produce maps of air pollutant levels at very high spatial resolution over the pilot agricultural domains, detailed input data are collected from open data sources and formatted to be used in the modelling applications. Data sources such as the Greek National Registry of Land and Property, which provides a digital soil model of 5 m resolution, are used.

4 Conclusion

The LIFE GAIA Sense project aims at presenting a very efficient and robust tool for implementing the EU policies in the areas of water, waste and air management, reducing the contribution of the agricultural sector over the major environmental burdens. Traditional modelling tools must be further developed in order to realistically cope with the complex system of characteristic soil-atmosphere interactions in crop areas. At the same time, implementations of the relevant physical modules should follow a pragmatic approach in view of the need of integration and robustness requirements of the operational decision-support tool. The atmospheric modelling is one of several components contributing to the comprehensive evaluation of the environmental impact of GAIA Sense application. In whole, possible environmental benefits and trade-offs of proposed farming regimes are identified, quantified and categorised in order to recommend best management practices and support policy formulation on Smart Farming in the EU.

Acknowledgements The "LIFE GAIA Sense" Project is co-funded by the LIFE Programme of the European Union under contract number LIFE17 ENV/GR000220.

References

Ehrhard, J., Khatib, I. A., Winkler, C., Kunz, R., Moussiopoulos, N., & Ernst, G. (2000). The microscale model MIMO: Development and assessment. *Journal of Wind Engineering and Industrial Aerodynamics, 85*, 163–176.

Moussiopoulos, N., Douros, I., Tsegas, G., Kleanthous, S., & Chourdakis, E. (2010). An air quality management system for Cyprus. *Global Nest Journal, 12*, 92–98.

Moussiopoulos, N., Douros, I., Tsegas, G., Kleanthous, S., & Chourdakis, E. (2012). An air quality management system for policy support in Cyprus, Hindawi Publishing Corporation. *Advances in Meteorology*. https://doi.org/10.1155/2012/959280.

Tsegas, G., Moussiopoulos, N., Barmpas, F., Akylas, V., & Douros, I. (2015). An integrated numerical methodology for describing multiscale interactions on atmospheric flow and pollutant dispersion in the urban atmospheric boundary layer. *Journal of Wind Engineering and Industrial Aerodynamics*, *144*, 191–201. ISSN 0167-6105, https://doi.org/10.1016/j.jweia.2015.05.006.

Modeling Chain Set up for the Assessment of Policy Impacts on Air Quality and Human Health

Valentina Agresti, Alessandra Balzarini, Maria Gaeta, Paolo Giani, Fabio Lanati, and Guido Pirovano

Abstract Private road transport segment is one of the main contributors to poor air quality, especially in densely populated cities. This study aims to simulate future mobility scenarios on the Italian peninsula and the associated impacts. A modeling chain composed by several modules is implemented to perform this analysis and the implications of a Reference and a Decarbonization scenarios are discussed. The first module is composed by an energetic model which outlines the car fleet evolution in terms of composition, vehicles kilometres travelled (VKT) and energy consumptions in 2030. A novel methodology is then applied to the energy model output to infer the private road transport emission variation respect to the base case year (2010). Then the estimation of the scenario's atmospheric concentration of NO_2, $PM_{2.5}$ and O_3, over a whole year, is obtained by means of a chemical transport model. Finally, some estimates of the health impact of two scenarios are provided, based on the variation of $PM_{2.5}$ and O_3 simulated concentration, respect to the base case year. Both scenarios expect an increase of the total demand for private transport in 2030 (18% for the Reference one), but at the same time a reduction of ICE cars in favour of hybrid and electric vehicles, with respect to the base case year. This trend leads to a general improvement of air quality, especially for the Decarbonization scenario for which the reduction of NO_2 concentration reaches 25% in some areas.

Keywords Energy scenarios · Atmospheric modeling · Decarbonization · Electric mobility · Air quality · Health impact

V. Agresti (✉) · A. Balzarini · M. Gaeta · P. Giani · F. Lanati · G. Pirovano
RSE Spa, via Rubattino 54, 20134 Milano, Italy
e-mail: valentina.agresti@rse-web.it

P. Giani
Department of Civil and Environmental Engineering and Earth Science, University of Notre Dame, Notre Dame, IN, USA

© The Author(s), under exclusive license to Springer-Verlag GmbH, DE, part of Springer Nature 2021

C. Mensink and V. Matthias (eds.), *Air Pollution Modeling and its Application XXVII*, Springer Proceedings in Complexity, https://doi.org/10.1007/978-3-662-63760-9_29

1 Introduction

The estimation of the environmental impact of future mobility is a challenging issue since on one hand, there is an ongoing transition towards low and zero emission vehicles and on the other hand, there is a growing demand for passenger transport. The object of this work is the implementation of a modeling chain, able to properly simulate the evolution of private road transport segment and related environmental impacts. In Sect. 2 all modules being part of the modeling chain are described as well as the methodology used to estimate the scenario road transport emissions. Then a description of the two scenarios analysed in this work is given. In Sect. 3 the impact of both *Reference* and *Decarbonization* scenarios, in terms of both air quality and human health is discussed by comparison with the base case and some final remarks can be found in Sect. 4.

2 Materials and Methods

2.1 Models

The processing of mobility scenarios is performed with a TIMES (The Integrated MARKAL-EFOM System) based approach (Seebregts et al., 2002) technical–economic model. TIMES-RSE model is implemented in Ricerca sul Sistema Energetico and it is a partial equilibrium model of the entire Italian energy system. It is driven by the demand for energy services (e.g. mobility demand) as well as by other drivers (such as fossil fuel prices evolution, technology parameters, investment costs) and it is based on the minimization of total costs for the energy system. Energy policies and / or energy and environmental constraints can be represented in the model. Afterwards the regionalization of TIMES-RSE output is entrusted to MONET energy model (Gelmini et al., 2011), which allows splitting future projections among the twenty Italian regions. Based on VKT data (vehicles kilometres travelled) associated to different fuelled vehicles in 2030, that the two energetic models outline, a novel methodology is developed to estimate scenario road transport emissions. Base case emissions are rescaled by the product with a grow matrix made by reduction coefficient C (Eq. 1). They are calculated as the ratio between VKT estimated by the TIMES-RSE model for the year 2030 multiplied by Euro6 cars emission factors, and VKT of 2010 multiplied by the 2010 emission factors from COPERT (Ntziachristos et al., 2000).

$$C = \frac{VKT_{2030} \times EF_{Euro6}}{VKT_{2010} \times EF_{Euro0-Euro5}} \tag{1}$$

The assumption that all vehicles belong to the Euro6 legislative class in 2030 is made. Moreover, zero emissions are associated to BEV. A coefficient is calculated

for the main pollutants (CO, SO_2, NMVOC, NO_X, NH_3, $PM_{2.5}$ and PM_{10}), for each Italian region, for each kind of fueled car distinguishing urban, rural street and highways. Starting from the grow matrix and some reference values, SMOKE (Sparse Matrix Operator Kernel Emissions) model allows to calculate road transport scenario emission field (Houyoux & Vukovich, 1999), which is an input of air quality model. Atmospheric pollutant concentration fields are calculated through the coupling of the meteorological model WRF (Weather Research and Forecasting meteorological model, Skamarock et al., 2008) and CAMx (Comprehensive Air Quality Model with Extensions, ENVIRON, 2016), which is a model able to simulate dispersion phenomena and chemical processes. Both models are implemented over the ITA domain (Fig. 2), which covers the Italian peninsula with 15 km of horizontal resolution, and that is a European nested domain. Additional details on WRF set-up and on CAMx configuration are available in Pepe et al. (2016). Three simulations are performed with these settings, one for the base case (2010 calendar year) and two for the scenarios (2030) with the rescaled road transport emission field. The final module of the modeling chain has been developed in RSE in order to estimate the impact of these scenarios on human health. This is achieved combining gridded changes in pollutant concentration fields, municipality-level population data and baseline incidence rates. Following the well-established European Environment Agency methodology (De Leeuw & Horálek, 2016), a log-linear model has been used to derive the health impact function. More details on this tool can be found on Agresti et al., (2019).

2.2 Scenarios

The two scenarios analyzed in this work are developed in the frame of the NECP, (National Energy Climate Plan) which aims to define actions and priorities for achieving the objectives that Italy intends to pursue by 2030, according to the targets set by the EU climate-energy policy and Paris Agreement (Falkner, 2016; Schleussner et al, 2016). These objectives are the reduction of greenhouse gas emissions and the increasing of both renewable energy and energy efficiency by 2030.

- The *Reference* scenario projects the energy system's evolution based on present trends, current and future technologies, economic and social development trends and recent legislation;
- The *Decarbonization* scenario follows the backcasting approach and it is outlined on the achievement of the main policy objectives: 32% share of RES (Renewable Energy Sources) in the 2030 Gross Final Consumption, with a 22% share of RES in the transport sector.

The evolution of the distribution of the car fleet for the latter scenario, from 2010 to 2030 is shown in Fig. 1. Most evident trends are a reduction of VKT by diesel-fueled vehicles and an increase of VKT by PHEV (Plug-in Hybrid Electric Vehicle).

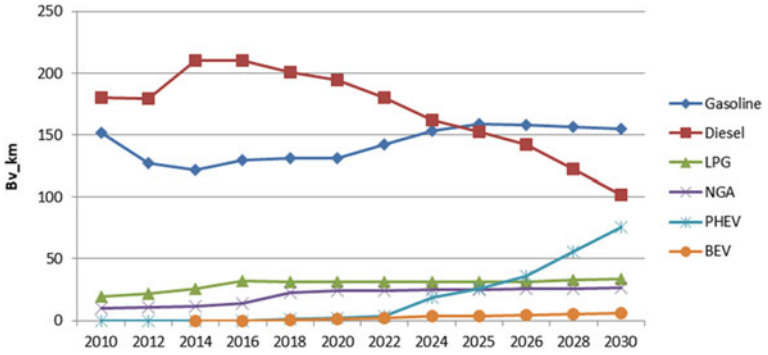

Fig. 1 Composition of the Italian car fleet by fuel, in terms of VKT (Billions of vehicle kilometer travelled), estimated with TIMES-RSE model for the *Decarbonization* scenario

3 Results and Discussion

Scenarios impacts on air quality are estimated by the comparison of pollutant concentrations with the base case ones. Atmospheric concentration of NO_2 is strongly affected by transport segment and the yearly mean concentration reaches 20 ppbV in Italy's most populated cities (Fig. 2a).

Figures 1b and 1c show that both scenarios entail an improvement of air quality with a stronger impact on the above-mentioned metropolitan areas, where the concentration of NO_2 is reduced by 3 ppbV (*Decarbonization* scenario).

$PM_{2.5}$ is the pollutant that most affects human health, with 59,630 premature deaths due to the exposure to this pollutant in Italy (EEA, European Environment Agency). As for the air quality, both scenarios have positive effects in terms of avoided hospitalizations and premature deaths. Most important benefits are reached in the cities of Milan, Turin, Florence, Rome and Naples. On a national level, the number of $PM_{2.5}$ premature deaths avoided annually in the *Reference* and *Decarbonization*

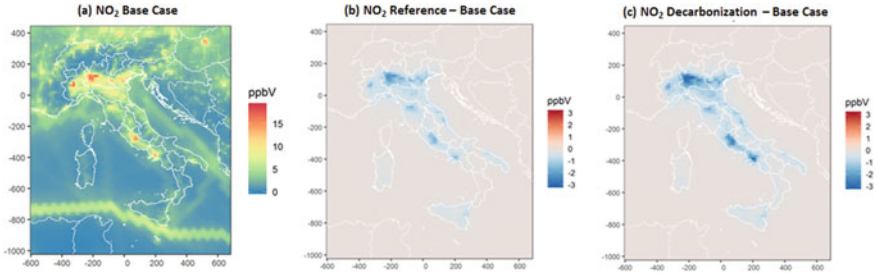

Fig. 2 Yearly mean NO_2 concentration (ppbV) for the base case in the ITA domain (**a**). Relative difference between the *Reference* scenario and the base case (%) (**b**) and between the *Decarbonization* scenario and the base case (**c**)

Table 1 Effects on human health due to the abatement of $PM_{2.5}$ ($\mu g*m^{-3}$) respect to the base case, due to the *Reference* and *Decarbonization* Scenarios (all the numbers refer to avoided effects)

	Reference	Decarbonization
Avoided premature deaths	3096 ± 51	3354 ± 55
Avoided hospitalizations	15,515 ± 80	16,814 ± 86

scenarios are 3096 and 3354 respectively (Table 1), which correspond to 5.1% and 5.6% of the total number of $PM_{2.5}$ deaths estimated by EEA.

4 Conclusion

This work shows all the steps of a modeling chain that allows to estimate which are the impacts of a certain policy, in terms of reduction of atmospheric pollutant concentrations, avoided hospitalizations and premature deaths in the Italian peninsula. The implications of a *Reference* and *Decarbonization* scenarios are discussed. Both scenarios assume an increase of the total demand for private transport (18% for the Reference one), but also a reduction of ICE cars in favor of hybrid and electric vehicles, with respect to the base case year (2010). This trend leads to a general improvement of air quality, especially for the *Decarbonization* scenario for which the reduction of NO_2 concentration reaches 25% in some areas, compared to the base case value. The obtained results also point out the relevance of developing harmonized modeling systems able to efficiently integrate optimized energy scenarios with the corresponding impacts on air quality and health. These results might provide a clearer understanding of the impacts for all stakeholders involved in energy and mobility topics.

Acknowledgements This work has been financed by the Research Fund for the Italian Electrical System in compliance with the Decree of Minister of Economic Development April 16, 2018.

References

Agresti, V., Giani, P., Pirovano, G., Lonati, G., & Pepe, N. (2019). Mobility scenarios in the Milan area: a modeling assessment of Air Quality. In *23rd transport and air pollution conference*.

De Leeuw, F. & Horálek, J. (2016). Quantifying the health impacts of ambient air pollution: methodology and input data.

ENVIRON. (2016). *CAMx (Comprehensive air quality model with extensions) User's Guide Version 6.3*. ENVIRON International Corporation

Falkner, R. (2016). The Paris Agreement and the new logic of international climate politics. *International Affairs, 92*(5), 1107–1125.

Gelmini, A., Lanati, F., Gargiulo, M. E., & De Miglio, G. (2011). *Il modello energetico multiregionale MONET*. RSE (p. 12001033), Ricerca di Sistema.

Houyoux, M. R., & Vukovich, J. M. (1999). Updates to the sparse matrix operator Kernel emissions (SMOKE) modeling system and integration with Models-3. *The Emission Inventory: Regional Strategies for the Future, 1461*, 1–11.

Ntziachristos, L., Samaras, Z., Eggleston, S., Gorissen, N., Hassel, D., & Hickman, A. J. (2000). *Copert iii. Computer Programme to calculate emissions from road transport, methodology and emission factors (version 2.1)*. European Energy Agency (EEA).

Pepe, N., Pirovano, G., Lonati, G., Balzarini, A., Toppetti, A., Riva, G. M., & Bedogni, M. (2016). Development and application of a high resolution hybrid modeling system for the evaluation of urban air quality. *Atmospheric Environment, 141*, 297–311.

Pepe, N., Pirovano, G., Balzarini, A., Toppetti, A., Riva, G. M., Amato, F., & Lonati, G. (2019). Enhanced CAMx source apportionment analysis at an urban receptor in Milan based on source categories and emission regions. *Atmospheric Environment*, *X*, 100020.

Schleussner, C. F., Rogelj, J., Schaeffer, M., Lissner, T., Licker, R., Fischer, E. M., & Hare, W. (2016). Science and policy characteristics of the Paris agreement temperature goal. *Nature Climate Change, 6*(9), 827.

Skamarock, W. C., Klemp, J. B., Dudhia, J., Gill, D. O., Barker, D. M., Duda, M. G., & Powers, J. G. (2008). *A description of the advanced research WRF version 3, NCAR Technical Note*. National Center for Atmospheric Research.

Seebregts, A. J., Goldstein, G. A., & Smekens, K. (2002). Energy/environmental modeling with the MARKAL family of models. In *Operations research proceedings 2001* (pp. 75–82). Springer

Modeling of Pollutant Emissions from a Diesel Power Station and Dispersion Over Extremely Complex Topography

Theodoros Nitis, George Tsegas, Eleftherios Chourdakis, Leonidas Ntziachristos, Nicolas Moussiopoulos, and Theodoros Giannaros

Abstract The operation of a diesel power station located near the urban area of Mytilene has resulted in elevated air pollution levels throughout the past decades, especially during the summer period. In order to assess the polluting potential of the plant, an evaluation of emissions from the diesel generators was performed on the basis of average and transient load and emission factors appropriate for the marine diesel mix used by the plant operator. The dispersion of emitted pollutants was calculated in a medium-term chemical dispersion simulation, performed using the mesoscale modelling system MEMO—MARS-aero for two selected multiday periods. The simulations underlined the important role of starting emissions, which under specific condition can lead to severe exceedances of the hourly concentration limits in nearby urban receptors. As a result, the need for continuous emissions monitoring, especially under identified unfavourable conditions, is highlighted.

T. Nitis (✉) · G. Tsegas
Laboratory of Environmental Quality and Geospatial Applications, Department of Marine Sciences, University of the Aegean, 81100 Mytilene, Lesvos, Greece
e-mail: theonitis@aegean.gr

G. Tsegas
e-mail: gtsegas@auth.gr

G. Tsegas · E. Chourdakis · L. Ntziachristos · N. Moussiopoulos
Laboratory of Heat Transfer and Environmental Engineering, Aristotle University, 54124 Thessaloniki, Greece
e-mail: chourdakis@auth.gr

L. Ntziachristos
e-mail: leon@auth.gr

N. Moussiopoulos
e-mail: moussio@eng.auth.gr

T. Giannaros
National Observatory of Athens, Institute for Environmental Research and Sustainable Development, Athens, Greece
e-mail: thgian@noa.gr

© The Author(s), under exclusive license to Springer-Verlag GmbH, DE, part of Springer Nature 2021

C. Mensink and V. Matthias (eds.), *Air Pollution Modeling and its Application XXVII*, Springer Proceedings in Complexity, https://doi.org/10.1007/978-3-662-63760-9_30

1 Introduction

An air quality study performed in the late 80's indicated that the town of Mytilene in the island of Lesvos, Greece is experiencing very high concentrations of air pollutants, both in terms of annual averages and summertime peak values. The latter were attributed to the operation of a diesel power station which operates near the border of the urban area of Mytilene and, to this day, is still covering more than 95% of the power needs of the island. Considering the age and specifications of the generator engines and the fuel used, as well as the limited application of emission-reduction measures, this power station remains a potentially important source of atmospheric pollution affecting the adjacent urban areas. Aiming to depict the contribution of the operation of the power station to the local air pollution levels, evaluation of the emissions from the diesel generators was initially carried out based on the average and transient load and emission factors appropriate for the marine diesel mix used by the plant operator. As a second step, the dispersion of emitted pollutants was calculated in a medium-term chemical dispersion simulation, performed using the mesoscale modelling system MEMO—MARS-aero with a resolution of 500 m covering the entire island of Lesvos, for two selected multi-day periods, representing the low and high wind situations, respectively. Results reveal that under specific meteorological conditions a persistent plume can affect the city of Mytilene leading to exceedances of limit values for PM_{10} and, to a lesser extend NO_2. The need for regulating the use of marine diesel and high-sulfur fuel mixes in isolated power plants is evident.

2 Methodology

2.1 Study Area

The island of Lesvos is situated in the North East Aegean Sea. It is the third biggest island of Greece with a population of approximately 95,000 habitants. The electricity generation infrastructure of Lesvos comprises of two wind parks and one diesel power plant. The diesel power plant consists of 10 electric generating sets and is located in the outskirts of the capital Mytilene.

2.2 Modelling Tools

A medium-term chemical dispersion simulation was performed, in a spatial resolution of 500 m:

- Regional scale driving meteorology: Advanced Research Weather Research and Forecasting Model (WRF; Skamarock & Klemp, 2008)

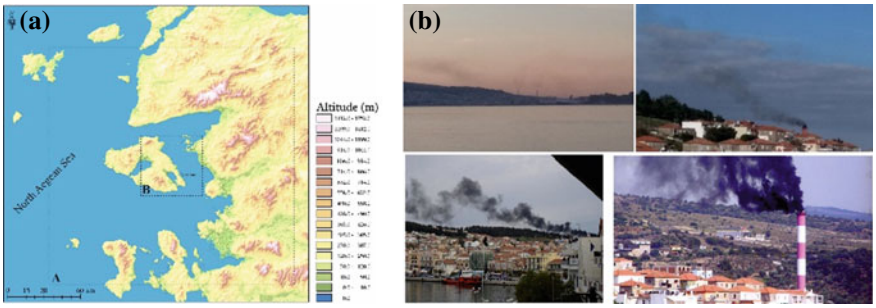

Fig. 1 **a** Relative location of the study area. Frames A and B indicate the coarse and the fine domain, respectively. **b** Pictures illustrating the degradation of the air quality in the area

- Meteorological driver: Mesoscale Model MEMO (Moussiopoulos et al., 2012)
- Chemical dispersion: MARS-aero (Moussiopoulos et al., 2010)

2.3 MEMO Input Data

Meteorological input information for MEMO, consisting of vertical profiles of wind speed, wind direction and temperature was acquired by application of the WRF Model. The WRF model is built over a mother domain with 9 km spatial resolution, which covers the Aegean Sea. The inner-most domain is centered over Island of Lesvos with a spatial analysis of 3×3 km^2.

A detailed orography dataset was derived from the Shuttle Radar Topography Mission—SRTM/90 m database (Farr et al., 2007). The land use dataset is based on the Corine Land Cover 2000 database. Initial night time Land and Sea Surface Temperature fields, as well as albedo data were derived from the Moderate-resolution Imaging Spectro-radiometer (MODIS; Rechid et al., 2009) instruments. Finally, the aerodynamic roughness length was derived by the application of simple empirical relationships between satellite radiometry and vegetation physiology (Nitis, 2016). To evaluate models (MEMO & WRF) performance, concurrent observations of air temperature and relative humidity, as well as wind speed and direction were employed (Lagouvardos et al., 2017) (Fig. 1).

2.4 Emission Estimations and MARS-aero Input Data

- Exhaust emissions from the power station were estimated on an hourly basis as average diurnal patterns for the periods under investigation.

- Activity data obtained from a previous study for the island of Lesvos in the form of electricity demand (in kWh; Giannoulis & Haralambopoulos, 2011).
- Separate emission factors were calculated for each pollutant, following the Tier-2 approach as specified in the Guidebook.
- Thermal efficiency of the engine assumed to be approximately 50%.

3 Results and Discussion

A. *Analysis of Meteorological Simulations*

The city of Mytilene comes under the influence of sea breeze and the Etesian winds, especially in summertime. The period under study confirms that the wind patterns in the area are categorized in these two groups. The first one (Fig. 2) is characterized by strong North-East winds, starts early at noon and blows until late in the evening (Etesian days).

In the second one (Fig. 3), the synoptic variations are light, the temperature gradient along the coastline is fully established and early in the afternoon drives to a North–West flow to the town. This flow pattern was selected in order to simulate the effect of the power plant on the air quality of the study area using the MARS-aero model.

B. *Analysis of Inert Pollutants Dispersion*

For calculating the effect of the power station on the air quality status of the nearby areas, especially in the city of Mytilene, dispersion calculations were performed in a nested grid configuration, covering the entire area of the island of Lesvos (50 km grid) in a resolution of 500 m. The Eulerian chemical dispersion model MARS-aero was

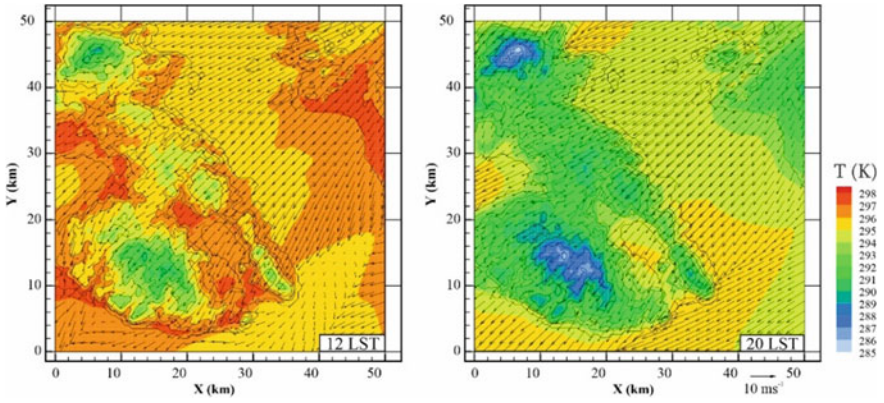

Fig. 2 Simulated surface wind fields and temperature (10 m AGL) for the fine domain at 12:00 and 20:00 LST for the 2nd of August 2018

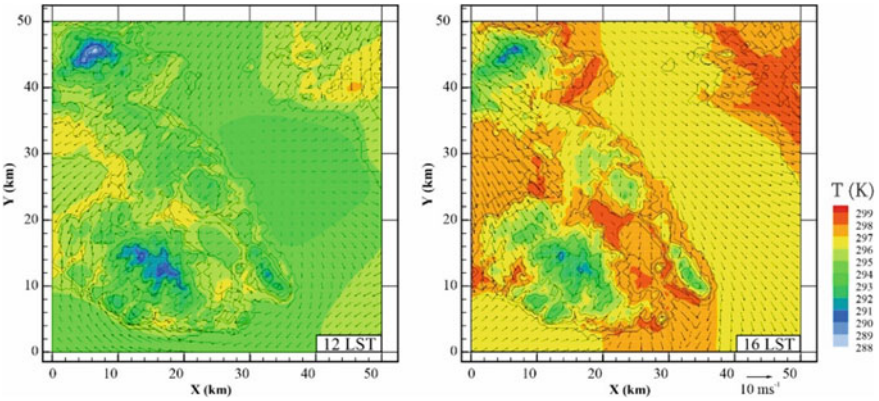

Fig. 3 Simulated surface wind fields and temperature (10 m AGL) for the fine domain at 12:00 and 16:00 LST for the 16th of August 2018

used to calculate concentrations of NO_2, PM_{10} and $PM_{2.5}$, using the meteorological fields of the non-hydrostatic meteorological model MEMO as input.

The impact of the operation of the power plant was quantified by means of an emissions scheme, whereby dispersion calculations are conducted for a scenario that excludes all emission sources except for the power station. The result of this calculation is shown in Figs. 4 and 5. It is noteworthy that the power station has a contribution on NO_2 in excess of 100 $\mu g/m^3$ and more than 20 $\mu g/m^3$ in the case of PM. The calculated concentrations indicate that the plant has a dominant contribution to the air pollution in the nearby areas.

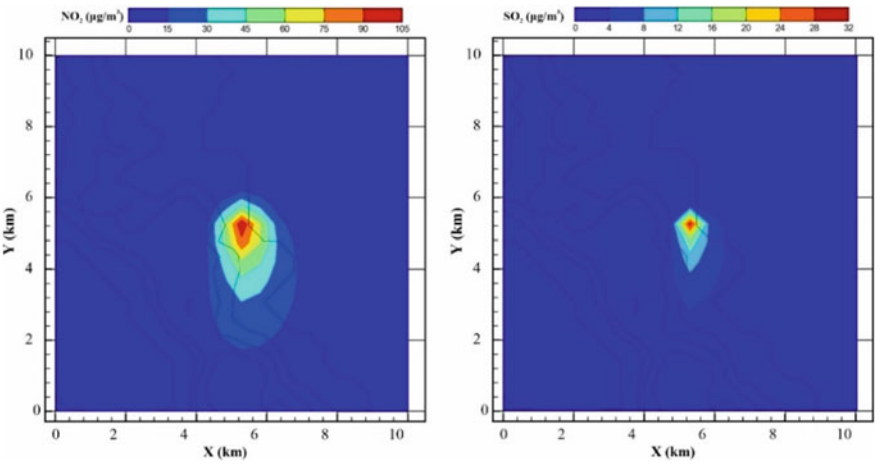

Fig. 4 Average calculated concentrations of NO_2 (left) and SO_2 (right) for the reference period

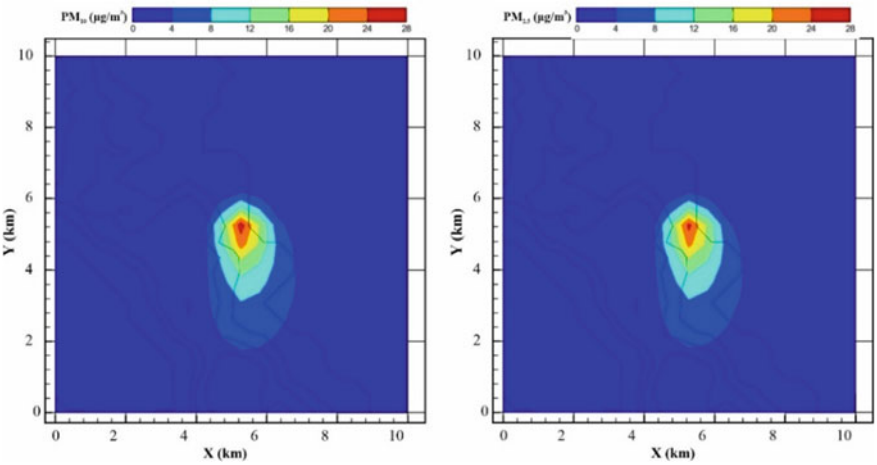

Fig. 5 Average calculated concentrations of PM_{10} (**left**) and $PM_{2.5}$ (**right**) for the reference period

Besides, in this point it should be noted that another factor affecting the air pollution levels in the city of Mytilene which can be attributed to the operation of the power station is its position in combination with the prevailing wind direction. More specifically, the plant is located in the north suburbs of the city, while the prevailing usually blows from the north. This fact increases the impact of the sta-tion on pollutant concentrations observed in the city of Mytilene.

4 Conclusions

Results reveal that under specific meteorological conditions a persistent plume can affect the city of Mytilene leading to exceedances of limit values for PM_{10} and, to a lesser extent, NO_2. The preliminary simulations highlighted the important role of starting emissions, which under specific conditions can lead to severe exceedances of the hourly concentration limits in nearby urban receptors. These results indicate the need for continuous emissions monitoring. Furthermore, the need for regulating the use of marine diesel and high-sulfur fuel mixes in isolated power plants is evident.

References

Farr, T. G., Rosen, P. A., & Caro, E. et al. (2007). The shuttle radar topography mission. *Reviews of Geophysics*, *45*.

Giannoulis, E. D., & Haralambopoulos, D. A. (2011). Distributed Generation in an isolated grid: Methodology of case study for Lesvos—Greece. *Applied Energy, 88*, 2530–2540.

Lagouvardos, K., Kotroni, V., Bezes, A., et al. (2017). The automatic weather stations NOANN network of the National Observatory of Athens: Operation and database. *Geoscience Data Journal, 4*, 4–16.

Moussiopoulos, N., Douros, I., Tsegas, G., et al. (2010). An air quality management system for cyprus. *Global NEST Journal, 12*, 92–98.

Moussiopoulos, N., Douros, I., Tsegas, G. et al. (2012). An air quality management system for policy support in cyprus. *Advances in Meteorology*.

Nitis, T. (2016). *An atmospheric environment management system incorporating the impact of urban areas and using geoinformatics*. Ph.D. thesis (p. 191), Aristotle University Thessaloniki.

Rechid, D., Hagemann, S., & Jacob, D. (2009). Sensitivity of climate models to seasonal variability of snow-free land surface albedo. *Theoretical and Applied Climatology, 95*, 197–221.

Skamarock, W. C., & Klemp, J. B. (2008). A time-split nonhydrostatic atmospheric model for weather research and forecasting applications. *Journal of Computational Physics, 227*, 3465–3485.

Local and Urban Scale Modeling

The Lagrangian Approach to Dispersion Modeling: Why We Like It (and What We Did with It)

Silvia Trini Castelli

Abstract An introduction to the Lagrangian approach for dispersion modeling and some historical notes are presented. In parallel, a brief review of our activity in Lagrangian particle models development and application, from the long range to the microscale, is proposed. Advantages and disadvantages of the Lagrangian approach are discussed, with a special highlight on the reasons why we like it and adopted it.

Keywords Lagrangian modeling approach · Historical notes · Lagrangian versus Eulerian models

1 Introduction

Giuseppe Luigi Lagrangia, alias Joseph-Louis Lagrange, was born in Torino, Italy, on the 25th of January 1736 (Fig. 1). However, this is not the only reason why we like the Lagrangian approach to dispersion modeling.

Lagrange was a mathematician and an astronomer, among his scientific contributions he reformulated the classical Newtonian mechanics into the "Lagrangian mechanics", where the motion equations are derived based on the principle of least action.

The Lagrangian modeling approach regards a variety of research fields, in atmospheric science, geoscience, oceanography, and their related applications. Here we limit our discussion to the Lagrangian modeling of the atmosphere (Lin et al., 2012) and to the study and simulation of the dispersion of tracers and pollutants in the atmosphere.

S. Trini Castelli (✉)
Institute of Atmospheric Sciences and Climate (ISAC), National Research Council (CNR), Torino, Italy
e-mail: s.trinicastelli@isac.cnr.it

© The Author(s), under exclusive license to Springer-Verlag GmbH, DE, part of Springer Nature 2021

C. Mensink and V. Matthias (eds.), *Air Pollution Modeling and its Application XXVII*, Springer Proceedings in Complexity, https://doi.org/10.1007/978-3-662-63760-9_31

Fig. 1 The monument dedicated to Joseph-Louis Lagrange in piazza Lagrange, Torino, Italy

In order to study the atmospheric dispersion, it is fundamental defining the **air parcel**, which is a portion of the atmosphere.

- Large enough to contain several molecules and to have well defined physical properties (temperature, density, humidity, pollutant concentration)
- Small enough to be considered infinitesimal, a «unit».

This concept applies also to the **tracer parcel**.

Considering an air parcel, in the Eulerian reference system an observer is fixed in space and is stationary in time t, so that it is tracking the changes in a variable $\varphi(t)$ as the parcel moves by its position (x, y, z). Instead, in the Lagrangian reference system, the observer is integral with the air parcel and is moving with it, thus tracking the changes of the variable $\varphi(t; x, y, z)$ as the parcel moves in the atmosphere (Fig. 2).

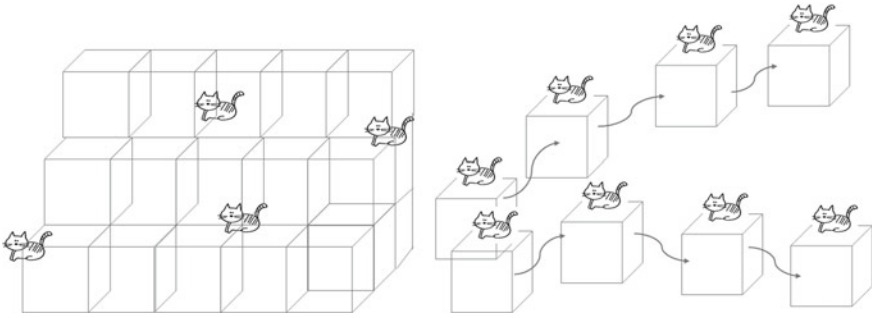

Fig. 2 Sketch of the Eulerian (left) and Lagrangian (right) reference frames, with air parcels (boxes) and observers (cats)

In equations, this implies that the rate of change of a state variable in the Lagrangian frame is determined by the total derivative:

$$\frac{d\varphi}{dt} = S \tag{1}$$

which in the Eulerian frame can be rewritten as:

$$\frac{\partial\varphi}{\partial t} + \boldsymbol{u} \cdot \nabla\varphi = S \tag{2}$$

where t is the time, S represents the source term and $\boldsymbol{u}$ is the velocity.

In numerical modeling, this translates in: Eulerian models solve the dynamical conservation equations at each (x, y, z) grid point of a numerical 3D grid; Lagrangian models are themselves "grid-free" and solve the trajectory of a parcel in a 3D domain, interpolating at the parcel position the meteorological variables needed to drive its motion.

Starting from mean trajectories, different Lagrangian models have been developed, boxes, puffs and particles. Their applicability depends not only on the degree of approximation with which the parcels are treated, but also on the scale that is considered. Lin (2012) provides a detailed description of the main characteristics of the different Lagrangian models, which are here summarized.

The **mean trajectory** modeling approach assumes that an air parcel retains its identity: from the Reynolds decomposition this implies that the air parcel trajectory is derived considering only the mean velocity and neglecting both molecular and turbulent diffusion. In the atmosphere, neglecting turbulence, thus the stochastic component of the flow, represents the main simplification in this approach. In Lagrangian **box models** air parcels are treated as aggregate, as boxes with variable volumes. The motion of the boxes is simulated by single or multiple mean wind trajectories, initialized at different locations. The dimension and volume of the boxes are determined by the mixing, the vertical extension of the box is determined by the varying

atmospheric boundary-layer height. With respect to the single-trajectory approach, the multiple trajectory box better describes the effect of the deformation of the flow in the dispersion. However, simulations are still based on mean-wind trajectories and do not account for wind shear, simplifying the representation of the dispersion in the atmospheric boundary layer. This is a limitation for describing the transport in the atmospheric boundary layer, where turbulence is an important component and diffusion cannot be neglected. Lagrangian **puff models** describe the dispersion of a sequence of puffs, representing a cloud of pollutant, with the transport determined by the mean wind and where the diffusion is solved on the basis of a Gaussian distribution or a distribution of a given form. Puff models are efficient when the mean winds and turbulence remain relatively constant, but they have difficulties capturing the interaction between wind shear and turbulence, distorting the plume into non-Gaussian shapes. This problem is faced with potentially ad hoc parameterizations, like puff splitting. In Lagrangian **particle dispersion models** (LPDM) the air/tracer parcel are represented as particles of equal mass (of the emitted substance) that are transported with random velocities generated by a Markov process. The behaviour of the airborne pollutant is simulated through the 'virtual' particles, their mean motion is defined by the local wind and the dispersion is determined by velocities obtained as solution of Lagrangian stochastic differential equations, able to reproduce the statistical characteristics of the turbulent flow. They calculate the concentration by computing the statistics of the trajectories of a large number of the fictitious particles. Here the focus is on the LPDM, which at present are the most advanced Lagrangian models.

2 Historical Trace

An overview on the turbulent dispersion theory and a summary of historical development of Lagrangian stochastic models can be found in Luhar (2012) and Thomson and Wilson (2012), respectively. Here the scientific milestones leading to the Lagrangian approach are briefly reviewed.

An homage is due to Leonardo da Vinci, who was the first one observing and describing the turbulence processes: "*Doue la turbolenza dellacqua rigenera, doue la turbolenza dellacqua simantiene plugho, doue la turbolenza dellacqua siposa*".

Robert Brown in 1827 observed that small pollen grains floating in water show an irregular and chaotic motion, then called *Brownian* after him. The brownian motion highlights that a small scale phenomenon (the molecular thermal collisions) leads to a larger scale effect (the random motion of a pollen grain). It is not possible to know in a deterministic way how next collision will be, thus the motion of a single pollen grain cannot be forecasted exactly. However, one can try describing the behaviour of the pollen after several collisions, when the effect of the single collision is 'forgotten'.

Osborne Reynolds in 1883 proposed the hypothesis for scale separation: any process $\varphi(\boldsymbol{x}, t)$—thus its variable—can be decomposed in a mean component (average) and a turbulent component (fluctuation): $\varphi = \bar{\varphi} + \varphi'$. The application

of averaging operators results in the appearance of new unknown terms in the equations, the second-order moments, i.e. the Reynolds stresses, which represent the turbulence contribution. The interpretation of the brownian motion was proposed and published by Albert Einstein in 1905 (and, independently, by Marian Smoluchowski in 1906), introducing for the first time the concept of stochastic model for a natural phenomenon: the motion of the pollen grain is so complex that its 'story' can be described only with a probabilistic approach. Einstein supposed that the instantaneous displacement of the grain is independent from the previous displacements: from this follows that the dimension of the 'cloud' of grains grows in time proportionally to the square root of the time itself. This analysis brought to a deterministic law describing not the position of the single grain but the dimension of the 'cloud' made up by several grains:

$$\sigma_x^2 = 2Kt, \tag{3}$$

where σ_x^2 is the displacement variance and K is the diffusivity.

A few years later, in 1908, Paul Langevin re-formulated, with an innovative approach, the equation of motion for the pollen grains. He made the assumption that two forces act on the pollen grain: a deterministic one, representing the friction of the fluid, and a stochastic one, accounting for the random collisions of the fluid molecules:

$$\frac{dv}{dt} = -\beta v + \lambda\mu(t), \tag{4}$$

where v is the velocity, μ a random function, β, λ are constants.

The equation, named after him, opened the door to a new mathematical framework: the stochastic approach, that found its rigorous description in the 1950s. The Langevin one is a Lagrangian equation. The corresponding Eulerian is the Fokker–Planck equation.

Geoffrey I. Taylor in 1921 provided an exact Lagrangian solution for the rate of spread of tracer in unbounded, stationary homogeneous turbulence. In 1D (z): the rate of increase in time of the ensemble mean spread, measured by the variance σ_z^2 of z displacement is given by:

$$\frac{d\sigma_z^2}{dt} = 2\int_0^t \overline{w'(t')w'(t'+\xi)}d\xi = 2\sigma_w^2 \int_0^t R_{ww}(\xi)d\xi \tag{5}$$

where σ_w^2, $R_{ww}(\xi)$ are the velocity variance and the Lagrangian velocity autocorrelation function.

He obtained a fundamental result: the standard deviation of the displacement is proportional to the time elapsed from the parcel release in the first phase of the diffusion process, and it is proportional to the square root of time for longer times, as found by Einstein.

3 More Recent Developments and Our Work in the Meantime

The theoretical basis for modern Lagrangian model dates back to the early 80s of former century, their numerical development began in following years, with the increasing power of computers. Starting from Alexander Obukhov, who in 1959 suggested that the Fokker–Planck equation can be used to model turbulent diffusion, more recent developments have been comprehensively reviewed by Rodean (1996). Here we recall the contributions by Steven Hanna, who in 1979 showed that a finite-difference equivalent of the Langevin equation is approximately valid for Lagrangian and Eulerian wind speed observations in the atmospheric boundary layer; by Frank Gifford, who in 1982 proposed that Langevin equation could be used to model horizontal diffusion in the atmosphere over diffusion times ranging from seconds to days; by Brian Sawford, who in 1984 noted that the Langevin equation is applicable to three-dimensional turbulence whereas relative diffusion on a global scale is quasi two-dimensional. Early numerical simulations highlighted the need of 'drift correction' terms and different approaches were proposed: Wilson et al. (1983), Legg and Raupach (1982), Thomson (1984). Han van Dop and coauthors in 1985 transformed the Langevin equation into its Eulerian equivalent, the Fokker–Planck. David Thomson in 1987 used more general forms of the Langevin and Fokker–Planck equations in evaluating several design criteria for stochastic Lagrangian models of turbulent diffusion. Many other scientists contributed to the development of Lagrangian models, more can be found in Lin et al. (2012).

While for long-range transport mean trajectories are still used, in order to account for the variability of the flow structure, also at the large scale more advanced models are needed. In the 90s, mostly long-range models were under development and assessment, with more urgency after the accident at the Chernobyl nuclear plant. International intercomparisons based on data collected in such dramatic occurrence were setup (ATMES programme), and further joint efforts to evaluate and validate models prosecuted (ETEX test case). The accidental release from Fukushima plant in 2011 renovated the interest in cross-borders transport of pollutants and several studies by different groups have been conducted. In this frame, based on a trajectory model our group developed a long-range Lagrangian particle model, MILORD (Anfossi et al., 1995). Yet, in even earlier years, a Lagrangian model for flat terrain, LAMBDA (Ferrero et al., 1995), and afterwards a more advanced model for complex terrain, SPRAY (Tinarelli et al., 2000), were built by our group to simulate the dispersion of pollutants at the regional scale. Several improvements followed in the years, in particular for SPRAY model, which is solving the Langevin stochastic differential equations for the velocity fluctuations, thus describing the statistical characteristics of the turbulent flow. SPRAY allows realistic reproductions of complex phenomena, such as strong temperature inversions, flow over topography, land use and terrain variability, and is able to simulate low wind-speed conditions, dense and light gas releases, also with two-phases (gaseous and liquid). All these improvements were then inherited by its microscale version, MicroSPRAY model (Tinarelli et al., 2012),

which contains special modules to treat the presence of obstacles. Modeling suites have been created, interfacing SPRAY and MicroSPRAY with RAMS atmospheric model (RMS and microRMS suites) and with MINERVE/SWIFT mass-consistent diagnostic model (MicroSwiftSpray, MSS, system). Recently, SPRAY has been interfaced with MOLOCH regional meteorological model, generating the SMART suite, for the Italian territory (Bisignano et al., 2018). A research version of SPRAY model, SPRAYWEB, has been lately setup with the intention of having an open community-modeling platform: a dedicated website is now available at http://sprayweb.isac.cnr.it/, with a link to the GitLab platform providing the core of the model after registration and under GNU license.

The models we developed have been applied to a number of different case studies, model intercomparisons, impact assessment evaluations, for both research aims and operational goals. Following the historical trace of the Lagrangian model developments in past three decades, our contributions to this research field have been presented at the conference, discussing our findings and results for several examples. In Figs. 3 and 4 some illustrative results are reported considering case studies at the different scales.

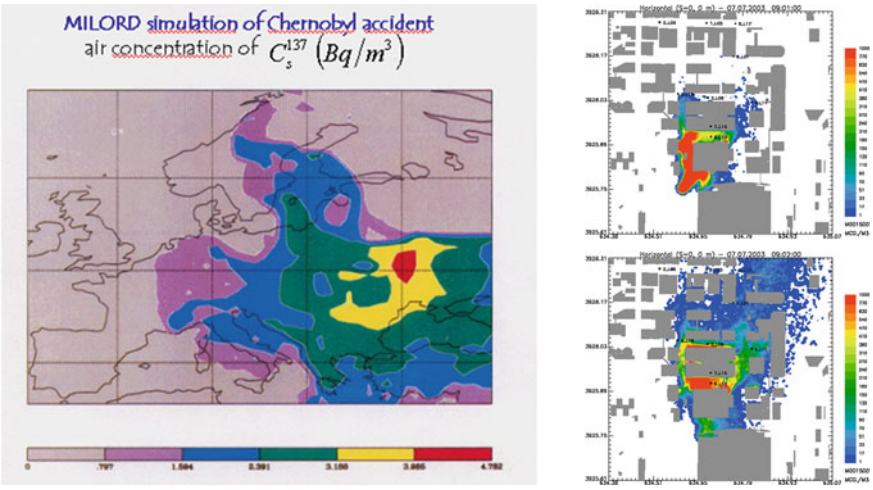

Fig. 3 From the long range to the microscale: MILORD model applied to ATMES intercomparison after Chernobyl accident (left) and MSS system applied to UDINEE project (Tinarelli and Trini Castelli, 2019), simulating puff releases from JU2003 experimental field campaign in Oklahoma City urban site (right)

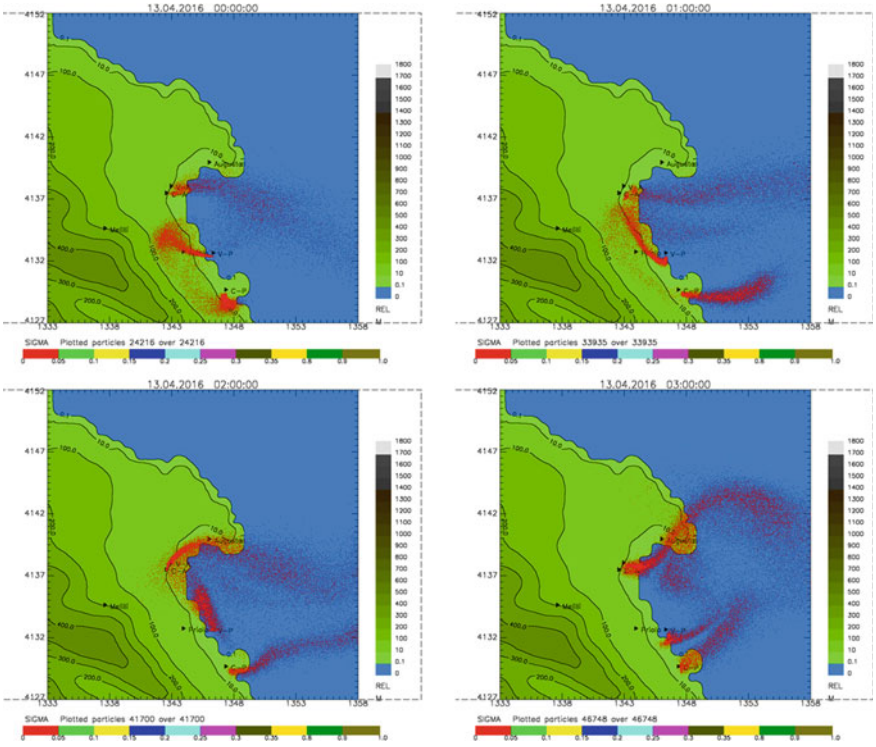

Fig. 4 Local and regional scale. SMART suite simulating the releases from two stacks (C-A and C-P) and two settling tanks (V-A and V-P) on the Sicilian coast: particles dynamics from 00 to 04 night hours, revealing the sensitivity to the local circulation

4 Discussion and Conclusion

Together with the Eulerian models, Lagrangian ones certainly need larger computational resources than Gaussian or parametric models, but they provide a more realistic and physical reproduction of the pollutant dispersion, better accounting for the variability of the meteorology, for the complexity and heterogeneity of topography and landuse, for the presence of obstacles at small scale.

Among the advantages of the Lagrangian models (see also Lin et al., 2012), we briefly cite that:

– For their nature, by following the air/tracer parcel motion, they mime realistically the atmospheric flow, they inherently maintain the conservation properties, they provide information of the trajectories of the parcels;
– Being grid-free, they follow the air/tracer parcels motions at all scales with the same accuracy, leading to a complete description of all the phases of dispersion and resolving the variability at the subgrid scale;

– Following previous point, they are more effective than Eulerian models in describing the first phase of the release close to the source and related subgrid diffusion, because not dependent on the grid resolution;
– With respect to simpler models, thanks to the independent particles, in the LPDM the plume responds to mean and turbulent motions in each point, not only at its centre of mass;
– Their formulation is not affected by the non-linearity of the advection term (see Eqs. (1) and (2)), thus its numerical integration and solution is stable;
– They are not conditioned by the requirement of a closure approximation for the non linear-term in the conservation equation for the concentration, as in Eulerian models, where the gradient-diffusion hypothesis is not physically acceptable for small diffusion time.

As for the disadvantages of Lagrangian models:

– They require in input meteorological variables that are generally provided on 3D Eulerian grids, thus the level of detail of the dispersion processes is conditioned by the resolution of the 3D fields, there might be inconsistencies with the Eulerian outputs and interfacing codes are mostly needed;
– The calculation of the concentration is not 'embedded' in the model as in the Eulerian approach: they need additional post-processing to produce the tracer concentration and deposition fields, using a regular mesh for parcel counting, or kernel estimators or other procedures to calculate these fields;
– They produce ensemble-averaged concentrations, developments towards two-particles models are needed for calculating instantaneous concentrations or concentration variances;
– Dealing with chemistry in a Lagrangian model is complicated, it is difficult to describe the parcels/particles interaction because the distances between air/tracer parcels change continuously; generally, LPDM cannot solve chemical reactions of second order: hybrid solution have been proposed but are still under investigation.

The reasons why we like the Lagrangian model are both its intuitive physical description of the atmospheric flow and diffusion, since air masses move as the Lagrangian parcels do, and its flexibility in simulating the tracer dispersion. A Lagrangian model can be run using both minimal or fully 3D meteorological inputs, it can follow the fate of a released mass forward or backward, thus reconstructing possible unknown sources of pollution. It allows reproducing different emissive and dispersive scenarios in the same meteorological condition, without the need of a complete re-run as for an Eulerian model. Such off-line approach is useful for impact assessment or monitoring network planning. An additional reason for promoting Lagrangian models is that they can represent an optimal compromise between physical accuracy and computational burden, when compared to simpler Gaussian models or advanced Eulerian-CFD models, respectively.

Somehow, it is also a matter of "philosophical" choice: firmly standing and looking at the flow passing by, or freely flying with it.

Acknowledgements I like to acknowledge the colleagues who have received me in the Lagrangian community and who have been the "Dei ex Machina" of our Lagrangian models, in alphabetical order: Domenico Anfossi, Giuseppe Brusasca, Enrico Ferrero, Gianni Tinarelli.

References

Anfossi, D., Sacchetti, D., & Trini Castelli, S. (1995). Development and sensitivity analysis of a Lagrangian particle model for long range dispersion. *Environmental Software, 10*(4), 263–287.

Bisignano, A., Trini Castelli, S., & Malguzzi, P. (2018). "Development and verification of a new meteo-dispersive modeling system for accidental releases in the Italian territory: SMART". In: C. Mensink, W. Gong & A. Hakami., (Eds.) *Air pollution modeling and its application XXVI.* Springer Proceedings in Complexity. Cham, Switzerland: Springer International Publishing.

Ferrero, E., Anfossi, D., Brusasca, G., & Tinarelli, G. (1995). Lagrangian particle model LAMBDA: Evaluation against tracer data. *International Journal of Environment and Pollution, 5*, 360–374.

Legg, B. J., & Raupach, M. R. (1982). Markov-chain simulation of particle dispersion in inhomogeneous flows: The mean drift velocity induced by a gradient in Eulerian velocity variance. *Boundary-Layer Meteorology, 24*, 3–13.

Lin, J. (2012). "Lagrangian modeling of the atmosphere: An introduction". In: *Lagrangian modeling of the atmosphere*, Geophysical Monograph Series, *200* (pp. 1–14). Washington DC: American Geophysical Union.

Lin, J., Brunner, D., Gerbig, C., Stohl, A., Luhar, A., & Webley, P. (Eds.). (2012). *Lagrangian modeling of the atmosphere.* Geophysical Monograph Series*, 200* (p. 349). Washington DC: American Geophysical Union.

Luhar, A. K. (2012). "Turbulent dispersion: Theory and parameterization—overview". In: *Lagrangian modeling of the atmosphere*, Geophysical Monograph Series, *200* (pp. 15–18). Washington DC: American Geophysical Union.

Rodean, H. C. (1996). *Stochastic Lagrangian models of turbulent diffusion.* Meteorological Monographs (Vol. *48*). Boston, Mass: American Meteorological Society.

Thomson, D. J. (1984). Random walk modeling of diffusion in inhomogeneous turbulence. *Quarterly Journal Royal Meteorological Society, 110*, 1107–1120.

Thomson, D. J. (1987). Criteria for the selection of stochastic models of particle trajectories in turbulent flows. *Journal of Fluid Mechanics, 180*, 529–556.

Thomson, D. J., & Wilson, J. D. (2012). "History of Lagrangian stochastic models for turbulent dispersion". In: *Lagrangian modeling of the atmosphere.* Geophysical Monograph Series, *200* (pp. 19–36). Washington DC: American Geophysical Union.

Tinarelli, G., Anfossi, D., Bider, M., Ferrero, E., & Trini Castelli S. (2000). "A new high performance version of the Lagrangian particle dispersion model SPRAY, some case studies". In S. E. Gryning & E. Batchvarova (Eds.) *Air pollution modeling and its application XIII 23* (pp. 499–506). New York: Plenum Press.

Tinarelli, G., Mortarini, L., Trini Castelli, S., Carlino, G., Moussafir, J., Olry, C., Armand, P., & Anfossi, D. (2012). "Review and validation of microspray, a Lagrangian particle model of turbulent dispersion". In *Lagrangian modeling of the atmosphere*, Geophysical Monograph Series, *200* (pp. 311–327). Washington DC: American Geophysical Union.

Tinarelli, G. L., & Trini Castelli, S. (2019). Assessment of the sensitivity to the input condition with a Lagrangian particle model in UDINEE Project. *Boundary-Layer Meteorology, 171*(3), 491–512.

van Dop, H., Nieuwstadt, F. T. M., & Hunt, J. C. R. (1985). Random walk models for particle displacements in inhomogeneous unsteady turbulent flows. *Physics of Fluids, 28*, 1639–1653.

Wilson, J. D., Legg, B. J., & Thomson, D. J. (1983). Calculation of particle trajectories in the presence of a gradient in turbulent-velocity variance. *Boundary-Layer Meteorology, 27*, 163–169.

Questions and Answers

Questioner: Peter Builtjes

Question: Nearly all observations, meteorological (wind speed, for instance) and concentrations are Eulerian. Is that an issue, a problem, for trajectory models?

Answer: Since the Lagrangian models are grid-free, this is not an issue. Meteorological observations can be an input to Lagrangian models; when enough densely distributed in the simulation domain, they can also be treated with a diagnostic mass-consistent model to provide the Lagrangian model with gridded input data. In the Lagrangian model, the observed (or modelled) meteorological variables of interest are interpolated at the particle position to provide the due thermo-dynamical values driving its motion. Observed concentrations are compared to the output model predictions: in this case, the pollutant mass brought by the particles which arrive at the observation point in the time interval of interest are used to calculate the simulated concentration, with different approaches (3D boxes, kernels…).

Questioner: Heinke Schlünzen

Question: How do you determine how many particles have to be released to calculate a minimum concentration that is given?

Answer: The number of particles N_p that have to be emitted at each time step to estimate a given minimum concentration can be determined, for instance, by a relationship that considers the volume $\Delta x \Delta y \Delta z$ of the cell in the concentration computational grid:

$$N_p = \frac{N_c}{C_x} \frac{Q \Delta t}{\Delta x \Delta y \Delta z}$$

where Q is the emission rate, Δt is the time step, N_c is the minimum number of particles wanted in the 3D grid cell in order to produce a sensible concentration value, C_x (given by $N_c = 1$) is the minimum concentration associated to a single particle found in a cell. In alternative, kernel-based methods can be used.

Question: What is the smallest distance (as time scale) a Lagrangian Model can be applied to? How close to a source are the determined concentrations reliable?

Answer: In principle, the concentrations predicted by a Lagrangian stochastic model are reliable at any distance from the source. In practice, the discrete simulation time step determines the minimum distance at which, given the driving mean wind and turbulence, a particle can be found, thus contributing to the calculation of the concentration in a volume close to the source. Clearly, the grid resolution of the meteorological input influences an effective estimation of the concentration because the particles are moved inside a single grid cell based on interpolation of the input variables.

Questioner: Andrey Vlasenko

Question: My naïve understanding of Lagrangian approach says me, that the size of a Lagrangian particle in the numerical model should be at least not larger than the Kolmogorov size. Am I right?

Answer: We need to refer to time scale. In high Reynolds-number turbulence, as in the atmospheric flows, the diffusion term of the Langevin equation is consistent with Kolmogorov theory of local isotropy in the inertial subrange, in that the correlation time scale of the particle accelerations is of the order of the Kolmogorov time scale. This last is much shorter than the Lagrangian integral time scale. In this sense, the related size of the Lagrangian particle has to be congruent with the Kolmogorov spatial scale in the inertial subrange.

Question: Why particles moving from Chernobyl towards Italy propagate in a narrow corridor? Is it because the corridor coincides with the computational domain?

Answer: It is just a graphical effect: in the figure we plotted a small percentage of the particles travelling in (and filling!) the computational domain, in order to highlight the areas that have been more affected by the plume impact during the release and simulation time.

Modeling Setup for Assessing the Impact of Stakeholders and Policy Scenarios on Air Quality at Urban Scale

Vera Rodrigues, Kevin Oliveira, Sílvia Coelho, Joana Ferreira, Ana Patrícia Fernandes, Sandra Rafael, Diogo Lopes, Vânia Seixas, Alexandra Monteiro, Carlos Borrego, Kris Vanherle, Peter Papics, Trond Husby, Iason Diafas, Angreine Kewo, Carlo Trozzi, Enzo Piscitello, Svein Knudsen, Evert Bouman, Enda Hayes, Jo Barnes, Stephan Slingerland, Hans Bolscher, and Myriam Lopes

Abstract ClairCity, a project funded by the EU Horizon 2020 research and innovation programme, developed an innovative quantification framework aiming to assess environmental, health and economic impacts. The quantification framework consists of (i) an integrated urban module based on the household and dwelling characteristics, (ii) emission rates linked with on-road transport, (iii) emission data linked with the industrial, residential, commercial and institutional sectors, (iv) daily and hourly consumption profiles based on the energy and power generation data, (v) air quality patterns and related population exposure, (vi) health-related impacts and costs, and (vii) carbon footprint estimates. This framework was applied for the baseline situation of 6 pilot cities. In particular, the second-generation Gaussian

V. Rodrigues (✉) · K. Oliveira · S. Coelho · J. Ferreira · A. P. Fernandes · S. Rafael · D. Lopes · V. Seixas · A. Monteiro · C. Borrego · M. Lopes
CESAM and Department of Environment and Planning, University of Aveiro, 3810-193 Aveiro, Portugal
e-mail: vera.rodrigues@ua.pt

K. Vanherle · P. Papics
Transport & Mobility Leuven, Leuven, Belgium

T. Husby · I. Diafas
Planbureau Voor de Leefomgeving, The Hague, Netherlands

A. Kewo
Danmarks Tekniske Universitet, Lyngby, Denmark

C. Trozzi · E. Piscitello
TECHNE Consulting, SRL, Milano, Italy

S. Knudsen · E. Bouman
Norsk Institutt for Luftforskning, Kjeller, Norway

E. Hayes · J. Barnes
University of the West of England, Bristol, UK

S. Slingerland · H. Bolscher
Trinomics Bv, Rotterdam, Netherlands

© The Author(s), under exclusive license to Springer-Verlag GmbH, DE, part of Springer Nature 2021

C. Mensink and V. Matthias (eds.), *Air Pollution Modeling and its Application XXVII*, Springer Proceedings in Complexity, https://doi.org/10.1007/978-3-662-63760-9_32

model URBAIR was setup and ran to simulate NO_2 and particulate matter concentrations for distinct computational domains covering the urban area of each case study for the full baseline year of 2015. The ClairCity impact assessment framework is applied to evaluate the impact of scenarios for 2025, 2035 and 2050, namely the Business As Usual (BAU) scenario and 3 additional scenarios translating the expectations of citizens and local experts based on data collected through engagement process. The outcomes of the assessment of impacts were used to inform the Policy Workshops for each case study to help decision-makers and local planners to define the final integrated Unified Scenario.

1 Introduction

The continuous growth of population living in urban areas worldwide has been increasing the number of air pollution episodes alarmingly threatening human health and well-being. In order to preserve healthy living conditions in urban areas, control and mitigation strategies of air pollution episodes are of utmost importance. For that, citizens need to become the key element at the centre of air pollution reduction strategies, being consider not only as a cause, but also as the main solution, making the scene for big changes in citizens' behaviour, activities and practices (Barnes et al., 2018; Chatterton & Wilson, 2014). The ClairCity project—Citizen-led air pollution reduction in cities—aims to improve future air quality and carbon policies in European cities by initiating new modes of engaging citizens, stakeholders and policy makers. ClairCity is putting citizens and their behaviour at the centre of air pollution and carbon management, applying the most recent advances in social sciences.

In this work, we discuss the application of the ClairCity quantification framework to assess the impacts on air quality focus on NO_2, PM10 and PM2.5 concentrations.

2 Air Quality Impacts Assessment

ClairCity applies a quantification framework to six European cities and regions: Bristol (UK), Amsterdam (The Netherlands), Ljubljana (Slovenia), Sosnowiec (Poland), Genoa (Italy) and the Aveiro region (Portugal). The application of the quantification framework encompassed the build-up of a ClairCity emissions database addressing distinct emission sectors, in line with statistics by sector, by time of day, establishing the link with citizen's behaviour. It includes emission rates for the 6 case studies, considering as point sources the large industry emissions, as well as, shipping emissions (in the case study of Genoa), the line sources with the road-traffic emissions, and the area sources covering the residential, commercial and industrial emissions, the IRCI module, as well as the shipping emissions for the case study of Amsterdam. The database is physically stored in the ClairCity Data Portal and will be fully public available by the end of the project.

The Gaussian model URBAIR (Borrego et al., 2016) was setup and run at urban scale for the computational domain over the urban area of each city/ region with a horizontal grid resolution of 200 m × 200 m. The baseline simulations were performed using as input data the meteorological vertical profiles provided by the WRF model, which was applied to the regional domain covering the urban area of each case study using as horizontal resolution 0.05 degrees. The air quality simulations of NO_2, PM10 and PM2.5 concentrations were performed for the full-year in an hourly basis using the emission rates available on the ClairCity emission database described above.

For Bristol (the pilot case study), a preliminary comparison of the URBAIR outputs with the observations pointed out an underestimation of the simulated concentrations. This underestimation was mainly associated with the lack of other emission sources contributing to the concentrations within the area, as well as the transboundary contribution. Therefore, a procedure was defined to account for the background concentrations and other remaining sources, following the background concentrations maps published by the UK's Department for Environment Food & Rural Affairs (DEFRA). The background air pollution maps made available by DEFRA are the total annual mean concentrations based on modelled data on 1 km × 1 km grid squares. The background concentrations added to the NO_2 concentrations simulated by URBAIR model included the contributions from aircraft, rail, other and rural, while for PM10 and PM2.5 the added background accounted for rail, other, secondary PM, residual and salt categories. The simulation results together with the added background concentrations were then calibrated against the measurements through an adjustment procedure. The adjustment procedure comprises the establishment of a linear regression between the measurements, including data from 107 diffusion tubes, 4 continuous measurement points and the St Paul's urban background station from the UK's automatic monitoring network, and the simulated concentrations obtained for the cells corresponding to the location of the measurement points. In case of NO_2 concentrations, the slope of 1.62 from the linear regression is applied as a correction factor over all the domain, together with a unique correction factor applied to each cell with a measurements available.

For Amsterdam, a similar procedure was defined to account for the background concentrations and other remaining sources, following the background concentrations maps for 2015 (available on http://geodata.rivm.nl/gcn/) published by the National Institute for Public Health and the Environment of The Netherlands (RIVM). The background air pollution maps made available by RIVM consist of annual average modelled concentrations at 1 × 1 km^2 resolution. The background concentrations added to the NO_2, PM10 and PM2.5 modelled concentrations included the contributions from the following categories: foreign sources, aviation, rail traffic, agriculture, and waste processing, based on source apportionment data from GGD Amsterdam. The resulting concentrations were again calibrated against the measurements through the adjustment procedure. For NO_2 concentrations, a slope of 1.3 obtained from the linear regression is applied as a correction factor over all the domain, together with a unique correction factor applied to each cell with measurements available. In case of particulate matter, the slope obtained from the linear regression is equal to 6.9 for PM10 and 9.1 for PM2.5 concentrations.

Based on the lessons learnt from the pilot case study (Bristol), a model adjustment procedure have been defined suited for the 4 remaining case studies. For Ljubljana, Sosnowiec, Genoa and Aveiro region the simulation results were calibrated with the measurements. The adjustment procedure comprised the establishment of the linear regression between the measurements and the simulated concentrations. The adjustment factors obtained from the linear regression for NO_2 concentrations were 2.1, 2.2, 1.7 and 2.9 for Ljubljana, Sosnowiec, Genoa and Aveiro region. These factors were applied as a correction factor over all the four domains, together with a unique correction factor applied to each cell with a measurement available.

2.1 Impact Assessment of Scenarios

To understand the impact of the measures that citizens and stakeholders put forward, the quantification framework assesses the impact of the designed policies on emissions, air quality, human health and related costs. Two different type of scenarios have been considered: (i) the business-as-usual "BAU" scenario, which aims to capture the changes on the air quality if no further measures are taken in the expected technological and behavioural changes. It reflects the normal trend without any policy or other interventions beyond the measures already established; (ii) the scenarios from the Stakeholders Dialogue Workshop (SDW) translate the vision and expectations of citizens and local stakeholders based on data collated through engagement processes (e.g. Stakeholders Dialogue Workshop, Delphi, ClairCity Skylines Game and Mutual Learning Workshop) plus evidence from the baseline policy assessment. These scenarios will be used to support and inform the development of city policy packages out to 2050. Therefore, the headline air quality of the BAU and SDW scenarios was quantified as an indicator of the scenarios' potential impact for 2025, 2035 and 2050. Figure 1 shows an overview of the results for the city of Sosnowiec,

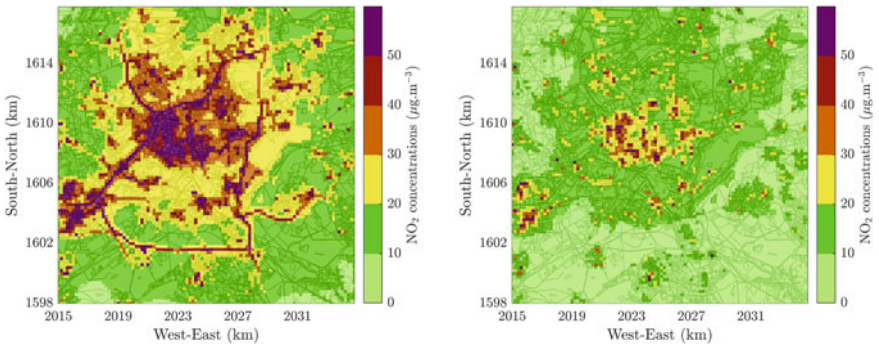

Fig. 1 NO_2 annual average concentrations for Sosnowiec for the baseline year (**a**) and for the high ambition level scenario from the SDW in 2050 (**b**)

as example, with the comparison between the annual average of NO_2 concentrations for the baseline year, in 2015, and the high ambition level scenario from the SDW, in 2050.

For Sosnowiec, the low ambition scenario (not presented) will promote a reduction of NO_2 concentrations over the urban area of 38%, while the high ambition scenario will promote a reduction of 47%. The European legal limit value for NO_2 concentrations will be potentially exceeded within an area corresponding to 10% of the total area of the computation domain in 2015, 2.2% in 2050 for the low ambition scenario, and 1.1% in 2050 for the high ambition scenario. Therefore, the overall air quality will significantly improve in 2050 with the application of the high ambition scenario, although Sosnowiec urban area will still register some exceedances to the European legal limit values for NO_2.

3 Conclusions

This work focuses on the modeling approach to assess the impacts on air quality of the ClairCity scenarios. The outcomes were used to inform the Policy Workshop to carry out in each city/region to help decision-makers and local planners to define the final integrated policy unified scenario, including citizens' visions and behaviour. The final unified scenario is quantified as input to the ClairCity Policy Report to be delivered at the end of the process to each city.

The ClairCity framework contribute to assess air pollution through the source apportionment of air pollutant emissions and concentrations, as well as, carbon emissions, not only by technology, but by citizens' behaviour. As a further outcome, ClairCity is currently addressing the impact of citizens' behaviour on air pollution and carbon footprint.

Acknowledgements This work was supported by the ClairCity project. ClairCity has received funding from the European Union's Horizon 2020 research and innovation programme under grant agreement n. 689289. J. Ferreira is funded by national funds (OE), through FCT—Foundation for Science and Technology, I.P., in the scope of the framework contract foreseen in the numbers 4, 5 and 6 of the article 23, of the Decree-Law 57/2016, of August 29, changed by Law 57/2017, of July 19. Thanks are also due for the financial support to the PhD grant of S. Coelho (SFRH/BD/137999/2018), and to CESAM (UID/AMB/50017/2019), to FCT/MCTES through national funds, and the co-funding by the FEDER, within the PT2020 Partnership Agreement and Compete 2020.

References

Barnes, J., Hayes, E., Chatterton, T., & Longhurst, J. (2018). Policy disconnect: A critical review of UK air quality policy in relation to EU and LAQM responsabilities over the last 20 years. *Environmental Science and Policy, 85*, 28–39.

Borrego, C., Amorim, J., Tchepel, O., Dias, D., Rafael, S., Sá, E., Pimentel, C., Fontes, T., Fernandes, P., Pereira, S., Bandeira, J., & Coelho, M. (2016). Urban scale air quality modeling using detailed traffic emissions estimates. *Atmospheric Environment, 131*, 341–351.

Chatterton, T., & Wilson, C. (2014). The 'Four dimensions of behaviour' framework: A tool for characterising behaviours to help design better interventions. *Transportation Planning and Technology, 37*(1), 38–61.

Question and Answer

Questioner: Peter Builtjes

Question: *You showed a range of NO_2 adjustment factors, ranging from 1.3 for Amsterdam to 2.3 for Aveiro. Does the factors depend on the size of the city*?

Answer: The adjustment factor procedure comprises the establishment of a linear regression between the measurements and the simulated concentrations obtained for the cells corresponding to the location of the measurement points. The variability of the calculated factors strongly depends on the number of stations with measurements available for the regression. The NO_2 observations available for 2015 include measurements from 107 diffusion tubes, 4 continuous measurement points and the St. Paul's urban background station from the UK's automatic monitoring network, in Bristol; 100 diffusion tubes with valid measurements available, and 16 continuous measurements, in Amsterdam; only one background site, part of the automatic monitoring network of Slovenia, in Ljubljana; one road traffic site and two urban background sites, in Sosnowiec; eight monitoring stations in Liguria region (four urban traffic, three urban background and one urban industrial site); and three monitoring stations in Aveiro region (one urban traffic, and two suburban background stations).

Urban Atmospheric Chemistry with the EPISODE-CityChem Model

Matthias Karl and Martin Otto Paul Ramacher

Abstract Photochemical ozone production in the urban area of Hamburg, Germany, was investigated using detailed emission inventories of ozone precursors and an urban-scale chemistry-transport model. Within the urban area, traffic-related emissions of nitric oxide destroy much of the inflowing ozone, mainly at night, leading to minimum concentrations along the traffic network and the port area. Net ozone production was determined based on the difference between the reference simulation, using an advanced photochemistry reaction scheme, and a simulation using photostationary state (PSS) assumption. Neglecting the photo-oxidation of VOC resulted in up to 4.5% lower average ozone in the city outflow in summer.

Keywords Urban air quality · Chemistry transport model · Photochemical ozone

1 Introduction

Episodes with elevated ozone (O_3) during summer are of specific interest, since these are associated with exceedances of the World Health Organization (WHO) guideline concentration limits. While the urban areas are the main sources of O_3 precursors, the stronger impacts of elevated O_3 (e.g. damaging of crops and natural vegetation) occur in rural areas with low population density (Querol et al., 2016). On the local scale, O_3 depletion may occur dominantly because of the chemical interaction with freshly emitted nitric oxide (NO) to form secondary nitrogen dioxide (NO_2), through so-called O_3 titration. Ozone is produced in complex formation mechanism that involves the photo-oxidation of VOC in the presence of nitrogen oxides ($NO_X = NO + NO_2$) following non-linear reaction pathways.

M. Karl (✉) · M. O. P. Ramacher
Department of Chemical Transport Modeling, Helmholtz-Zentrum Hereon,
Max-Planck-Strasse 1, 21502 Geesthacht, Germany
e-mail: Matthias.Karl@hzg.de

© The Author(s), under exclusive license to Springer-Verlag GmbH, DE, part of Springer Nature 2021

C. Mensink and V. Matthias (eds.), *Air Pollution Modeling and its Application XXVII*,
Springer Proceedings in Complexity, https://doi.org/10.1007/978-3-662-63760-9_33

2 The EPISODE-CityChem Model

The urban-scale chemistry-transport model EPISODE-CityChem (Karl et al., 2019) was applied. CityChem (City-scale Chemistry) is an extension of the urban dispersion model EPISODE of the Norwegian Institute for Air Research (NILU). EPISODE systematically combines a 3-D Eulerian grid model with sub-grid Gaussian dispersion models, allowing computation of pollutant concentrations near road traffic and industrial point sources with high spatial resolution. EPISODE-CityChem solves the photochemistry of multiple reactive pollutants on the 3-D Eulerian grid by using detailed chemical schemes and includes specific treatments of street canyons and industrial stacks (Fig. 1).

In the setup for Hamburg, EPISODE-CityChem model was driven with meteorological data generated by the prognostic meteorology module of TAPM (The Air Pollution Model; Hurley, 2008). Chemical boundary conditions were provided from a regional air quality simulation. The model was set-up with a main grid of 30 × 30 grid cells of 1 × 1 km^2 size and a receptor grid of 300 × 300 grid cells of 100 × 100 m^2 size. Urban emission input included geo-referenced point sources, line sources and area source categories using sector specific temporal profiles and vertical profiles. Simulations were performed for summer (JJA) 2012 using two chemical configurations on the Eulerian grid: (1) photo-stationary state assumption involving O_3/NO/NO_2 (PSSA) and (2) EmChem09-mod (reference simulation). The photolysis of nitrous acid (HONO) is an important source of hydroxyl (OH) radicals in urban areas. The reference run included a light-dependent ground surface source of HONO and direct emissions of HONO from vehicles.

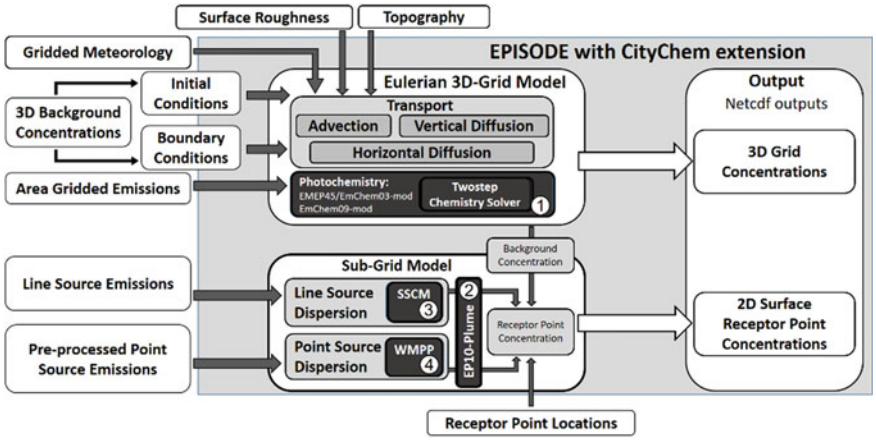

Fig. 1 Schematic diagram of the EPISODE-CityChem model. Modules belonging to the CityChem extension (dark boxes) are: (1) photochemistry on the Eulerian grid, (2) EP10-Plume chemistry in the sub-grid components, (3) simplified street canyon model (SSCM), and (4) WORM Meteorological Pre-Processor (WMPP)

3 Results

Following the inflow-outflow direction in space from west to east (30 km), modelled summer mean O_3 concentration (reference run) decreases from ~70 $\mu g\ m^{-3}$ at the western border to 10–30 $\mu g\ m^{-3}$ in the inner city; and over the eastern part gradually increases to ~50 $\mu g\ m^{-3}$ (Fig. 2a). Within the urban area, traffic-related emissions of NO destroy much of the inflowing ozone, leading to minimum concentrations along the traffic network and the port area. An evaluation of daily 8-h max. O_3 for the summer months with observations of five urban background stations revealed an underestimation of the daily maximum O_3 by 10–24% in summer, which was highest at the inner-city background site (13ST). In the inner city and near highly trafficked streets and motorways, ozone production is small (Fig. 2b; difference <0.6 $\mu g\ m^{-3}$), confirming that the PSS is a valid assumption close to the sources of NO_X pollution.

The highest O_3 concentration difference between the PSSA and the reference run is in the range of 1.6–2.2 $\mu g\ m^{-3}$ occurs in the outflow of polluted air to the southeast of the city (Fig. 2b). The time series of hourly O_3 extracted at station 27TA, which lies in the southeast outflow, shows that photochemical formation occurred almost every day in July (Fig. 3). The ozone-precursor relationship in urban environments is a consequence of the fundamental division into NO_X-sensitive and VOC-sensitive regimes (Sillman, 1999). From the city centre to the rural areas inside the city domain, summer mean VOC/NO_X increases from 0.5 to 4.0 (not shown), indicating that the outflow is still governed by the VOC-limited regime, where O_3 increases with increasing VOC and decreases with increasing NO_X.

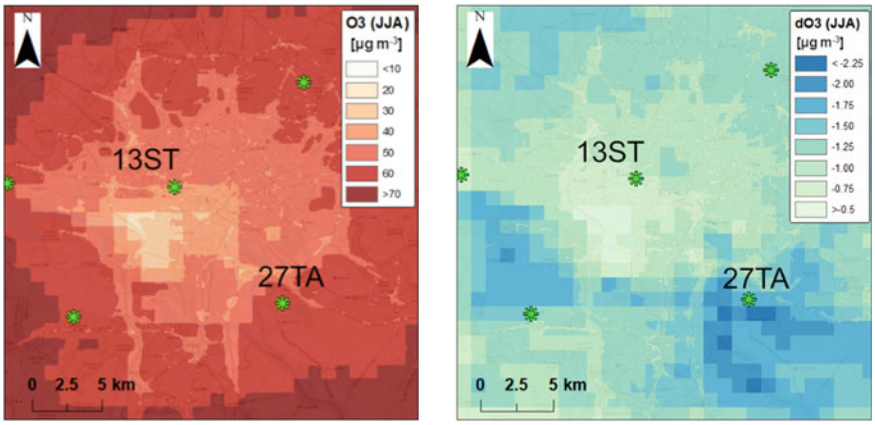

Fig. 2 Spatial maps of the summer average of **a** O_3 (reference); and **b** difference O_3 between PSSA and reference run. Green asterisks represent the urban background stations (13ST: inner-city; 27TA is in the southeast)

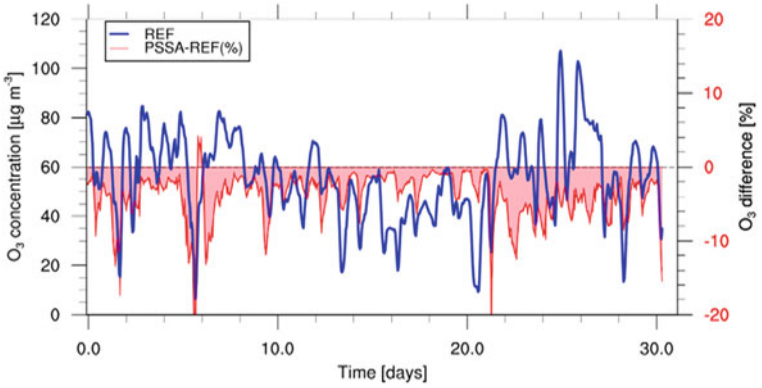

Fig. 3 Time series of hourly O_3 concentration for July at station 27TA and the percentage difference of O_3 between PSSA run and reference run (red shaded)

4 Conclusion

Net ozone production accounted for 1.5–4.5% of the summer mean ozone concentrations in the urban area of Hamburg, Germany. The highest photochemical ozone production occurred in the outflow of polluted air to the southeast of the city. Higher VOC emissions, such as biogenic VOC from vegetation, in the outflow area have the potential to enhance photochemical ozone production.

Acknowledgements This work was funded by the ERA-PLANET trans-national project SMURBS (SMart URBan Solutions for air quality, disasters and city growth), Grant Agreement no. 689443, under the EU Horizon 2020 Framework Programme.

References

Hurley, P.J. (2008). *TAPM V4. Part 1: Technical description.* CSIRO marine and atmospheric research paper, 025, (p. 59). CSIRO, Aspendale, Vic., Australia.

Karl, M., Walker, S.-E., Solberg, S., Ramacher, M. O. P. (2019). "The Eulerian urban dispersion model EPISODE. Part II: Extensions to the source dispersion and photochemistry for EPISODE-CityChem v1.2 and its application to the city of Hamburg". *Geoscience Model Development Discussions* 1–62. https://doi.org/10.5194/gmd-2018-325

Querol, X., Alastuey, A., Reche, C., Orio, A., Pallares, M., Reina, F., Dieguez, J. J., Mantilla, E., Escudero, M., Alonso, L., Gangoiti, G., & Millan, M. (2016). On the origin of the highest ozone episodes in Spain. *Science of Total Environment, 572*, 379–389. https://doi.org/10.1016/j.scitotenv.2016.07

Sillman, S. (1999). The relation between ozone, NO_X and hydrocarbons in urban and polluted rural environments. *Atmospheric Environment, 33*(12), 1821–1845.

Zhang, et al. (2016). Potential sources of nitrous acid (HONO) and their impacts on ozone: A WRF-Chem study in a polluted subtropical region. *Journal of Geophysical Research: Atmospheres*, *121*, 3645–3662. https://doi.org/10.1002/2015JD024468.

Questions and Answers

Questioner: Bruce R. Denby.

Question: The EPISODE model is a combined Eulerian/Gaussian model. The chemistry you use is only in the Eulerian model; so what is the chemistry in the Gaussian model?

Answer: In the Gaussian models for line and point sources, the PSSA has been replaced by the EP10-Plume chemical scheme (Karl et al., 2019). EP10-Plume includes reactions of O_3, NO, NO_2, nitrous acid (HNO_3), carbon monoxide (CO) and formaldehyde (HCHO). EP10-Plume was shown to give very similar results as PSSA for O_3, NO and NO_2 concentrations up to a distance of 300 m from a line source (Karl et al., 2019). It is planned to include reactions of HONO in the chemical scheme of the Gaussian model.

Questioner: Golam Sarwar.

Question: (1) Can you elaborate on boundary conditions used in the study? Are they fixed in time? (2) What is the gamma value used in the model (gamma for HONO source)?

Answer: (1) The setup of this study used hourly varying 3-D concentrations at the lateral and vertical boundaries from regional air quality simulations with the Community Multiscale Air Quality Modeling System (CMAQ) model as initial and boundary conditions. CMAQ v5.0.1 was run over the European domain with 64 km horizontal resolution and an intermediate nested domain over Northern Europe with 16 km horizontal resolution. Within the northern Europe domain, an inner domain over the Baltic Sea region with 4 km horizontal resolution was nested, that provided the initial and hourly boundary conditions for the chemical concentrations in the Hamburg model domain. (2) The ground surface reaction producing HONO was parameterized according to Zhang et al. (2016) with an NO_2 uptake coefficient (gamma) depending on light intensity. When light intensity is less than 400 W m^{-2}, a gamma value of 2×10^{-5} is used. When it is higher, a factor of (light intensity)/400 is used to scale the gamma value.

The Impact of BVOC Emissions from Urban Trees on O_3 Production in Urban Areas Under Heat-Period Conditions

Martin Otto Paul Ramacher, Matthias Karl, Johannes Bieser, and Josefine Feldner

Abstract Heat-periods in summer occurred more frequently in this decade and affected the well-being of citizens in several ways. One effect of heat-periods is a higher photochemical ozone (O_3) production rate, which leads to higher O_3 concentrations. Strategies to influence urban climate and air pollution more often include urban trees. A side effect of urban trees is the emission of biogenic VOCs (BVOCs), which are participating in urban O_3 production. In this study, we investigate the effect of urban tree BVOCs during heat-period conditions on O_3 formation using an integrated urban-scale biogenic emissions and chemistry transport model chain. To demonstrate the possibility of investigating the effect of urban trees on O_3 production under heat-period conditions, we performed simulations in the densely populated Rhein-Ruhr area (DE) in July 2018. The results show impacts of up to 4% higher averaged maximum daily 8 h mean (MDA8) O_3 concentrations due to local isoprene emissions and up to additional 15% higher MDA8 O_3 values when decreasing NO_x emissions from traffic and increasing urban tree emissions. In general, the relevance of biogenic emissions is expected to increase in future due to higher frequency of heat-period events related to climate change and due to the decreasing trend of anthropogenic emissions in response to current legislation. Therefore, the established model chain can be a valuable tool for urban planning.

Keywords Urban air quality · Urban trees · BVOC · Tropospheric ozone · Heat-period

M. O. P. Ramacher (✉) · M. Karl · J. Bieser · J. Feldner
Department of Chemical Transport Modeling, Institute of Coastal Research, Helmholtz-Zentrum Hereon, Max-Planck-Strasse 1, 21502 Geesthacht, Germany
e-mail: Martin.Ramacher@hzg.de

© The Author(s), under exclusive license to Springer-Verlag GmbH, DE, part of Springer Nature 2021

C. Mensink and V. Matthias (eds.), *Air Pollution Modeling and its Application XXVII*, Springer Proceedings in Complexity, https://doi.org/10.1007/978-3-662-63760-9_34

1 Heat-Periods, Urban Trees and Urban Air Quality

Heat-periods and other extreme events are a serious threat for urban citizens and occurred more frequently in Europe during the last decades. Besides climatic effects during these events, synergistic effects between high temperature and air pollution, e.g. due to elevated levels of ground-level ozone (O_3), have been observed to have led to an increase in hospital admissions as a result of cardiovascular and respiratory diseases (Aström et al., 2013), even more during extreme heat events (Levy & Patz, 2015). Ground-level O_3 is produced during the oxidation of volatile organic compounds (VOC) and carbon monoxide (CO) in the presence of nitrogen oxides (NO_x), with increased reactivity at higher temperatures (Camalier et al., 2007). Consequently, high temperatures are often associated with elevated surface O_3 and its associated impacts (Fiore et al., 2015).

Strategies to influence urban air pollution more often include urban trees, which can influence air quality due to several biophysical processes: (1) deposition of gaseous and particle pollution onto plant surfaces and uptake via leaf stomata, (2) modification of air circulation, (3) formation of O_3 through emission of biogenic volatile organic compounds (BVOCs), such as isoprene, monoterpenes and sesquiterpenes and (4) production of pollen (Eisenman et al., 2019). However, urban trees are widely recognized as possibility to mitigate virtually all-kinds of environmental problems (Escobedo et al., 2011). But in terms of the local regulation of tropospheric O_3 concentrations, the impacts of urban trees are complex and largely influenced by species-specific and climate-dependent emission rates of BVOCs and O_3 deposition rates (Fitzky et al., 2019; Grote et al., 2016). Thus, there might be positive or negative effects of trees in urban context on formation of ground-level O_3 in urban areas. These effects need to be studied area-, climatic- and tree-specific to prevent that the negative effect of urban trees on O_3 formation outweighs other positive effects.

In this study, we investigate the effect urban tree BVOCs during heat-period conditions on O_3 formation using an integrated urban-scale biogenic emissions and chemistry transport model chain. Therefore, we integrated modelling of BVOC emissions in an urban-scale chemistry transport model (CTM). We performed CTM simulations in the densely populated Rhein-Ruhr area (DE) under heat-period conditions in July 2018 to identify the impact BVOC emissions on O_3 formation.

2 Research Domain and CTM Setup

The research domain is the Rhein-Ruhr area (Fig. 1) located in the west of Germany close to the Dutch border and inhabiting more than 2 Million people, most of them living in urban areas. The research area contains the cities Duisburg and Düsseldorf, the river Rhine and multiple forests. Both, Duisburg and Düsseldorf are urban areas with more than 40% of urban green infrastructure. In July 2018, the daily temperature

Fig. 1 The Rhein-Ruhr research domain and its location in Europe. The red dots show LUQS air quality measurements stations. Maps are created with © ArcGIS Pro and are based on open street map

maximum exceeded on 28 days the 30 year annual mean of the maximum temperature averaged over four stations in the research domain and showed a maximum temperature of 36.02 °C. The July 2018 period was widely recognized as heat-period event. Additionally, the mean values of the daily maximum 8 h average (MDA8) O_3 concentrations have been exceeded up to eight times at different stations of the federal urban air quality monitoring network (Luftüberwachungssystem, LUQS) in the Rhein-Ruhr area.

The Rhein-Ruhr research domain was setup in the CTM EPISODE-CityChem (Karl et al., 2019) with a spatial resolution of 100 × 100 m^2 and an extent of 50 × 50 km^2. The focus of EPISODE-CityChem is the simulation of complex atmospheric chemistry involved in the photochemical production of O_3 in urban areas and accurate representation of dispersion in proximity of emission sources. The EPISODE-CityChem simulations were driven by meteorological fields for July 2018, which were simulated with the TAPM model (Hurley et al., 2005). The TAPM simulation were driven by three-hourly ECMWF ERA5 synoptic scale reanalyses ensemble means on a longitude/latitude grid with 0.3 × 0.3 degrees resolution and assimilated local wind field measurements. To account for background concentrations we applied hourly regional measurements from nearby EBAS:EMEP air quality measurement stations. To account for anthropogenic emissions, we applied annual emission totals in the Urban Emission Conversion Tool (Hamer et al., 2019), to calculate hourly emissions of area, line and point sources. The emission totals were provided by the Landesamt für Natur, Umwelt und Verbraucherschutz Nordrhein-Westfalen (LANUV) and are based on federal emission reporting for the year 2016. Urban tree-specific BVOC emissions are considered by a tree-specific emission inventory for isoprene, monoterpenes, sesquiterpenes and oxygenated VOC as introduced in the next chapter.

With the introduced CTM system we performed simulations in the Rhein-Ruhr research area and identified the impact of isoprene emissions on MDA8 O_3 values.

Table 1 Emissions scenarios to investigate isoprene impact on O_3 production in CTM simulations

Scenario	Isoprene emissions	NOx emissions
Base	100% forests & urban trees	100% NO_x all sources
No isoprene	None	100% NO_x all sources
Half traffic	100% forests & urban trees	50% NO_x traffic, 100% NO_x other sources
Double urban trees	100% forests, 200% urban trees	100% NO_x all sources

We chose to investigate the impact of isoprene, because it is the most common BVOC and has a reactivity which is 22 times higher than that of the important anthropogenic VOC (AVOC) benzene (Wagner & Kuttler, 2014). We performed simulations with different scenarios, to investigate the impact of isoprene emissions and traffic NO_x sources on O_3 production (Table 1).

3 Modeling Urban Tree-Specific BVOC Emissions in Urban Areas

To account for BVOC emissions from urban trees we created a European tree specific BVOC emissions inventory with a resolution of $100 \times 100\ m^2$. Therefore, we identified tree cover using the Copernicus Land Monitoring Service's (CLMS) Tree Cover Density map (TCD). This was then combined with probability maps of the 39 most common tree species in Europe (San Miguel-Ayanz, 2016). Additionally we used the CLMS Forest Type Additional Support Layer to identify trees in urban context on a map with $100 \times 100\ m^2$ resolution and conducted a literature review to identify urban tree species mixes for different bioclimatic zones. These maps are then combined with tree species specific foliar biomass density and standard emission potentials for isoprene, monoterpenes, sesquiterpenes and oxygenated VOCs (Karl et al., 2009). In the next step we calculated the BVOC emissions in dependence of temperature (Guenther et al., 2012) and radiation for the Rhein-Ruhr research domain in July 2018. To account for BVOCs in the EPISODE-CityChem model we integrated isoprene, α-pinene & limonene in the chemistry mechanism EMCHEM09Mod.

4 Simulated Effects of UGI BVOC Emissions on Ozone

First, the simulated hourly O_3 concentrations were compared with measured hourly ozone concentrations at four urban air quality measurement sites in the research domain (Fig. 1). The comparison showed correlations of 0.62–0.73 and negative normalized mean biases of −0.31 to −0.12. Thus, the model underestimates the O_3

hourly concentrations, which holds also true for the comparison of measured and modeled MDA8 O_3 values.

Second, we analysed the impact of isoprene emissions on monthly averaged MDA8 O_3 values by calculating the monthly averaged difference of MDA8 O_3 values in the total domain (Fig. 2).

Local isoprene emissions have an effect of up to ~4% on MDA8 O_3 values, close to sources of high NO_x emissions, such as highways and urban-centres. Calculated as an average for the total domain, local isoprene emissions are increasing the MDA8 O_3 value with ~2%.

Third, we made a transect analysis for a day with measured exceedance of MDA8 O_3 values (25th July). Therefore, we analyzed the MDA8 O_3 values for each 100 × 100 m^2 grid cell following a West–East-transect (Fig. 3). Moreover, we calculated the impacts of all scenarios on MDA8 O_3 values. The transect analysis for 25th July shows contributions of local isoprene emissions on MDA8 O_3 values of 2 to 12%. Moreover, a 50% reduction of traffic NO_x emissions leads to an increase of 2–10%. If then the amount of emissions from urban trees is doubled, there is an additional increase in MDA8 O_3 values of 0–3%. In terms of absolute values, the MDA8 O_3 value can be raised by up to 5 µg/m^3 in the analyzed transect.

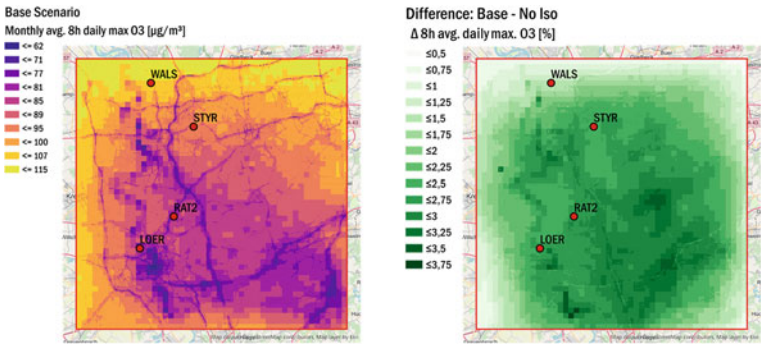

Fig. 2 Monthly averaged MDA8 ozone values in the base scenario (left) and as relative difference of base and no isoprene scenarios (right)

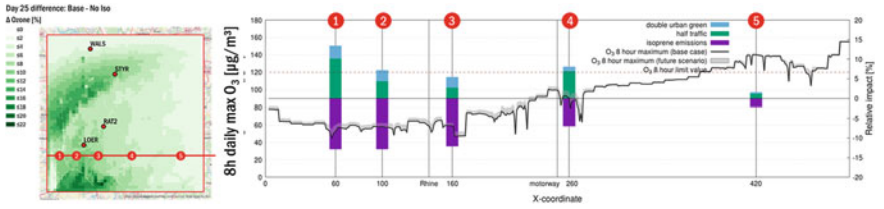

Fig. 3 Simulated West–East transect of MDA8 O_3 values on 25th July. The absolute MDA8 O_3 values are on the left y-axis and plotted as black line. The relative impact on MDA8 O_3 values of different scenarios is shown on the right y-axis

In total, the simulated results show a high spatial variability for the impact of different isoprene emissions and NO_x reductions on the formation of ground level MDA8 O_3 values.

5 Conclusion

We setup an urban CTM system with a novel approach to account for city- and tree-specific BVOC emissions, to identify the impact of isoprene emissions on ground level O_3 formation under heat-period conditions in the Rein-Ruhr area in July 2018. The results of the simulations show a monthly averaged impact of ~2% on MDA8 O_3 values in the total research domain, with a maximum of ~4% in areas close to sources of NO_x emissions. Moreover, we simulated possible future conditions by halving NO_x and doubling urban tree isoprene emissions, which led to total maximum increases in MDA8 O_3 values of up to 15%. The relevance of biogenic emissions is expected to increase in the future due to higher frequency of heat-period events related to climate change and due to the decreasing trend of anthropogenic emissions in response to current legislation. Therefore, the established model chain can be a valuable tool for urban planning in view of finding trade-offs between lowering the urban carbon footprint, regulating urban climate, and reduce urban air pollution.

Acknowledgements This work was funded by the CLINSH project, under the EU Horizon 2020 Framework Programme. We thank Dieter Busch at the LANUV for providing emission data and the LUQS for providing AQ monitoring data.

References

Aström, C., Orru, H., Rocklöv, J., Strandberg, G., Ebi, K. L., & Forsberg, B. (2013). Heat-related respiratory hospital admissions in Europe in a changing climate: A health impact assessment. *BMJ open, 3*(1).

Camalier, L., Cox, W., & Dolwick, P. (2007). The effects of meteorology on ozone in urban areas and their use in assessing ozone trends. *Atmospheric Environment, 41*(33), 7127–7137.

Eisenman, T. S., Churkina, G., Jariwala, S. P., Kumar, P., Lovasi, G. S., Pataki, D. E., et al. (2019). Urban trees, air quality, and asthma: An interdisciplinary review. *Landscape and Urban Planning, 187*, 47–59.

Escobedo, F. J., Kroeger, T., & Wagner, J. E. (2011). Urban forests and pollution mitigation: Analyzing ecosystem services and disservices. *Environmental Pollution (Barking, Essex: 1987), 159*(8–9), 2078–2087.

Fiore, A. M., Naik, V., & Leibensperger, E. M. (2015). Air quality and climate connections. *Journal of the Air and Waste Management Association (1995), 65*(6), 645–685.

Fitzky, A. C., Sandén, H., Karl, T., Fares, S., Calfapietra, C., Grote, R., et al. (2019). The interplay between ozone and urban vegetation—BVOC emissions, ozone deposition, and tree ecophysiology. *Frontiers in Forests and Global Change, 2*, 403.

Grote, R., Samson, R., Alonso, R., Amorim, J. H., Cariñanos, P., Churkina, G., et al. (2016). Functional traits of urban trees: Air pollution mitigation potential. *Frontiers in Ecology and the Environment, 14*(10), 543–550.

Guenther, A. B., Jiang, X., Heald, C. L., Sakulyanontvittaya, T., Duhl, T., & Emmons, L. K., et al. (2012). The model of emissions of gases and aerosols from nature version 2.1 (MEGAN2.1): An extended and updated framework for modeling biogenic emissions. *Geoscientific Model Development, 5*(6), 1471–1492.

Hamer, P. D., Walker, S.-E., Sousa-Santos, G., Vogt, M., Vo-Thanh, D., & Lopez-Aparicio, S., et al. (2019). The urban dispersion model EPISODE. Part 1: A Eulerian and subgrid-scale air quality model and its application in Nordic winter conditions. *Geoscientific Model Development Discussions*, 1–57.

Hurley, P. J., Physick, W. L., & Luhar, A. K. (2005). TAPM: A practical approach to prognostic meteorological and air pollution modelling. *Environmental Modelling and Software, 20*(6), 737–752.

Karl, M., Guenther, A., Köble, R., Leip, A., & Seufert, G. (2009). A new European plant-specific emission inventory of biogenic volatile organic compounds for use in atmospheric transport models. *Biogeosciences, 6*(6), 1059–1087.

Karl, M., Walker, S.-E., Solberg, S., & Ramacher, M. O. P. (2019). The Eulerian urban dispersion model EPISODE—Part 2: Extensions to the source dispersion and photochemistry for EPISODE–CityChem v1.2 and its application to the city of Hamburg. *Geoscientific Model Development*, *12*(8), 3357–3399.

Levy, B. S., & Patz, J. (Hrsg.) (2015). *Climate change and public health.* Oxford University Press.

San Miguel-Ayanz, J. (Hrsg.) (2016). *European atlas of forest tree species.* Unión Europea.

Wagner, P., & Kuttler, W. (2014). Biogenic and anthropogenic isoprene in the near-surface urban atmosphere–a case study in Essen, Germany. *The Science of the Total Environment, 475*, 104–115.

Questions and Answers

Questioner: Silvia Trini Castelli

Question: You showed that green infrastructures have a number of benefits, then illustrated the "drawbacks" in ozone increase. To avoid pressing the message that trees and vegetation bring negative contributions to the environment, would you be able to provide a list of "final budget" that account for all aspects, pros and cons?

Answer: In many recent reviews (Eisenman et al., 2019; Fitzky et al., 2019) the need for more modeling studies to answer the question on possible drawbacks in terms of ozone formation, while planning urban green infrastructure to mitigate other impacts is emphasized. Thus, the presented study was designed to show a framework that can be used to help answering the question of a "final budget" of pros and cons of urban green infrastructure.

Questioner: Heinke Schlünzen

Question: Can you rec urban areas that should be best used to improve urban climate and have little impact on ozone formation?

Answer: This kind of question shall be answered with the introduced modeling chain and is highly dependent on existing local tree species and meteorological conditions.

Nevertheless, our first results show higher ozone concentrations due to isoprene especially in areas close to high sources of NOx emissions. But more analysis and research is needed to finally answer this question.

Questioner: Calvin Arter

Question: Have you considered impacts of BVOC emissions in urban areas on SOA formation.

Answer: We are working on the integration of the interaction of BOVC emissions and SOA formation in the EPISODE-CityChem model, but in the presented results we did not account for this effect.

Implementation and Application of the Online Coupled Chemistry Model of the Microscale Urban Climate Model PALM-4U

Sabine Banzhaf, Edward C. Chan, Renate Forkel, Basit Khan, Farah Kanani-Sühring, Matthias Sühring, Klaus Ketelsen, Mona Kurppa, Yvonne Breitenbach, Florian Tautz, Volker Diegmann, Björn Maronga, Matthias Mauder, Martijn Schaap, and Siegfried Raasch

Abstract The microscale urban climate model PALM-4U (i.e. PALM for Urban applications) is based on the PALM model and can be run in both LES (Large Eddy Simulation) and RANS (Reynolds Averaged Navier–Stokes) mode. Within the joint project MOSAIK (Model-based city planning and application in climate change), an online chemistry model has been implemented into PALM-4U, including both gas-phase and aerosol chemistry. In this study, we have set up PALM-4U for a nested simulation for a city quarter of Berlin with a 'parent' domain on 10 m grid resolution and a 'child' domain, which is a cut-out of the 'parent' domain, on 1 m grid resolution. For the simulation a real-time traffic emission data set has been used. The model results for both, the 'parent' and the 'child' domain are presented.

S. Banzhaf (✉) · E. C. Chan · M. Schaap
Institute of Meteorology, Freie Universität Berlin, Berlin, Germany
e-mail: sabine.banzhaf@met.fu-berlin.de

R. Forkel · B. Khan · M. Mauder
Institute for Meteorology and Climate Research (IMK-IFU), Karlsruhe Institute of Technology (KIT), Garmisch-Partenkirchen, Germany

F. Kanani-Sühring · M. Sühring · B. Maronga · S. Raasch
Institute of Meteorology and Climatology, Leibniz Universität Hannover, Hannover, Germany

K. Ketelsen
Independent Software Consultant, Hannover/Berlin, Germany

M. Kurppa
University of Helsinki, Helsinki, Finland

Y. Breitenbach · F. Tautz · V. Diegmann
IVU Umwelt GmbH, Freiburg, Germany

© The Author(s), under exclusive license to Springer-Verlag GmbH, DE, part of Springer Nature 2021

C. Mensink and V. Matthias (eds.), *Air Pollution Modeling and its Application XXVII*, Springer Proceedings in Complexity, https://doi.org/10.1007/978-3-662-63760-9_35

1 Introduction

Urban settlements increase worldwide. Such rapid urbanization has a negative impact on urban climate, and its vulnerability is intensified by urban soil sealing, profligate consumption of resources, and high energy demand, resulting in increased air pollution. Although Large-Eddy Simulation (LES) models can capture the transient flow structures of atmospheric turbulence and advection by explicitly resolving relevant scales of turbulent motion, these models are rarely used for urban air quality studies, especially if chemical transformation of pollutants is accounted for. In this study we have performed a high resolution nested simulation of a city quarter of Berlin using the new microscale urban climate model PALM-4U (Maronga et al., 2019) in LES-mode. A self-nesting capability has recently been developed to simultaneously run a series of two or more LES model domains with different spatial extents and grid resolutions with PALM-4U. The outermost model is called root model and is a parent model to the so- called child models whose domains are nested completely inside the root domain. A child model obtains boundary conditions for the prognostic quantities from its parent model through interpolation from the coarse to the fine grid. Furthermore, PALM-4U includes a fully coupled 'online' chemistry module (Khan et al., 2021). In the following, the chemistry module and emission input are described and first results of the study are presented.

2 PALM-4U Chemistry Implementation

The microscale urban climate model PALM-4U is based on the PALM model (Maronga, 2015). Within the joint project MOSAIK an online chemistry model has been implemented into PALM (Khan et al., 2021) as one of the PALM-4U components (Maronga et al., 2019). The gas-phase chemistry has been implemented using the Kinetic PreProcessor (Damian, 2002; http://people.cs.vt.edu/asandu/Software/Kpp/) in order to obtain the necessary flexibility in the choice of complexity of the chemistry mechanisms. Automatic adaptation of KPP generated code for PALM-4U is based on KP4 (Jöckel, 2010). PALM-4U includes a set of available chemistry mechanisms of different complexity. Currently the following chemistry options are included:

- CBM4 (Carbon Bond Mechanism, Gery et al., 1989, 32 compounds, 81 reactions)
- SMOG (simple photochemical smog mechanism, 12 compounds, 12 reactions)
- SIMPLE (further simplification of SMOG, 9 compounds, 7 reactions)
- PHSTAT (photo-stationary state only, 3 compounds, 2 reactions)
- PASSIVE (just 2 passive tracers, no chemical reactions).

Furthermore, aerosol processes have been introduced (Kurppa et al., 2019) based on the sectional aerosol module SALSA (Sectional Aerosol module for Large Scale Applications) (Kokkola, 2008). Anthropogenic emissions can be supplied either by

gridded NetCDF files with hourly emission data or traffic emissions are parameterized depending on street type information from OpenStreetMap.

3 Case Study for a City Quarter of Berlin, Germany

A 24 h nested simulation for July 30th 2017 started at 0 UTC was conducted in LES-mode. The extent of the 'parent' domain was 1600 × 1600 m^2 with 10 m resolution and the extent of the 'child' domain was 480 × 240 m^2 on 1 m resolution. The investigation area covered a city quarter of Berlin around the Ernst-Reuter-Platz, a junction with some high buildings and heavy car traffic. Only gas-phase chemistry was switched on for the simulation shown here. The chosen chemistry option PHSTAT includes the following reactions:

$$NO_2 + hv \rightarrow NO + O_3 \quad (1)$$

$$NO + O_3 \rightarrow NO_2 \quad (2)$$

Gridded hourly real-time traffic emission data sets were used for both simulations. The emission data was based on calculations applying the IMMIS^{em,h} emission model (Version 7.0; IVU Umwelt, 2018) which is using HBEFA 3.3 emission factors (INFRAS, 2017) and real-time traffic counts and temperature time series. The resulting emission information on street segments was superpositioned on a rasterized street map. As an example, Fig. 1 shows the traffic emission information for NO for the Ernst-Reuter-Platz area on 10 m resolution for January 17th 2017 at 7 am. As the figure shows main roads can easily be distinguished from side roads and emissions are enhanced at the junctions.

The model was initialized with meteorological data from the regional scale model COSMO (COnsortium for Small-scale MOdelling). Furthermore, cyclic boundary conditions were applied for the 'parent' simulation. First results are presented in Fig. 2. Horizontal cross sections of NO_2 concentration at 8:25 am of Juli 30th 2017 are shown for the 'parent' domain and NO_2 concentration and O_3 concentrations for the 'child' domain. As solely traffic emissions have been used concentrations of NO_2 are highest in the streets. NO_2 and O_3 concentrations vary in space and time due to the chemical transformation of the atmospheric trace gases and advection by turbulent motions. The nesting option was successfully applied and Fig. 2 nicely illustrates the added value of the higher resolution in the 'child' domain compared to the 'parent' domain.

Fig. 1 Underlying traffic emission information for Ernst-Reuter-Platz domain (10 m resolution) for NO (in g/m^2/h) for January 17th 2017 at 7:00 am

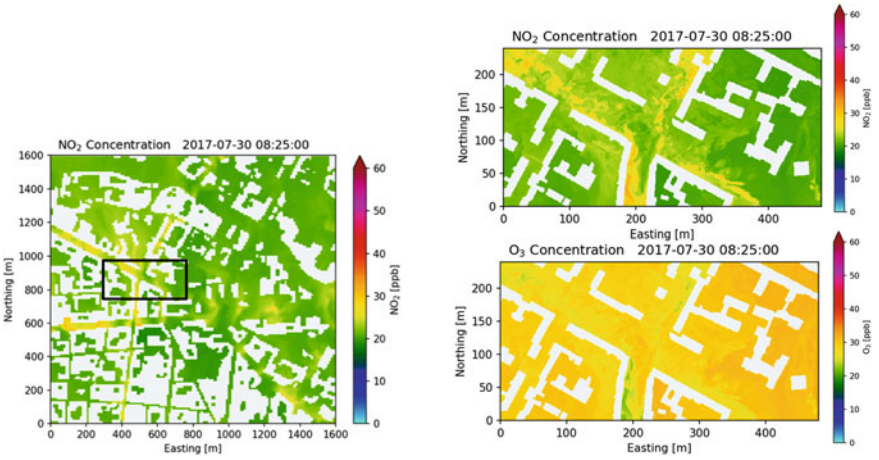

Fig. 2 Simulated 'parent' domain concentrations of NO_2 (in ppb) at 8:25 am (left panel) and 'child' domain concentrations of NO_2 (in ppb, upper right panel) and O_3 (in ppb, lower right panel) at 8:25 am for July 30th 2017 for the Ernst-Reuter-Platz area in Berlin, Germany. Horizontal cross sections are displayed 5 m above the ground

4 Conclusions and Outlook

The presented work has shown that PALM-4U is capable to simulate the resolved turbulence and chemical transformations in the urban canopy. The nesting option of the model was successfully applied. The self-nesting approach allows to use the model as a magnifying-lens tool that helps resolving areas of interest with a finer grid spacing. In a next step a comprehensive evaluation of the model will be conducted.

The model is still under further development, which also holds for its chemistry module. In the near future time dependent lateral boundary conditions from a regional scale model will be supplied for chemical species. Furthermore, the effect of shading will be considered in the photolysis scheme, domestic heating emissions will be included in the parameterized emissions scheme, biogenic VOC emissions will be accounted for and a wet deposition scheme will be implemented.

Acknowledgements MOSAIK is funded by the BMBF (German Federal Ministry of Education and Research) under grant 01LP1601 within the framework of Research for Sustainable Development (FONA; www.fona.de).

References

Damian, V., Sandu, A., Damian, M., Potra, F., & Carmichael, G. R. (2002). The kinetic preprocessor KPP—A software environment for solving chemical kinetics. *Computers and Chemical Engineering, 26*, 1567–1579.

INFRAS, MK, TU Graz. (2017). Handbuch emissionsfaktoren des straßenverkehrs. HBEFA version 3.3. Autoren: INFRAS AG, MK Consulting GmbH, TU Graz. Auftraggeber: Umweltbundesamt (Deutschland); Bundesamt für Umwelt (Schweiz), Umweltbundesamt (Österreich), Trafikverket (Schweden), ADEME (Frankreich), SFT (Norwegen) und JRC (Joint Research Center der Europäischen Kommission).

Jöckel, P., Kerkweg, A., Pozzer, A., Sander, R., Tost, H., Riede, H., Baumgaertner, A., Gromov, S., & Kern, B. (2010). Development cycle 2 of the Modular Earth Submodel System (MESSy2). *Geoscientific Model Development, 3*, 717–752. https://doi.org/10.5194/gmd-3-717-2010

Khan, B., Banzhaf, S., Chan, E. C., Forkel, R., Kanani-Sühring, F., Ketelsen, K., Kurppa, M., Maronga, B., Mauder, M., Raasch, S., Russo, E., Schaap, M., & Sühring, M. (2021). Development of an atmospheric chemistry model coupled to the PALM model system 6.0: implementation and first applications. *Geoscientific Model Development, 14*, 1171–1193. https://doi.org/10.5194/gmd-14-1171-2021.

Kokkola, H., Korhonen, H., Lehtinen, K. E., Makkonen, R., Asmi, A., Järvenoja, S., Anttila, T., Partanen, A. I., Kulmala, M., Järvinen, H., & Laaksonen, A. (2008). SALSA—A sectional aerosol module for large scale applications. *Atmospheric Chemistry and Physics, 8*, 2469–2483. https://doi.org/10.5194/acp-8-2469-2008

Kurppa, M., Hellsten, A., Roldin, P., Kokkola, H., Tonttila, J., Auvinen, M., Kent, C., Kumar, P., Maronga, B., & Järvi, L. (2019). Implementation of the sectional aerosol module SALSA2.0 into the PALM model system 6.0: Model development and first evaluation. *Geoscientific Model Development, 12*, 1403–1422. https://doi.org/10.5194/gmd-12-1403-2019

Maronga, B., Banzhaf, S., Burmeister, C., Esch, T., Forkel, R., Fröhlich, D., Fuka, V., Gehrke, K.F., Geletič, J., Giersch, S., Gronemeier, T. (2019). Overview of the PALM model system 6.0. Geoscientific Model Development Discuss. https://doi.org/10.5194/gmd-2019-103

Maronga, B., Gryschka, M., Heinze, R., Hoffmann, F., Kanani-Sühring, F., Keck, M., Ketelsen, K., Letzel, M. O., Sühring, M., & Raasch, S. (2015). The parallelized large-eddy simulation model (PALM) version 4.0 for atmospheric and oceanic flows: model formulation, recent developments, and future perspectives. *Geoscientific Model Development, 8*, 2515–2551. https://doi.org/10.5194/gmd-8-2515-2015

Umwelt, I. V. U. (2018). *IMMISem/luft/lärm—Handbuch zur Version 7*. IVU Umwelt GmbH.

Questions and Answers

Question: Can you give us a typical order of magnitude of the computational duration of your simulations?

Answer: I will give an estimate for simulations for the parent domain on 256 cores for two different resolutions:

10 m resolution: 18 h simulation time corresponds to about 8 h wall clock time

1 m resolution: 30 min simulation time corresponds to about 24 h wall clock time

Questioner: L. Ran

Question: Do you have urban morphology data in your urban scheme? If yes, how do you obtain or process them (sources)?

Answer: Yes, the input data includes a comprehensive data set of the urban morphology within the simulation domain. The data was gathered (from e.g. local authorities, remote sensing etc.) and processed (to NetCDF) by one of the project partners, the DLR (German Aerospace Center). PALM-4U can also deal with less comprehensive data sets of the urban morphology that can be defined via the so-called static driver (format: NetCDF) of PALM-4U. However, the accurancy of the input data will of course have impact on your results.

Urgency Management of Adverse Atmospheric Releases with a Forefront Multi-scale High Resolution Modeling and Decision-Support System

Patrick Armand and Christophe Duchenne

Abstract This paper presents the principal features of the CEA Modeling and decision-support system dedicated to the dispersion and health impact assessment of Chemical, Biological or Radiological materials released into the air in case of an accident or a malicious action. The chain of models allows the prediction of the weather and simulation of the dispersion from the closest vicinity of the release to the far extent of the affected area taking account of the topography and buildings at high resolution. The chain also includes the CFD computations of the indoor/outdoor transfers of "hazmat" in and out of critical infrastructures. The experimental validation of the models and their compliance with the acceptance criteria for dispersion in built-up areas confirm the CEA rigorous approach to the system development. The application of the Modeling chain to the huge Paris urbanized domain (40 km × 40 km) at 3 m resolution to predict the local scale meteorology each day for the next one and simulate fictitious dispersions with a time acceleration factor of five demonstrates the feasibility and interest of such calculations in the frame of an emergency. All these considerations favorably augur for the operational use in a near future of our Modeling system to support decision-making of the firefighters and their authorities facing contingency radioactive, toxic and/or explosive releases.

1 Introduction

Accidental or malicious releases of gases or fine particles into the atmosphere are highly topical as they may involve hazardous Chemical, Biological or Radiological materials (potentially mixed with Explosives) threatening people health and the environment. While such events are infrequent, they are a major concern of the public security services and their local and national authorities as their societal consequences would be huge, especially in crowded urban areas or industrial sites.

P. Armand (✉) · C. Duchenne
CEA, DAM, DIF, 91297 Arpajon, France
e-mail: patrick.armand@cea.fr

© The Author(s), under exclusive license to Springer-Verlag GmbH, DE, part of Springer Nature 2021

C. Mensink and V. Matthias (eds.), *Air Pollution Modeling and its Application XXVII*, Springer Proceedings in Complexity, https://doi.org/10.1007/978-3-662-63760-9_36

In the same time, releases resulting from an accident or a terrorist attack are poorly known, and simulations may be necessary from the vicinity of the release to a large distance from it. Moreover, when buildings or infrastructures are present, releases are likely to be transferred inside them. To tackle these complex situations, Modeling has to combine the influence of the terrain, land-use, and buildings, in evolving meteorological conditions. Thus, only a chain of CFD models is able to provide realistic and reliable impact assessment of the releases with appropriate level of details.

The French Atomic and alternative Energies Commission (CEA) is involved in R&D activities devoted to the preparedness and response in case of hazardous releases into the air, of which the development and validation of state-of-the-science 3D Modeling and decision support systems.

This paper intends to sum up the strategy at CEA regarding multi-scale dispersion Modeling. Three parts are successively dedicated to the presentation of the downscaling and upscaling chain of models, to the experimental validation of the local scale Modeling system and to the application of this system to a huge urban domain in the prospective framework of the civilian security.

2 Downscaling and Upscaling Flow and Dispersion Modeling

For about 25 years, multi-scale Modeling of atmospheric dispersion has experienced impressive improvements as discussed in Benamrane et al. (2013). The development of simplified or full CFD models has been motivated by the awareness that Gaussian models are inappropriate to deal with rough topography and built-up, industrial or urban, areas. This development has been accompanied by the steep increase of the computational capabilities of standard laptops to multicore parallelized machines making meshed computations on very large domains now possible (Oldrini et al., 2013).

At CEA, we have pushed forward a suite of models whose successive evolutions enabled the progressive construction of a comprehensive multiscale computational chain for atmospheric flow and dispersion. This suite comprises basically WRF weather reconstruction and forecast model and Parallel-Micro-SWIFT-SPRAY (PMSS) which includes a diagnostic mass-consistent (optionally a momentum) flow model and a Lagrangian particle dispersion model (Tinarelli et al., 2013). PMSS main feature is to explicitly account for buildings influence on the flow and on the dispersion.

Originally, Micro-SWIFT-SPRAY (MSS) was developed as a trade-off between a rigorous, still quickly produced, solution of the flow and dispersion in built-up environments. The introduction of nesting in SWIFT allowed the calculation of the wind flow from the mesoscale to the local scale at an increasingly finer resolution (Duchenne & Armand, 2010). More recently, efficient parallel versions of SWIFT

and SPRAY were developed leading to the PMSS system (Oldrini et al., 2011, 2017) and a momentum solver was implemented in PSWIFT to simulate the velocity and pressure fields more accurately than it is done with the diagnostic flow model (Oldrini et al., 2014, 2016a, 2016b).

Furthermore, PSWIFT has been coupled with Code_SATURNE in order to compute the flow both outside and inside buildings (among them critical infrastructures are of high interest). Then, PSPRAY uses together PSWIFT and Code_SATURNE as flow inputs to evaluate the distribution and the possible transfers of harmful materials both indoor and outdoor (Nibart et al., 2011).

3 Validation of the Local Scale Modeling System

Validation is a key asset to make models trustworthy for end-users, especially when these users are emergency players and protection of the population is at stakes. In parallel with the Modeling system development and the growth of its applications, the greatest attention has been paid to the validation of PMSS against numerous experimental trials, notably in the frame of COST Action ES1006 (Armand et al., 2016, Trini Castelli et al., 2016), in which the test-cases included both idealized and realistic urban mock-ups, wind tunnel and field trials, continuous and puff releases.

All predicted results were compared to measurements and the performances of PMSS evaluated through a statistical analysis based principally on the fractional bias (FB), normalized mean square error (NMSE), and fraction of predictions in a factor of two of measurements (FAC2) utilizing the acceptance criteria for the results of dispersion in built-up environments (Hanna & Chang, 2012). All results of this validation exercise are in Trini Castelli et al. (2018) with a summary given here.

3.1 Description of the Experimental Test-Cases

Within COST Action ES1006, the wind tunnel facility of Hamburg University was leveraged to make measurements for continuous and puff releases in a neutrally stratified boundary layer flow. The Michelstadt experiment was designed to validate dispersion models with the building structure representing an idealized city. In addition, the Complex Urban Terrain Experiment (CUTE) was developed to test dispersion models in the real densely built-up downtown of a Central-European city including measurements from field and wind tunnel. Most of the trials were blind tests with minimum information available for the inflow as it would be the case during a real accident.

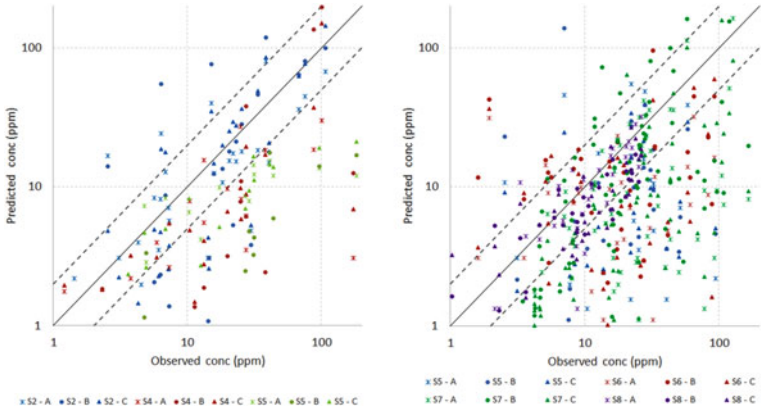

Fig. 1 Scatter plots of Michelstadt continuous releases mean concentrations, for the non-blind (left) and the blind (right) test-cases in three PMSS configurations

3.2 Overview of PMSS Validation Against Michelstadt Wind Tunnel Results

PMSS was run by independent teams of modellers giving the rare opportunity to investigate the sensitivity of the Modeling system to different meteorological input data or numerical options.

The scatter plots in Fig. 1 compare the predicted and observed mean concentrations for all continuous releases. The main part of the numerical results is in a factor of two of the experimental results. The agreement is better for a release taking place in an open square (S2) than for a release occurring in a street-canyon (S4 and S5), at a crossroad (S6 and S7), or inside a courtyard (S8).

The scatter plots in Fig. 2 compare the predicted and observed mean dosages and puff mean durations for all puff releases. Notwithstanding the complexity of the tests, the passage of the puff is timely captured, and a reasonable accuracy is obtained for the largest values of the dosage; for the puff duration, quite all numerical results are in a factor of two of the experimental results.

3.3 Overview of PMSS Validation Against CUTE Field and Wind Tunnel Results

Here again, PMSS was run by independent teams of modellers to study the sensitivity of the Modeling system to the turbulence input data, the wind input profile, and the flow model.

The scatter plots in Fig. 3 compare the predicted and observed mean concentrations for all continuous releases. For the field experiment, the best agreement is found

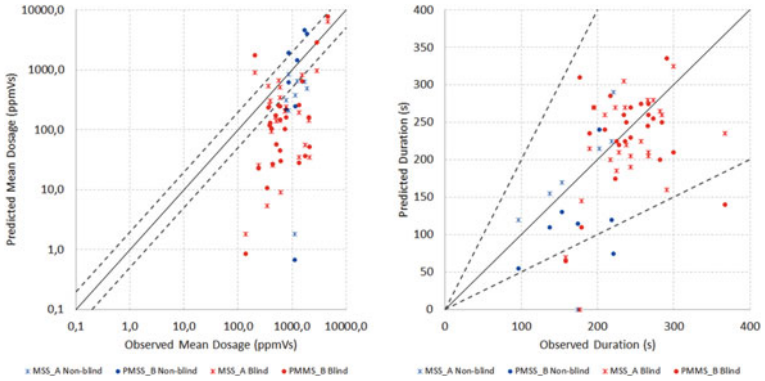

Fig. 2 Scatter plots of Michelstadt puff releases dosages (left) and puff durations (right), for the non-blind (blue) and the blind (red) test-cases in three PMSS configurations

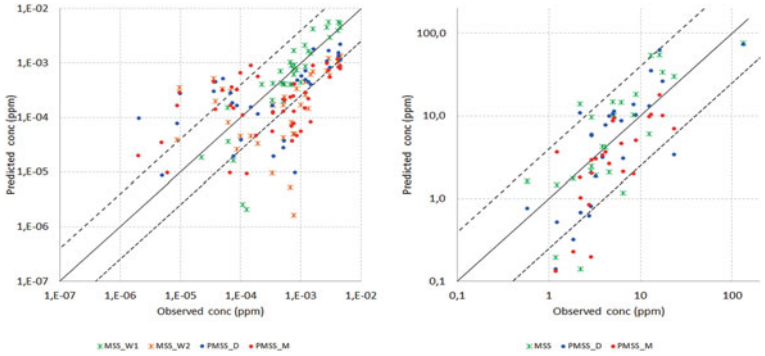

Fig. 3 Scatter plots of CUTE field experiment continuous release (left) and wind tunnel continuous release (right) concentrations in five PMSS configurations

with the most relevant wind direction profile ("MSS_W2"). For the wind-tunnel experiment, the predictions fairly agree with the measurements in all configurations, especially for the highest concentrations.

The scatter plots in Fig. 4 compare the predicted and observed mean dosages and mean puff durations for the wind tunnel puff releases. While the paired data are few, they provide interesting insights as there is a tendency to underestimate the lowest dosages, whereas the highest values are well reproduced by the predictions. These results are in line with the findings in Michelstadt cases.

In the whole, albeit there is some variability among the PMSS configurations, FAC2, FB and NMSE are predominantly satisfying. The quality of the results is not better for the non-blind or blind cases suggesting that PMSS performances are well established. It is worth noticing that the concentrations are more accurate with the momentum flow model compared to the diagnostic one.

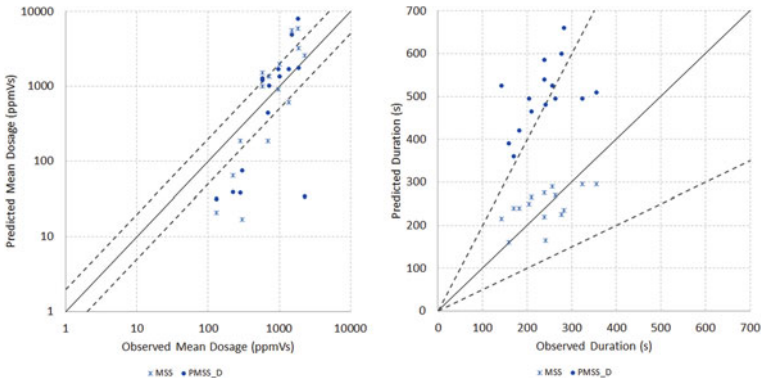

Fig. 4 Scatter plots of CUTE wind tunnel puff releases mean dosage (left) and mean duration (right) in two PMSS configurations

4 Application of the Modeling Chain to the EMERGENCIES Project

EMERGENCIES project was launched in 2014 with the twofold aim (1) to apply the Modeling chain based on PMSS to fictitious atmospheric releases in a giant domain covering the whole Paris city, its urbanized vicinity and airports which are under the responsibility of Paris Fire Brigade and (2) to demonstrate the feasibility and interest of these computations to support decision-making in an emergency implying noxious or explosive releases into the air (Oldrini et al., 2016a, 2016b).

The simulations were operated at the High Performance Computing (HPC) centre of the CEA on an intensive cluster using from 1,000 to 25,000 computational cores. PMSS domain had more than 6 billion nodes with horizontal dimensions of 40 km $\times$ 40 km and a vertical extent of 1,000 m. It was meshed at 3 m horizontally, and divided in 1,088 sub-domains (namely the "tiles") distributed to cores efficiently computing in parallel the flow and the dispersion (Oldrini et al., 2017).

Weather was predicted with WRF over Paris region at 1.6 km resolution and downscaled to the PMSS domain accounting for the fine scale topography and 1.5+ million buildings. The turbulent flow field computed with PSWIFT was used by PSPRAY to transport and disperse noxious agents fictively released near or inside public buildings in Paris (museum, train station and administrative building). Nested domains were defined to mesh the inside of the buildings at 1 m resolution and computations done with Code_SATURNE coupled to PMSS to evaluate indoor/outdoor transfers.

As an illustration, Fig. 5 shows the hazardous plumes in the districts of the train station and administrative building and inside the buildings 20 min after the releases and Fig. 6 shows the print of the plumes 2 h after the first release. Eventually, using an optimal number of about 2,000 cores, the performance was to predict 1 day of urban meteorology in less than 2 h (thus, forecast can be carried out each day for the next one) and 5 h of dispersion in about 1 h.

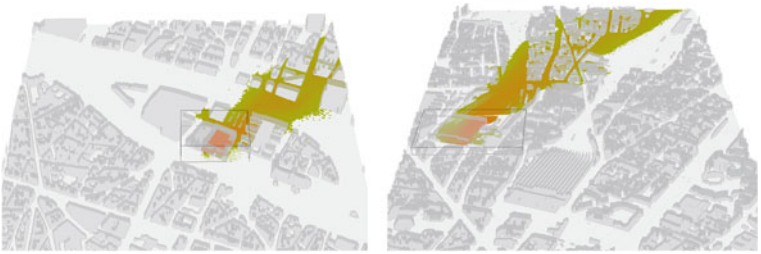

Fig. 5 Close views of the plume near the ground in the vicinity of the administrative building (left) and train station (right)

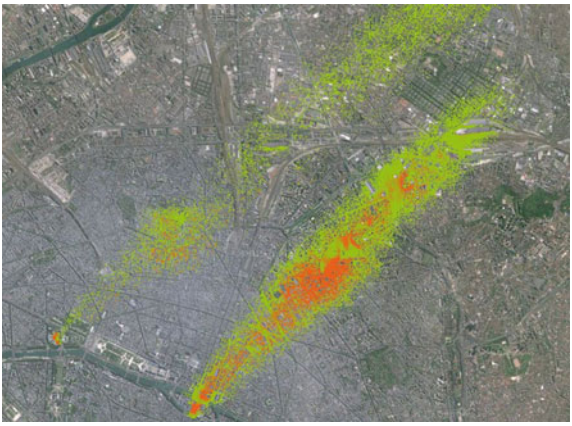

Fig. 6 Web GIS view of the plumes 2 h after the first release

5 Conclusion and Perspectives

This paper describes a multiscale system chaining WRF, PMSS and Code_SATURNE models, the deep validation effort dedicated to PMSS and the application of the system to fictive accidental or malicious dispersion events occurring in the giant domain encompassing Paris city and vicinity. The underlying principles of the simulations are generic and applicable to any dispersion situation. The chain is flexible as the computational domains can be easily moved to any place in the world.

These highly resolved 3D computations cascading from the mesoscale to the urban local scale and the inner part of infrastructures are worldwide unique as they combine a huge geographical print with a metric resolution. We argue that they are not an exercise in style, but the only way to account for the flow and dispersion in complex natural or built-up environment, and subsequently, to realistically and reliably estimate the health impact on the population and the first responders.

In the nowadays practice, first responders are still provided with results of simplistic models not appropriate for a built-up environment. Response procedures

based on these models may thus be not effective or incisive, or even misleading. The validation and application of the CEA modeling chain address the reliability and timeliness of 3D models in the conditions of an emergency in a built-up environment, demonstrating the support of these models to get control over the situation.

For the recent years, R&D carried out at CEA in the field of atmospheric dispersion and health impact assessment has not only focused on modeling, but also encompassed the decision-support tools adequacy with the organization and missions of the emergency players. Several participations of the CEA to security exercises have implied the production and transmission of danger zones or counter-measures maps to the firefighters and their authorities during the exercises (Armand et al., 2013, 2014, 2015, 2017). We argue that this approach is essential to promote the usage of state-of-the-art 3D models in computational tools whose results are accepted and trusted by practitioners.

Even if still prospective, it is very likely that supercomputing will become more and more usual and benefit to first-responders and their authorities in the preparation, diagnosis, and anticipation of emergency situations, notably in the case of radioactive, toxic, and/or explosive releases.

References

Armand, P., et al. (2016). Best practice guidelines for the use of atmospheric dispersion models at local scale in case of hazmat releases into the air. In *Proceedings of the 17th International Conference on Harmonisation within Atmospheric Dispersion Modelling for Regulatory Purposes* (pp. 459–465), Budapest, Hungary, May 9–12, 2016.

Armand, P., Duchenne, C., Benamrane, Y., Libeau, C., Le NouëneT., Brill, F. (2013). Meteorological forecast and dispersion of noxious agents in the urban environment—Application of a modelling chain in real-time to a fictitious event in Paris city. In *Proceedings of the 15th International Conference on Harmonisation within Atmospheric Dispersion Modelling for Regulatory Purposes* (pp. 724–728), Madrid, Spain, May 6–9, 2013.

Armand, P., Duchenne, C., & Bouquot, E. (2014). Atmospheric dispersion modelling and health impact assessment in the framework of a CBRN-E exercise in a complex urban configuration. In *Proceedings of the 16th International Conference on Harmonisation within Atmospheric Dispersion Modelling for Regulatory Purposes* (pp. 638–643), Varna, Bulgaria, September 8–11, 2014.

Armand, P., Duchenne, C., Oldrini, O., & Perdriel, S. (2017). EMERGENCIES Mediterranean—a prospective high-resolution modelling and decision-support system in case of adverse atmospheric releases applied to the French Mediterranean coast. In *Proceedings of the 18th International Conference on Harmonisation within Atmospheric Dispersion Modelling for Regulatory Purposes*, Bologna, Italy, October 9–12, 2017.

Armand, P., Duchenne, C., & Patryl, L. (2015). Is it now possible to use advanced dispersion modelling for emergency response? The example of a CBRN-E exercise in Paris. In*Air Pollution Modeling and its Application XXIV* (pp. 433–446). Springer International Publishing Switzerland.

Benamrane, Y., Wybo, J.-L., & Armand, P. (2013). Chernobyl and Fukushima nuclear accidents: What has changed in the use of atmospheric dispersion modeling? *Journal of Environmental Radioactivity, 126*, 239–252.

Duchenne, C., & Armand, P. (2010). Development of a 3D modelling suite from the global scale to the urban scale using MM5 and Micro-SWIFT-SPRAY—application to the dispersion of a

toxic release in New York City. In *Proceedings of the 13th Conference on Harmonisation within Atmospheric Dispersion Modelling for Regulatory Purposes*, Paris, France, June 1–4, 2010.

Hanna, S. R., & Chang, J. C. (2012). Acceptance criteria for urban dispersion model evaluation. *Meteorology and Atmospheric Physics, 116*, 133–146.

Nibart, M., Armand, P., Olry, C., Duchenne, C., & Albergel, A. (2011). The indoor/outdoor pollutant transfer of a hazardous release: application to a Parisian railway station. In *Proceedings of the 14th International Conference on Harmonisation within Atmospheric Dispersion Modelling for Regulatory Purposes*, Kos, Greece, October 2–6, 2011.

Oldrini, O., Armand, P., Duchenne, C., Olry, C., & Tinarelli, G. (2017). Description and preliminary validation of the PMSS fast response parallel atmospheric flow and dispersion solver in complex built-up areas. *Journal of Environmental Fluid Mechanics, 17*(3), 1–18.

Oldrini, O., Nibart, M., Armand, P., Olry, C., Moussafir, J., & Albergel, A. (2013). Multi-scale build-up area integration in Parallel SWIFT. In *Proceedings of the 15th International Conference on Harmonisation within Atmospheric Dispersion Modelling for Regulatory Purposes* (pp. 485–489), Madrid, Spain, May 6–9, 2013.

Oldrini, O., Nibart, M., Armand, P., Olry, C., Moussafir, J., & Albergel, A. (2014). Introduction of momentum equation in Micro-SWIFT. In *Proceedings of the 16th International Conference on Harmonisation within Atmospheric Dispersion Modelling for Regulatory Purposes* (pp. 412–417), Varna, Bulgaria, September 8–11, 2014.

Oldrini, O., Nibart, M., Duchenne, C., Armand, P., & Moussafir, J. (2016a). Development of the parallel version of a CFD—RANS flow model adapted to the fast response in built-up environments. In *Proceedings of the 17th International Conference on Harmonisation within Atmospheric Dispersion Modelling for Regulatory Purposes*, Budapest, Hungary, 9–12 May 2016.

Oldrini O., Olry, C., Moussafir, J., Armand, P., & Duchenne, C. (2011). Development of PMSS, the parallel version of micro SWIFT SPRAY. In *Proceedings of the 14th International Conference on Harmonisation within Atmospheric Dispersion Modelling for Regulatory Purposes* (pp. 443–447), Kos, Greece, October 2–6, 2011.

Oldrini, O., Perdriel, S., Nibart, M., Armand, P., Duchenne, C., & Moussafir, J. (2016b). EMERGENCIES—a modelling and decision-support project for the Great Paris in case of an accidental or malicious CBRN-E dispersion. In *Proceedings of the 17th International Conference on Harmonisation within Atmospheric Dispersion Modelling for Regulatory Purposes*, Budapest, Hungary, May 9–12, 2016.

Tinarelli, G., Mortarini, L., Trini-Castelli, S., Carlino, G., Moussafir, J., Olry, C., Armand, P., & Anfossi, D. (2013). Review and validation of Micro-Spray, a Lagrangian particle model of turbulent dispersion. In*Lagrangian modeling of the atmosphere, Geophysics. Monograph* (Vol. 200, pp. 311–327). American Geophysical Union.

Trini Castelli, S., et al. (2016). Evaluation of local-scale models for accidental releases in built environments—results of the modelling exercises in COST Action ES1006. In*Air pollution modeling and its application XXIV* (pp. 497–502). Springer International Publishing Switzerland.

Trini Castelli, S., Armand, P., Tinarelli, G., Duchenne, C., & Nibart, M. (2018). Validation of a Lagrangian particle dispersion model with wind tunnel and field experiments in urban environment. *Journal of Atmospheric Environment, 193*, 273–289.

Air Quality Modeling in Dense Urban Areas at Ground Level—CFD, OSM or Gauss?

Marie Haeger-Eugensson, Christine Achberger, Helen Nygren, Erik Bäck, Anna Bjurbäck, Marian Ramos Garcia, and Jens Forssén

Abstract There is an ongoing intensive urban densification in many cities. The need for advanced modeling methods that realistically simulate dispersion at ground level in complex urban areas have increased. As more modeling is done outside usual model communities, guidelines supporting the selection of suitable models is needed. Dispersion of air pollutants in street canyons is affected by width, height, length and building structure. Studies show that concentration of NO_2 in street canyons can become 5-times higher, compared to open conditions. Since Gaussian models cannot simulate dispersion at ground level in dense urban settlements models that include 3D information (buildings) is therefore required, such as CFD or OSM models to obtain realistic results. The purpose of the project is to investigate the effect from building on air quality and giving recommendations to authorities and consultants helping with model choices. This is based on calculations with three different model types, CFD, OSM and Gaussian for four urban environments, from dense to open suburban areas using the same input. Validation was done with continuous measurements of

M. Haeger-Eugensson (✉)
Department of Earth Sciences, Gothenburg University, Gothenburg, Sweden
e-mail: mrhr@cowi.com

M. Haeger-Eugensson · C. Achberger · H. Nygren · E. Bäck · A. Bjurbäck · M. R. Garcia
COWI, Gothenburg, Sweden
e-mail: char@cowi.se

H. Nygren
e-mail: heny@cowi.se

E. Bäck
e-mail: erbk@cowi.se

A. Bjurbäck
e-mail: AABJ@cowi.com

M. R. Garcia
e-mail: mrga@cowi.com

J. Forssén
Chalmers University of Technology, Gothenburg, Sweden
e-mail: jens.forssen@chalmers.se

© The Author(s), under exclusive license to Springer-Verlag GmbH, DE, part of Springer Nature 2021

C. Mensink and V. Matthias (eds.), *Air Pollution Modeling and its Application XXVII*, Springer Proceedings in Complexity, https://doi.org/10.1007/978-3-662-63760-9_37

NO_2 at each site. The CFD modeling gave best results at all sites, the OSM modeling quality varied between the sites, with slight to about 50% underestimation. The Gaussian modeling generally underestimated the concentration with 50%. The aspect ratio H/W $\geq$ 0.7 favors development of vortices and lateral dispersion of pollutants in street canyons. It was shown that with at least this aspect ratio locally emitted NO_2 frequently becomes at least 2–3 times higher compared an open road case. A methodology has been developed visualized in a flow chart, for help choosing an appropriate model for each environment. Most important factors are; street canyon structure; local concentration level; proximity to high emissions/risk of leakage into calculation area.

Keywords CFD-modeling · Air quality · Street canyon dispersion · Urban structure · Choice of models

1 Introduction and Background

There is an ongoing worldwide intensive urban densification in many cities, often leading to more dense building morphology and more distinct and closed street canyons. It is well known that this largely affects ground-based dispersion conditions, often called" breathability", which locally can, lead to up to five times higher concentration levels of air pollutants, compare to more open areas (Kwak et al., 2016; Sajani, 2018). Canyons structures can be classified using aspect ratios of the either street height/width (H/W) or width/length (W/L) (Yazid, 2014). Oke (2017) complemented H/W with numerical values explaining commonly occurring vortexes and dispersion patterns (e.g. H/W $\leq$ 0.4 small lateral flow; 0.7 < H/W < 1 start of development of vortex systems and large potential for lateral flow between streets). However, connections between air quality and structural classifications are difficult to find. As densification of urban areas is possibly increasing and for planning purposes it is essential to understand when and how more detailed modeling (e.g. CFD-modeling) of the air quality is required to achieve relevant results. According to Yazid et al. (2014) and Tominaga and Stathopoulos (2017) there is visible decline in air quality, mainly around heavily trafficked roads partly due to dense building morphology in closed and semi-closed street canyons. One reason why this has not been generally noticed may possibly be that measurements and modeling for regulating purposes is not usually performed for these environments. Within the so-called Fairmode modeling community (fairmode.jrc.ec.europa.eu), discussions of when CFD models is to be used. Many opinions point toward using it in planning but not yet for regulated purposes. Today, it is still common to use Gauss models in these types of investigations for planning purposes. However, in order to ensure good air quality in urban areas with the ongoing change in urban geometry, increased requirements of fine scale modeling in 3D, e.g. CFD-modeling, is likely going to become necessary in the planning stages. This task is assumed to be carried out by consultants rather than by authorities or model developers. Thus, given the complexity and the

special skills required, guidelines on when and how to use CFD modeling is needed for ensuring accurate results. The purpose of this work is to:

- investigate the relationship between different street canyon geometries and its impact on air pollution concentrations using a CFD-model.
- investigate different model types and their suitability for usage in different urban environments.
- an attempt for recommendations in choice of model for different urban areas.

2 Method

The results of dispersion modeling depend on the type of model used, what and how detailed input data is used and if/how the result is post-processed (e.g. NO_x to NO_2). In order to investigate how the air quality varies in different Swedish urban type environments, four test sites have been selected that represent different building structures, emission environments, meteorology conditions and background levels. The chosen street canyons were located in Gothenburg, Stockholm and Jönköping and the open road in Lerum (on the Swedish west coast). At the test sites there were air quality measurements which were used for validation. Additionally, to increase the number of environments more sites was included, but without the possibility to validate the results.

To obtain comparable results with the different models, the same input data has been used as far as possible. When the data is not similar it is mentioned in the text. The type of models used were two Gauss models (ADMS and Dispersion-Road), OSM (SIMAIR) and CFD (Miskam). To evaluate the effect of the urban structure on the air quality (here NO_2) the ratio between calculated concentration with CFD-modeling in different street canyons and open roads fore the same emissions.

3 Results and Conclusion

Calculations of NO_2 concentration using CFD, OSM and Gauss models have been performed at four different urban areas as 98-percentiles of daily (environmental standard in Sweden commonly exceeded). Validation between calculated and contiguous monitored NO_2 is shown in Fig. 1.

It becomes clear from Fig. 1 that the results from the CFD model best represent the monitored concentration levels at all sites, even if also the OSM model performs rather well for Stockholm and Jönköping. However, in Gothenburg OSM underestimates the NO_2 with 48%, possibly mainly due to that this model does not include the export of polluted air between different canyons. For the open road case, Lerum, the difference between the CFD and Gauss modeling is very small. To validate calculations (with CDF) in smaller street canyons, passive samplers (NO_2) have been used on weekly basis at five sites, and apart from site 1, all is narrow street canyons

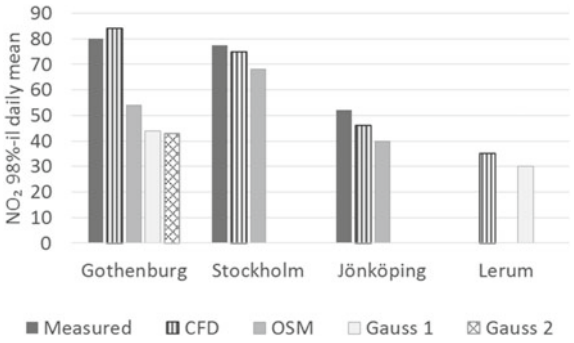

Fig. 1 Comparison between calculated NO_2 concentration as 98-percentile of daily means using CFD, OSM and Gauss models at four different urban areas. Measurements are shown where available

(Fig. 2). It is apparent that the consistency is good between measured and modeled concentration levels at all sites, although with some underestimation of the highest levels.

Further, calculations of the NO_2 concentrations at 38 different street canyons both with and without buildings at the same site, with same emissions and meteorology. The ratio between the NO_2 concentration in street canyon/open road is shown in Fig. 3 and plotted against different aspect ratios of street canyons (a) H/W and (b) L/W (c) H/W and L/W together with the NO_2 ratio.

Based on the results in Fig. 3 it is clear that NO_2 is commonly 1.5–2 and three sites show ratios between about 4–7 times higher in the canyon compare to open road. However, by only using the aspect ratios it is difficult to predict the enhancement of the NO_2 concentration level from the emissions in the street itself. The three sites with NO_2 ratios ≥ 3 all have both high H/W and W/L. In Fig. 3c H/W and W/L is plotted together and the color of the markers indicate the level of the NO_2 ratio. It is visual that with H/W between about 0.7–1 the NO_2 ratios are frequently between

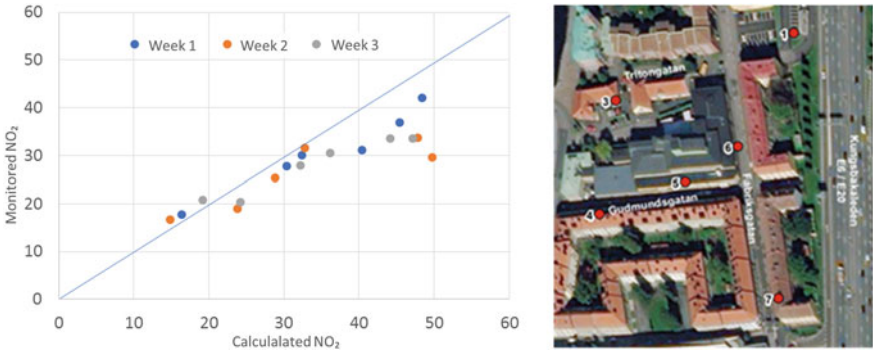

Fig. 2 Comparison between measured and calculated NO_2 concentration for three weeks in 2017 at site 1, 4, 5, 6, and 7 using the CFD-model Miskam

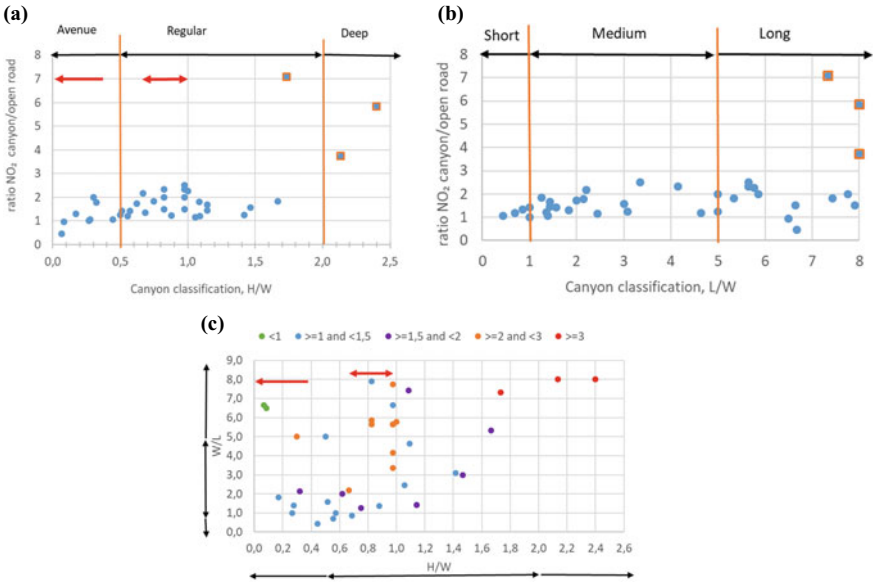

Fig. 3 Ratio calculation of NO_2 concentration from traffic in canyon/open road respectively compared with aspect ratios of two classification system **a** H/W and **b** L/W, **c** H/W and L/W and the level of ratio. The black arrows are classification systems by Yazid et al. (2014) and the red ones by Oke et al. (2017)

2 and 3. This is where Oke et al. (2017) defined that vortices in canyons begins to develop and is also the largest potential for lateral dispersion between streets. Thus, by using Oke's lower limit of the aspect ratio H/W $\geq$ 0.7 it can become an indication of when the vertical dispersion becomes poor in street canyons and when emissions in surrounding streets is going to influence the concentration level in street canyons. In many urban areas an increase with 2–3 times of the NO_2 contribution from the street canyon emissions solely due to the building morphology can become an issue.

When a model is to be choosen for an area some questions shold be answered. That is: What is the primary purpose of the modeling? Is it for monitoring/regulation or planning? Local prerequisites such as building and street morphology, emissions and background concentration. Is there high surrounding street emissions? A suggested workflow for modeling for planning purposes is summerized in Fig. 4.

In Fig. 4, the methodology is visualized showing that at first the complexity of the building morphology is to be decide with three choices (blocks with orange text). Thereafter, depending on the first choice, there is one to three sub-choices, which is the level of the local background concentration, size of emissions and risk of export of pollutions from surrounding streets. The model choices are shown in blue. Finally, for those cases with H/W $\geq$ 0.7 a CFD model should possibly be used to achieve relevant results, but if the local urban background is very low CFD modeling might not be necessary. However, the result in Fig. 4 is based on somewhat too few data to

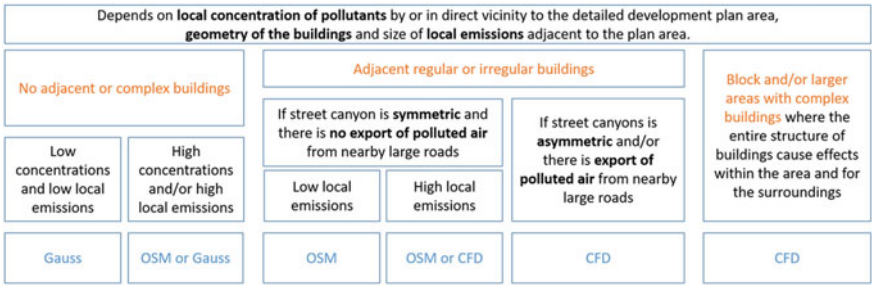

Fig. 4 Suggested workflow for the choice of model for specific areas/street canyons for planning purposes

give a reliable result but it will hopefully give some starting help to choose model type. Thus, since there is a shortage of model recommendations the method may possibly be used for other sites.

Acknowledgements This work was mainly funded by the Swedish Environmental Protection Agency but also partly by COWI and FORMAS. We would also like to acknowledge Meta Berghauser Pont and Andreas Gustavsson with development of realistic urban structures fore test cease scenarios.

References

Kwak, K. H., Baik, J. J., Ryu, Y. H., & Lee, S. H. (2015). Urban air quality simulation in a high-rise building area using a CFD model coupled with mesoscale meteorological and chemistry-transport models. *Atmospheric Environment, 100*, 167–177.

Oke, T., et al. (2017). Urban climates. *Cambridge University Press.* https://doi.org/10.1017/9781139016476

Sajani, S., et al. (2018). Vertical variation of $PM_{2.5}$ mass and chemical composition, particle size distribution, NO_2, and BTEX at a high rise building. *Environmental Pollution, 235*, 339–349.

Tominaga, Y., & Stathopoulos, T. (2017). Ten questions concerning modeling of near-field pollutant dispersion in the built environment. *Building and Environment, 105*, 390–402.

Yazid, A. W. M., et al. (2014). A review on the flow structure and pollutant dispersion in urban street canyons for urban planning strategies. *SIMULATION, 90*(8), 892–916.

Assessment of Air Quality Impacts from the Deployment of an Intelligent Transport System in Balkan Cities

George Tsegas, F. Barmpas, Nicolas Moussiopoulos, and Eleftherios Chourdakis

Abstract In line with the requirements of the European Commission's Transport White Paper 2011 (Roadmap to a Competitive and Resource Efficient Transport), an original Interoperable Open Architecture System for urban transport management and environmental impact assessment was developed in the frame of the Step2Smart INTERREG project. The system relies on Intelligent Transport Systems (ITS) application to associate city transport management with the reduction of atmospheric pollutant concentrations. The pilot ITS application in the city of Nicosia, Cyprus takes advantage of an advanced Air Quality Management System (AQMS) based on the MEMO/MARS-aero modeling system, used by the city authorities for the operational assessment of air quality. Real-time measurements of the main atmospheric pollutants and traffic data are collected from monitoring sensors at two locations in Nicosia, one at the street level and one as an urban background station, in order to quantify traffic contribution in air pollution levels. A new module is incorporated into the AQMS for the on-line assimilation of traffic and air quality measurement data. The monitoring data are then incorporated in air quality model simulations combined with a database of current and future emission scenarios, for rapidly assessing potential traffic management strategies. Pilot actions in Nicosia are coordinated with parallel deployments in the Greek island cities of Chania and Kos, which will be interconnected in the Interoperable Open Architecture System, providing a complete traffic picture of the three cities and will quantify traffic impact on air pollution along major road axes, as well as at the urban scale.

G. Tsegas (✉) · F. Barmpas · N. Moussiopoulos · E. Chourdakis
Laboratory of Heat Transfer and Environmental Engineering, Aristotle University, 54124 Thessaloniki, Greece
e-mail: gtsegas@auth.gr

F. Barmpas
e-mail: fotisb@auth.gr

N. Moussiopoulos
e-mail: moussio@auth.gr

E. Chourdakis
e-mail: chourdakis@auth.gr

© The Author(s), under exclusive license to Springer-Verlag GmbH, DE, part of Springer Nature 2021

C. Mensink and V. Matthias (eds.), *Air Pollution Modeling and its Application XXVII*, Springer Proceedings in Complexity, https://doi.org/10.1007/978-3-662-63760-9_38

1 Introduction

The interconnection of environmental issues with the transport sector is reinforced through the Transport White Paper 2011 (URL1) where an action guide for a competitive, low-emission and energy-efficient economy is created by 2050. The aim was to reduce pollutants from 80 to 95% by 2050 compared to 1990 levels. In this frame, the EU funded Step2Smart project (URL2) aims to develop an open architecture methodology, building on both existing and new systems, which will be implemented and evaluated in pilot actions in the cities Nicosia, Chania and Kos. Pilot campaigns of Intelligent Transport Systems (ITSs) will be used to link transport to cities with reducing environmental pollutants. The basic tool for this is an operational Air Quality Management System (AQMS) which has been adopted by the Department of Labour Inspection of the Ministry of Labour, Welfare and Social Insurance as the official software platform for air quality management in Cyprus (Moussiopoulos et al., 2016). This system provides up-to-date air quality nowcasting and 24-h air quality forecasts for regulated atmospheric pollutants for Cyprus and its five largest cities, including the capital city of Nicosia. The pilot applications of the Step2Smart Open Architecture System are supported mainly by the AQMS.

2 Methodology

An operational AQMS has been installed and used operationally in the Department of Labour Inspection (DLI) of the Republic of Cyprus. The core of the AQMS consists of a model system which performs nested-grid meteorological and photochemical model simulations in two parallel operational modes, providing nowcasting and forecasting concentration maps for the entire island of Cyprus. The mesoscale meteorological model MEMO (Moussiopoulos et al., 2012) and the chemistry-transport model MARS-aero (Moussiopoulos et al., 2010) are used for this purpose. In addition, air quality assessment and decision making is supported by the AQMS by enabling DLI users to interactively configure custom emission scenarios and computationally assess air quality trends over user-defined domains of interest. More details as regards the structure and the special features of the AQMS can be found in Moussiopoulos et al. (2016).

The implementation of the AQMS is based on a flexible infrastructure of Python script programs incorporating the various operational and off-line workflows as presented in Fig. 1. As it can be deduced from this structure diagram, there is a noticeable need for workflow optimization, as many subsystems are interlinked and working in parallel. Moreover, it is evident that there is a mixture of information flows from in-situ measurements and models running operationally. Consequently, one of the Step2Smart objectives is to implement a streamlined link between traffic management and air quality assessment with the aid of a data assimilation module which

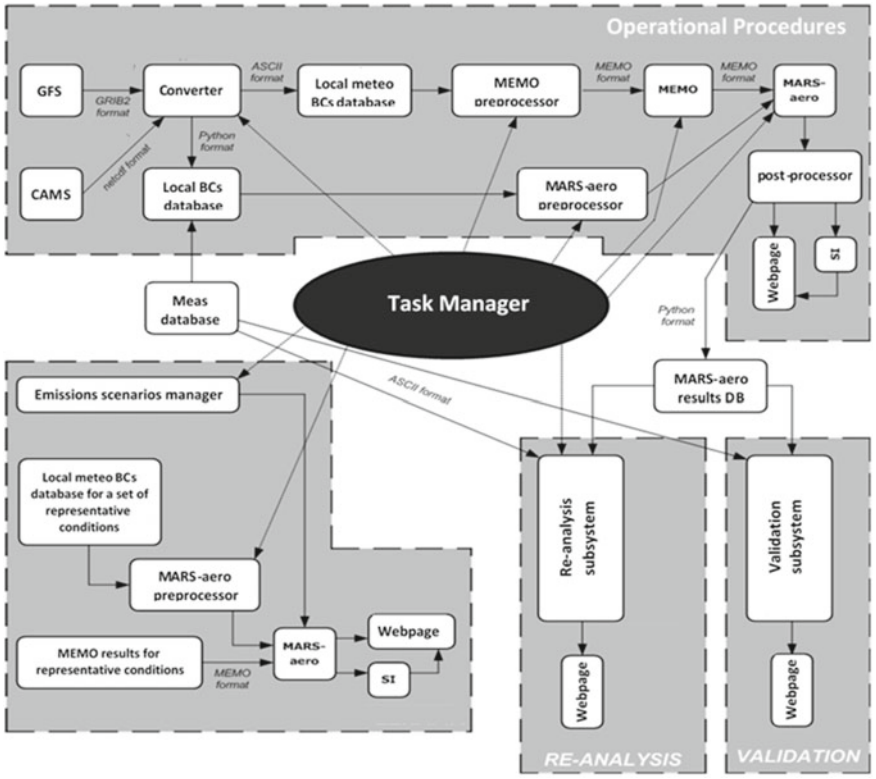

Fig. 1 AQMS system architecture and interfacing

are developed and incorporated in the AQMS. Regarding the operational structure of this module, the following features are established:

- Transfer of concentration data
- Timebase checking and rejection of out-of-sequence data
- Sanity checking: ranges (species-dependent), derivatives, spatial correlation
- Classification (regional background, urban background, street-scale) and normalisation
- Calculation of numerical tendencies (forcing terms)
- Spatial "smearing" of tendencies
- Incorporation of tendencies in the dynamical terms and timestep integration
- Extraction of corrective terms, to be used in next assimilation/integration steps.

3 Preliminary Deployment

As regards the AQMS operational application, at the end of each day a wide range of statistical indicators are calculated according to the guidelines set by COST728 (2008), for the station locations and pollutants of interest, and numerous charts are produced for visually assessing the accuracy of the simulations in both nowcasting and forecasting mode. Moreover, in order to have a better overview of the system's performance, validation charts for meteorological parameters are also produced presenting comparisons between the calculated and the observed timeseries of wind speed and wind direction. A previous evaluation of the baseline AQMS operational core had revealed that short-term forecasts were in good agreement with the corresponding urban background measurements (Fig. 2). Nevertheless, the forecast accuracy in predicting air pollution levels at the local/street scale is consistently lower. A statistical approach for determining "street increments" of concentrations was evaluated in a pilot two-month application, using the AQMS's operational mesoscale calculations of urban background concentrations and meteorological fields in order to provide the functional relationship with the required input parameters. The results of this pilot application were then compared with observational data. The validation process indicated a clear improvement in the AQMS's ability to predict pollution levels at the street scale.

On the other hand, a number of further potential enhancements were identified and are currently under implementation, such as the incorporation of additional variables in the semiempirical calculation (e.g. traffic-induced turbulence). On a practical level, information obtained through this optimized operation of the AQMS is expected to contribute to the reduction of the urban environmental footprint and the promotion of public means of transport, through interventions in pilot projects/transport improvement applications and measures to upgrade the administrative capacity in the design and monitoring of the environmental footprint. These pilot interventions include the provision of real-time information on traffic conditions and emissions, the prioritization of busses on signalling nodes, the development of a bus management fleet and public information to attract passengers and the adaptation of traffic light signals according to current traffic.

4 Conclusions

The AQMS developed and installed in the Department of Labour Inspection (DLI) of the Republic of Cyprus is an integrated operational state-of-the-art air quality management system for meteorological and photochemical model simulations which offers a range of features for nowcasting, forecasting and performing scenario calculations for air quality in areas of interest. Within the Step2SMART INTERREG project, the efficiency of pilot measures in terms of emission reduction and air quality improvement will be assessed using the AQMS. In this direction, a two-way link

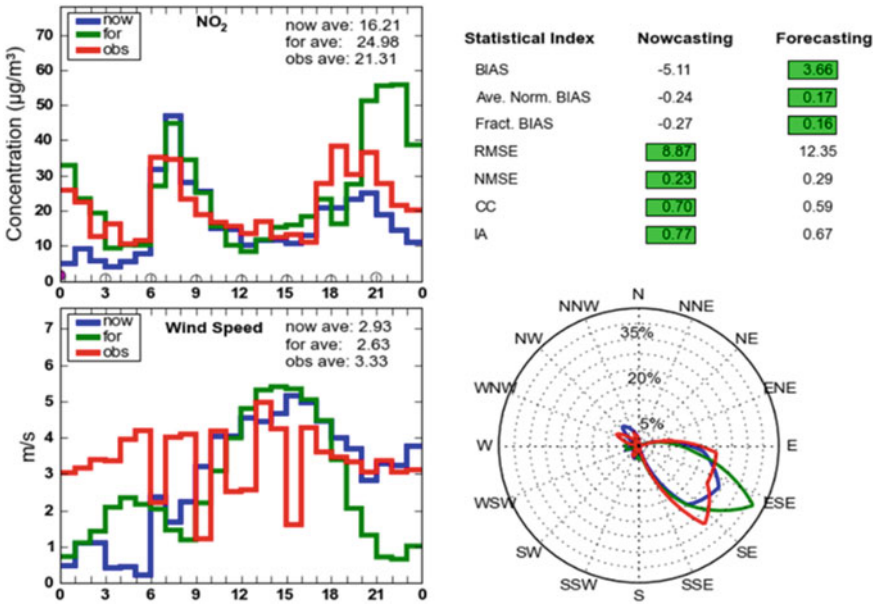

Fig. 2 Comparison between AQMS results and in-situ observations for a typical weekday in the city of Nicosia

between the AQMS and the traffic loads monitoring software of the Department of Public Works of the Ministry of Transport, Communications and Works of Cyprus is implemented. Measured traffic loads in Nicosia are taken into account by the AQMS in real-time, for calculating accurate pollutant emissions to be fed into AQMS. The final results of this work will be used as guidelines for the future development of Sustainable Urban Mobility Plans (SUMPs) for similar mid-sized island cities.

Acknowledgements The "Step2Smart" Project is co-funded by the European Union and national funds of the participating countries.

References

COST728, 2008. *Overview of Tools and Methods for Meteorological and Air Pollution Mesoscale Model Evaluation and User Training.*

Moussiopoulos, N., Douros, I., Tsegas, G., Kleanthous, S., & Chourdakis, E. (2010). An air quality management system for Cyprus. *Global Nest Journal, 12*, 92–98.

Moussiopoulos, N., Douros, I., Tsegas, G., Kleanthous, S., & Chourdakis, E. (2012). An air quality management system for policy support in Cyprus. In *Advances in meteorology* (Vol. 2012). Hindawi Publishing Corporation. https://doi.org/10.1155/2012/959280.

Moussiopoulos, N., Chourdakis, E., & Tsegas, G. (2016). An air quality management system for Cyprus: Evaluation and improvements. In *Proceedings of the 13th International Conference on*

Meteorology, Climatology and Atmospheric Physics (COMECAP 2016), Thessaloniki, Greece, September 19–21.
URL1: https://ec.europa.eu/transport/sites/transport/files/themes/strategies/doc/2011_white_paper/white-paper-illustrated-brochure_en.pdf.
URL2: http://www.eng.ucy.ac.cy/step2smart/.

Question and Answer

Questioner: Rostislav Kouzmetsov.

Question: How do you handle VOC composition from CAMS boundaries?

Answer: The operational dispersion model is not particularly sensitive on the exact NMVOC split used for the boundary conditions. As an adequate approximation, the same system of split factors has been used as previous applied for the emissions disaggregation. The split is based on the EDGAR data assuming the SNAP sector distribution of the Cypriot emissions inventory.

High-Resolution Air-Quality Modeling in Urban Areas—A Case Study for the City of Leipzig

Bernd Heinold, Michael Weger, Oswald Knoth, Roland Schrödner, Thomas Müller, and Liina Tõnisson

Abstract A multi-scale framework for urban air-pollution modeling is presented, which has been developed for the mid-sized City of Leipzig, Germany, and potential application in other cities. The model system consists of the urbanized chemistry-transport model COSMO-MUSCAT, which is enhanced by a newly developed CFD model to bridge the gap between neighborhood scale and street level. A first application of COSMO-MUSCAT as air-quality forecast model at continental to urban neighborhood scales for Central Germany and the City of Leipzig is presented for spring 2019. In addition, the CFD model is tested to be able to capture the typical urban flow patterns.

1 Introduction

The urban atmosphere is strongly influenced by a range of short-lived pollutants from multiple spatially and temporally varying sources. Many of them are known to cause adverse health effects (ultrafine particulate matter, soot, nitrogen oxides, ozone). Because of short lifetimes, these air pollutants show a high spatio-temporal

B. Heinold (✉) · M. Weger · O. Knoth · R. Schrödner · T. Müller · L. Tõnisson
Leibniz Institute for Tropospheric Research (TROPOS), 04318 Leipzig, Germany
e-mail: Bernd.Heinold@tropos.de

M. Weger
e-mail: Michael.Weger@tropos.de

O. Knoth
e-mail: Oswald.Knoth@tropos.de

R. Schrödner
e-mail: Roland.Schroedner@tropos.de

T. Müller
e-mail: Thomas.Mueller@tropos.de

L. Tõnisson
e-mail: Liina.Tonisson@tropos.de

© The Author(s), under exclusive license to Springer-Verlag GmbH, DE, part of Springer Nature 2021

C. Mensink and V. Matthias (eds.), *Air Pollution Modeling and its Application XXVII*, Springer Proceedings in Complexity, https://doi.org/10.1007/978-3-662-63760-9_39

variability, which currently cannot be adequately captured by stationary observations and air-quality models.

For a better exposure evaluation, and to scientifically study the small-scale variability and controls of air pollutants in cities, a flexible multi-scale system for air-quality modeling has been developed. It is based on a state-of-the-art chemistry-transport model (CTM), which is enhanced by a new Computational Fluid Dynamics (CFD) solver for application across entire urban areas. The model framework was first tested for the mid-sized City of Leipzig, Germany, within the knowledge-transfer project WTimpact. The model system was run operationally up to the 500-m scale for field campaigns in spring 2019 and as hindcast for the hot summer 2018. For model evaluation, long-term stationary and extensive mobile air quality measurements with sensor backpacks are available.

2 Methods

2.1 Multi-Scale Air-Quality Modeling Framework

A flexible framework for high-resolution air-quality modeling has been developed for the City of Leipzig and potential application in other cities. The core is an urbanized version of the multi-scale CTM COSMO-MUSCAT (Consortium for Small-scale Modeling model of the German Weather Service DWD—MUltiScale Chemistry Aerosol Transport model; Schättler et al., 2018; Wolke et al., 2012). The model system includes up-to-date production parameterizations for natural aerosol, including an advanced scheme for biogenic emissions and secondary aerosol formation, and considers complex multiphase chemistry. Anthropogenic air pollutant emissions are prescribed from latest inventories. In order to account for the impact of city morphology on air flow and radiation, the model is equipped with the Double Canyon Effect Parametrization (DCEP) by Schubert (2012). The required statistical input is calculated from a detailed 3-D city model in CityGML format using preprocessor tools in python language.

The simulations are realized with a nesting chain, where the horizontal resolution is gradually increased from 28 km over Europe to about 550 m over the city area. The outer domain, which provides the background concentrations over Germany, is driven by the global ICON forecast of DWD. Copernicus Atmosphere Monitoring Service (CAMS) forecasts provide the input for the aerosol and gas boundary conditions of the coarse domain. The meteorological initial and boundary data for the German domain come from the DWD COSMO-D2 forecast. The subsequent domains use the boundary conditions of the respective coarser model run. For the European domain, TNO-CAMS emissions are used, while for Germany, high-resolved point, area and road emissions are available from the German Environment Agency (Umweltbundesamt, UBA).

The system can be run in quasi-operational mode, which allows to accompany field campaigns. Another important feature is the visualization by interactive online mapping on the project website.

2.2 Urban CFD Model

In order to bridge the gap between the COSMO-MUSCAT results at neighborhood scale and street level, dynamical downscaling is applied. For the computation of wind fields considering the full physical presence of buildings, a CFD solver for incompressible flow equations has been developed following Gowardhan et al. (2011). The spatial discretization of the tendency terms involves a finite volume method on a uniformly structured cuboidal mesh. The velocity components are defined on the cell faces, while the pressure is a cell-centered quantity. Detailed building geometry data is used to compute effective volumes, as well as effective face areas of the grid cells. Advection is upwind biased and 3rd order spatial accurate. Time integration involves the fractional step pressure projection method, which is essentially an operator splitting. In a first step, the advection and diffusion tendencies are integrated explicitly using the classic 4th-order Runge–Kutta procedure. The pressure-gradient correction is computed afterwards implicitly from the divergence of the intermediate wind field using an efficient multigrid solver. After pressure projection, the final wind field satisfies the continuity equation. Turbulence closure is currently provided by a simple algebraic eddy-viscosity model, and skin-friction drag is parameterized from the effective cell-face areas. Finally, the air pollutant dispersion is computed by an advection–diffusion routine. In this approach, obstacles are represented by permeability fields, which allows spatial resolutions that can be significantly lower than needed to explicitly resolve buildings. This way computational costs are considerably reduced and, in future, the scheme may be used online in the CTM MUSCAT.

3 Results and Discussion

The multi-scale modeling framework was first tested in hindcast mode for the hot summer 2018, and as 48-h forecast for the field phases of the WTimpact project in spring 2019. Long-term stationary observations at four sites in the City of Leipzig and extensive mobile measurements from the WTimpact field campaigns are available for evaluation. The first comparison of the model results from the innermost domain to the monitoring station measurements shows a reasonably good agreement for the temporal evolution of PM_{10}, NO_2, and O_3 at all sites. The levels of PM_{10} and NO_2 are matched well by the model at the urban background stations, as well as the concentration of PM_{10} in the city center. However, the observed values of NO_2 and O_3 are underestimated, in particular, at high traffic locations. This requires further analysis. A likely reason is a still too coarse horizontal resolution, but possibly

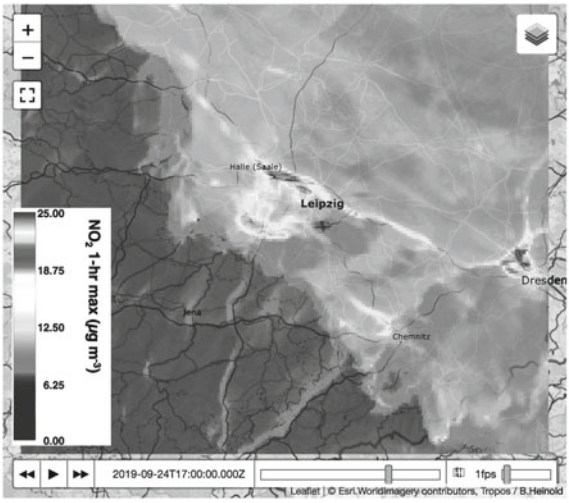

Fig. 1 Maximum hourly NO_2 concentration at surface as computed with COSMO-MUSCAT for Leipzig on 24 September 2019, 17 UTC. Screenshot of the interactive web map as provided within project WTimpact

also adjustments to the prescribed road traffic emissions may be needed. During WTimpact, the urban air-quality forecast was provided to the volunteers in the project via interactive web mapping for experimental planning and the interpretation of observations (Fig. 1).

In addition, the new urban CFD solver was tested for a subdomain over Leipzig with 150 × 100 grid cells and 20 m horizontal resolution. In Fig. 2, the CFD simulation is initialized and driven with a uniform wind field ($u = 5$ m s^{-1}, $v = 0$ m s^{-1}) at the domain boundaries. The building structure is described by permeability fields, calculated from detailed building-geometry data. For test purposes, a point source of arbitrary strength is placed at a building roof at 25 m height and another source emitting into the first model layer at the inner ring road of Leipzig. The dispersion of the tracers is as expected, e.g. with channeling in narrow inner-city roads and more diluted spread in wider areas, as well as downward mixing of the lofted plume in the lee of buildings (Fig. 2). The CFD solver is fully parallelized and efficient to be applied for the entire urban area of Leipzig. In a next step, the COSMO-MUSCAT model will be combined with the CFD solver for downscaling.

4 Conclusions

The multi-scale framework for urban air-pollution modeling presented here allows to visualize air-quality issues in cities, and provides a better exposure evaluation. The model system consists of the urbanized CTM COSMO-MUSCAT, which is applied at

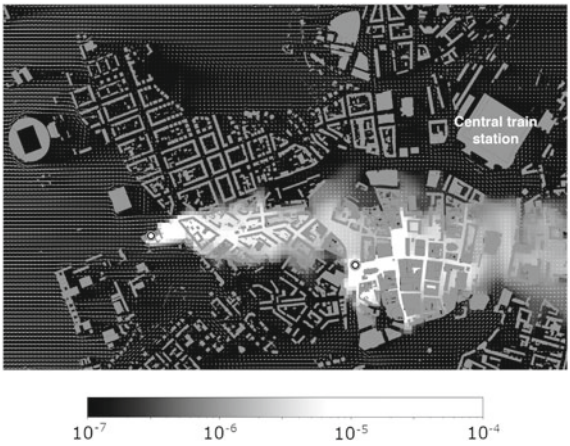

Fig. 2. 1st-layer tracer concentration over central Leipzig after one hour of simulation with the new CDF model. Point sources of arbitrary strength emit at a 25 m rooftop (left dot) and into the first layer (right dot)

continental to urban neighborhood scales (<500 m). A first application of COSMO-MUSCAT in urban air-quality forecast for the City of Leipzig is presented for May 2019. For downscaling to street-level, in a next step, the urban-scale modeling will be combined with a new CFD solver, which uses permeability fields to represent buildings that allow grid spacings larger than a typical street width. As shown in a first test, the CFD model is able to represent characteristic flow patterns. Near future work includes a thorough model evaluation of the coupled model framework with the unique set of mobile and stationary measurements available at Leipzig. Ultimately, it will be used to investigate the small-scale variability of short-lived air pollutants and their controlling factors in Leipzig, as well as potentially in other cities.

Acknowledgements This work is funded by the Bundesministerium für Bildung und Forschung (BMBF) as part of the "WTimpact" project under grant 01IO1726. Recent emission data were provided by the Umweltbundesamt (UBA). We thank the Deutscher Wetterdienst (DWD) for good cooperation and support.

References

Gowardhan, A., Pardyjak, E., Senocak, I., & Brown, M. (2011). A CFD-based wind solver for an urban fast response transport and dispersion model. *Environmental Fluid Mechanics, 11*, 439–464. https://doi.org/10.1007/s10652-011-9211-6

Schättler, U., Doms, G., & Schraff, C. (2018). *A description of the nonhydrostatic regional COSMO-Model. Part VII: User's Guide.* Deutscher Wetterdienst (DWD).

Schubert, S., Grossman-Clarke, S., Martilli, A. (2012). A double-canyon radiation scheme for multi-layer urban canopy models. *Boundary-Layer Meteorology*, *145*(3), 439–468. https://doi.org/10.1007/s10546-012-9728-3

Wolke, R., Schröder, W., Schröder, R., & Renner, E. (2012). Influence of grid resolution and meteorological forcing on simulated European air quality: A sensitivity study with the modeling system COSMO–MUSCAT. *Atmospheric Environment, 53*, 110–130. https://doi.org/10.1016/j.atmosenv.2012.02.085

Question and Answer

Questioner: Dr. Ronny Petrik.

Question: Is the jump from 28 to 2.2 km not much too high for the model dynamics?

Answer: This is not an issue, since the outermost 28-km domain covering Europe only provides the aerosol-chemical boundary conditions for the ‘German’ nest with 2.2 km grid spacing. The 2.2 km nest is driven by initial and boundary conditions from the DWD COSMO-D2 forecast, which also has a horizontal grid spacing of 2.2 km.

Assessment of the Sensitivity to the Input Condition Using MicroSpray Lagrangian Particle Model for Puff Releases in UDINEE Project

Gianni L. Tinarelli and Silvia Trini Castelli

Abstract In the frame of the UDINEE Project the MicroSpray Lagrangian particle dispersion model is run to simulate puff emissions in four different test cases carried out in Oklahoma city during the JU2003 experiment. For each case, two different wind velocity inputs, both representative of the incoming flow, are considered. The difference in the output concentration field is discussed and the uncertainty depending on the input variation is assessed.

Keywords Puff releases · Lagrangian particle models · Urban site · UDINEE project

1 Introduction

The uncertainty on the driving input conditions for modeling the dispersion of pollutants in the atmosphere is a critical issue, particularly in the context of emergency response to accidental releases of harmful substances. Mostly, only single values of wind speed and direction are available in real scenarios as information for model simulations. Especially in built environments, observations are inevitably affected by local effects and might not be fully representative of the actual incoming flow. The model predicted concentrations are in turn determined by the availability or the possible choice of the wind field data driving the simulation. Here we focus on the sensitivity of the simulation results connected to the choice of the wind velocity used as input. In the UDINEE Project (Urban Dispersion INternational Evaluation Exercise), different modeling approaches were compared in application to the Joint Urban 2003 (JU2003) puff-releases field campaign in Oklahoma City,

G. L. Tinarelli
ARIANET Srl, Milano, Italy

S. Trini Castelli (✉)
CNR—Institute of Atmospheric Sciences and Climate, Torino, Italy
e-mail: s.trinicastelli@isac.cnr.it

© The Author(s), under exclusive license to Springer-Verlag GmbH, DE, part of Springer Nature 2021

C. Mensink and V. Matthias (eds.), *Air Pollution Modeling and its Application XXVII*, Springer Proceedings in Complexity, https://doi.org/10.1007/978-3-662-63760-9_40

U.S.A. (Hernández-Ceballos et al., 2019a, 2019b). Four selected JU2003 IOPs (intensive operating periods) cases, each composed by four puff releases, were simulated with MicroSpray model, driven by MicroSwift diagnostic model fields, using wind velocity data from two different observed datasets, both representative of the flow at the time of the release. The analysis and discussion of the single IOP case, including a comparison with observed concentrations at the sampling sensors, is presented in Tinarelli and Trini Castelli (2019), investigating the influence of the meteorological data supplied as input to the model on the predicted concentration distribution, and on its representativeness of the observed pattern. Here we consider the differences between the output fields corresponding to the alternative input flows, looking at distribution of the differences in concentration at the ground.

2 The Case Study and the Simulations

For each IOP, two sets of wind speed and direction are considered in input to build the MicroSwift flow field driving the puff dispersion simulations: those calculated as the averages of 80 fixed anemometers placed at street level, on building roofs, in the suburbs and nearby airports, and over each IOP of 8 h duration (AW case, hereafter) and those measured at a sensor located 10 m above the roof of the city post office, 1 km upwind the central business district, supplied as 10 s averaged time series (MW case, hereafter). The two inputs differ in time and for their spatial representativeness of the wind field. In AW case spatially-averaged and constant values are assigned to the wind velocity for the full simulation of the single IOP, thus representing a situation where minimum information is available. In MW case the wind velocity input is time-varying and correspond to a location upwind the urban area of interest, thus representing a more detailed information for the incoming flow. In Table 1 the main details about the different IOPs are provided.

In Fig. 1 a sketch of the four IOPs configuration is given. The IOPs were selected considering cases where the two wind directions are similar (IOP3 and IOP7) or rather different (IOP5 and IOP8). This allows evaluating how much the dissimilarity in the

Table 1 Details on the selected IOPs

IOP N	Release time of puffs (CST)	AW wind speed (m/s) and dir (°)	Average of MW wind speed (m/s) and dir(°)
IOP 3	2003/07/07 08:00; 08:20; 08:40; 09:00	3.7; 196	4.6; 200
IOP 5	2003/07/09 14:00; 14:20; 14:40; 15:00	2.8; 191	4.5; 162
IOP 7	2003/07/18 04:00; 04:20; 04:40; 05:00	2.5; 217	1.8; 209
IOP 8	2003/07/24 04:00; 04:20; 04:40; 05:00	3.8; 157	2.1; 130

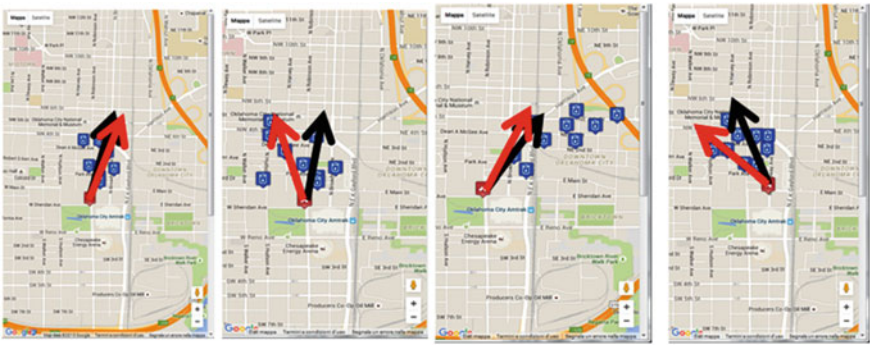

Fig. 1 AW (black arrow) and MW (red arrow) wind directions for IOP3, IOP5, IOP7 and IOP8, from left to right. Red flag: release point; blue flags: measurement points

input wind field affects the distribution of the concentration and the area covered by the pollutant puffs.

The computational domain has dimensions 1600 m × 1400 m × 770 m, the horizontal resolution of the meteorological grid is 5 m, the vertical meteorological grid has 57 points of higher resolution closer to the ground (about 2 m in the first 20 m), as required and suggested for the UDINEE intercomparison. In this configuration the obstacles, seen by the modeling system as filled cells of the computational grid, are well resolved.

3 Results and Discussion

In Fig. 2 the maps of the difference between the concentration simulated by MW and AW are plotted. Larger differences are found in proximity to the release point, also because concentrations there are higher. Even when the two wind directions are similar (IOP3 and IOP7), the areas affected by the puffs may result to be quite different. This can clearly be an issue, especially in complex built environments, when emergency response actions are planned and taken. The uncertainty related to the input used for the simulation was assessed in Tinarelli and Trini Castelli (2019) based on some statistical indexes, among them the normalized absolute difference (NAD). Averaging their values for the 'similar wind direction' (IOP3 and IOP7) and 'diverging wind direction' (IOP5 and IOP8) cases, the NAD between the concentrations predicted by AW and MW simulations takes values 0.55 and 0.88, respectively. These estimates provide a quantification of the possible bias in the simulation outputs associated to the variability and uncertainty in the input wind field. As for other statistics, fractional bias (FB) values between the two simulations are found to be comparable to the typical bias between predictions and observations.

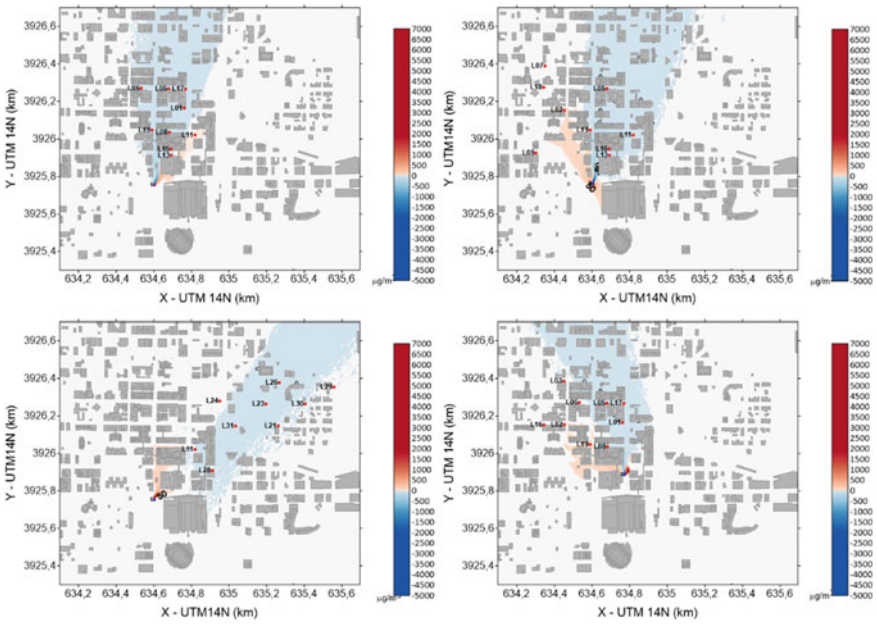

Fig. 2 Maps of the difference of ground level concentrations between MW and AW simulations for IOP3 (top left), IOP5 (top right), IOP7 (bottom left) and IOP8 (bottom right)

The estimation of the deviation provides information on the uncertainty of the predicted concentration, connected to the possible limited representativeness of the input flow data used in model simulations. It can represent the 'error' to be associated to the concentration distribution, and related affected areas, given as output by model simulations. The calculated bias can thus be taken into account to have a conservative approach when the impact of a release, and its affected areas, are to be evaluated, in particular in response to emergency situations.

References

Hernández-Ceballos, M. A, Hanna, S., Bianconi, R., Bellasio, R., Chang, J., Mazzola, T., Andronopoulos, S., Armand, P., Benbouta, N., Čarný, P., Ek, N., Fojcíková, E., Fry, R., Huggett, L., Kopka, P., Korycki, M., Lipták, L., Millington, S., Miner, S., Oldrini, O., Potempski, S., Tinarelli, G., Trini Castelli, S., Venetsanos, A., & Galmarini, S. (2019). UDINEE: evaluation of multiple models with data from the JU2003 puff releases in Oklahoma City. Part II: simulation of puff parameters. *Boundary-Layer Meteorology, 71*(3), 351–376.

Hernández-Ceballos, M.A, Hanna, S., Bianconi, R., Bellasio, R., Chang, J., Mazzola, T., Andronopoulos, S., Armand, P., Benbouta, N., Čarný, P., Ek, N., Fojcíková, E., Fry, R., Huggett, L., Kopka, P., Korycki, M., Lipták, L., Millington, S., Miner, S., Oldrini, O., Potempski, S., Tinarelli, G., Trini Castelli, S., Venetsanos, A., & Galmarini, S. (2019). UDINEE: evaluation of

multiple models with data from the JU2003 puff releases in Oklahoma City. Part I: comparison of observed and predicted concentrations. *Boundary-Layer Meteorology, 171*(3), 323–349.
Tinarelli, G. L., & Trini Castelli, S. (2019). Assessment of the sensitivity to the input condition with a Lagrangian Particle Model in UDINEE Project. *Boundary-Layer Meteorology, 171*(3), 491–512.

Test of Gas Phase Chemistry Mechanisms and Boundary Conditions for the LES Model with Online Coupled Chemistry PALM-4U

Renate Forkel, Basit Khan, Sabine Banzhaf, Matthias Sühring, Farah Kanani-Sühring, Klaus Ketelsen, Johannes Werhahn, Mona Kurppa, Edward C. Chan, Björn Maronga, Matthias Mauder, and Siegfried Raasch

Abstract The microscale urban model PALM-4U is based on the Parallelized Large-Eddy Simulation Model PALM, which was extended by a gas phase chemistry module within the joint project MOSAIK (https://palm.muk.uni-hannover.de/mosaik). The performance of different chemistry mechanisms of different complexity within the PALM-4U and the impact of lateral boundary conditions from a regional scale model are tested and discussed.

1 Introduction

Large Eddy Simulation (LES) models can capture the inherent unsteadiness of atmospheric turbulence and therefore, permit to resolve local scale urban processes. Within the joint project MOSAIK (Modellbasierte Stadtplanung und Anwendung im Klimawandel/Model-based city planning and application in climate change), the micro-scale urban climate model PALM-4U has been developed under the lead of the Institute of Meteorology and Climatology at the Leibniz Universität Hannover (Maronga et al., 2019). PALM-4U, which is based on the Parallelized Large-Eddy

R. Forkel (✉) · B. Khan · J. Werhahn · M. Mauder
Institute for Meteorology and Climate Research (IMK-IFU), Karlsruhe Institute of Technology (KIT), Kreuzeckbahnstr. 19, 82467 Karlsruhe, Garmisch-Partenkirchen, Germany
e-mail: renate.forkel@kit.edu

S. Banzhaf · E. C. Chan
Institute of Meteorology, Freie Universität Berlin, Berlin, Germany

M. Sühring · F. Kanani-Sühring · B. Maronga · S. Raasch
Institute of Meteorology and Climatology, Leibniz Universität Hannover, Hannover, Germany

K. Ketelsen
Berlin, Germany

M. Kurppa
Institute for Atmospheric and Earth System Research, University of Helsinki, Helsinki, Finland

© The Author(s), under exclusive license to Springer-Verlag GmbH, DE, part of Springer Nature 2021

C. Mensink and V. Matthias (eds.), *Air Pollution Modeling and its Application XXVII*, Springer Proceedings in Complexity, https://doi.org/10.1007/978-3-662-63760-9_41

Simulation Model PALM (Maronga et al., 2015) includes online coupled gas phase chemistry.

An outline of the chemistry implementation in PALM and an application example is shown here.

2 Method

The microscale urban climate model PALM-4U is based on the well-established LES model PALM (Maronga et al., 2015).

In order to obtain the necessary flexibility in the choice of the chemistry mechanisms the gas-phase chemistry was implemented using the Kinetic PreProcessor KPP (Damian et al., 2002; http://people.cs.vt.edu/asandu/Software/Kpp/). Automatic adaptation of KPP generated code for PALM-4U is based on KP4 (Jöckel et al., 2010).

Currently a sample of about ten mechanisms is implemented (Khan et al., 2021) with varying complexity and degree of detail that ranges from the photostationary equilibrium via strongly reduced mechanisms with a simple O_3-NO_2-NO-VOC-HO_x chemistry and a small number of products to larger mechanisms which are typically used in regional air quality models, such as CBM4 (Gery et al., 1989). Additional mechanisms can easily be added by the user. Aerosol is described either by an option for passive aerosol compounds or by the sectional aerosol module SALSA (Kurppa et al., 2019).

Anthropogenic emissions are supplied either by gridded NetCDF files with hourly emissions or traffic emissions are parameterized depending on street type information (e.g. from OpenStreetmap).

3 Results

With PALM-4U it is possible to go beyond the simulation of single street canyons and simulate chemical transformation, advection and deposition of air pollutants in the larger urban canopy. In this context, compromises may be required regarding the degree of detail of the gas-phase chemistry for larger model domains due to the very high computational demands of an LES-based model.

As an example PALM-4U is applied to an area of Berlin around the Ernst-Reuter-Platz for a grid spacing of 10 m. Table 1 gives an overview of the additional computational demand for the transport of the chemical constituents and indicates that transport is more time consuming than the computation of gas phase chemistry.

Figure 1 shows distributions of NO_2 and ozone for a simulation of a 2 km by 2 km area with 10 m grid spacing. In this case PALM with photostationary state chemistry was applied for a clear summer day and traffic emissions based on street types from OpenStreetmap.

Table 1 Additional computational demand for the transport of the chemical compounds and for the full chemistry module: Ratio relative to a simulation without chemistry ('Baseline')

Case/mechanism	Description	Transport only	Transp. + chemistry
Baseline	Meteorology only	1	–
Photostationary	3 compounds, 2 reactions	1.3	1.5
Smog	13 compounds, 12 reactions	2.2	2.9
CBM4	32 compounds, 81 reactions	4.1	6.5

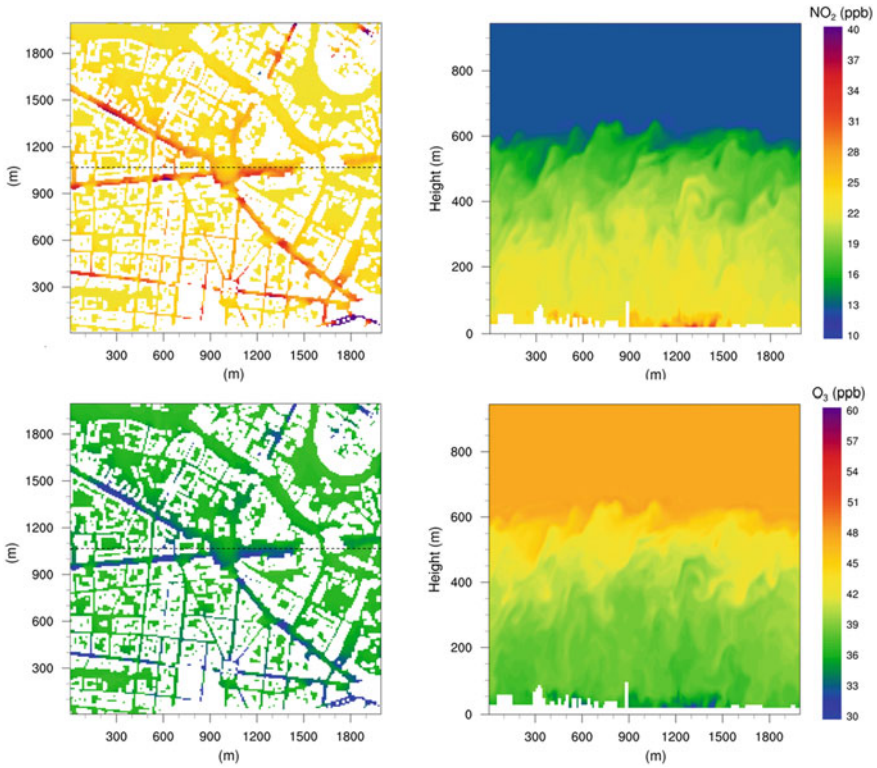

Fig. 1 Concentrations of NO_2 (top) and O_3 (bottom) as simulated for photostationary state chemistry over a 4 km^2 domain around the Ernst-Reuter-Platz in Berlin, Germany, at July 29 2017, 10:00 h. Initial conditions with typical values and cyclic boundary conditions were applied. Horizontal cross sections are displayed 5 m above the ground, vertical cross sections in west–east direction in the middle of the domain as indicated by line in the horizontal cross sections

Figure 2 shows NO_2 and O_3 concentrations from a simulation with lateral boundary conditions from a regional simulation with WRF-Chem. Since turbulent fluctuations are not included in the boundary conditions from the regional simulation, turbulence is weaker than for cyclic boundary conditions, which indicates

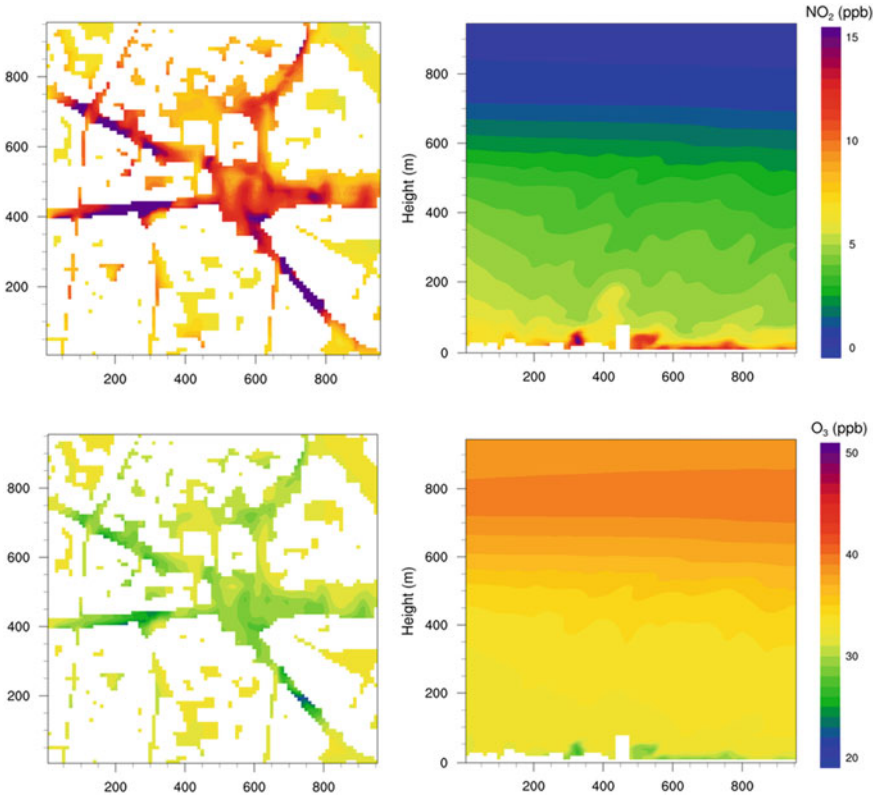

Fig. 2 Same as Fig. 1, but for a 1 km^2 domain and initial conditions and time dependent lateral and top boundary conditions from a WRF-Chem simulation

that a larger domain needs to be considered in order to capture the development of turbulence when boundary conditions from regional simulations are applied.

4 Concluding Remarks

PALM-4U is able to simulate resolved turbulence and chemical transformations—also allowing for more comprehensive chemical mechanisms than shown here—in the urban environment.

The model is still under further development. For example the application of time dependent lateral boundary conditions from WRF-Chem for chemical species and meteorology still needs further testing in order to develop an optimum nesting strategy. Further work will include the effect of shading in the photolysis scheme. Furthermore, it is planned to include domestic heating emissions to the parameterized emissions scheme, biogenic VOC emissions, and wet deposition.

Acknowledgements MOSAIK is funded by the BMBF (German Federal Ministry of Education and Research) under grant 01LP1601 within the framework of Research for Sustainable Development (FONA; www.fona.de).

References

Damian, V., Sandu, A., Potra, F., & Carmichael, G. R. (2002). The kinetic PreProcessor KPP—a software environmentfor solving chemical kinetics. *Computers & Chemical Engineering, 26*, 1567–1579.

Gery, M. W., Whitten, G. Z., Killus, J. P., & Dodge, M. C. (1989). A photochemical kinetics mechanism for urban and regional scale computer modeling. *Journal of Geophysical Research, 94*, 12925–12956.

Jöckel, P., Kerkweg, A., Pozzer, A., Sander, R., Tost, H., Riede, H., Baumgaertner, A., Gromov, S., & Kern, B. (2010). Development cycle 2 of the modular earth submodel system (MESSy2). *Geoscientific Model Development, 3*, 717–752. https://doi.org/10.5194/gmd-3-717-2010

Khan, B., Banzhaf, S., Chan, E. C., Forkel, R., Kanani-Sühring, F., Ketelsen, K., Kurppa, M., Maronga, B., Mauder, M., Raasch, S., Russo, E., Schaap, M., & Sühring, M. (2021). Development of an atmospheric chemistry model coupled to the PALM model system 6.0: implementation and first applications. *Geoscience Model Development, 14*, 1171–1193. https://doi.org/10.5194/gmd-14-1171-2021.

Kurppa, M., Hellsten, A., Roldin, P., Kokkola, H., Tonttila, J., Auvinen, M., Kent, C., Kumar, P., Maronga, B., & Järvi, L. (2019). Implementation of the sectional aerosol module SALSA2.0 into the PALM model system 6.0: Model development and first evaluation. *Geoscientific Model Development, 12*, 1403–1422. https://doi.org/10.5194/gmd-12-1403-2019.

Maronga, B., Gryschka, M., Heinze, R., Hoffmann, F., Kanani-Sühring, F., Keck, M., Ketelsen, K., Letzel, M. O., Sühring, M., & Raasch, S. (2015). The parallelized large-eddy simulation model (PALM) version 4.0 for atmospheric and oceanic flows: Model formulation, recent developments, and future perspectives. *Geoscientific Model Development, 8*, 2515–2551. https://doi.org/10.5194/gmd-8-2515-2015

Maronga, B., Gross, G., Raasch, S., Banzhaf, S., Forkel, R., Heldens, W., Kanani-Sühring, F., Matzarakis, A., Mauder, M., Pavlik, D., Pfafferot, J., Seckmeyer, G., Sieker, H., & Trusilova, K. (2019). Development of a new urban climate model based on the model PALM—Project overview, planned work, and first achievements. *Meteorologische Zeitschrift*. https://doi.org/10.1127/metz/2019/0909

Emergency Local-Scale Dispersion (ELSI) Software

Hana Chaloupecká, Michala Jakubcová, Radka Kellnerová, Zbyněk Jaňour, and Klára Jurčáková

Abstract Operational softwares predicting a situation in case of short-term gas leakages are usually based on simple models because of time demands. But the project COST ES1006 revealed that predictions of these models for the short-term gas leakages can be as inaccurate as one order of magnitude. In contrast, predictions of simple models for continuous sources are not as much inaccurate. Hence, the aim of this paper is to introduce a new operational software for short-term gas leakages. The software is validated on data from experiments of short-term gas releases in a wind tunnel. The data describe the situation in different landscapes, a typical idealized European city centre and a rural area. The model of city centre was composed of buildings with pitched roofs organised into closed courtyards. The model of rural area was simulated by a surface roughness. The puff experiments were repeated a few hundred times for each measurement position at the models to get statistically representative datasets. Concentrations were measured by a fast flame ionisation detector. Ethane was utilized as a tracer gas. The introduced software uses mean concentrations calculated by a simple plume model as one of its inputs. The outputs are probability density functions of puff characteristics. This distinguishes the software from the usually utilized ones in which the outputs are only the ensemble-averaged puff outlines and concentration fields.

Keywords Dispersion model · Wind-tunnel modeling · Puffs

1 Introduction

Chemical industry changes the world. On one hand, it enhances life of many people. But on the other hand, accidents in industry threaten people. An example of such a recent incident is an explosion at a Russian factory in June 2019 (the Guardian, 2019). Chemical accidents are often associated with gas leakages. They usually last

H. Chaloupecká (✉) · M. Jakubcová · R. Kellnerová · Z. Jaňour · K. Jurčáková
Institute of Thermomechanics, Academy of Sciences of the Czech Republic, Prague, Czechia
e-mail: hana.chaloupecka@it.cas.cz

© The Author(s), under exclusive license to Springer-Verlag GmbH, DE, part of Springer Nature 2021

C. Mensink and V. Matthias (eds.), *Air Pollution Modeling and its Application XXVII*, Springer Proceedings in Complexity, https://doi.org/10.1007/978-3-662-63760-9_42

less than one hour, belonging therefore to the turbulent part of the atmospheric spectrum. Hence, many accident scenarios can happen under the same mean conditions (Chaloupecká et al., 2017). During such an accident, emergency services utilize mathematical models to predict how the accident will evolve. The models must be very fast to get the results in a few minutes at latest. Unfortunately, predictions of these models utilized for short-term gas leakages can be as inaccurate as one order of magnitude (Baumann-Stanzer et al., 2015). Hence, the aim of this paper is to introduce a new operational software for short-term gas leakages.

2 Methods

The software ELSI (emergency local-scale dispersion model) is based on a simple model for a continuous source and a new model developed in the project TJ01000383. It uses usual input parameters, such as wind speed, direction, and released material. The input is initially utilized by a simple plume model (e.g. Gaussian model). Then the model output is along with the input data used by a short-term gas dispersion model.

The equations of the short-term gas dispersion model were developed using wind tunnel modeling. In the experiments, scaled models of different landscapes (city centre, rural area; Fig. 1) were utilized. The city centre was composed of buildings with pitched roofs organised into closed courtyards. The model scale was 1:400. The rural area was simulated by roughness. Its scale was 1:650. Concentrations released from a gas source were measured at the pedestrian level by a fast flame ionisation

(a) **b)**

Fig. 1 Scaled models in a wind tunnel: **a** city centre in scale 1:400 with roughness elements and turbulent generators; **b** rural area in scale 1:650 with roughness elements and turbulent generators

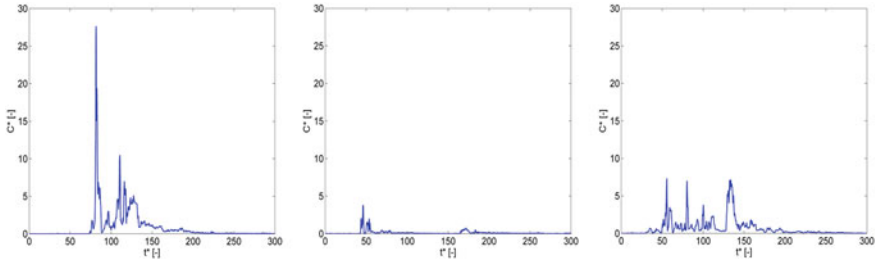

Fig. 2 Examples of concentration measurements at one sampling position for repetitions of the short-term gas release experiment under the same mean conditions (C* denotes dimensionless concentration, t* dimensionless time—VDI, 2000)

detector (Fig. 1a) at individual sampling positions. The results were transformed into dimensionless variables (VDI, 2000). Experiments of results independence on Reynolds number and source intensity were conducted to set appropriate experimental conditions for both models. The experiments of ground level short-term gas releases were repeated a few hundred times for each measurement position to get statistically representative datasets since under the same mean conditions many dispersion scenarios can happen (Fig. 2).

Concentration time series of individual repetitions of the experiments were analysed for each measurement position. In such a way, puff characteristics (arrival time—Chaloupecká et al., 2017, departure time—Chaloupecká et al., 2018, dosage, maximum concentration, high percentiles of concentrations—Chaloupecká et al., 2019) for each repetition and sampling position were obtained for puffs. For each measurement position and puff characteristic, datasets were fitted with a suitable distribution utilizing chi square goodness of fit test (de Sá, 2017). One value of mean concentration was obtained for each measurement position for the continuous source. Finally, relations between parameters of the fitted distributions for puffs and mean concentrations for continuous sources/position of the sampling positions were searched (Chaloupecká et al., 2019).

3 Results

In the software, user writes input data into a table. The model switches between two modes according to the length of a leakage—for long-term and short-term sources of contaminants. In case of the leakage duration shorter than one hour belonging to the turbulent part of the atmospheric spectrum, the model uses the mode for the short-term leakage. In the other case, the model mode is switched to the long-term mode.

The long-term mode of the model utilizes ISC3 model (EPA, 1995). It is a traditionally used Gaussian model for emergency purposes. The model requires a decision

whether the place of leakage is surrounded by an urban or rural area. Making this decision, a set of horizontal and vertical dispersion curves is chosen. While the rural area sub-mode utilizes Pasquill–Gifford relations, the urban development sub-mode utilizes McElroy-Pooler relations. The output of the model for either sub-mode is a plume presenting expected mean concentrations from the source.

The short-term mode of the model utilizes the model for long-term source and the model recalculating the results valid for the long-term source into the ones valid for the short-term source. This sub-model was found utilizing wind tunnel modeling (Chaloupecká et al., 2019). The output of this model mode is a probability density function of individual puff characteristics at each exposed place. Two most important values of the probability density functions are then calculation to ensure clarity and easy interpretability of the output. These values are the most probable value and an extreme value that can cause most complications for emergency services (Fig. 3).

The model is being developed for the emergency services of the Czech Republic. Hence, the model output for either mode is plotted along with a map-background of the Czech Republic. The map is created utilizing open-street-maps data. The user enters GPS coordinates of a leakage place and a size of the surrounding that should be plotted in the model output.

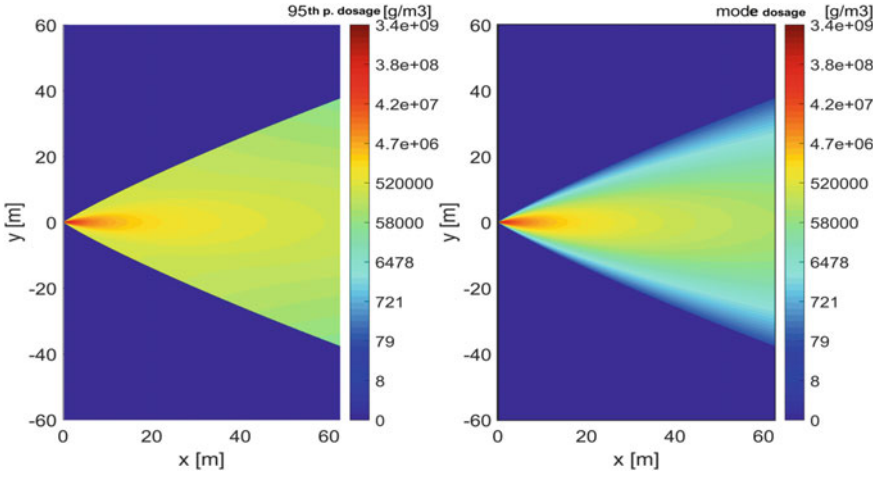

Fig. 3 Example of software output for dosage: 95th percentile and mode. The gas source is placed in [0,0]

4 Conclusion

The paper presents a new software. The software is usable for both, long-term and short-term gas leakages. The model outputs are mean concentrations for the long-term mode. The outputs for the short-term mode are the most probable values and extreme values of puff characteristics.

Acknowledgements The authors would like to thank the Technology Agency of the Czech Republic—TA CR (TJ01000383) and the Institute of Thermomechanics (RVO 61388998) for their financial support.

References

Baumann-Stanzer, K., Andronopoulos, S., Armand, P., Berbekar, E., Efthimiou, G., Fuka, V., Gariazzo, C., Gasparac, G., Harms, F., Hellsten, A., Jurcakova, K., Petrov, A., Rakai, A., Stenzel, S., Tavares ,R., Tinarelli, G., & Trini Castelli, S. (2015). *COST ES1006—Model Evaluation Case Studies, COST Action ES1006*.

Chaloupecká, H., Jaňour, Z., Mikšovský, J., Jurčáková, K., & Kellnerová, R. (2017). Evaluation of a new method for puff arrival time as assessed through wind tunnel modeling. *Process Safety and Environmental Protection, 111*, 194–210.

Chaloupecká, H., Jaňour, Z., Jurčáková, K., & Kellnerová, R. (2018). Sensitivity of puff characteristics to maximum-concentration-based definition of departure time. *Journal of Loss Prevention in the Process Industries, 56*, 242–253.

Chaloupecká, H., Jakubcová, M., Jaňour, Z., Jurčáková, K., & Kellnerová, R. (2019). Equations of a new puff model for idealized urban canopy. *Process Safety and Environmental Protection, 126*, 382–392.

de Sá, J. P. M. (2017). *Applied statistics using SPSS, Statistica, Matlab and R*. Springer.

EPA. (1995). *User's guide for the industrial source complex (ISC3) dispersion models. EPA-454/B-95–003b*. U.S. Environmental Protection Agency.

The Guardian. (2019). *Scores injured after blast at Russian explosives factory*. https://www.theguardian.com/world/2019/jun/01/russia-factory-explosion-kristall-people-injured.

VDI—Verein Deutcher Ingenier. (2000). Environmental meteorology Physical modeling of flow and dispersion processes in the atmospheric boundary layer. *Application of wind tunnels, VDI-Standard: VDI 3783 Blatt 12*, Dusserdorf.

A Modeling Study of the Influence of Biogenic Emissions on Ozone Concentration in a Mediterranean City

Rita Cesari, Riccardo Buccolieri, Alberto Maurizi, and Silvana Di Sabatino

Abstract This work discusses the impact of biogenic VOC (bVOC) emissions from an idealized park of *Quercus ilex* L. on the ozone ground concentration in a Mediterranean city located in southern Italy. Emissions were calculated as a function of leaf temperature and photosynthetically active radiation. Numerical simulations were performed for a week in July 2012 using the local-scale ADMS-Urban model coupled with the mesoscale model BOLCHEM. Preliminary results show that emitted bVOC lead to an increase of ozone concentration in the central hours of the day.

Keywords Biogenic emissions · Mesoscale model BOLCHEM · Local scale model ADMS-urban · Urban air quality · Ozone

1 Introduction

The inclusion of vegetation in urban areas and its effects on city liveability has become an important task in urban planning. Scientific literature mainly addresses the deposition/absorption effect of vegetation (PM_{10} deposition, O_3 uptake) and the influence of vegetation on urban flow (Buccolieri et al., 2018). Recently attention is being devoted to the role of urban vegetation on O_3 formation, especially during

R. Cesari (✉)
National Research Council of Italy, Institute of Atmospheric Sciences and Climate (CNR-ISAC), Strada Prov.Le Lecce-Monteroni Km 1,200, 73100 Lecce, Italy
e-mail: r.cesari@isac.cnr.it

R. Buccolieri
Dipartimento di Scienze e Tecnologie Biologiche ed Ambientali, University of Salento, S.P. 6 Lecce-Monteroni, 73100 Lecce, Italy

A. Maurizi
National Research Council of Italy, Institute for Microelectronics and Microsystems (CNR-IMM), Via Gobetti 101, 40129 Bologna, Italy

S. Di Sabatino
Department of Physics and Astronomy, ALMA MATER STUDIORUM - University of Bologna, Viale Berti Pichat 6/2, 40127 Bologna, Italy

© The Author(s), under exclusive license to Springer-Verlag GmbH, DE, part of Springer Nature 2021

C. Mensink and V. Matthias (eds.), *Air Pollution Modeling and its Application XXVII*, Springer Proceedings in Complexity, https://doi.org/10.1007/978-3-662-63760-9_43

period characterized by high temperature values (Churkina et al., 2017). It is not superfluous to recall that the oxidation process of VOC in the presence of nitrogen oxides (NOx) lead to the formation of ozone (O_3). While most NOx emissions can be ascribed to anthropogenic sources, an important part of VOC is released by vegetation, in particular in the Mediterranean area during summer.

2 Methodology

The aim of the study is the investigation of the impact of vegetation on O_3 ground concentrations. The study area is the city of Lecce located in the southern Italy (Fig. 1), a medium-size city characterized by a Mediterranean climate. As a preliminary work, we analyze an idealised scenario consisting in the inclusion of a park of *Quercus ilex* L. of size 500 m × 500 m in the city.

Numerical simulations have been performed for the period 10–17 July 2012 by means of the local scale advanced-Gaussian model ADMS-Urban (CERC, 2017) coupled with the meso-scale model BOLCHEM (Cesari et al., 2019, 2021). BOLCHEM is an on-line model that includes the photochemical mechanisms SAPRAC90 and the aerosol dynamic model AERO3. ADMS-Urban is a comprehensive system for modeling air quality in large urban areas, cities and towns. It

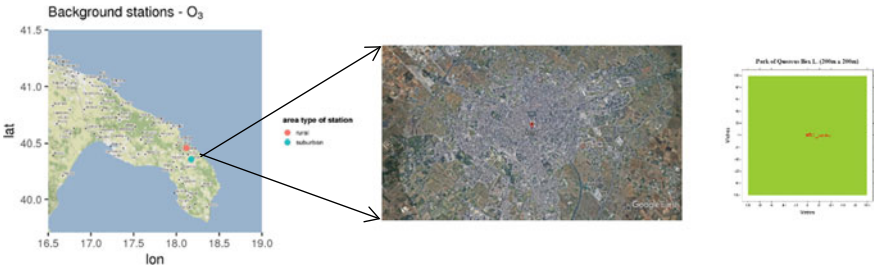

Fig. 1 The city of Lecce (middle), the idealized park (right) and the Apulia region in South-East Italy (left) with indication of background Airbase stations

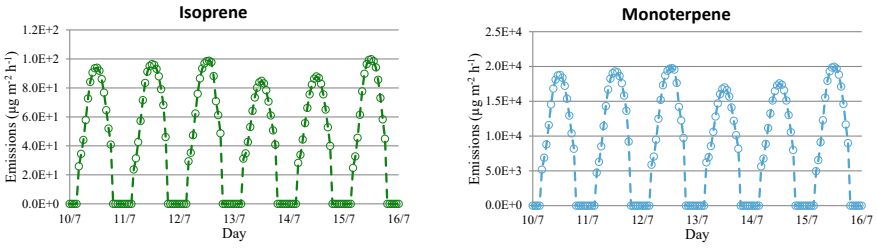

Fig. 2 Emissions of bVOC used as input in ADMS-urban

models NOx chemistry using the 8 reaction Generic Reaction Set (GRS) that includes reactions with ozone and hydrocarbons. Recent examples of coupling are given in Buccolieri et al. (2016) and Cesari et al. (2018).

For bVOC emissions, isoprene and monoterpene have been considered. Following Guenther et al. (1995), the flux F ($\mu g\ m^{-2}\ h^{-1}$) (see Fig. 2) has been calculated as:

$$F = \varepsilon \cdot D \cdot \gamma \tag{1}$$

where ε is the emission rate expected for a particular plant species at a reference temperature of 30 °C and a photosynthetically active radiation (PAR) of 1000 μmol photons (400–700 nm) ($\mu g\ g^{-1}\ h^{-1}$), D is the foliar biomass density (g m^{-2} DW) and γ is a dimensionless environmental correction factor. ε and D are ecosystem dependent, while γ is independent of plant species.

For the *Quercus ilex* L., γ is the product of C_L and C_T, which account respectively for the effect of PAR levels and leaf temperature T:

$$\gamma_{isoprene} = \gamma_{monoterpene} = C_L \times C_T = \frac{\mathrm{aC}_{L1}\mathrm{PAR}}{\sqrt{1 + a^2\mathrm{PAR}^2}} \times \frac{\exp\frac{C_{T1}(T-T_S)}{\mathrm{RT}_S T}}{1 + \exp\frac{C_{T2}(T-T_M)}{\mathrm{RT}_S T}} \tag{2}$$

For isoprene $\varepsilon = 0.1\ \mu g\ g^{-1}\ h^{-1}$ and for monoterpene $\varepsilon = 20\ \mu g\ g^{-1}\ h^{-1}$, $D =$ 500 g m^{-2} DW. a (0.0027), C_{L1} (1.066), β (0.09 K^{-1}), C_{T1} (95,000 J mol^{-1}), C_{T2} (230,000 J mol^{-1}) and T_M (314 K) are empirical coefficients, R is the ideal gas constant (8.314 J K^{-1} mol^{-1}) and T_S is a standard temperature of 303 K (Simpson et al., 1999). PAR levels and leaf temperature T have been obtained from BOLCHEM.

BOLCHEM simulations have been performed at horizontal resolution dx = dy = 0.06°, in a one-way nested grid configuration. Meteorological IC e BC were taken from ECMWF, chemical IC e BC were based on climatological data, anthropogenic emissions were based on TNO 2010, natural emissions were calculated run time.

As for ADMS-Urban local scale simulations, the main input data used to run the model were source (park) parameters and emissions, hourly meteorological data from the ARPA-Puglia meteorological station located in Lecce (http://www.arpa.puglia.it/web/guest/serviziometeo), the surface roughness z_0 for both the study area and the meteorological site (equal to 0.75 m being an urban area), the latitude (40.35°) and the background concentrations of VOC, NO_X and O_3 provided by BOLCHEM. To investigate the effects of VOCs on O_3 formation, sensitivity test by varying the ADMS default value of the weighted reactivity coefficient AROC used by the reaction representing the processes leading to radical production from VOC through photo-oxidation, have been performed.

3 Results

To evaluate BOLCHEM simulations in reproducing the background surface concentration, model results have been compared (see Fig. 3) with data from the European Environmental Agency AIRBASE (https://www.eea.europa.eu/data-and-maps/data/airbase-the-european-air-quality-database-2) at background stations indicated in Fig. 1. To investigate the impact of bVOC emissions from the park of *Quercus ilex*, the percentage variation of O_3 concentrations (averaged along the whole week) between ADMS-Urban (C_{ADMS}) and background (C_{back}) has been calculated at a receptor point located in the centre of the park as follows:$(C_{ADMS} - C_{back}) \times 100/C_{back}$. Figure 4 shows the percentage variation of O_3 concentration obtained with different values of AROC. First the default value (AROC = 0.1) of ADMS has been used. It is an artificial value to take into account that normally the modeling does not include all the VOC contributions. In an urban atmosphere, a good estimate is AROC = 0.0067 (Johnson, 1984). A modified value, calculated as AROC $= \frac{0.1 \times \overline{C}_{bVOC} + 0.0067 \times \overline{C}_{back}}{\overline{C}_{bVOC} + \overline{C}_{back}} =$ 0.06, where $\overline{C}_{bVOC}$ is the bVOC estimated concentration, has been used.

These preliminary results show that, during a summer day, bVOC emitted by the vegetation lead to an increase of O_3 ground concentration in the central hours of the day.

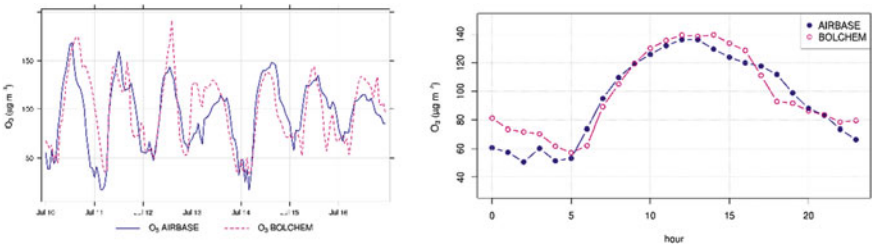

Fig. 3 Comparison of O_3 ground concentration simulated by BOLCHEM with observed values at background stations AIRBASE for the simulation period: hourly value (left) and daily cycle averaged over the two background station (right)

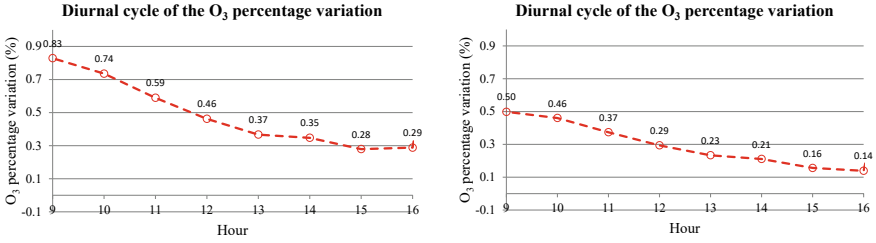

Fig. 4 Relative impact of park emissions on O_3 concentration obtained from the model system ADMS-Urban + BOLCHEM, with AROC = 0.1 (left) and AROC = 0.06 (right)

4 Future Perspectives

This work is a preliminary study analyzing the ability to model the impact of urban vegetation on O_3 production using ADMS-Urban coupled with BOLCHEM. Since bVOC are more reactive than anthropogenic VOC, further investigation on the reactivity coefficient to be used in the GRS scheme and on the photochemical regime of the study area is needed. The inclusion in the ADMS-Urban model of more detailed chemical reactions may be necessary. Further study will also include the effect of dry deposition of O_3 on leaf surfaces and the impact of different plant species on O_3 production.

Acknowledgements We kindly acknowledge CERC for making available ADMS-Urban for this study and for useful discussion about the GRS scheme.

References

Buccolieri, R., Cesari, R., Dinoi, A., Maurizi, A., Tampieri, F., & Di Sabatino, S. (2016). Impact of ship emissions on local air quality in a Mediterranean city's harbour after the European sulphur directive. *International Journal of Environment and Pollution, 59*, 30–42.

Buccolieri, R., Santiago, J.-L., Rivas, E., & Sanchez, B. (2018). Review on urban tree modeling in CFD simulations: Aerodynamic, deposition and thermal effects. *Urban Forestry & Urban Greening, 31*, 212–220.

CERC. (2017). *ADMS-Urban Model*. Cambridge Environmental Research Consultant, Cambridge. http://www.cerc.co.uk

Cesari, R., Buccolieri, R., Maurizi, A., Landi, T., & Di Sabatino, S. (2018). Influence of ship emissions on ozone concentration in a Mediterranean area: A modeling approach. In *Air Pollution Modeling and its Application XXV, Springer Proceedings in Complexity* (pp. 317–321).

Cesari, R., Landi, T., & Maurizi, A. (2019). The coupled chemistry-meteorology model BOLCHEM: An application to air pollution in the Po Valley (Italy) hot spot. *International Journal of Environment and Pollution, 65*, 1–24.

Cesari, R., Landi, T. C., D'Isidoro, M., Mircea, M., Russo, F., Malguzzi, P., Tampieri, F., et al. (2021). The on-line integrated mesoscale chemistry model BOLCHEM. *Atmosphere*, *12*, 192.

Churkina, G., Kuik, F., Bonn, B., Lauer, A., Grote, R., Tomiak, K., & Butler, T. M. (2017). Effect of VOC emissions from vegetation on air quality in berlin during a heatwave. *Environmental Science & Technology, 51*, 6120–6130.

Guenther, A., Hewitt, C., Erickson, D., Fall, R., Geron, C., Graedel, T., Harley, P., Klinger, L., Lerdau, M., McKay, W., Pierce, T., Scholes, B., Steinbrecher, R., Tallamraju, R., Taylor, J., & Zimmerman, P. (1995). A global model of natural volatile organic compound emissions. *Journal of Geophysical Research-Atmospheres, 100*, 8873–8892.

Johnson, G. M. (1984). A simple model for predicting the ozone concentration of ambient air. In *Proceedings of 8th International Clean Air Conference*, Melbourne, 6–11 May (pp. 715–731).

Simpson, D., Winiwarter, W., Börjesson, G., Cinderby, S., Ferreiro, A., Guenther, A., Hewitt, C. N., et al. (1999). Inventorying emissions from nature in Europe. *Journal of Geophysical Research-Atmospheres, 104*, 8113–8152.

A CFD Model to Assess the Impact of Cruise Ship Emissions in the Port of Naples

Domenico Toscano, Benedetto Mele, and Fabio Murena

Abstract The port of Naples is one the most important in the Mediterranean Sea for passengers' traffic. Due to the proximity of the port to the urban area, ship emissions can have an important impact on air pollution in Naples. The presence of buildings very near to the docks can modify significantly the wind field and, as a consequence, the transport of pollutants emitted when ships are at berth. Models (Calpuff, SPRAY) normally adopted to assess the impact of ship emissions do not take in account this effect. For this reason, a CFD model was developed to assess the impact of cruise ship emissions during the hoteling phase in the port of Naples. A calculation domain of about 7 $km^2 \times 1$ km height with 10 million cells has been created. Unsteady CFD simulations have been carried out adopting the Scale Adaptive Simulation (SAS) hybrid model that allows a satisfactory accuracy in the calculation of the turbulence. In particular, the impact of SO_2 emissions on seafront building facades and inside the port area are evaluated. Some differences between the results of the CFD model and those obtained by CALPUFF are observed. The CFD model, taking in count the presence of buildings, gives more reliable results about the dispersion of pollutants.

1 Introduction

Over the last years, dispersion models have often been used to assess the impact on air quality of ship emissions in ports. The most commonly dispersion models used are Gaussian models (CALPUFF, AERMOD), or Lagrangian models (SPRAY,

D. Toscano (✉) · F. Murena
Chemical, Materials and Production Engineering Department, University of Naples "Federico II", Naples, Italy
e-mail: domenico.toscano@unina.it

F. Murena
e-mail: murena@unina.it

B. Mele
Industrial Engineering Department, University of Naples "Federico II", Naples, Italy
e-mail: benmele@unina.it

© The Author(s), under exclusive license to Springer-Verlag GmbH, DE, part of Springer Nature 2021

C. Mensink and V. Matthias (eds.), *Air Pollution Modeling and its Application XXVII*, Springer Proceedings in Complexity, https://doi.org/10.1007/978-3-662-63760-9_44

HYSPLIT). Poplawski et al. (2011) and Murena et al. (2018) used CALPUFF to investigate the impact of cruise ships emissions in James Bay (Canada) and on the urban area of Naples (Italy) respectively. Gariazzo et al. (2007) used a Lagrangian particle model to assess the impact of harbour, industrial and urban activities on air quality in the Taranto area (Italy). Urban canopies due to their complexity can influence significantly the dispersion of atmospheric pollutants. Above reported models take in count the effect of the presence of buildings mainly in terms of roughness. Urban dispersion models (ADMS, SIRANE) can better simulate dispersion inside even large urban areas. However, the most precise description can be achieved only with Computational Fluid Dynamics (CFD) models that require a larger amount of resources in terms of analyst skill and CPU time. Due to the increase of computer performances, CFD models are now applied to simulate, at local scale, the dispersion of pollutant also in urban areas (Di Sabatino et al., 2007; Gousseau et al., 2011). However, because of the varsity and complexity of areas involved, the use of CFD models to assess the impact of ship emissions in ports, is still quite rare.

In the case of the port of Naples, there is the presence of buildings in face of the port, that even though, do not determine building downwash effects, can influence significantly the wind flow. For this reason, we have developed a CFD model and compared the results with those obtained with CALPUFF.

2 Methodology

A CFD model has been generated for the prediction of pollutants dispersion deriving from the shipping traffic in the port of Naples. The computational domain extends for an area of about 7 km^2 with a height of 1 km and counting about 10 million hexahedral cells with refinement at the walls. The unsteady incompressible formulation of Navier–Stokes equations has been adopted with species transport (air-SO_2 mixture) neglecting chemical reactions. Turbulence in the numerical simulations has been modelled adopting the SAS (Scale Adaptive Simulation) model by Menter and Egorov (2010). The Scale-Adaptive Simulation (SAS) is a hybrid method that switch between an LES and URANS approach on the basis of the computed cell Courant numer (CFL = 1 LES, CFL > 1 URANS). It has been proved to be an optimal compromise between the accurate resolution of the turbulent spectrum and computational effort requirements. The SAS model has been used with success by Murena and Mele (2014) and (2016) for street canyon flows. Second order central numerical scheme in space and time has been used. The boundary conditions are velocity inlet at the inflow and outflow conditions with extrapolated variables at the outlet that depend on the wind direction with respect to the computational domain. Pressure outlet boundary condition has been set on the top of computational domain and mass flow inlet at the source points (funnels of the ships). The natural convection due to the difference of temperatures in the flow field has been taken into account adopting a gas model with variable density due to temperature (incompressible ideal gas model) activating the gravitational forces. Furthermore, the flow field has been

initialized with ISA (International Standard Atmosphere) temperature and pressure conditions at temperate latitudes. Also, the boundary conditions for temperature and pressure at the side and top of the computational domain have been set at ISA conditions. The results of CFD model are compared with those obtained with CALPUFF, a multi-layer, multi-species non-steady-state puff dispersion model. The simulations were conducted with a wind blowing from SE with a speed of 2 m/s, because this is the most impacting case for buildings laying in front of the port. For the same reason, the simultaneous presence of three cruise ships at hotelling was considered. As pollutant we have selected SO_X because it is a marker of ship emissions. SOx emission rates were calculated as the product of the emission factors for the power applied in the hotelling phase by each ship. The S content in the fuel was assumed at 0.1% by weight following a resolution by the Port Authority of Naples.

3 Results

SO_2 concentration at ground level are reported in Figs. 1 and 2. Contour maps obtained with CFD and CALPUFF are similar. However, higher concentrations are obtained with CALPUFF. In fact, the maximum SO_2 concentration on the ground is $\approx$5 $\mu g/m^3$ by CFD and $\approx$10 $\mu g/m^3$ by CALPUFF.

Higher differences are observed considering counter maps on a vertical surface in correspondence of the facades of buildings laying in front of the port (Figs. 3 and 4). Two of the three plumes emitted by funnels collapse in a single plume (on the right in Figs. 3 and 4). The dispersion of the plume on the left does not impact with the buildings and is estimated in a similar way by the two models. The presence of buildings determines the elevation of the plume on the right in Figs. 3 and 4. This phenomenon is captured by the CFD model but not by CALPUFF. In fact, the center of the plume is at about 180 m height for CFD and 120 m for CALPUFF. A significant difference is also observed in the maximum concentration $\approx$130 $\mu g/m^3$ by

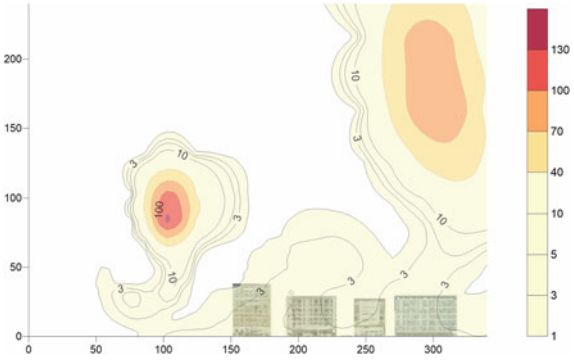

Fig. 1 CFD—contour map of SO_2 concentration at front port facades of first line buildings

Fig. 2 CFD—distribution of SO_2 concentration [$\mu g/m^3$] in the calculation domain at ground level

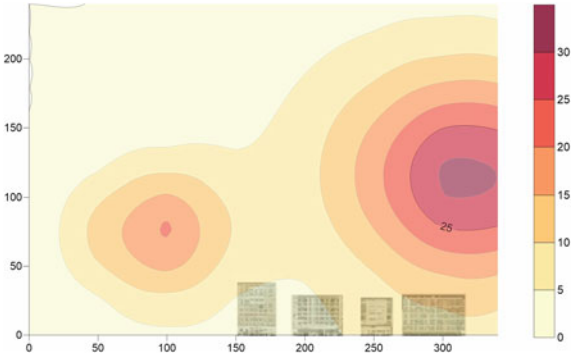

Fig. 3 CALPUFF—contour map of SO_2 concentration at front port facades of first line buildings

CFD and ≈30 $\mu g/m^3$ by CALPUFF. This difference in SO_2 levels may be attributed to a less effective dispersion in the horizontal direction showed by CFD simulations. This effect could depend on an inappropriate simulation by CFD of the horizontal mixing mechanism. The results indicate that the presence of buildings with height of 30–40 m at about 150–200 m from cruise ships docks can influence significantly the dispersion of atmospheric pollutant emitted during the hoteling phase and would be better considered in the assessment of port emissions on the urban areas.

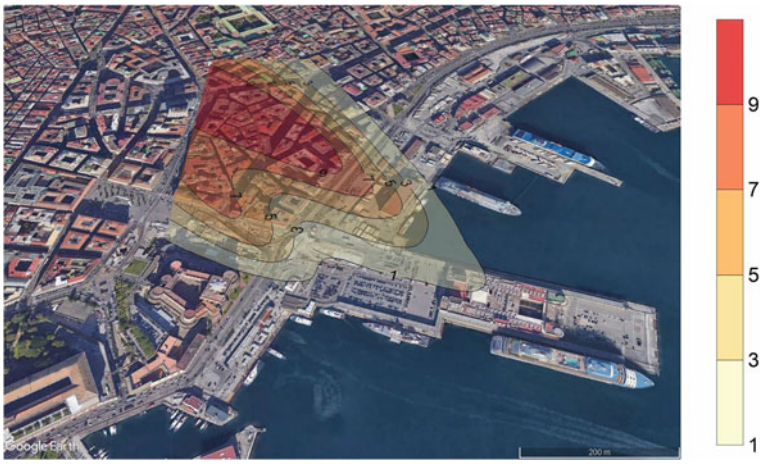

Fig. 4 CALPUFF—Distribution of SO_2 concentration [$\mu g/m^3$] in the calculation domain at ground level

References

Di Sabatino, S., Buccolieri, R., Pulvirenti, B., & Britter, R. (2007). Simulations of pollutant dispersion within idealised urban-type geometries with CFD and integral models. *Atmospheric Environment, 41*(37), 8316–8329.

Gariazzo, C., Papaleo, V., Pelliccioni, A., Calori, G., Radice, P., & Tinarelli, G. (2007). Application of a Lagrangian particle model to assess the impact of harbour, industrial and urban activities on air quality in the Taranto area Italy. *Atmospheric Environment, 41*(30), 6432–6444.

Gousseau, P., Blocken, B., Stathopoulos, T., & Van Heijst, G. J. F. (2011). CFD simulation of near-field pollutant dispersion on a high-resolution grid: A case study by LES and RANS for a building group in downtown Montreal. *Atmospheric Environment, 45*(2), 428–438.

Menter, F. R., & Egorov, Y. (2010). The scale-adaptive simulation method for unsteady turbulent flow predictions. Part 1: Theory and model description. *Flow, Turbulence and Combustion, 85*(1), 113–138.

Murena, F., & Mele, B. (2014). Effect of short–time variations of wind velocity on mass transfer rate between street canyons and the atmospheric boundary layer. *Atmospheric Pollution Research, 5*(3), 484–490.

Murena, F., & Mele, B. (2016). Effect of balconies on air quality in deep street canyons. *Atmospheric Pollution Research, 7*(6), 1004–1012.

Murena, F., Mocerino, L., Quaranta, F., & Toscano, D. (2018). Impact on air quality of cruise ship emissions in Naples, Italy. *Atmospheric Environment, 187*, 70–83.

Poplawski, K., Setton, E., McEwen, B., Hrebenyk, D., Graham, M., & Keller, P. (2011). Impact of cruise ship emissions in Victoria, BC Canada. *Atmospheric Environment, 45*(4), 824–833.

Study of the Effects of Urban Vegetation on Thermal Comfort in a Neighbourhood of Lahti (Finland)

Elisa Gatto, Riccardo Buccolieri, Eeva Aarrevaara, Leonardo Perronace, Rohinton Emmanuel, Zhi Gao, and Jose Luis Santiago

Abstract This study investigates the effect of urban vegetation on thermal comfort in a neighbourhood of Lahti (Finland) by means of modeling simulations performed with the Computational Fluid Dynamics-based and microclimate model ENVI-met. A scenario without vegetation and the current one (with vegetation) are considered to assess the effects of vegetation in different seasons and provide suggestions for thermal comfort improvement.

1 Introduction

Urban vegetation could be a strategy to improve microclimate, air quality and mitigate the effects of climate change and Urban Heat Island (UHI). A careful planning of vegetation planting is necessary because its effects are strictly dependent on the

E. Gatto (✉) · R. Buccolieri
Dipartimento di Scienze e Tecnologie Biologiche ed Ambientali, University of Salento, Lecce, Italy
e-mail: elisa.gatto@unisalento.it

R. Buccolieri
e-mail: riccardo.buccolieri@unisalento.it

E. Aarrevaara
Faculty of Technology, LAB University of Applied Sciences, Lahti, Finland

L. Perronace
Fagus Lab S.R.L, Roma, Italy

R. Emmanuel
School of Computing, Engineering and Built Environment, Glasgow Caledonian University, Galsgow, UK

Z. Gao
School of Architecture and Urban Planning, Nanjing University, Nanjing, China

J. L. Santiago
Department of Environment, CIEMAT, Madrid, Spain

© The Author(s), under exclusive license to Springer-Verlag GmbH, DE, part of Springer Nature 2021

C. Mensink and V. Matthias (eds.), *Air Pollution Modeling and its Application XXVII*, Springer Proceedings in Complexity, https://doi.org/10.1007/978-3-662-63760-9_45

interaction of local factors, such as site geometry and meteorological conditions. This study aims to investigate the effects of urban vegetation on the microclimate through modeling simulations in a neighborhood of Lathi (Finland) under typical winter and summer days. Specifically, the Computational Fluid Dynamics (CFD)-based and microclimate model ENVI-met is employed to evaluate the optimum scenarios tailored to the improvement of thermal.

2 Methodology

2.1 Description of the Study Neighborhood

The neighborhood analyzed here is located in Lahti, a medium-size city of southern Finland, representative, for the climate and architectural design, of European Northern cities (Fig. 1, top left). The neighborhood (referred to as "Aleksanterinkatu"

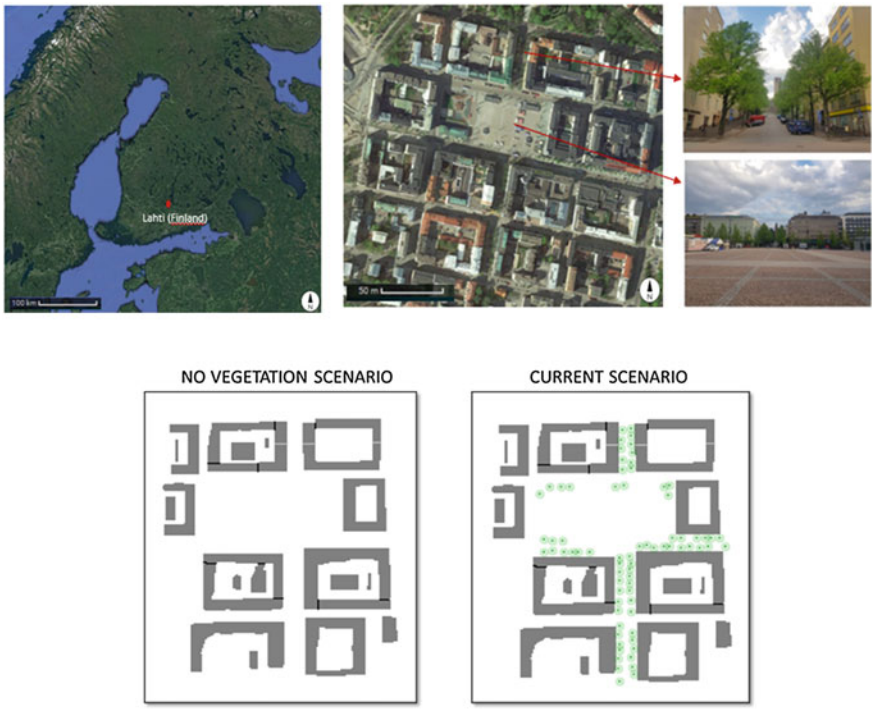

Fig. 1 Top left: the city of Lahti located in southern Finland; top center: the study area located in the city center and here referred to as "Aleksanterinkatu" (from Google Earth); top right: some pictures of *Tilia cordata* Mill. (top) and of the square inside the study area; bottom: investigated scenarios

hereinafter), is located in the city center (Fig. 1, bottom left). Buildings, despite the different heights, are distributed in a rather regular pattern. The neighborhood is characterized by buildings heights ranging from 16 to 22 m and by rows of *Tilia cordata* Mill., with an average height of 15 m and a Leaf Area Density (LAD) equal to 1.00 m^2m^{-3} (Fig. 1, right). Two scenarios have been investigated (Fig. 1): (i) the current scenario, (ii) a no vegetation scenario for comparison and evaluation of the effects of vegetation.

2.2 Numerical Simulations

ENVI-met is a prognostic non-hydrostatic model for the simulation of surface-plant-air interactions composed by a 3D main model and in addition a one dimensional (1D) atmospheric boundary layer (ABL) model which extends from the ground surface up to 2500 m. ENVI-met has a typical horizontal resolution from 0.5 to 5 m and a typical time frame of 24–48 h with a time step of 1–5 s, which meet the criteria for the accurate simulation of physical processes, suitable for microclimate studies at the neighborhood scale. The atmospheric system solves Reynolds-averaged Navier–Stokes equations using a turbulence closure k-ε model. See the ENVI-met official website (http://www.envi-met.info/doku.php?id=kb:review) for a complete review of validation studies.

The 3D simulation area (computational domain) has a dimension of 400 m × 450 m and a vertical height of 30 m. The area was meshed with a grid resolution of 2 m × 2 m × 2 m, except for the lowest five cells whose vertical resolution was 0.4 m. To improve model accuracy and stability, 5 nesting grids were also employed. Hourly air temperature and relative humidity were forced at the model boundary to drive the simulation with meteorological input obtained from a 10 m high meteorological station (FMIdata®Finnish Meteorological Institute) located at about 4 km far from the study area. 18 February and 17 July were selected as representative of a typical winter and summer day. The cyclic type method was selected for the Lateral Boundary Conditions (LBC) because the study area is located in the city where the neighborhood space layout is similar to the residential district. For each case, ENVI-met was run for a 16 h period, starting at 06:00 (see Table 1). The model set-up was previously validated with field measurements (Buccolieri et al., 2019).

3 Results

3.1 Spatially-Averaged Values of Microclimate Variables

Air temperature, relative humidity, wind velocity and mean radiant temperature were obtained from ENVI-met at 1.4 m (pedestrian level) and used to calculate

Table 1 Initial and boundary conditions used in ENVI-met simulations

Parameter	Definition	Value
Simulation time	Start date	18 February 2018 (winter) 17 July 2018 (summer)
	Start of simulation (h)	06:00
	Total simulation time	16 h (4 h spin-up + 12 h)
Meteorological conditions	Wind speed	1.1 m/s
	Wind direction	0°
	Temperature of atmosphere (forced)	Daily profile
	Roughness length	0.1 (urban area)
	Relative humidity (%) (forced)	Daily profile
Computational domain and grid	Grid cells (x, y, z)	200 × 225 × 15
	δx × δy × δz	2 m × 2 m × 2 m (equidistant: 5 cells close to the ground)
	Nesting grids	5
	Boundary conditions	Cyclic

the predicted mean vote PMV (Jendritzky & Nübler, 1981) for the evaluation of the thermal comfort. It takes into consideration also the personal factors heat resistance of clothing and human activity. Outdoor PMV ranges from −4 (very cold) to 4 (very hot), with 0 being neutral.

The spatial distribution of PMV is shown in Fig. 2 for all the scenarios investigated at 11:00. As expected, since the simulations were performed for a hot summer day, mean values are high, indicating that overall the area is characterized by very hot (PMV = 4) to hot (PMV = 3) conditions.

The presence of vegetation leads to an average PMV reduction in summer and an increase in winter day. The average improvement of thermal comfort in summer is equal to 0.1 in the current scenario and it is more evident looking at the maximum and minimum values and occurs especially within the street canyons due to the effect on air temperature and relative humidity (through shading and evapotranspiration) and wind velocity (through obstruction to the wind). In winter, an increase equal to 0.1 and so an improvement of thermal comfort is appreciated. This improvement, equal to 0.30, is larger in the street canyon at the bottom of the study area.

4 Conclusions

This study analyses the effect of vegetation on thermal comfort in the city of Lahti. Results show that the vegetation has an effect on thermal comfort where it is located, but the effect can spread over the whole neighbourhood. The presence of trees can

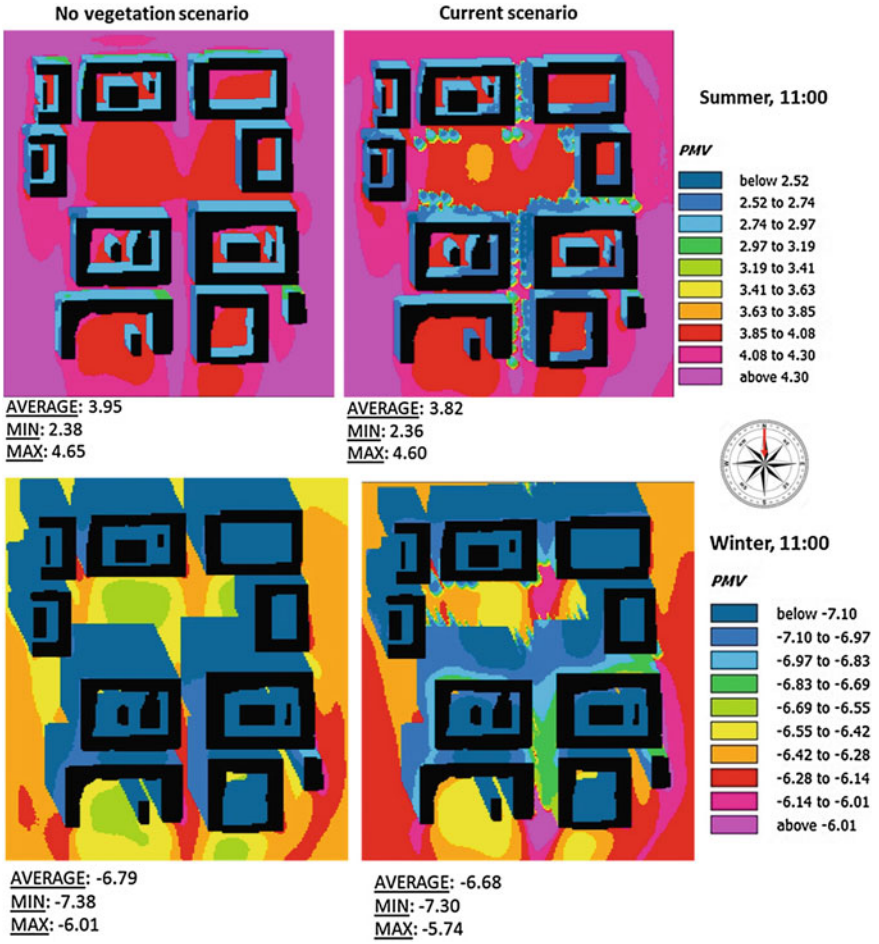

Fig. 2 PMV spatial distribution for the no veg (left) and current (right) scenarios at 11:00

improve the thermal comfort both in summer and winter. However, the effects of vegetation are highly dependent on the urban geometry. In fact, different effects are observed inside street canyons both in winter and summer day. We also expect further different effects by changing the wind direction and speed. Therefore, it is necessary to study the effects of vegetation on a case-by-case basis. This study will compare, in the near future, with those obtained for the city of Lecce, as well as other urban and suburban neighbourhoods in order to provide adaptation and mitigation solutions to improve citizens' quality of life and urban planners' decisions.

References

Buccolieri, R., Gatto, E., Ippolito, F., Rispoli, G., De Luca, V., Gao, Z., Aarrevaara, E., & Perronace, L. (2019). Study of the effects of urban vegetation on the microclimate and thermal comfort in neighbourhoods of Lecce (Italy). In *19th International Conference on Harmonisation within Atmospheric Dispersion Modeling for Regulatory Purposes*, 3–6 June 2019, Bruges, Belgium.

Jendritzky, G., & Nübler, W. (1981). A model analysing the urban thermal environment in physiologically significant terms. *Archives for Meteorology, Geophysics and Bioclimatology Series B, 29*, 313–326.

WRF/Chem Evaluation and Application for Impacts Assessment of Point Sources

Roberto San José, Juan L. Pérez, Libia Pérez, and Rosa Maria Gonzalez Barras

Abstract The objectives of this research are to analyze the contribution of two elevated point sources (plants for waste or residual treatment) to the Madrid air quality. Identifying in time and space the percentage of in mission concentrations due to the industrial plants. And the evaluation and benchmarking the simulations results using the statistics and criteria defined by DELTA tool (European Environment Agency and the European Commission Joint Research Centre) against agreed quality standards. The air quality system is based on WRF/Chem and the emission model EMIMO (UPM). The zero-out emission methodology (ON/OFF) has been used. We present the results for one year simulation with 1 km of spatial resolution. EMIMO-WRF/Chem fulfils all criteria for correlation, bias, standard deviation and RMSEu <1 (100% of satiations) for O_3 and NO_2, so it can be used for applications. The simulations showed that point source emissions were contributors to NO_2 exceedances in the nonattainment area of Madrid city. Also the sources reduced the number of O_3 exceedances. The differences (OFF–ON) distributions show heterogeneity patterns in spatial and temporal scales due to significant topographic diversity and meteorological variations over short distances. The magnitude of these concentration changes is potentially significant and illustrates that accurate of the EMIMO-WRF/Chem tool and how it can be used in forecasting mode to provide meaningful and policy-relevant information for the stakeholders. The results show that the modeling system is capable to determine the impact of the emission sources in real-time and forecasting mode.

R. S. José (✉) · J. L. Pérez · L. Pérez
Environmental Software and Modeling Group, Computer Science School, Technical University of Madrid (UPM), Madrid, Spain
e-mail: roberto@fi.upm.es

J. L. Pérez
e-mail: jlperez@fi.upm.es

L. Pérez
e-mail: lperez@fi.upm.es

R. M. G. Barras
Department of Physics and Meteorology, Faculty of Physics, Complutense University of Madrid (UCM), Ciudad Universitaria, Madrid, Spain
e-mail: rgbarras@fis.ucm.es

© The Author(s), under exclusive license to Springer-Verlag GmbH, DE, part of Springer Nature 2021

C. Mensink and V. Matthias (eds.), *Air Pollution Modeling and its Application XXVII*, Springer Proceedings in Complexity, https://doi.org/10.1007/978-3-662-63760-9_46

1 Introduction

A typical methodology for knowing the impact on air quality of the emission sources is the well-known "brute force" (BF) method, in which the results of a "base" air quality simulation are compared with the results of a changed simulation using an altered parameter or data set. The traditional zero-out method (a case of BF) involves running the model twice: first with base scenario emissions (ON simulation) and then without emissions where the input of emissions from the sources to be studied is set to zero (OFFs simulations). The differences between the two simulations (OFF–ON) estimate the impacts or contributions of the sources. This approach has been used extensively in the past to isolate the response to changes in inputs from complex, non-linear systems such as air pollution (Samali et al.).

In this paper, the methodology for the evaluation of air quality modeling systems presented at Thunis et al. (2013) and Pernigotti et al. (2013), and implemented in the Delta Tool software (European Environment Agency and Joint Research Centre of the European Commission) has been applied. The objective is to evaluate and benchmark the results of the simulations using the statistics and criteria defined by the Delta Tool against the agreed quality standards to validate the contributions of the sources that are extracted from the analysis of the simulations.

2 Methodology

The WRF/Chem modeling system (Grell et al., 2005), which is commonly used in air quality prediction studies, was implemented to simulate meteorology as well as the dispersion and transport of pollutants in Madrid during 2016. The model has been configured with three unidirectional domains of 25.5 and 1 km of network separation representing Spain, the Community of Madrid and the city of Madrid with its surroundings. In this work, we have configured WRF/Chem to simulate using the same parameters as in the ES1 simulations carried out for the second phase of the AQMII (Air Qualiy Modeling International Initiative) (San Jose et al., 2015). This configuration has already been tested and evaluated with very good results in different applications. Anthropogenic emissions data are obtained from a top-down strategy implemented in the EMIMO emission model, developed by UPM (San Jose et al., 2008).

Two elevated point sources have been analysed in this study. Both sources are companies whose activity is focused on waste treatment. The first source (S1) emitted 282,713 kg/year of NO_x in 2016 after treating 2095 tons/year of waste. The second point source (S2) emitted 177,213 kg/year of NO_x and treated 216,907 tons/year of waste. The data are public and can be obtained from the European Pollutant Release and Transfer Register (E-PRTR) which provides key environmental data easily accessible from industrial sites in EU Member States. The base case or simulations ON, all sources emit. The next is the OFF simulation, whose emissions from sources 1 and

2 are set to zero. Differences between OFF and ON (OFF–ON) simulations report impacts of the two sources when working together. Finally, the simulations OFF1, emissions from source 1 are reset to zero and OFF2 where emissions from source 2 are reset to zero, run to discover the individual impacts of sources on air pollution, which are calculated by making the differences OFF1-ON and OFF2-ON.

3 Results

The modeling system has been comprehensively evaluated to ensure reasonable estimates of concentrations of the pollutants involved. For the evaluation, data from 23 monitoring stations of the Madrid region's air quality network and 24 monitoring stations of the Madrid city's air quality network were used, so that a total of 47 different sites were used to compare hourly modelled concentrations with the measured values. We have developed several R scripts that implement the main statistical parameters (i. e. bias, root mean square error, correlation coefficient, standard deviation) as well as different types of diagrams (scatterplot, time-series, Taylor and Target graphs) based on Delta Tool software, that is not scriptable (no automation process, no web services …). Figure 1 shows the Taylor diagrams for NO_2 and O_3. It allows different statistical indicators to be represented on a single graph—the correlation coefficient R2, the CRMSE of centralised mean-square root error (calculated by the pairing of observations and predictions in time and space), and the standard deviation coefficient between model and observations (Sigma_M/Sigma_O). Figure 1 that there are no large differences between the values modeled and observed in terms of variability measured by the three most important statisticians. We can observe that

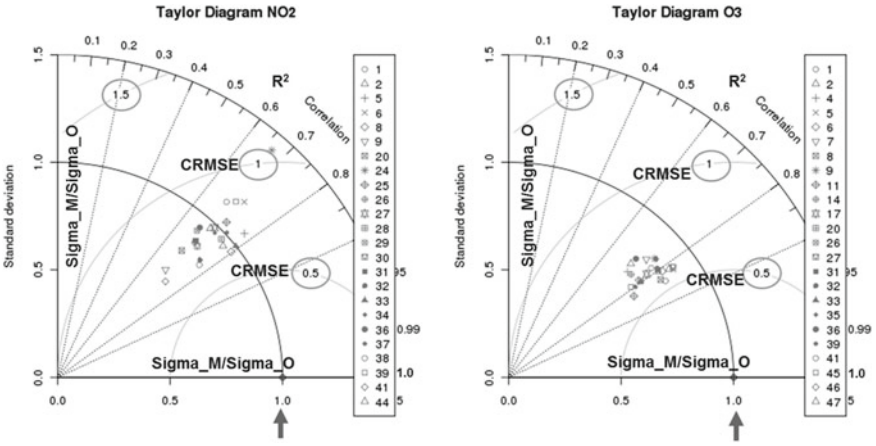

Fig. 1 Taylor diagrams displaying WRF/Chem model performance for NO_2 (left) and O3 (right) for 47 monitoring stations locations. Ideal model is indicated by the arrow

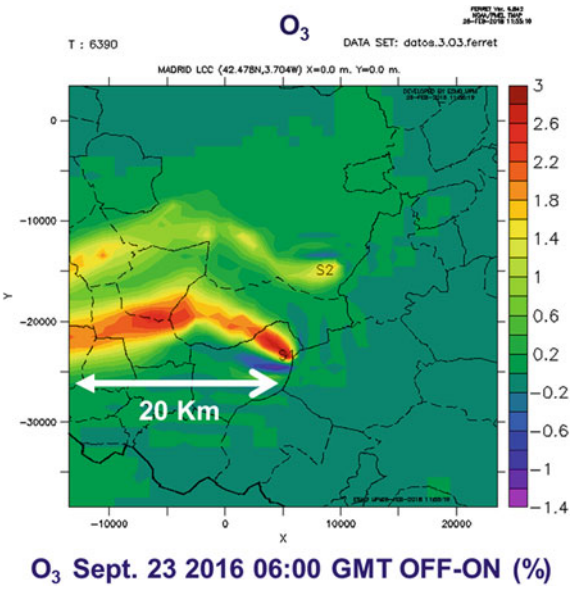

Fig. 2 Spatial distributions of hourly percentage contributions to the concentrations of O3 WRF/Chem 1 km. September 23, 2016 06:00 GMT

in the case of NO_2, the values of R2 are between 0.7 and 0.8, for O_3 all the locations of the stations are very close to 0.8. In all station locations, the mean square error of the central root (CRMSE) is less than 1 and in the case of O_3 the values are very close to 0.5. Only modelled ozone values tend to be less variable (standard deviation) than observations (Sigma_M/Sigma_O >0.5 and <1.0).

Figure 2 shows the spatial distribution of the impacts of emissions from sources S1 and S2 on the pollutant O_3. Positive impacts of up to 3% and negative impacts of −1.4% can be observed. This implies that not emitting NO_x in some areas would increase O_3 concentrations and in others it would be reduced, which can be modelled thanks to the non-linear chemical model of the system. It is also important to note how the impacts occur at points far from the emission sources, in this case impacts have been observed 20 km away from the emitting sources, which matches the end of the computational domain. If computational resources were available, it would be useful to design a more extended domain in order to capture all the areas affected by the two industries.

4 Conclusion

The impact of two sources of emissions (plants for waste treatment) on air quality concentrations in the Madrid area was investigated for one year using four simulations carried out alternately with emissions (ON) and without consideration of point emissions (OFF, OFF1, OFF2). The modeling system has been evaluated through a

series of R-scripts developed based on Delta Tool software that is used to diagnose and evaluate the performance of air quality models. The assessment of performance has been very satisfactory.

The differences (OFF–ON) represented spatially, shows a large heterogeneity of impacts. These high variations between relatively close locations are caused by the high diversity of the topography in the modelled area, which causes differences in meteorological flows that affect concentrations. The range of changes in concentration is significant enough to demonstrate the accuracy and utility of the presented EMIMO-WRF/Chem tool that can be used to provide relevant information to the authorities when using the forecast mode.

Acknowledgements The UPM authors acknowledge the computer resources and technical assistance provided by the Centro de Supercomputación y Visualización de Madrid (CeSViMa). The UPM authors thankfully acknowledge the computer resources, technical expertise and assistance provided by the Red Española de Supercomputación.).

References

Grell, G., Peckham, S., Schmitz, R., McKeen, S., Frost, G., Skamarock, W., & Eder, B. (2005). Fully coupled "online" chemistry within the WRF model. *Atmospheric Environment, 39*(37), 6957–6975. https://doi.org/10.1016/j.atmosenv.2005.04.027

Pernigotti, D., Gerboles, M., Belis, C., & Thunis, P. (2013). Model quality objectives based on measurement uncertainty. Part II: NO2 and PM10. *Atmospheric Environment, 79*, 869–878. https://doi.org/10.1016/j.atmosenv.2013.07.045

San José, R., Pérez, J., Morant, J., & González, R. (2008). European operational air quality forecasting system by using MM5–CMAQ–EMIMO tool. *Simulation Modeling Practice and Theory, 16*(10), 1534–1540. https://doi.org/10.1016/j.simpat.2007.11.021

San José, R., Pérez, J., Balzarini, A., Baró, R., Curci, G., Forkel, R., et al. (2015). Sensitivity of feedback effects in CBMZ/MOSAIC chemical mechanism. *Atmospheric Environment, 115*, 646–656. https://doi.org/10.1016/j.atmosenv.2015.04.030

Thunis, P., Pernigotti, D., & Gerboles, M. (2013). Model quality objectives based on measurement uncertainty. *Part i: Ozone. Atmospheric Environment, 79*, 861–868. https://doi.org/10.1016/j.atmosenv.2013.05.018

A New Methodology to Propagate Uncertainties from Regional Climate Models to Urban Impact Model: Feasibility Study

François Duchêne, Bert Van Schaeybroeck, Steven Caluwaerts, Andy Delcloo, Rozemien De Troch, Rafiq Hamdi, and Piet Termonia

Abstract The demand from the city planners and stakeholders concerning climate change impact on cities is increasing. Due to the global warming, cities, which are already more vulnerable, will experience an increasing number of extreme events such as heat waves. However, the information about long-term climate projections are extracted from global or regional climate models that are not conducted at city-scale resolutions. Additional simulations are therefore required. The computational cost of running a high-resolution regional climate model (RCM) coupled with a land surface model (LSM) to get the full atmospheric feedback from cities is extremely high. Moreover, an ensemble of simulations is required in order to estimate the uncertainties in part related to urban projections. Using a LSM in standalone mode is a cheaper solution. However, to downscale climate simulations from a RCM without urban parameterisation to a LSM, an extra step is required in order to present accurate results to compensate for the lack of atmosphere-land feedback. A simple and relatively fast statistical–dynamical downscaling approach is developed to fulfil this step and correct the LSM forcing. In this study, a description and a validation of the methodology is presented. The RCM used is ALARO, and the LSM is SURFEX. They are run over the Brussels Capital Region and forced with ERA-Interim reanalysis during the summers of 1981–2010. The validation is performed for the urban heat island.

1 Introduction

The global mean surface temperature is increasing since the preindustrial period and is projected to continue rising. Cities usually feature climate conditions with temperatures that are typically higher than the surrounding rural areas, this is called

F. Duchêne (✉) · B. V. Schaeybroeck · A. Delcloo · R. D. Troch · R. Hamdi · P. Termonia
Royal Meteorological Institute of Belgium (RMI), Brussels, Belgium
e-mail: francois.duchene@meteo.be

S. Caluwaerts · A. Delcloo · R. Hamdi · P. Termonia
Department of Physics and Astronomy, University of Ghent, Brussels, Belgium

© The Author(s), under exclusive license to Springer-Verlag GmbH, DE, part of Springer Nature 2021

C. Mensink and V. Matthias (eds.), *Air Pollution Modeling and its Application XXVII*, Springer Proceedings in Complexity, https://doi.org/10.1007/978-3-662-63760-9_47

the Urban Heat Island (UHI) (Oke et al., 2017; Bader et al., 2018). Furthermore 50% of the population is currently living in cities and this proportion is projected to rise. City inhabitants are then likely to feel more heat stress during warm events. Therefore, it is relevant to improve the climate projection at the city scale (Berckmans et al., 2019).

The goal of this work is to develop a simple method that enables the translation of an ensemble of regional atmospheric data from its regional scale up to city-level scale, as shown on Fig. 1. Using high-resolution (H-RES) dynamic downscaling is too computationally expensive for climate studies especially when applied for different cities. Therefore, based on a limited set of RCM-LSM at H-RES, a method is proposed here to imprint the "urban signature". Once this signature is constructed one can skip the downscaling step. For this work, the intermediate step is at 4 km resolution while the urban resolution of the standalone LSM is 1 km.

The greater benefit of the proposed statistical–dynamical methodology is the computational time that is very cheap as compared to a full climate-scale dynamical downscaling. Furthermore, the proposed method corrects the data that forces the LSM models instead of applying the correction on the final model output. This insure that the output time series are guaranteed to be physically realistic among

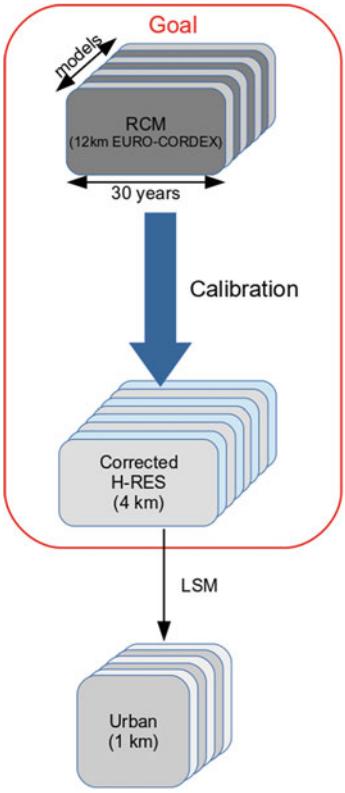

Fig. 1 Purpose of the methodology. The goal is to translate an ensemble of RCM (12 km resolution) to the city scale (1 km resolution). An additional intermediate step is required to correct for the urban-atmosphere interactions

space, time and variables and could then be used for impact studies such as human comfort, etc.

The validation is limited here for the summer during the 30-year period 1981–2010 with respect to the urban heat island only.

2 Methodology

As stated, the aim is to correct RCM data to H-RES scale by applying the hourly spatial signature of the urban-atmosphere interactions to all meteorological variables required by the LSM. The corrected H-RES data is in a second step used to force the LSM in offline mode at 1 km resolution.

The first step of the calibration consists of creating a database of two types of simulations. A H-RES climate simulation with no urban parametrization active (H-RES NO-UP) and one with urban parametrization (H-RES UP). In our study, the database's extend consist of a period of 4 summers. The signature $\Delta(d)$ corresponds to the difference between the corresponding variables with (UP) and without (NO-UP) urban parametrization activated for each day d of this period. More specifically, for variable i, location r and hour-of-the-day t:

$$Signature \equiv \Delta_{i,r,t}(d) = X_{i,r,t}^{H-RES,UP}(d) - X_{i,r,t}^{H-RES,NO-UP}(d) \tag{1}$$

where $X^{H-RES,UP}$ and $X^{H-RES,NO-UP}$ are the forcing variables from the H-RES RCM data with and without urban parametrization, respectively.

The second step of the calibration, consists of imprinting the signature. To determine the signature to apply, we choose the day in the database that most strongly resembles the RCM day which needs correction. All variables are first rescaled by subtracting their mean and dividing by their standard deviation (for each grid point separately). The day d_{min} that is most resemble to a day d_1 (taken from the RCM run) is obtained by minimizing the following cost function with respect to d_2:

$$J(d_1, d_2) = \sum_r \sum_{t=1}^{24} \sum_i \left(\bar{X}_{i,r,t}^{RCM}(d_1) - \bar{X}_{i,r,t}^{H-RES,NO-UP}(d_2) \right)^2 \tag{2}$$

where $\bar{X}_{i,r,t}^{RCM}$ and $\bar{X}_{i,r,t}^{H-RES,NO-UP}$ are the rescaled RCM and H-RES NO-UP variables, respectively.

Finally, the day of the RCM is corrected by adding the signature for all forcing variables i, all spatial points r and all times-of-the-day t:

$$Correction \equiv X_{i,r,t}^{Cor-RCM}(d) = X_{i,r,t}^{RCM}(d) + \Delta_{i,r,t}(d_{min}) \tag{3}$$

Table 1 Mean, bias and RMSE of the night-time UHI (UHI_N) during summer and HW events for the reference (REF) and calibrated (CAL) runs. The bias and RMSE are evaluated with respect to the control run (CTR) and all are averages over the 26 year validation period

	REF UHI_N		CAL UHI_N	
	Summer (°C)	HW (°C)	Summer (°C)	HW (°C)
Mean	1.0	0.6	1.6	2.2
Bias	−0.5	−1.5	0.0	0.0
RMSE	0.5	2.2	0.1	0.5

3 Results

The focus of the results is on the performance of the calibration to improve the simulation of the UHI. Table 1 summarizes the average night-time UHI during summer and during HW events for the reference (REF) and calibrated (CAL) runs. The bias and root-mean-square error with respect to the control run (CTR) is also presented. The calibration fully corrects the large negative bias (−0.5 °C) of the summer UHI of the reference run. The usually observed rising UHI during HWs is not reproduced by the reference run. As it is shown by the negative night-time UHI bias of −1.5 °C (third column of Table 1). It further enhanced the fact that direct coupling of a RCM data to a LSM requires corrections to get more accurate results. Here, the calibration also almost perfectly removes of the bias during HWs. Note that the day-time UHI is also fully corrected, both during the summer period and during HWs events (not shown here).

In addition to the overall suppression of the bias, the calibration methodology also strongly reduces the RMSE of the calibrated run CTR. Both for the entire summer (80% reductions) and only during the HW events (77% reduction). The UHI used in this study is determined from the difference between the temperatures at one rural and one urban station only. However, our calibration method also corrects the UHI for the entire domain over the Brussel region.

4 Conclusion

The calibration methodology is able to efficiently correct RCM's data prior to feed a LSM to downscale climate projections at urban scale. And it does not only correct a single variable such as UHI but also the correlations among different variables. For example, we also investigate the Humidex (a measure of the human comfort) which is calculated based on temperature and humidity. The calibration methodology strongly improves the spatial pattern of the Humidex, especially during the night. Which proves the huge benefit of using this simple methodology for statistical–dynamical downscaling.

References

Bader, D. A., Blake, R. A., Grimm, A., Hamdi, R., Kim, Y., Horton, R. M., Rosenzweig, C., Alverson, K., Gaffin, S. R., Crane, S. (2018). Urban climate science. In C. Rosenweig, W. Solecki, P. Romer-Lankao, S. Mehotra, S. Dhakal, & S. Ali Ibrahim (Eds.),*Climate Change and Cities: Second Assessment Report of the Urban Climate Change Research Network* (ARC3.2). Cambridge University Press (pp. 27–60).

Berckmans, J., Hamdi, R., & Dendoncker, N. (2019). Bridging the gap between policy-driven land use changes and 1 regional climate projections 2. *Journal of Geophysics Research.*

Oke, T., Mills, G., Christen, A., & Voogt, J. (2017). *Urban climates.* Cambridge University Press. https://doi.org/10.1017/9781139016476

AtMoDat (Atmospheric Model Data)—Creation of a Model Standard for Obstacle Resolving Models

Vivien Voss, K. Heinke Schlünzen, and David Grawe

Abstract To assess processes and phenomenon in complex urban areas, obstacle resolving micro-scale models of the atmosphere are increasingly used. But the comparison of results of different obstacle resolving models (ORM) is hindered by the various data formats used for different models and approaches. For global model data a data standard exist within the WCRD Coupled Model Intercomparison Project (CMIP) and therefore model data can be compared more easily. Micro scale ORM results are more difficult to compare, because of the lack of a tailored data standard for these types of model results. As a part of project AtMoDat (Atmospheric Model Data) the creation of a standard for obstacle resolving models, which should be based on existing model standards is in progress. In this study a first attempt to create a standard will be based on the needs of the user community. A web based inventory is developed, where model user can provide information during this conference on their requirements for this tailored model data standard.

Keywords AtMoDat · Data standard · Obstacle-resolving model

1 Introduction

Obstacle resolving micro-scale models of the atmosphere are used to assess processes in complex urban areas. Each ORM generates different results, which is due to the different model types and approaches used. A comparison of results is time consuming. This includes different filtering methods (RANS, LES), with different numerical grids (Arakawa A, B, C), numerical solution techniques (finite elements,

V. Voss (✉) · K. H. Schlünzen · D. Grawe
Meteorological Institute, CEN, University of Hamburg, Hamburg, Germany
e-mail: vivien.voss@uni-hamburg.de

K. H. Schlünzen
e-mail: heinke.schlunzen@uni-hamburg.de

D. Grawe
e-mail: david.grawe@uni-hamburg.de

© The Author(s), under exclusive license to Springer-Verlag GmbH, DE, part of Springer Nature 2021

C. Mensink and V. Matthias (eds.), *Air Pollution Modeling and its Application XXVII*, Springer Proceedings in Complexity, https://doi.org/10.1007/978-3-662-63760-9_48

finite volume, finite differences) and with different temporal and spatial resolutions (Schlünzen et al., 2017). This hinders reusability of model results by the model user group as well as by others.

Because of the WCRD Coupled Model Intercomparison Project (CMIP) a model data standard for global model data exists (Taylor & Doutriaux, 2010). Model data can therefore be compared more easily. Micro scale ORM results are more difficult to compare, because of the lack of a tailored data standard for these type of model results. Simply applying CMIP standards to micro scale model results may not fit the need of the micro scale model results. The project AtMoDat funded by the Federal Ministry of Education and Research (BMBF) start an attempt to create a standard for ORM results based on the existing Climate and Forecast (CF) conventions for CMIP. To aim for a better usability and reusability of ORM results, for data storage in archive systems and for a better citation of the used data a standard format is helpful and necessary. As a part of project AtMoDat (Atmospheric Model Data) the creation of a standard for ORMs, which should be based on existing model standards is in progress. A standard enable a better comparison of model data and helps to declare the data for the storage in an archive. In this study, a first attempt for a standard should be created based on the currently used models and the needs of the user community. Therefore, we want to ask the user community about their usage with model data. We want to know if the user is aware about model standards, what they are missing when handling model data and what should be considered for the final ORM data conventions. The users can suggest us, how the data should look like to enable a better comparison. Or if their model output is already based on the currently available standard for global model data. During this conference model users can provide us some information via a web based inventory. The next step is to extend the collection of model characteristics and eventually a generic scheme shall be provided.

In this project involved are the German Climate Computing Center (Deutsches Klimarechenzentrum, DKRZ), Leibniz Information Centre for Science and Technology University Library (Technische Informationsbibliothek, TIB), Meteorological Institute of the University of Hamburg and the Institute for Meteorology of the University of Leipzig (AtMoDat, 2019).

The DKRZ is hosting the world data center for climate and a long-term archive for scientific data. Working with the aspects of data curation, preparation, identification and long-term-archivation for global model data, DKRZ wants to extend these services towards other modeling communities and their data. The TIB was involved in the processes of creating the DOI citation, which leads to the Data Cite organisation and concerns with the management and quality of data and metadata.

The Meteorological Institute of the University of Hamburg are part of the project with the micro scale obstacle resolving model MITRAS (Salim et al., 2018; Schlünzen et al., 2003) and the wind tunnel laboratory and provides obstacle resolving model data, on which the data standard should be tested. The Institute for Meteorology of the University of Leipzig concerns with cloud formatting, aerosol and precipitation. As a part of the AeroCom project they worked with high resolution modeling of cloud-formatting processes in global models, which also are part of MIP.

2 Method

The survey was created with the online survey tool limesurvey (www.limesurvey.org). During the conference, an online survey will be active. In this survey, we ask the community of ORM user to answer the following questions, which are divided into three question groups:

(1) Used Models—Which models were used by the user so far, which models provided data, that have been used and was not been generated by the users themselves.
(2) Model Settings—What are the specifications of the used models? Are initialization and model set up stored? What grid uses the model? What is the data format of the results?
(3) Conventions—Are the user aware of conventions? Does the model data already adhered to conventions?

Based on the answers to this question, a first attempt for a model standard will be created.

3 Conclusion

The results of the survey should provide some information about the currently used models and model the output data, also the needs and suggestions of the model user for handling the data. These information will be considered during the development of the model data standard.

References

AtMoDat. (2019). Homepage of the Project. https://www.atmodat.de/

Salim, M. H., Schlünzen, H., Grawe, D., Boettcher, M., Gierisch, A. M. U., & Fock, B. (2018). The microscale obstacle-resolving meteorological model MITRAS v2.0: Model theory. *Geoscientific Model Development*, 11(8), 3427–3445. https://doi.org/10.5194/gmd-11-3427-2018

Schlünzen, K. H., Hinneburg, D., Knoth, O., Lambrecht, M., Leitl, B., López, S., Lüpkes, C., Panskus, H., Renner, E., Schatzmann, M., Schoenemeyer, T., Trepte, S., & Wolke, R. (2003). Flow and transport in the obstacle layer: First results of the micro-scale model MITRAS. *Journal of Atmospheric Chemistry, 44*, 113. https://doi.org/10.1023/A:1022420130032

Schlünzen, K. H., Leitl, B., & Lunkeit, F. (2017). Meteorologische Modellierung (MOD). *Lecture Notes, Version, 1*(5), 88.

Survey Link: uhh.de/orm-survey, this survey is active until June 2022.

Taylor, K. E., & Doutriaux, C (2010). CMIP5 model output requirements: File contents and format, data structure and metadata. Program for climate model diagnosis and intercomparison (PCMDI).

Model Assessment and Verification

How Accurate are Dust Surface Concentrations Forecasts from Numerical Models? A Preliminary Analysis of the Multi-model Median Forecasting in Eastern Mediterranean Region

A. Eleftheriou, P. Mouzourides, and M. K. -A. Neophytou

Abstract Transboundary transport of dust is a phenomenon encountered across the globe, where pollution is generated in one area and impacts another, sometimes travelling thousands of kilometres, as in the case of desert dust storms. There is a relatively wide range of tools and methods for monitoring dust storms in the atmosphere, extending from near-ground measurements to satellite observations and numerical simulations. Evaluation of the numerical models is systematically conducted with the use of sun-photometers and satellite aerosol products which are integrated over the atmospheric column rather than exclusively near the ground. In this work we evaluate the performance of the ensemble numerical model Multi-Model Median (MMM), which forecasts the long-range transport of desert dust in the Mediterranean Region, using PM_{10} near-ground concentration measurements, collected at monitoring stations from three (3) different regional areas: Cyprus, Greece and Israel for the period of 2012–2016. The measurements represent background concentrations, removed from anthropogenic influence. Here we present the results from a preliminary evaluation analysis which shows that the ensemble numerical model generally underestimates the near-ground measurements for all sites.

1 Introduction

Long-range transport of dust to areas far from the source is estimated to 1536 $Tg/year^{-1}$ and 75% of it, is from natural processes as desert dust emissions (Ginoux et al., 2012). Querol et al. (2009) observed a systematic increase of PM_{10} and $PM_{2.5}$ concentrations from the Western Mediterranean Basin to the Eastern Mediterranean Basin and from North to South, thus making the Eastern Mediterranean Region

A. Eleftheriou (✉) · P. Mouzourides · M. K. .-A. Neophytou
Laboratory - Isle of Excellence of Environmental Fluid Mechanics, Department of Civil & Environmental Engineering, School of Engineering, University of Cyprus, Nicosia, Cyprus
e-mail: eleftheriou.g.andreas@ucy.ac.cy

© The Author(s), under exclusive license to Springer-Verlag GmbH, DE, part of Springer Nature 2021

C. Mensink and V. Matthias (eds.), *Air Pollution Modeling and its Application XXVII*, Springer Proceedings in Complexity, https://doi.org/10.1007/978-3-662-63760-9_49

(EMR) one of the most heavily impacted areas by desert dust globally. High concentrations of PM_{10} has been proven to result in many serious human health problems such as cardiovascular diseases (Middletton, 2017; European Environment Agency, 2019).

For the monitoring of dust storms in the atmosphere, there is a wide range of tools and methods which extend from near-ground measurements to satellite observations and numerical simulations, which are used by regulatory authorities to issue announcements or warnings in order to inform the public of high PM_{10} concentrations in the area. The forecasting process of dust storms uses a combination of monitoring data with satellite products and numerical modeling. Input data are the core of correct and accurate forecasts of dust transport and deposition. Under the Sand and Dust Storm Warning Advisory and Assessment System (SDS-WAS) initiative, the need for reliable sand and dust storm forecasts is aimed to be met, using assimilation of different models into a MMM or use of individual ones. These numerical dust models cover at regional scale, a large part of Africa and the Middle East and have been used numerously under the directive 2008/50/EC for PM_{10} exceedances (e.g. Mouzourides et al., 2015) or as a research database in investigating dust processes (Basart et al., 2014).

The evaluation of the numerical models for dust load and dust surface concentration products, is regularly performed with the use of sun photometers through the AERONET network and satellite aerosol products (MODIS). However, dust surface concentration forecasts cannot exhaustively be evaluated, as both aforementioned methods use integrated data over the atmospheric column rather than exclusively near the ground. Generally, dust models have different first layer calculation heights, ranging from ~20m to 100 m above the sea or ground level, take into account different particle sizes, ranging from ~0.03μm to 20 μm, and also use different schemes in applying physics in the models (e.g. Knippertz & Stuut, 2014). In addition, the use of near-ground PM_{10} monitoring stations for evaluation of dust surface concentration forecasts can be difficult in deriving conclusions of the real fraction of desert dust in the measurements (Garcia-Castrillo & Tarradellas, 2017). Thus, very few studies exist in evaluating numerical models with the use of near-ground monitoring stations and to the best of our knowledge, none for the EMR. For the evaluation of the ensemble numerical model, we analyze near-ground measurements, of 24h-time-average of PM_{10} concentrations, collected at monitoring stations representing background conditions in the following areas: Agia Marina Xyliatou (AM) in Cyprus, Finokalia-Crete (FK) in Greece, and Be'er Sheva (BS) in Israel. First, we assess the trends of long-range transport of dust for the whole period of study; then we use the top percentiles of 75^{th}, 85^{th} and 95^{th}, of the daily average PM_{10} concentration measurements depicting the major dust events in each area and the corresponding dust surface concentrations forecasts of the MMM for each site, in order to evaluate the model's performance.

2 Site and Data Description

The study area with the monitoring stations is situated in the EMR as shown in Fig. 1. FK and AM are in the European Monitoring and Evaluation Programme (EMEP) and the BS is an urban monitoring station. In this study, these stations were selected because they are located away from anthropogenic sources or are least impacted by anthropogenic sources, in order to assess the long-range transport of dust. At each site continuous monitoring is being held using high temporal resolution equipment: a Tapered Element Oscillating Microbalance (TEOM) for Cyprus and Israel, and a FH 62 I-R Thermo for Greece. The measurements are taken at a height of 2m–5m from the ground for AM and FK, and on top of a building in the case of BS (at a height of 10m–15m). High PM_{10} concentrations have been frequently associated with desert dust storms (e.g. Mouzourides et al., 2015). Achilleos et al. (2019) used the characteristics of the 3 sites during dust storms to develop threshold rules for when a dust storm occurs in each area. The study found that the PM_{10} concentrations exhibit a rise of 20% to 59% of the normal average measurements in a year during a dust event. In this study we used the 75^{th}, 85^{th} and 95^{th} percentiles of PM_{10} concentrations of the whole period to include only the days with substantial dust transport. Then by using the BOOT Model Evaluation Methodology (Hanna et al., 2004), we evaluate the best performance of MMM model. Forecasting products for dust surface concentrations were obtained from the SDS-WAS on-line available database (https://sds-was.aemet.es/). The forecasting products are generated every 3 hours in UTC, on a spatial resolution of $0.5° \times 0.5°$ and are taken for each site to be evaluated with the relevant PM_{10} concentrations. Both datasets obtained from near-ground PM_{10} concentrations measurements and forecasts were time-averaged in 24-h values. The study period was selected from January of 2012 to December of 2016 due to the fact that this is the longest period with commonly available data from all datasets.

Fig. 1 Site area with station

3 Results and Discussion

The time-series data of PM_{10} concentrations were used in order to evaluate the trends of the particulate matter concentrations in the EMR. Figure 2 presents in time-series plots, the daily averages of PM_{10} concentrations measurements (shown as blue continuous line) compared to the daily forecasting data of the dust surface concentrations (shown as red dots) for the three study areas. This figure shows the trends of the data that are found in the whole period of study. The boxplots next to each time-series show the distribution of the concentrations for each year, for the 3 sites. The top and bottom quantiles indicate the 75^{th} and the 25^{th} percentile of the recorded measurements respectively, while the centre of the box shows the median value. The highest concentrations are found in BS area, followed by the AM and FK with lower concentrations. From the time-series it can be deduced that in all three sites, during periods of low concentrations (i.e. lower than the yearly median concentration), the agreement between PM_{10} near-ground concentration measurements and forecasts, as shown by the GM and VG model performance indicators, is poor. The results of the BOOT Model Evaluation Methodology show that the best agreement between PM_{10} near-ground measurements and forecasts is found above the 75^{th} percentile. As it can be deduced from the analysis, the larger the number of outliers in measurements indicating more extreme dust events, the better the agreement between near-ground measurements and forecasts while the higher peaks (spikes) in concentrations in Fig. 2, are a result of transboundary air pollution which can be dust.

Figure 3 shows graphically the evaluated performance of the MMM for the 3 sites. The Geometric Mean (MG) is a measure of relative bias and the Geometric Variance (VG) is a measure of the relative scatter. For a perfect model an MG = VG = 1

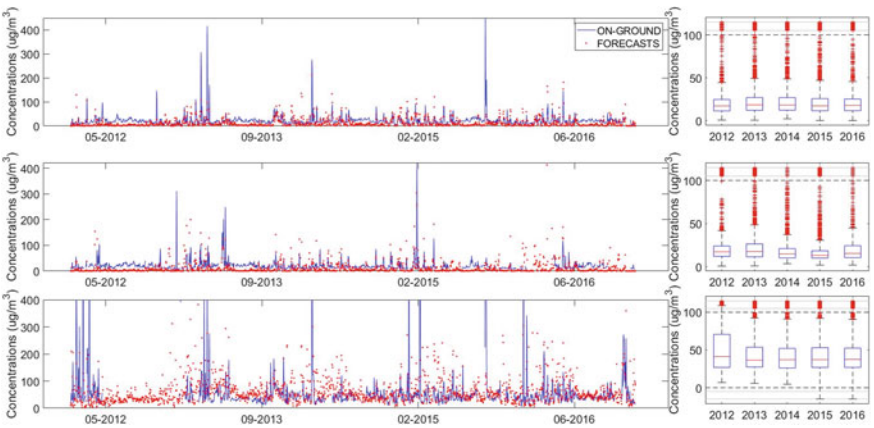

Fig. 2 Comparison between near-ground monitoring station measurements and model predictions for **a** Agia Marina Xyliatou (AM) (Cyprus), **b** Finokalia-Crete (FK) (Greece) and **c** Be'er Sheva (BS) (Israel) for 2012–2016 and the relevant boxplot showing the distribution of frequency of measurements for each year of study

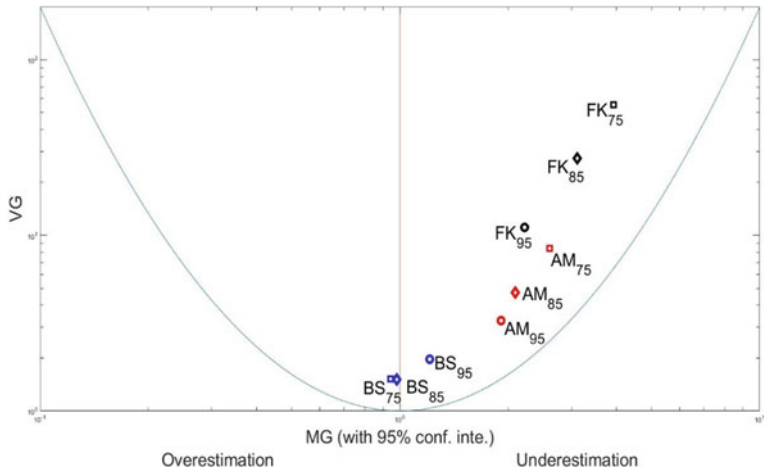

Fig. 3 The geometric mean (MG) versus geometric variance (VG) summarizing the over and under estimations of the model to near-ground measurements for different percentiles for each site

score is yielded and will be shown at the lowest point of the curve. In this analysis we used the daily averages of the PM_{10} concentrations and their corresponding 75^{th}, 85^{th} and 95^{th} percentiles, of the whole period of study, to evaluate the MMM as shown above. As it can be seen from Fig. 3, overall, the model performance is better for the BS station (due to the lowest MG value exhibited) compared to the other stations, and using different percentile for measurements makes an observable difference in the performance indicators. Specifically, using the lowest percentiles 75^{th} and 85^{th} for AM and FK yield larger deviations than the 95^{th} percentiles, while for BS 75^{th} and 85^{th} percentiles yield better performance indicators as seen through the MG and VG values. Generally, the model underestimates transport of dust in areas further away from sources such as AM and FK but for more extreme dust events (95^{th} percentile) provide better forecastings. On the other hand, for BS, slight overestimations are found (based on 75^{th} and 85^{th} percentiles), but for the most extreme events (95^{th} percentile) we have underestimations. This is probably due to the fact that the forecasts of transboundary particulate transport include relatively little information for what is happening near ground where monitoring stations are placed, and therefore their agreement is best when dust events are extreme which allows the dust transport information at higher levels to penetrate to lower levels - near ground, thus making monitoring stations reflecting better the transboundary phenomenon.

4 Concluding Remarks

In this work, a preliminary evaluation analysis of the MMM forecasts using near-ground measurements is conducted. We use different thresholds, specifically the 75th, 85th and 95th percentiles, for representation of PM_{10} near-ground measurements in the process of evaluation of the MMM performance. In general, the near-ground measurements are observed to be highest in BS (Israel), lowest in FK (Crete-Greece) and in AM (Cyprus) an intermediate situation is observed. The 75th and 85th percentiles for PM_{10} near-ground concentrations represent major dust events while the 95th percentile represent the most extreme dust events during the period of study. All datasets, near-ground PM_{10} concentrations and forecasts were averaged in daily values. The results of the evaluation show that the transport of dust further away from the source of dust, as in the areas of AM and FK, tends to be underestimated but becomes more accurate with increasing severity of the dust events. for an area closer to dust sources as BS, dust events are better represented and slightly overestimated but the model underestimates the most extreme events in the area. It should be taken into account that there are some model forecast issues such as geomorphology of the sites that is not addressed as accurately as it should be in the MMM model, as well as the fact that in dust models particles sizes that are being considered, vary, while the first height layer that simulations are taking place from dust models can vary greatly from the near-ground concentration measurement height.

Despite the preliminary evaluation of the MMM, a more detailed evaluation needs to be conducted for more conclusive deductions. To address this, gravimetric analysis of filters and particle size analyzers for the variation of dust particles transported during dust storms shall be used. Furthermore, a detailed investigation on a monthly, daily or dust event by dust event resolution, might be necessary to find where the model is best performing.

Acknowledgements The authors would like to acknowledge, the Department of Labour and Inspection of the Cyprus Ministry of Labour, Welfare and Social Insurance, the University of Crete, and the University of the Negev/Soroka Medical Center for the provision the PM_{10} concentration datasets. SDS-WAS (https://sds-was.aemet.es/) is acknowledged for the provision of the Multi-Model-Median forecast data. This work was supported by the European Union within the framework of the LIFE MEDEA 570 Program under the Grant Agreement LIFE16CCA/CY/000041.

References

Achilleos, S., Mouzourides, P., Kalivitis, N., Katra, I., Itai, K., Kouis, P., & Koutrakis, P. (2019). Spatio-temporal variability of desert dust storms in eastern mediterranean (Crete, Cyprus, Israel) between 2006–2017 using a uniform methodology. *Journal of the Total Environment*.

Basart, S., Dulac, F., Baldasano, J. M., Nabat, P., Mallet, M., Solmon, F., & Delbarre, H. (2014). Air pollution modeling and its application XXII (pp. 79–83). https://doi.org/10.1007/978-94-007-5577-2

European Environment Agency. (2019). Air quality in Europe—2018 report. EEA Report No. 12/2018. https://doi.org/10.2800/55823

García-Castrillo, G., & Terradellas, E. (2017). Evaluation of the dust forecasts in the canary Islands, WMO SDS-WAS. Barcelona, 21 (pp. SDS-WAS-2017–002).

Ginoux, P., Prospero, J. M., Gill, T. E., Hsu, N. C., & Zhao, M. (2012). Global-scale attribution of anthropogenic and natural dust sources and their emission rates based on MODIS deep blue aerosol products.

Hanna, S., Fabian, P., Chang, J., Venkatram, A., Britter, R., Neophytou, M. K.-A., & Brook, D. (2004). Use of urban 2000 field data to determine whether there are significant differences between the performance measures of several urban dispersion models. In *5th Symposium on the Urban Environment* (pp. 303–316).

Knippertz, P., & Stuut, J. B. W. (2014). *Mineral dust: A key player in the earth system.* https://doi.org/10.1007/978-94-017-8978-3

Middleton, N. J. (2017). Desert dust hazards: A global review. *Aeolian Research, 24*, 53–63. https://doi.org/10.1016/j.aeolia.2016.12.001

Mouzourides, P., Kumar, P., & Neophytou, M. K. A. (2015). Assessment of long-term measurements of particulate matter and gaseous pollutants in South-East mediterranean. *Atmospheric Environment. Elsevier Ltd, 107*(2), 148–165. https://doi.org/10.1016/j.atmosenv.2015.02.031

Querol, X., Pey, J., Pandolfi, M., Alastuey, A., Cusack, M., Pérez, N., & Kleanthous, S. (2009). African dust contributions to mean ambient PM10 mass-levels across the mediterranean basin. *Atmospheric Environment, 43*(28), 4266–4277. https://doi.org/10.1016/j.atmosenv.2009.06.013

Questions and Answers

Questioner: George Tsegas

Question: Would it be a preferable assessment approach to use short-term correlation analysis only for episode days, also evaluating the time-of-arrival error of individual models?

Answer: We have focused only on days (daily average concentrations) with high PM_{10} concentrations measured near ground by background stations indicating dust transport, using the methodology and the results for the same region as described in Achilleos et al. (2019).

Questioner: Pavel Kishcha

Question: In the summer months, PM10 measurements in Crete and Cyprus do not represent desert dust by but monthly anthropogenic aerosols. So, I would recommend to limit your study to the dust period from February to April.

Answer: We have focused only on days (daily average concentrations) with high PM_{10} concentrations measured near ground by background stations indicating dust transport. For future work, we intent to extent our analysis, taking into account the seasonal variation of dust periods. Also we will evaluate the performance of the model under different meteorological and air quality conditions.

Questioner: Christian Hogrefe

Question: Do you plan to look at the forecast ensemble range in addition to the median and the best member?

Answer: The next step is to examine each model included in the Multi Model Median to find out which have better forecasts in the Eastern Mediterranean Region.

Evaluating Long-Term Ozone and $PM_{2.5}$ Simulations Over the United States

Christian Hogrefe, K. M. Foley, K. W. Appel, S. Roselle, D. Schwede, J. O. Bash, and Rohit Mathur

Abstract In this study, we analyzed ozone and total and speciated $PM_{2.5}$ fields from two sets of WRF/CMAQ simulations over the continental US. Results show that differences in trends of ozone boundary conditions affect trends in modeled surface ozone concentrations within the domain, especially during fall and winter. The analysis of total and speciated $PM_{2.5}$ showed best model performance for SO_4^{2-} and revealed that modeled seasonal cycles of organic carbon in urban areas differed from observations for both simulations. It is likely that uncertainties in primary $PM_{2.5}$ emissions along with assumptions about the volatility of primary organic aerosols and the formation of secondary organic aerosols made in these simulations caused these differences and that recent updates made to the treatment of organic aerosol processes in CMAQ would lead to improved model performance.

C. Hogrefe (✉) · K. M. Foley · K. W. Appel · S. Roselle · D. Schwede · J. O. Bash · R. Mathur
Atmospheric and Environmental Systems Modeling Division, Center for Environmental Measurements and Modeling, US Environmental Protection Agency, 109 T.W. Alexander Dr, Research Triangle Park, NC 27711, USA
e-mail: hogrefe.christian@epa.gov

K. M. Foley
e-mail: foley.kristen@epa.gov

K. W. Appel
e-mail: appel.wyat@epa.gov

S. Roselle
e-mail: roselle.shawn@epa.gov

D. Schwede
e-mail: schwede.donna@epa.gov

J. O. Bash
e-mail: bash.jesse@epa.gov

R. Mathur
e-mail: mathur.rohit@epa.gov

This is a U.S. government work and not under copyright protection in the U.S.; foreign copyright protection may apply 2021

C. Mensink and V. Matthias (eds.), *Air Pollution Modeling and its Application XXVII*, Springer Proceedings in Complexity, https://doi.org/10.1007/978-3-662-63760-9_50

Keywords Trends · Dynamic evaluation · Emission inventories · Boundary conditions

1 Introduction

Performing decadal regional air quality model simulations has become more feasible due to increased computational resources. Evaluating how well such long-term simulations represent changes in air quality resulting from small- and large-scale changes in emissions and meteorology can help to build confidence in the modeling systems' use for air quality planning applications. In this study, we analyze ozone and total and speciated $PM_{2.5}$ fields from two sets of WRF/CMAQ simulations over the continental US. Our analysis also includes a comparison of emission and boundary condition input files to investigate to which extent they may have caused differences in the simulated pollutant levels, variations, and trends.

2 Model Simulations and Observations

Both sets of simulations analyzed in this study were performed over the contiguous US with version 3.4 of the WRF meteorological model and version 5.0.2 of the CMAQ chemical transport model. The first set of simulations (hereafter referred to as "DOE") was performed at 36 km resolution for 1990–2010 using the emission fields described in Xing et al. (2013) and lateral boundary conditions derived from hemispheric CMAQ simulations performed for the same time period (Xing et al., 2015). The second set of simulations (hereafter referred to as "ECODEP") was performed at 12 km resolution for 2002–2012 using emissions from multiple National Emission Inventories and lateral boundary conditions derived from multiple GEOS-CHEM simulations. Further details on the DOE simulations can be found in Gan et al. (2015) and Xing et al. (2013), Xing et al. (2015)) while further details on the ECODEP simulations can be found in Zhang et al. (2019). The analysis presented here focuses on the 2002–2010 time period included in both simulations.

To illustrate differences in emissions, Fig. 1 shows time series of domain-total NO_x, VOC, SO_2, and $PM_{2.5}$ emissions excluding biogenic sources. All emissions show a decreasing trend. While the SO_2 emissions are very similar for both simulations, there are noticeable differences in the magnitude of NO_x emissions (primarily due to different mobile source emission estimates) and $PM_{2.5}$ emissions. Differences in the representation of wildfires likely are a major contributor to the differences in $PM_{2.5}$ emissions but the differences also reflect a higher level of uncertainty in specifying these emissions for a range of sectors compared to other pollutants, especially SO_2 and NO_x.

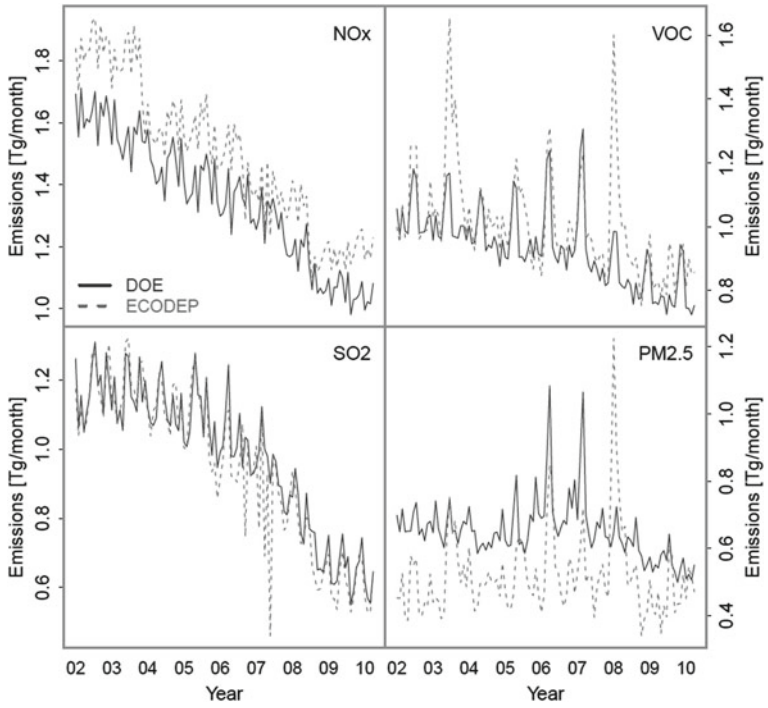

Fig. 1 Time series of monthly domain-total NO_x, VOC, SO_2, and $PM_{2.5}$ emissions (excluding biogenic sources but including wildfires) used in the DOE and ECODEP WRF/CMAQ simulations

Observations of ozone were obtained from the Air Quality System (AQS) database and total and speciated $PM_{2.5}$ mass were obtained from the Chemical Speciation Network (CSN) and the Interagency Monitoring of Protected Visual Environments (IMPROVE) network.

3 Results and Discussion

To investigate the effect of differences in ozone boundary conditions on simulated trends, Fig. 2 shows vertical profiles of 2002–2010 trends in seasonal average ozone boundary conditions at the western domain boundary, while Fig. 3 shows observed and modeled surface ozone trends as function of percentile and season at AQS stations in the Western US (all AQS stations west of −100° longitude). It should be noted that data for the year 2004 was excluded from this analysis due to a problem with the ozone boundary conditions in the ECODEP simulations for the first half of that year. Throughout all seasons, the trends in the ECODEP western boundary

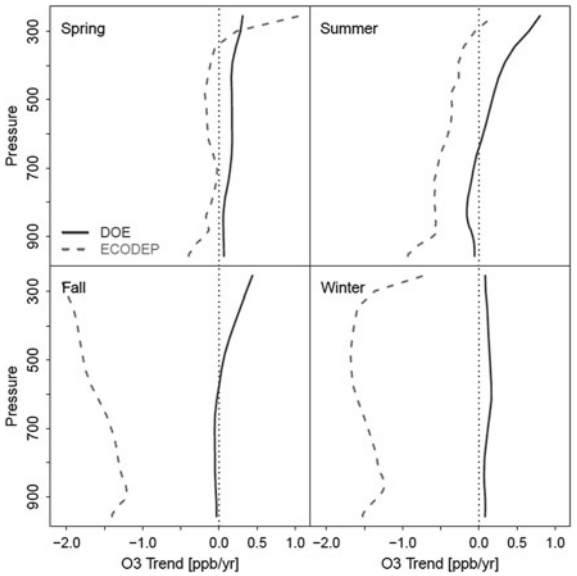

Fig. 2 Vertical profiles of trends in seasonal average ozone boundary conditions at the western domain boundary

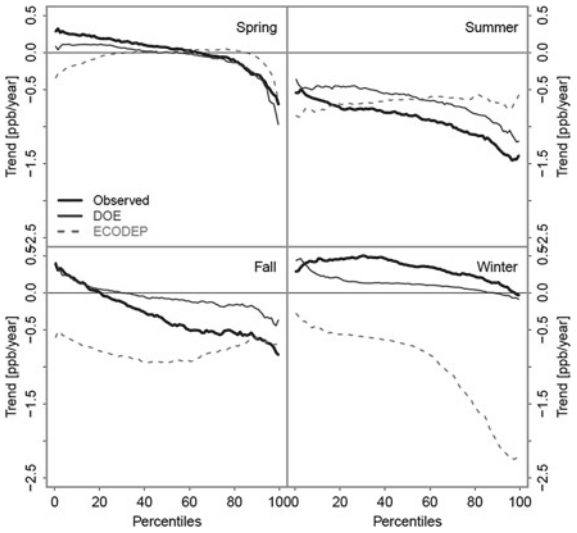

Fig. 3 Observed and modeled ozone trends as function of percentile and season at AQS stations in the Western US

conditions are negative (downward) below 400 mb while those for the DOE western boundary conditions are close to zero. The differences in these western boundary conditions trends are most pronounced in fall and winter. When comparing the DOE and ECODEP surface ozone trends in Fig. 3, the differences for spring, fall and winter mirror those for the boundary condition trends. During spring, both simulations show similar surface trends while during fall and winter, the ECODEP simulations show strong decreasing trends across all percentiles that are consistent with the strong negative trends in the western boundary conditions. During summer, the differences in boundary conditions have a smaller effect on simulated surface ozone trends due to the increased importance of photochemical production from local and regional emission sources.

Figure 4 shows time series of observed and modeled monthly domain-averaged $PM_{2.5}$, sulfate (SO_4^{2-}), and organic carbon (OC) concentrations at IMPROVE and CSN monitors. While many IMPROVE monitors are located in more rural areas in the western US, many CSN monitors are located in urban areas in the eastern US

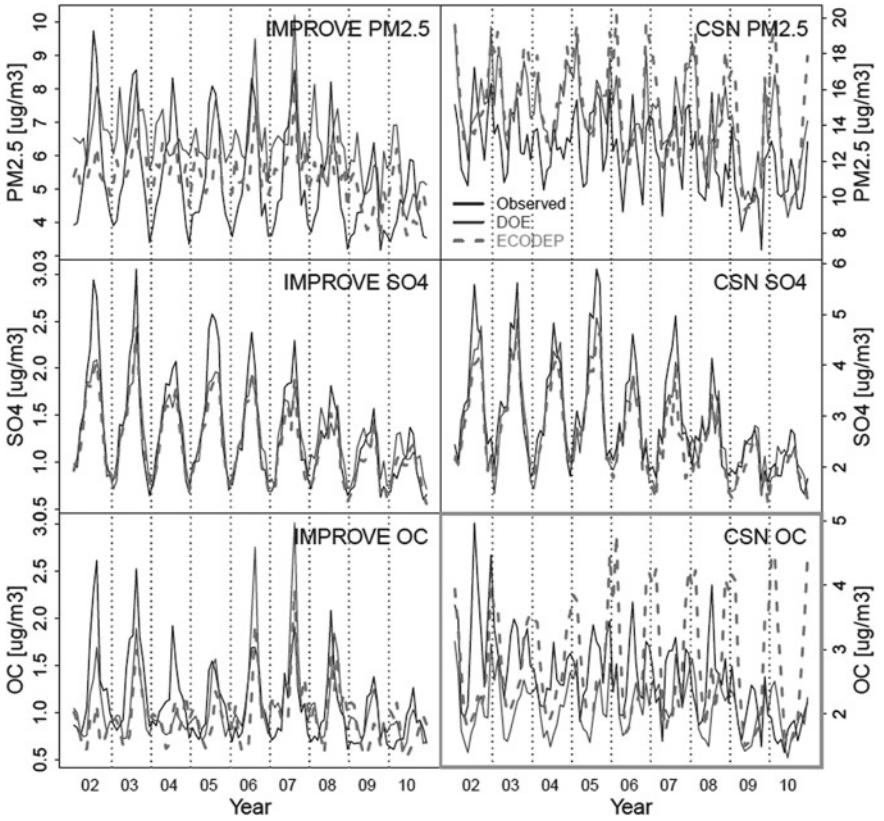

Fig. 4 Observed and modeled time series of monthly domain-averaged $PM_{2.5}$, SO_4^{2-}, and OC concentrations at IMPROVE and CSN monitors

and tend to experience higher concentration levels. The best performance for both simulations in terms of capturing the observed magnitude, seasonality, and trend is seen for SO_4^{2} at both CSN and IMPROVE monitors. On the other hand, differences between observations and simulations as well as between the two sets of simulations are evident for OC at IMPROVE and especially CSN monitors, and these differences affect the comparison of total $PM_{2.5}$ mass at both sets of monitors as well. For example, simulated OC at CSN stations shows wintertime maxima, while observed OC shows summertime peaks in many years. These discrepancies between observed and modeled OC likely can be explained by the treatment of primary and secondary organic aerosols in the older version of CMAQ (version 5.0.2) used in these long-term simulations. Recent updates to these treatments (Murphy et al., 2017; Xu et al., 2018) have been shown to reduce wintertime OC while increasing summertime OC by updating the volatility assumptions for primary organic aerosols and increasing the production of secondary aerosols. Moreover, differences can be seen for OC and total $PM_{2.5}$ between the DOE and ECODEP simulations. While part of these differences may be due to grid resolution (with higher simulated wintertime concentrations in emissions-rich urban areas for the 12 km ECODEP simulation compared to the 36 km DOE simulation), the difference in primary $PM_{2.5}$ emissions mass (see Fig. 1) also is a factor, with generally higher OC and $PM_{2.5}$ concentrations for the DOE simulation at the location of the IMPROVE monitors.

Overall, the analysis of both ozone and $PM_{2.5}$ reaffirms that decisions made when preparing emissions and boundary conditions for such long-term simulations have a significant impact on modeled variability and trends.

Disclaimer The views expressed in this paper are those of the authors and do not necessarily represent the view or policies of the US Environmental Protection Agency.

References

Gan, C.-M., et al. (2015). Assessment of long-term WRF–CMAQ simulations for understanding direct aerosol effects on radiation "brightening" in the United States. *Atmospheric Chemistry and Physics, 15*, 12193–12209. https://doi.org/10.5194/acp-15-12193-2015

Gan, C.-M., et al. (2016). Assessment of the effects of horizontal grid resolution on long-term air quality trends using coupled WRF-CMAQ simulations. *Atmospheric Environment, 132*. https://doi.org/10.1016/j.atmosenv.2016.02.036

Murphy, B. N., et al. (2017). Semivolatile POA and parameterized total combustion SOA in CMAQv5.2: Impacts on source strength and partitioning. *Atmospheric Chemistry and Physics, 17*, 11107–11133. https://doi.org/10.5194/acp-17-11107-2017

Xing, J., et al. (2013). Historical gaseous and primary aerosol emissions in the United States from 1990 to 2010. *Atmospheric Chemistry and Physics, 13*, 7531–7549. https://doi.org/10.5194/acp-13-7531-2013

Xing, J., et al. (2015). Observations and modeling of air quality trends over 1990–2010 across the Northern Hemisphere: China, the United States and Europe. *Atmospheric Chemistry and Physics, 15*, 2723–2747. https://doi.org/10.5194/acp-15-2723-2015

Xu, L., et al. (2018). Experimental and model estimates of the contributions from biogenic monoterpenes and sesquiterpenes to secondary organic aerosol in the southeastern United States. *Atmospheric Chemistry and Physics, 18*, 12613–12637. https://doi.org/10.5194/acp-18-12613-2018

Zhang, Y., et al. (2019). A measurement-model fusion approach for improved wet deposition maps and trends. *Journal of Geophysical Research: Atmospheres, 124*, 4237–4251. https://doi.org/10.1029/2018JD029051

Questions and Answers

Questioner: Limei Ran

Question: Do the two runs use the 12 km domain grid? What is the influence of grid resolution on the trend?

Answer: No, the DOE simulations were performed on a 36 km grid while the ECODEP simulations were performed on a 12 km grid. Gan et al. (2016) investigated the effects of grid resolution on selected periods of the DOE simulations and found that simulated O_3 and $PM_{2.5}$ trends were generally comparable between the 36 and 12 km grids.

Questioner: Volker Matthias

Question: In a previous investigation of SO_2 and SO_4^{2-} trends in Europe we found that SO_4^{2-} doesn't decrease as much as the emissions would imply. I wonder if you found that for your study in the US as well.

Answer: We did not yet analyze these simulations from that perspective but would be interested in doing so in the future.

Questioner: K. Wyat Appel

Question: Are there any plans to do additional long-term simulations with updated model version, more consistent emissions across time, etc.?

Answer: Yes, our group is currently preparing new emission and boundary condition inputs to perform 2002–2017 simulations with CMAQv5.3.1

Validation of WRF with Detailed Topography Over Urban Area in Complex Terrain

Hristina Kirova, Ekaterina Batchvarova, Reneta Dimitrova, and Evgeni Vladimirov

Abstract The urban convective atmospheric boundary layer (ABL) structure and its evolution were studied with Weather Research and Forecasting (WRF) model for the period of Sofia Experiment 2003. The experimental data of 2003 used for model validation encompass turbulent fluxes and profiles of temperature, humidity, wind speed and direction. Configuration using two datasets for topography (SRTM, NASA) and land cover (CORINE 2012) was implemented in WRF model. The spatial distribution of modelled maximal values of sensible and latent heat fluxes clearly indicated the location of big green areas in Sofia city, water bodies and mountain ridges. The model was able to reproduce sensible heat flux adequately for the entire period of the experiment with exception of September 30th when 2.6 mm rain was recorded. The model was able to capture the sharp jump in the latent heat flux after the rainfall, but with two hours delay. The model maximal values of friction velocity were overestimated compared to the measured ones.

H. Kirova
National Institute of Meteorology and Hydrology, Sofia, Bulgaria

E. Batchvarova (✉)
Climate, Atmosphere and Water Research Institute, Bulgarian Academy of Sciences (CAWRI-BAS), Sofia, Bulgaria
e-mail: Ekaterina.Batchvarova@cu.bas.bg

R. Dimitrova · E. Vladimirov
Sofia University "St. Kliment Ohridski", Sofia, Bulgaria

R. Dimitrova
NIGGG-BAS, Sofia, Bulgaria

E. Vladimirov
BULATSA, Sofia, Bulgaria

© The Author(s), under exclusive license to Springer-Verlag GmbH, DE, part of Springer Nature 2021

C. Mensink and V. Matthias (eds.), *Air Pollution Modeling and its Application XXVII*, Springer Proceedings in Complexity, https://doi.org/10.1007/978-3-662-63760-9_51

1 Sofia Experiment 2003

Up-to-date mesoscale meteorological models have parameterization and dynamic options that allow description of different scales of atmospheric processes from meters to thousands of kilometres. An observation data set with high spatial and temporal resolution is necessary for model validation to be able to find the best model configuration. Such data set was collected during the experimental campaign (Batchvarova & Rotach, 2005; Batchvarova et al., 2007) conducted in Sofia from September 27nd to October 3rd, 2003. The experiment program has contained measurements of turbulent fluxes and aerological observations tracking the development of the convective ABL in urban environment. Acoustic anemometers and fast hydrometer were mounted on the research tower at NIMH-BAS at height of 20 and 40 m above the ground and they were set with 30-min averaging time. The sondes were launched every 2 h (from 04 to 16 GMT).

2 WRF Model Setup

Numerical simulations are performed with the Advanced Research WRF (ARW) Version 3.8. (http://www.mmm.ucar.edu/wrf/users/docs) initialized with 0.25 degree NCEP Final Operational Analyses every 6 h. Four nested domains are used based on a Lambert Projection, centred at 42.68 N and 23.36 E with resolution of 32 km (D1), 8 km (D2), 2 km (D3) and 500 m (D4). Two new datasets for topography (SRTM, NASA) and land cover (CORINE 2012) were implemented in WRF. Four dimensional data assimilation (FDDA) is used for domain D1 at all vertical levels, and for domains D2, D3 only above the first 10 model levels. The FDDA option is not applied for D4. The parametrization of physical processes used in this study is listed in Table 1. Vertical structure of the atmosphere is presented through 50 levels going up to 50 hPa. A 48-h simulation period is performed for each day of the experiment, considering 24 h spin-up period.

Table 1 Parametrization of physical processes

Microphysics	2 = Lin et al.
Longwave radiation	1 = RRTM: Rapid Radiative Transfer Model
Shortwave radiation	2 = Dudhia
Surface layer	4 = Quasi-Normal Scale Elimination (QNSE)
Land surface	2 = Noah LSM
Planetary boundary layer	2 = QNSE
Cumulus parametrization	4 (only for D1 and D2) = Arakawa–Schubert

3 Model Results Validation

The model performance is estimated using standard statistic measures - mean values, mean bias (MB, model-observation), normalized root mean square error (NRMSE), standard deviation (SD), mean absolute error (MAE) and Pearson correlation coefficient (r). Observations for the potential temperature (Θ), relative humidity (RH), mixing ratio (MR) and wind speed (WS) are interpolated to the model levels. Comparison between simulated and observed parameters for all hours up to 8000 m (Table 2) shows a positive very strong correlation. All parameters are slightly underestimated by the model, except potential temperature.

The transition from stable to convective boundary layer in the morning hours is clearly displayed in both observed and modelled Θ profiles. Both profiles at 04 GMT (Fig. 1) show a stable layer approximately 250 m, residual convective layer between 1000 and 1800 m, and vast entrainment zone between them. The convective layer (CL) starts to grow at 8 GMT. The simulated Θ is 2 K lower than observed at the ground at this time. The model results are in agreement with observations for the height of CL. It is approximately 750 m at 10 GMT, 1750 m at 12 GMT and 2000 m at 14 GMT. The model Θ values are lower close to the ground during the day, but the biases reduce with the CL development.

Turbulent characteristics—sensible heat flux (*HFX*), latent heat flux (*LH*) and friction velocity (U_*) are also validated. Figure 2 shows that the model adequately describes the *HFX* except for September 30th after the rainfall, when the model overestimates about 2 times observations. WRF describes the sharp jump in *LH* value after the rain on September 30th, but with about 2 h delay. The simulated

Table 2 Summary of statistics (integrated data up to 8000 m)

	Mean	MB	SD	NRMSE	MAE	r
T [K]	280.9	−0.9	1.2	0.0	1.2	0.998
Θ[K]	300.5	0.1	1.0	0.0	0.8	0.995
RH [%]	55.0	−0.2	10.4	0.2	7.3	0.890
MR [g kg^{-1}]	5.4	−0.2	0.6	0.1	0.5	0.970
WS [ms^{-1}]	4.4	−0.5	2.0	0.4	1.6	0.908

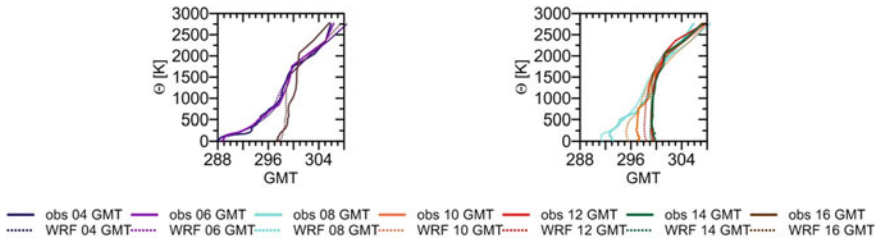

Fig. 1 Comparison of *Θ* model profile and observations up to 3000 m on September 29th

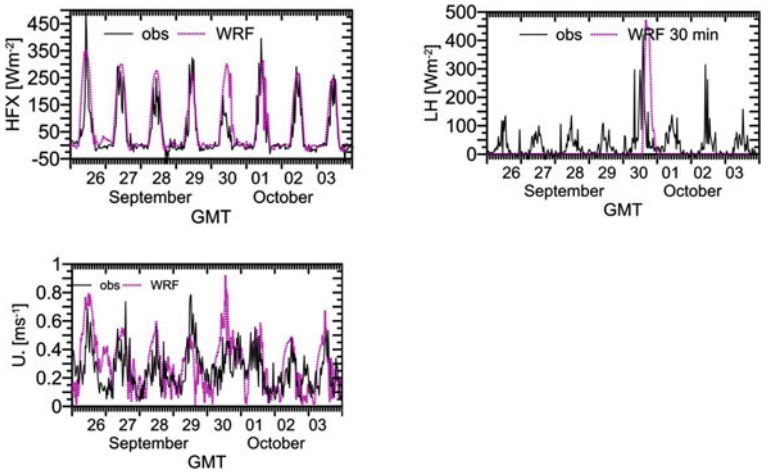

Fig. 2 Sensible heat flux (*HFX*), latent heat flux (*LH*) and friction velocity (U_*) validation

maximal values of U_* are overestimated by the model (with exception on September 29th), while WRF generally underestimates nocturnal U^* values, except night on September 26th.

The spatial distribution of modeled maximal *HFX* and *LH* (Fig. 3) clearly indicates that the model describes correctly city parks with lower values of *HFX* and higher

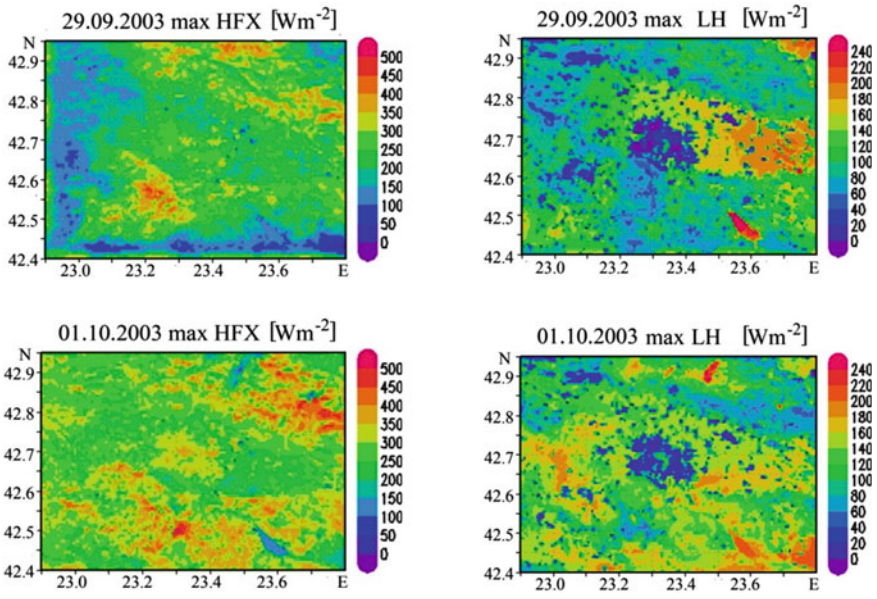

Fig. 3 Maximal simulated HFX and LH (first row: 29.09.2003, second row 01.10.2003)

for *LH*. High values of LH are calculated for the water basins around the city and low for the built-up areas. High *HFX* values are calculated in the city and on the ridges of the surrounding mountains.

4 Conclusions

The results of validation of WRF over Sofia urban area located in complex terrain show that the model adequately describes vertical profiles and turbulent fluxes with the selected parametrization of physical processes.

Acknowledgements This research is supported by the project DN4/7 (Study of the PBL structure and dynamics over complex terrain and urban area), funded by the National Science Fund of the Bulgarian Ministry of Education and Science.

References

Batchvarova, E., & Rotach, M. W. (2005). *Bilateral co-operation on urban boundary layer studies. Turbulence measurements for urban boundary layer research in Sofia* (pp. 185–188). Final report COST action 715, ISBN: 978-954-9526-30-1.

Batchvarova, E., Gryning, S.-E., Rotach, M. W., & Christen, A. (2007). Comparison of modeled aggregated turbulent fluxes and measured turbulent fluxes at different heights in an urban area. In C. Borrego & A. Norman (Eds.), *Air Pollution Modeling and its Application XVII* (pp. 363–370). Kluwer Academic/Plenum Publishers.

Author Index

© The Editor(s) (if applicable) and The Author(s), under exclusive license to Springer-Verlag GmbH, DE, part of Springer Nature 2021

C. Mensink and V. Matthias (eds.), *Air Pollution Modeling and its Application XXVII*, Springer Proceedings in Complexity, https://doi.org/10.1007/978-3-662-63760-9